Fall 2016

Advancing microalgae culturing via bubble dynamics, mass transfer, and dynamic growth investigations

Aastha Ojha

Department: Chemical and Biochemical Engineering

ADVANCING MICROALGAE CULTURING VIA BUBBLE DYNAMICS, MASS TRANSFER, AND DYNAMIC GROWTH INVESTIGATIONS

by

AASTHA OJHA

A DISSERTATION

Presented to the Graduate Faculty of the

MISSOURI UNIVERSITY OF SCIENCE AND TECHNOLOGY

In Partial Fulfillment of the Requirements for the Degree

DOCTOR OF PHILOSOPHY

in

CHEMICAL ENGINEERING

2016

Approved by:

Dr. Muthanna Al Dahhan
Dr. Oliver Sitton
Dr. Daniel Forciniti
Dr. Joontaek Park
Dr. Melanie Mormile

PUBLICATION DISSERTATION OPTION

This dissertation consists of the following articles, formatted in the style utilized by the Missouri University of Science and Technology.

Paper I, Pages 13-55, has been submitted to the Chemical Engineering Science Journal.

Paper II, Pages 56-96, is intended for submission to the Chemical Engineering Journal.

Paper III, Pages 97-150, is intended for submission to the Biotechnology and Bioengineering Journal.

Paper IV, Pages 151-185, is intended for submission to the Biotechnology and Bioengineering Journal.

Paper V, Pages 186-213, is intended for submission to the Biotechnology Journal.

ABSTRACT

The major hindrances to large scale cultivation of microalgae are the problems associated with the design, operation, and scale-up of airlift photobioreactors (PBRs), due to a lack of a comprehensive understanding of the gas-liquid interaction process in real microalgae cultures. Thus, the overall objective of this work is to advance the fundamental understanding of microalgae culturing via gas holdup, bubble dynamics, mass transfer, and dynamic growth investigations.

First, a four-point optical fiber probe technique was employed to study the local gas holdup, and bubble dynamics properties such as bubble passage frequency, chord length and bubble velocity distribution, and interfacial area in an air-water system in a split airlift PBR at superficial gas velocities between 0.3-2.8 cm/s. These properties were then studied in green fresh-water microalgae, *Scenedesmus*, grown inside the PBR, and their variation with a change in the optical density and rheology of the medium due to microalgae growth was also studied.

For mass transfer investigation, the significance and development of a new approach to calculate the liquid side and the local volumetric mass transfer coefficient was established in an air-water system. This new approach was then applied to estimate the local mass transfer coefficient in the *Scenedesmus* culture, as it grew in optical density.

Finally, a separate-effects experiment was developed to estimate the dynamic growth kinetics parameters of microalgae *Scenedesmus*, by measuring its growth rate and fluorescence in a tubular airlift PBR.

ACKNOWLEDGEMENT

First, I would like to thank my advisor, Dr. Muthanna H. Al-Dahhan for his guidance, encouragement, and critical comments through the years. I am immensely grateful to Dr. Oliver Sitton, for not only being on my defense committee but also for always being there to answer my questions. His profound fundamental understanding and meticulous work ethic were a major source of inspiration for me. I would also like to thank my defense committee members Dr. Daniel Forcinit, Dr. Joontaek Park, and Dr. Melanie Mormile for their time and effort, and constructive feedback that helped improve this work.

I wish to acknowledge the members of my research group for their cooperation and valuable discussions through the course of this work. I would also like to thank Dean Lenz, whose strong technical expertise helped ensure the smooth functioning of all the equipment through the course of this research. I am also grateful to the department secretaries Marlene Albrecht, and former secretaries, Krista Welschmeyer, Morgan Coonrod, and Julia Burnette for all their help, and more so for their emotional support in times of need.

Lastly, and most importantly, I would like to thank my parents, Naval and Meena, for being my strength and inspiration, my ever-so-understanding parents-in-law, Anju and Krishan, for their continuous support and cooperation, my late uncle, Om Rattan, for getting me started on pursuing my doctorate, my brother, Akhilesh, for lightening the mood during stressful days, and my better half, Amitesh, for being my rock and believing in me and the future that awaits us. Thank you, family. This dissertation belongs to you.

TABLE OF CONTENTS

LIST OF FIGURES

Figure Page

PAPER I

LIST OF TABLES

SECTION

1. INTRODUCTION

Microalgae are fast growing, simple organisms that convert light, CO_2, nitrates and phosphates into complex organic molecules like lipids, proteins, and sugars, through the process of photosynthesis. They can be cultivated on otherwise non-productive land, in saline water, or in other available wastewater. They gained popularity as the third generation of biofuels, overcoming the limitation of competing with food sources and low biomass productivity associated with the first and the second generation biofuels, respectively. Microalgae require higher amounts of carbon dioxide than terrestrial plants and thus help in carbon sequestration. In addition to fixing the atmospheric CO_2, they also utilize nitrates and phosphates present in atmosphere and aid in abating environmental pollution. Microalgae biomass can also be processed to produce pharmaceutical products, food additives, aquaculture, and single cell proteins, etc. [1]–[3]. Microalgae have the versatility to be genetically engineered to enhance lipid production and carbon dioxide fixation [4]–[6].

Photobioreactors used for microalgae culturing vary from open systems (such as ponds and lakes) to closed systems like bubble columns, airlifts, tubular and panel reactors, supplemented with pumps, propellers, and pneumatic mixers to ensure proper mixing of the culture, and avoid gradient buildup. The choice of reactor depends on the availability of parameters like nutrients, light, etc. that affect growth, and the geographic location. The source of illumination varies from the sun to LEDs and fluorescent lamps.

Contamination is a serious problem in outdoor ponds, rendering the microalgae biomass unfit for food and pharmaceutical applications, whereas indoor reactors have been shown to have better process control and higher biomass productivity [7]. The space requirement for culturing large volumes of microalgae can also be minimized in indoor reactors by increasing the size vertically, as opposed to the large land requirement for outdoor reactors such as ponds and lakes. They are also the choice for culturing species that are less resistant to environmental changes as they allow the algal cultures to grow in an environment much more tuned to optimal growth [8]–[13]. Temperature, pH, the duration and intensity of the light, availability of carbon dioxide and other nutrients, and adequate mixing are critical parameters that affect the growth of algae.

Since algae grow via the process of photosynthesis, light is one of the most important parameters that affect growth rate. Adequate intensity and duration of light are essential to maintaining a healthy culture. Deficiency of light can lead to insufficient cell energy and result in photolimitation. As the cell culture multiplies in number and grows in density, the light distribution within the culture is drastically affected due to mutual shading among the cells, further limiting the availability of light to the cells. On the other hand, an excess of light can also inhibit the growth of algae leading to photoinhibition, sometimes to the extent of completely shutting down the process. Also, light intensity decreases from the outer surface to the center of the reactor. This attenuation may be attributed to the material of construction and thickness of the reactor, cellular absorption, mutual shading among the cells, and scattering of light particles by the liquid and cellular elements. As the algae cells move from one point in the photobioreactor to the other, they are exposed to the well-lit exterior as well as the dark interior of the reactor, and thus

experience the flashing lights effect. The flashing lights effect has shown to improve the productivity of biomass [14], [15], while overexposure to either the well-lit exterior or the dark interior can lead to photoinhibition and photolimitation. The increase in the culture density or the size of operation further amplifies the phenomenon of photolimitation and photoinhibition leading to an inefficient distribution and supply of light energy to the cells. Thus, efficient mixing strategies, that provide proper movement between the random light and dark regions present throughout the reactor, are essential for maintaining healthy cultures.

Mixing also affects gas liquid interaction and ensures supply of carbon dioxide and other nutrients to the cells for primary and secondary metabolisms. This further helps in avoiding concentration gradients inside the reactor as CO_2 concentration build-up can severely alter the pH of the medium making it unfit for culturing algae. Low mixing rates can interfere with gaseous mass transfer and cause biomass settling. Pumping, mechanical stirring, and gas injection are some commonly used methods to aid in mixing. While both pumping and mechanical stirring provide fairly good mixing, the gas transfer rate for pumping is much lesser than that for stirring. Also, they both apply a significant hydrodynamic stress on the system. A high hydrodynamic stress on the cells can often lead to the rupturing of the cell walls [16], releasing the cytoplasm into the medium. The cell walls can stick to reactor walls, or interfere with the other components of the system, and together with the cytoplasm can hinder light distribution inside the medium [17].

Although, research and development to advance photobioreactor design and configuration and the potential uses of microalgae and has grown in recent years, the commercialization of microalgae technologies for biofuels and bio-based chemicals

production, and CO_2 and waste water treatment is still in its early stages. This is mainly due to the complexity of the algae culturing process and the lack of integration of the gas-liquid interaction and bubble dynamic properties with changes in the fundamental properties of the culturing medium. Therefore, to tap all the advantages of this microorganism, a thorough understanding of the gas-liquid interaction phenomenon in a real microalgae culture is essential for the optimization, design, scale-up and operation of all the elements of the system.

2. MOTIVATION

The process of cultivating microalgae has been in practice since the 1950s. The photobioreactor designs and configurations available in literature have been only used for investigational purposes, and have not been successful for large-scale cultivation operations [9]. Knowledge of gas holdup, hydrodynamics, and transport properties inside a real microalgae culture, as well as the operating parameters of the photobioreactor, are essential for successful scale-up and optimization for mass cultivation of microalgae [9], and a lack of the same has made commercial-scale microalgae culturing a costly affair.

Of the available photobioreactor configurations, bubble columns and airlift photobioreactors are very promising for culturing algae on a large scale [18] (Ugwu, 2008). They are also compact and easy to construct and operate. Since gas injection is used for mixing as well as introduction of nutrient gases into the system, they provide low shear stress to algae along with proper mixing and mass transfer [18]–[21]. Airlift photobioreactors supply a controlled concentration of CO_2 (with air and nitrogen), typically by sparging the gas into the algal culturing media, where the bubbles help in distributing the gas and agitating the culture as they move.

In bubble columns even though there are light and dark regions present inside the reactors (thus allowing for the flashing light effect), research has shown that properly ordered mixing strategies must be introduced to facilitate movement of cells between these zones [22]. Thus the draft tube and split airlift reactor are a better choice for microalgae cultivation. Both of these airlift reactors provide efficient circulation leading to ordered mixing leading and movement of cells between the light and dark phases.

However, in draft tube airlift reactors, the presence of microalgae culture in the annular region, and the walls of the internal draft tube attenuate the light intensity reaching the core of the reactor, thus creating a huge dark zone at the core. This problem is overcome in split airlift reactors which have been shown to be better at growing microalgae than draft-tube airlift reactors [17].

When gas flows through the microalgae culture inside the reactor, the gas holdup and bubble dynamics determines the transfer of the gasses from the gas phase to the liquid phase, and also the transfer of oxygen (produced during photosynthesis) from the liquid to the gas phase. Gas-liquid interaction is affected by the local gas holdup, bubble frequency, chord length and velocity, interfacial area, and mass transfer. These parameters are critical not only to ensure that the nutrients are supplied to the cells at an effective rate but also to avoid oxygen build-up in the medium. Some studies on estimating the gas holdup, bubble dynamics, and mass transfer in airlift reactors are available in the literature. There are also many correlations for calculating the flow dynamic properties of the system, but the empirical or semi-empirical nature of these studies limits their applicability.

As the culture grows and increases in density, the rheological properties of the system such as density, viscosity, and surface tension also change. These dynamic changes in the physical properties of the medium, in turn, alter the structure, size, and frequency of the gas bubbles, and hence the bubble dynamics of the system. Hence, it is essential to study the changes in the physical properties during the process of dynamic growth in conjunction with the bubble dynamics, to characterize the system accurately, and study mass transfer inside the medium. Very few studies in the literature have

addressed this essential issue. Most of these studies do not deal with a biological system, and hence fail to take into account the rheological changes in the system. Furthermore, these studies focus on the overall parameters (gas holdup, interfacial area, mass transfer coefficient). Since gas flow, liquid circulation, and light attenuation can lead to the formation of light and dark regions in the reactor, especially as the culture grows in density, the dynamics of the system changes from one point in the reactor to another. Additionally, overall parameters fail to describe the true phenomenon going on inside large scale reactors and mass cultures. Studies have also suggested that mass transfer properties vary from the riser to downcomer of the reactor, as well as along the length of the reactor [23]. Also, to truly understand the overall mass transfer coefficient, it is important to separately analyze the local mass transfer coefficient and the local interfacial area. Thus, a study of the overall parameters [24], [25] is insufficient, making it essential to investigate the changes in the local gas hold-up, bubble dynamics, and mass transfer coefficient as the physical properties such as optical density, viscosity, and surface tension of the system change.

Also, during the process of photosynthesis, microalgae generate oxygen, which is transferred from the liquid to the gas phase. As the culture photosynthesizes and grows in density, more and more oxygen is produced, which tends to accumulate inside the medium. Accumulation of oxygen hinders the process of photosynthesis and is detrimental to the growth of algae [26]. A pilot plant in Spain was shut down as oxygen accumulation inside the reactor inhibited cell growth, eventually killing most of the cells [20]. Hence, to achieve efficient growth rate and get a good culture density, the excess

accumulated oxygen must be removed regularly. This further emphasizes to fully understand the mass transfer process in real microalgae culturing systems.

Another crucial step in the process of optimizing the growth and biomass productivity of microalgae cultures is the integration of the dynamic and kinetic growth studies. As mentioned earlier, the duration and intensity of light are critical to the rate of growth of algae. As microalgae grow and the cells multiply in number, the light intensity drops drastically on moving from the illuminated region of the reactor to the core. A high photon flux density on the outer wall of the reactor can help reduce the attenuation of the light signal across the reactor and thus prevent a decrease in growth rate due to photoinhibition. But since a long duration of time spent in a high photon density region can also hamper growth through the process of photoilimitation, it is inevitable to achieve a dynamic balance between the light and the dark phases. Also, due to the movement of the cells from one point in the reactor to another, the light intensity experienced by the cells varies based on the cell's trajectory (flashing lights effect). However, the static growth models commonly used in literature to study the growth rate of microalgae are based on the assumption that all cells receive the same light intensity, which becomes grossly inaccurate on moving to large scale reactors and denser cultures. Thus, the application of a dynamic growth kinetics model to microalgae cultures becomes essential as they account for the hydrodynamics of the system and the true, varying light intensity experienced by each cell.

3. RESEARCH OBJECTIVES

The overall objective of this work is to advance the fundamental understanding of culturing microalgae via local gas holdup, bubble dynamics, mass transfer, and dynamic growth investigations. The specific research objectives are as follows:

1. Implementation of a four-point optical fiber probe technique in an air-water system in a split airlift reactor to study the local variation in properties such as gas holdup, bubble passage frequency, bubble chord length, bubble velocity, and interfacial area under different superficial gas velocities. This will help lay the foundation for implementing the technique in a real microalgae culture.

2. Estimation of the mass transfer coefficient in an air-water system through a new approach assuming a constant liquid-side mass transfer coefficient and incorporating the local gas holdup and interfacial area data from objective 1 to study the local volumetric mass transfer coefficient and observe its variation through the reactor.

3. Implementation of the optical fiber probe technique in a real microalgae culture inside the split airlift photobioreactor to study the local gas holdup, and bubble dynamics properties over the entire growth period of microalgae. The variation in these local properties with changes in optical density and viscosity of the microalgae culture will also be measured.

4. Application of the new mass transfer modeling approach, developed in objective 2, in a real microalgae culture inside the split airlift photobioreactor, using the local properties determined in objective 3. Also, analyzing the effect of an increase in

density and viscosity of the microalgae culture on the local volumetric mass transfer coefficient.

5. Estimation of the true dynamic growth parameters of microalgae *Scenedesmus* in a separate effects experiment adopting the methodology and modifications to the three states model [27] developed by Wu and Merchuk, 2001 [28].

The procedures and methodologies to carry out the objectives mentioned above, along with their results and discussion have been presented in the form of five papers included in this dissertation. The results and findings of this research give an insight into the dynamic changes in the physical properties of the medium, and its impact on local gas holdup, bubble dynamics and mass transfer. Also, these measurements can serve as valuable benchmarking data for evaluation and validation of computational fluid dynamics (CFD) models and interfacial forces closures to predict the flow field of microalgae culture during the growth where the physical properties of the medium vary.

PAPER

I. INVESTIGATION OF LOCAL GAS HOLDUP AND BUBBLE DYNAMICS USING FOUR-POINT OPTICAL PROBE TECHNIQUE IN A SPLIT AIRLIFT BIOREACTOR

ABSTRACT

Four-point optical fiber probe technique was employed in a split airlift reactor with an air-water system. Effect of superficial gas velocities- 0.3, 1.0, 2.0, and 2.8 cm/s- was studied on the local gas holdup and bubble dynamic properties namely, bubble passage frequency, interfacial area, bubble chord length, and bubble rise velocity in both the riser and downcomer sections of the reactor. The bubble chord length and bubble velocity in the riser and downcomer followed log-normal distribution and normal distribution respectively. For a superficial gas velocity increase from 0.3 to 2.8 cm/s the gas holdup and interfacial area in the riser increased by 900 and 800 %, respectively. No bubbles were detected in the downcomer at superficial gas velocity of 0.3 cm/s. The local gas holdup and interfacial area at the top of the downcomer increased by 500, and 400%, respectively, for a superficial gas velocity increase from 1.0 to 2.8 cm/s, respectively. At each superficial gas velocity, the bubble passage frequency, gas holdup, and interfacial area did not vary significantly along the axis of the riser. An axial variation in bubble passage frequency, gas holdup, and interfacial area was observed in the downcomer. A correlation for the variation of gas holdup in the riser was developed based on superficial gas and liquid circulation velocities. The correlation for the gas holdup in the downcomer was developed to account for the axial variation observed.

Keywords: Airlift Photobioreactors, Local Bubble Dynamics, Local Gas Holdup, Local Interfacial Area, Bubble Chord Length Distribution, Bubble Rise Velocity Distribution, Downward Bubble Velocity Distribution

1. INTRODUCTION

Airlift reactors are pneumatic devices commonly used for gas-liquid and gas-slurry contact. They consist of two main parts, namely the riser and the downcomer. The air or gas stream is introduced through an orifice or a sparger and serves the purpose of agitating and mixing the contents of the reactor. Often, the air/gas stream also acts as a reactant, or as a source of nutrients, like in microalgae culturing. The introduction of air at the bottom of the riser lowers the density of the mixture and also creates a difference in the gas holdup between the riser and the downcomer regions, resulting in fluid circulation. Fluid inside the reactor is lifted upwards in the riser due to the airlift action, and flows downwards through the downcomer, before entering the riser again due to the resulting circulation. Airlift reactors provide a more efficient gas-liquid contact in terms of heat and mass transfer while maintaining low shear stress, which is particularly beneficial in the case of fermenters and photobioreactors [1]–[3]. Due to a lack of moving parts like stirrers and mixers etc., they are fairly simple to construct, and their scale-up is easier as compared to bubble columns and continuously stirred tank reactors (CSTRs) [4], [5]. They are widely used in the field of fermentation, anaerobic digesters, wastewater treatment, photobioreactors for culturing algae and cyanobacteria among other multiphase reactor applications [2], [6]–[10].

Airlift reactors are of two types, external and internal loop reactors. In external loop reactors, the riser and downcomer sections are two separate parts (columns or tubes) connected externally via horizontal or inclined sections at the top and the bottom. Internal loop reactors are modified bubble columns, divided into the riser and downcomer

sections by a baffle [4]. Based on the type of baffle (separation) used, internal loop reactors can be of two types- draft-tube or split airlift reactors. Draft tube airlift reactors consist of two concentric tubes, with either the inner tube or the annular region sparged with air (thus forming the riser). A plate or partition is used to divide the column into the riser and the downcomer sections in a split airlift reactor.

The hydrodynamics in airlift reactors has a strong influence on gas-liquid interaction. Bubble dynamic properties like local gas holdup, interfacial area, bubble chord length distribution, and bubble passage frequency thus become critical parameters for mass transfer and the reactor performance during scale up operations and are important to understanding the true process inside the reactor. A number of correlations are available in literature to calculate the gas holdup [11]–[14], and interfacial area [11]–[18]. However, these correlations are either empirical or semi-empirical in nature and are thus limited in their application. Most of the researchers have focused on calculating the global hydrodynamic properties like overall gas holdup by measuring a difference between the static and dynamic liquid height in the column and differential pressure measurements [19]–[23]. Other properties like liquid circulation velocity and mixing time have also been measured [24], [25]. Even though the study of overall parameters is of significance to the study of airlift reactors, it is the local parameters that affect the reactor or culturing performance and their understanding is essential to advance the development and operation of the actual process. In fact, local parameters become crucial as the size of the reactor increases such as in industrial processes [26]. Also, since most of the applications of airlift reactors involve some form of interphase or bulk mass transfer, the local fluctuations in bubble properties in gas-liquid systems must be considered as they

can significantly affect the process. This becomes particularly important when the air/gas stream also acts as a source of nutrients supply, like in the case of culturing microorganisms. Due to lack of reliable data on local properties, and the difficulty associated with carrying out local measurements, researchers, even recently, have used the overall gas holdup for modeling mass transfer operations [26], [27]. There are very few studies in literature that have used techniques like monofiber optical fiber probes, electrical resistivity probes, and computed tomography to evaluate the local bubble properties and gas holdup, but did not study the axial variation in them, if any [28], [29].

Thus, a good understanding of the local variation of the bubble dynamics in an airlift reactor will not only help advance the current knowledge in the field but also add to the database for benchmarking CFD validation studies. For this purpose, this study aims at using a sophisticated 4-point optical probe to investigate local gas holdup, and for the first time, specific interfacial area, bubble chord length, and bubble passage frequency at different axial locations inside a split-column airlift reactor, and study axial variation in the aforementioned hydrodynamic properties, if any.

Luo et al., 2012 [5], studied the growth rate of microalgae *Porphyridium* in split airlift, draft tube and bubble column reactors, and found the split airlift photobioreactor to outperform the other two. This was possibly due to the presence of insufficient light inside the draft tube and a lack of ordered mixing in the bubble column. Therefore, in this study, a split airlift photobioreactor was used to investigate the local gas holdup and bubble properties.

Albdiri et al., 2015 [30], carried out a similar study in the same experimental setup as discussed in section 2. The results found in their study are different from those

presented in this paper, possibly due to a lack of proper statistical analysis. These shortcomings have been overcome in this study. Also, Albdiri et al., 2015 [30], did not study the bubble dynamic properties such as bubble passage frequency, bubble chord length, and bubble velocity, which have also been estimated in the present work.

2. EXPERIMENTAL SETUP

The split-column airlift reactor used in this study has been adapted from Luo et al., 2012 [5]. In addition to the conventional advantages of higher mass and heat transfer rates, simple construction, efficient mixing, and easier scale-up as compared to other types of reactors, the split airlift reactor has also been shown to perform better than draft-tube or bubble columns for microalgae culturing [5]. Luo and Al Dahhan, 2012 [5] studied the radial variation of the gas holdup in air water, and microalgae system using the Gamma Ray Computed Tomography (CT), and Radioactive Particle Tracing (RPT) techniques.

The split airlift reactor was constructed from acrylic with an inner diameter of 13 cm and a total height of 150 cm. A 105 cm tall acrylic plate, placed 5 cm above the base, divided the reactor into two zones of equal cross-sectional areas- the riser and the downcomer. The liquid volume in the reactor was about 15 liters. At the bottom of the riser, in the middle, a ring-type sparger was installed. Fifteen 1mm orifices were located equidistantly on the sparger ring for the introduction of air into the reactor (riser). Five ports were provided in both the riser and the downcomer sections for carrying out local measurements. The setup was operated in a batch mode at room temperature and pressure conditions. The liquid phase used was reverse-osmosis water, and dry compressed air was used as the gas phase. The column was run at riser superficial gas velocities of 0.3 cm/s, 1.0 cm/s, 2.0 cm/s, and 2.8 cm/s, which was calculated by dividing the volumetric gas flow rate by the riser cross-sectional area. A four-point optical fiber probe technique was employed at the radial center to study the axial gas holdup, interfacial area, bubble

passage frequency, and chord length distribution at the five ports provided in the riser and the downcomer sections (Figure 2.1). Figure 2.1 gives a schematic of the split airlift reactor and the sparger used in this work.

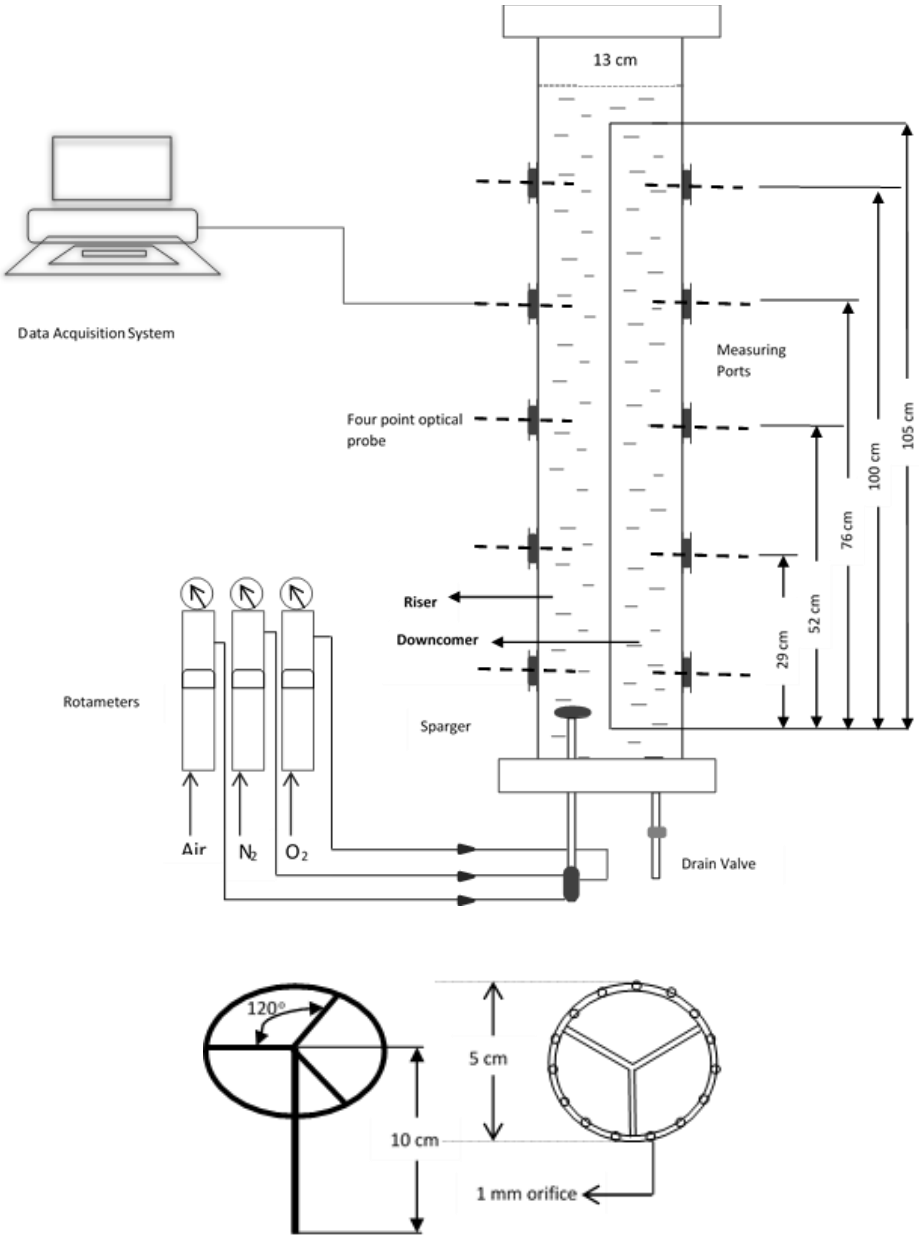

Figure 2.1: Schematic representation of the split airlift photobioreactor and sparger design

3. MEASUREMENT TECHNIQUE

A four-point optical probe technique, shown in Figure (2), was employed to investigate the local gas holdup and bubble dynamic properties such as interfacial area, bubble passage frequency, and chord length in the riser and downcomer of the split-column airlift reactor. This technique was developed by Xue et al., 2003 [31], and has been successfully employed in bubble columns for local measurements of the properties [32], [33]. It technique is based on the difference in the refractive indices of liquid and gas phases due to which the light being refracted back by the optical fibers varies depending on the phase it is in contact with at that moment of time. The system consists of a light source to send light to the probe tips, and a photodiode detector to detect the light refracted back from the tips and convert it into voltage signals. Figure 3.1 is a schematic diagram of the technique, Figure 3.2 gives the configuration of the probe tips, and Figure 3.3 is the typical response when a bubble strikes the four tips. Readers are referred to Xue et al., 2003 [31] for more details of the technique.

The tips of the four-point optical probe were positioned downwards in the riser, and upwards in the downcomer to capture the upcoming and down flowing bubbles, respectively. A data processing algorithm developed by Xue et al., 2003 [31] was used to calculate the local gas hold-up and specific interfacial area at each of the 10 locations (5 in the riser and 5 in the downcomer). The measurements were repeated three times at the radial center at each location, and an average was taken for each port in the riser and the downcomer for U_G equal to 0.3, 1, 2, and 2.8 cm/s.

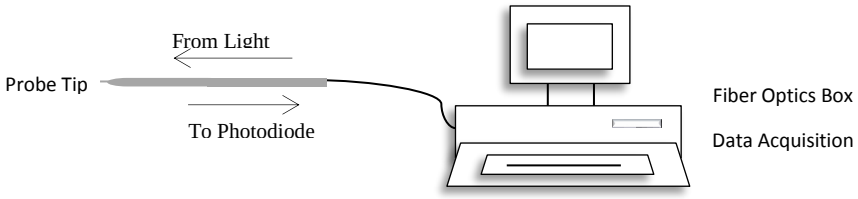

Figure 3.1: Schematic representation of the 4-point optical fiber probe technique

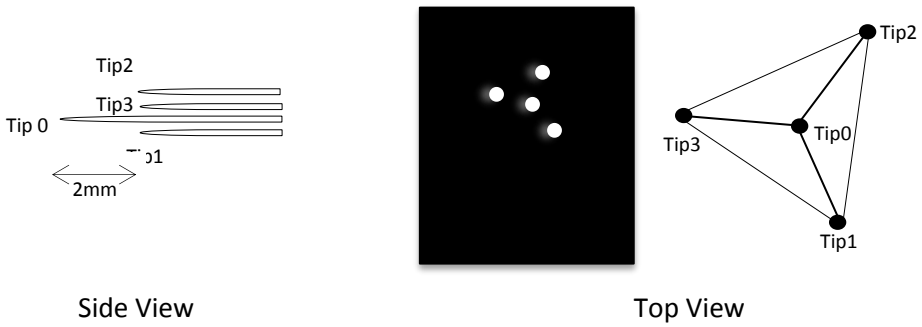

Figure 3.2: Schematic representation of the probe tip

For local gas holdup, Xue, et al., 2003 [31], invoked the ergo dynamic hypothesis and calculated the local gas holdup based on the time spent by the tip in the gas phase (T_G) versus the total measurement time (T).

$$\varepsilon_g = \frac{T_G}{T} \tag{1}$$

Taking the total number of bubbles hitting the tip, the Equation (1) can be rearranged to Equation (2).

$$\varepsilon_g = \frac{\sum (v_i . t_{G,i})}{\sum (v_i . (t_{G,i} + t_{L,i}))} \tag{2}$$

Where, v_i is the velocity of the i[th] gas-liquid interface (bubble leading phase), $t_{G,i}$ is the time interval that the probe tip spends in the i[th] gas section (bubble), $t_{L,i}$ is the time interval that the probe tip spends in the i[th] liquid section (Xue et al., 2003).

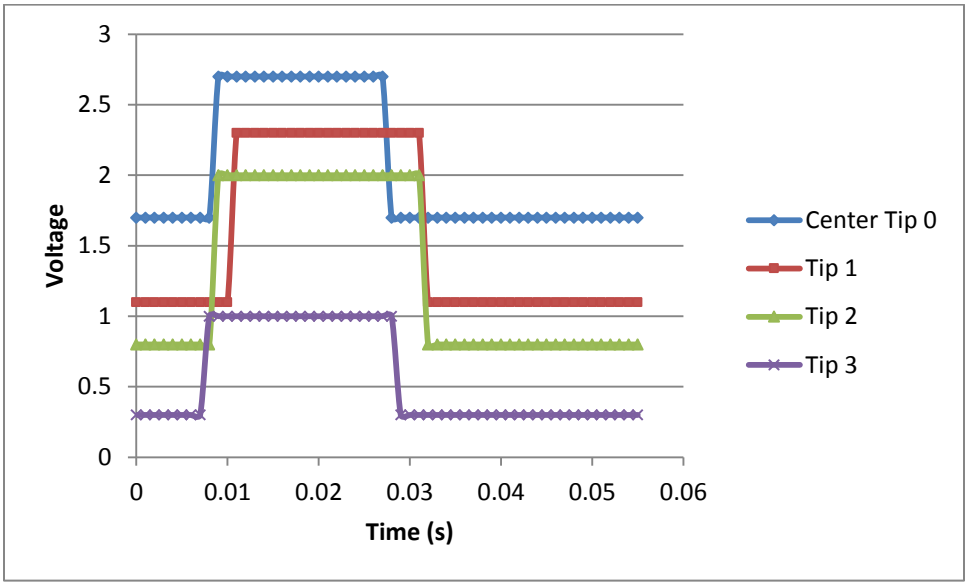

Figure 3.3: Typical response of a bubble striking the probe tip

For the measurement of interfacial area, equation (3) for the local specific interfacial area (a) in the gas-liquid system was derived by Kataoka et al., 1986 [34].

$$a = \frac{1}{\Delta T}\sum_{N}\frac{1}{V\cos\phi} \tag{3}$$

The above equation was modified by Xue et al., 2003 [31], to account for the bubbles that hit the center tip, but miss the others. The modified equation is based on the total number of the gas-liquid interfaces (N) passing by the probe in time (ΔT), the angle (ϕ) between the velocity vector and the normal vector of the interface (bubble's surface),

and the magnitude of the bubble velocity vector (V). The resulting correlation used by Xue et al., 2003 [31] to calculate the local interfacial area is given below.

$$a = \frac{1}{\Delta T}\sum_{N}\frac{1}{V\cos\phi} \cong \frac{1}{\Delta T}\frac{N}{N_{measured}}\sum_{N_{measured}}\frac{1}{V\cos\phi} \tag{4}$$

$$N = N_{measured} + N_{missed}$$

The bubble passage frequency is based on the total number of bubbles hitting the probe tip over a period of time. For further details, and for bubble chord length and bubble velocity measurement technique, the readers are referred to Xue et al., 2003 [31].

4. RESULTS AND DISCUSSION

4.1 GAS HOLDUP

For initial experimentation, at a fixed axial location, the four-point optical fiber probe was placed at three different radial positions in the middle of the riser and downcomer for gas holdup measurements. The four-point optical fiber measurement technique gave an error when employed close to the walls, possibly due to physical constraints posed by the shape, design, and placement of the probe. Thus a very fine mesh for radial measurements could not be obtained through this technique, and gamma-ray computed tomography (CT) must be employed to study radial gradients and obtain a clear and more comprehensive radial profile.

During preliminary experiments in the middle of the riser and downcomer sections, no significant statistical radial variation of gas holdup was observed, and hence, the gas holdup data reported at each axial location is the average of three measurements carried out at the radial center. Gas holdup data reported for both the riser and the downcomer is studied against the riser superficial gas velocity, U_g, which is calculated by dividing the volumetric gas flow rate by the riser cross-sectional area, as mentioned earlier.

4.1.1 Gas Holdup in the Riser. Superficial gas velocities varying from 0.3 cm/s to 2.8 cm/s were employed in the riser to study the local gas holdup at each of the five ports in the riser. No statistically significant axial variation of gas holdup was observed in the riser, and hence an average of the gas holdup at the five ports was used to calculate the riser gas holdup. Figure 4.1 depicts the variation of riser gas holdup with superficial

gas velocity. The gas holdup in the riser was found to increase with an increase in superficial gas velocity (Figure 4.1). This trend is similar to that found in the literature [15], [19], [35]–[37].

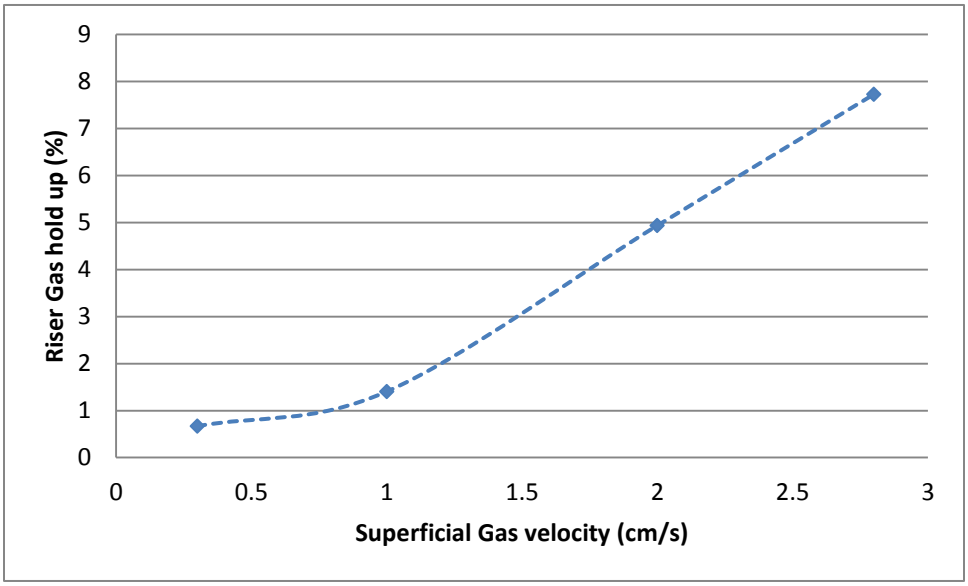

Figure 4.1: The effect of riser superficial gas velocity, Ug, on the gas holdup in the riser

With an increase in superficial gas velocity, the number of bubbles increases increasing the bubble passage frequency. The variation of bubble passage frequency with superficial gas velocity is shown in Figure 4.2. Increase in the bubble passage frequency increases mixing and interaction, which further results in an increase in the gas holdup in the riser.

In Figure 4.1, the rate of increase of gas holdup can be seen to increase slowly up to superficial gas velocities of 1.0 cm/s, beyond which the rate becomes higher. For superficial gas velocities less than 1.0 cm/s, all the bubbles were disengaged in the

separation zone at the top of the reactor, and thus, no bubbles could be seen entering the downcomer. At gas velocities above 1.0 cm/s, the increase in liquid circulation velocity was enough to entrap some bubbles and transport them to the downcomer. When the circulation velocity was high enough, a few bubbles could be seen reentering the riser at the bottom along with the circulating liquid, causing a greater increase in riser gas holdup at higher superficial gas velocities.

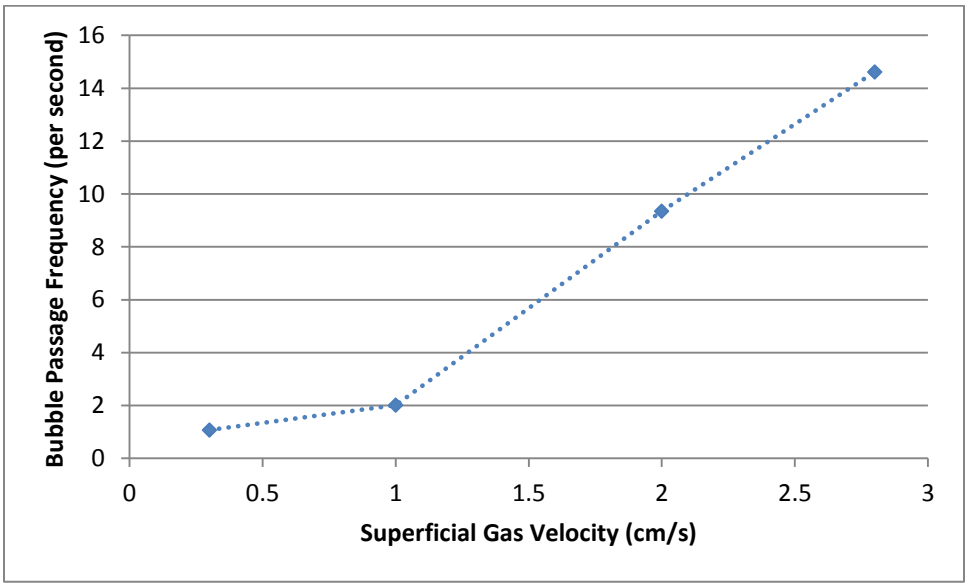

Figure 4.2: Effect of riser superficial gas velocity on the bubble passage frequency in the riser

The literature reported correlations available for gas holdup in bubble columns and airlift reactors are very specific and empirical in nature. While good agreement is found for correlations of gas holdup in bubble columns, the case for airlift reactors is quite different [12]. Most of the reactor configurations studied for developing these correlations are either external loop airlift reactors or draft-tube internal loop airlift

reactors. Table 4.1 gives a few correlations for internal loop airlift reactors available in the literature.

As can be seen in Table 4.1, the liquid phase used to develop the correlations varies from water to different concentrations of salt and alcohols all the way to non-Newtonian fluids. Also, the superficial gas velocities, the ratio of the area of the downcomer to the riser, and the reactor heights used in these studies vary greatly. Thus, the applicability of these correlations outside the studied conditions is highly limited which is clearly exhibited by Figure 4.3.

Figure 4.3 compares the experimental data of this study with some of the correlations for gas holdup. As is evident from Figure 4.3, none of the correlations can predict all the experimental values of the gas holdup obtained at the conditions studied in this work. The gas holdup values based on the correlation given by Blazej et al., 2004 [15] are the most different form the experimental values in this work, and are in fact an order of magnitude higher at the higher superficial gas velocities. Also, as can be seen from Figure 4.3, at the lower superficial gas velocities of 0.3 and 1.0 cm/s, Miyahara et al., 1986 [14], and at the higher velocities of 2.0 and 2.8 cm/s, Chisti et al., 1988 [38] comes close to predicting the riser gas holdup. However, no single correlation can predict the gas holdup in the riser for the entire range of superficial gas velocities of this study. This can be attributed to the theoretical assumptions used for developing these correlations. The value of the riser gas hold up being quite different from that calculated using the correlations, stresses the inherent ambiguity of empirical and semi-empirical correlations.

Table 4.1: Literature reported correlations for overall gas holdup, ε_g
(Subscript 'r' denotes the riser and 'd' denotes the downcomer)

Reference	Parameters	Correlation
Bello et al., 1985 [23]	Air - Water/NaCl solution A_d/A_r = 0.11-0.69	$\epsilon_{gr} = 0.16 * \left(\frac{U_{gr}}{U_l}\right)^{\alpha} (1 + \frac{A_d}{A_r})$ $\epsilon_{gd} = 0.89 * \epsilon_r$ $\alpha = 0.56\ for\ water$ $\alpha = 0.58\ for\ NaCl\ solution$
Blazej et al., 2004 [15]	Air – Water Reactor Volume : 10.5 L A_d/A_r = 1.23	For 10.5 L $\epsilon_{gr} = 0.829 * U_{gr}^{0.505}$ $\epsilon_{gd} = 0.875 * \epsilon_{gr} - 0.0095$
Chakravarty et al., 1973 [11]	$\epsilon_{gr} = \left[(\mu_l - \mu_w)^{2.75} + 161\frac{(73.3-\sigma)}{(74.1-\sigma)}\right] x10^{-4} U_{gr}^{0.88}$ $\epsilon_{gd} = 1.23x\left[\frac{(74.2-\sigma)}{(79.3-\sigma)}\right] x10^{-2} x U_{gr}^{0.88} (\frac{A_r}{A_d})^{1.08} \mu_l{}^{0.45}$	
Chisti et al., 1988 [38]	A_d/A_r = 0.25 -0.44	$\epsilon_{gr} = 0.65 * U_{gr}^{0.603} (1 + \frac{A_d}{A_r})^{-0.258}$ $\epsilon_{gd} = 0.46 * \epsilon_{gr} - 0.0244$
Miyahara et al., 1986 [14]	Air – Non-Newtonian Sols A_d/A_r = 0.128 – 0.808	$\epsilon_{gr} = \frac{0.4\sqrt{Fr}}{1 + 0.4\sqrt{Fr}(1 + \frac{U_l}{U_{gr}})}$ $Fr = \frac{(U_{lr} + U_{gr})^2}{g d_r}$
Kawase et al., 1998 [13]	$\frac{\epsilon_{gr}}{1 - \epsilon_{gr}} = \frac{(\frac{U_{gr}}{n})^{(n+2)/(2(n+1))}}{2^{\frac{3n+5}{n+1}} \left(\frac{g^n k}{\rho_l}\right)^{\frac{1}{2(n+1)}} (1 + \frac{A_d}{A_r})^{3(n+2)/4(n+1)}}$ N=1 for Newtonian fluids; K= viscosity of fluid	

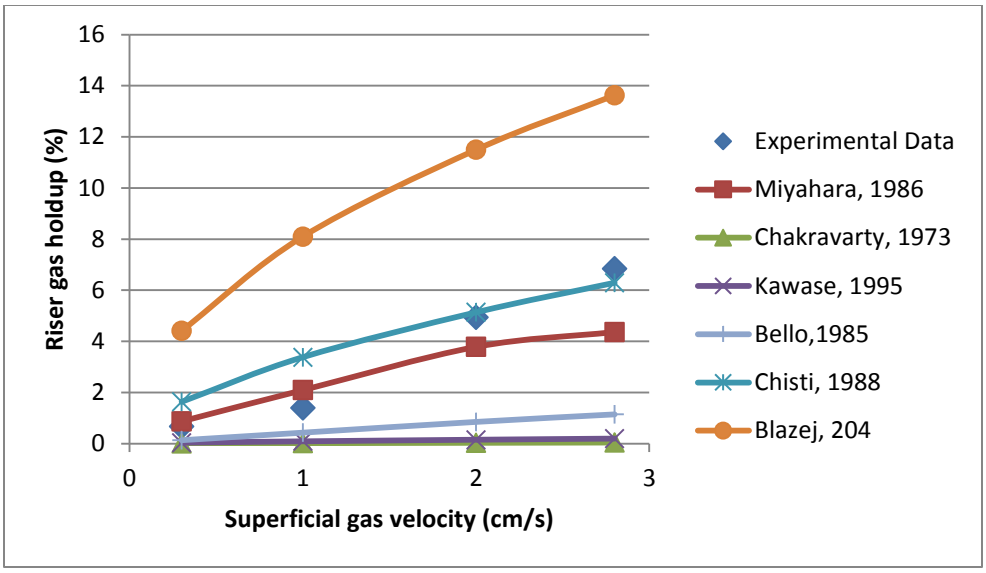

Figure 4.3: Comparison of experimental values of gas holdup in the riser and the correlations

4.1.1.1 Developed correlation. Based on the study by Chisti et al., 1988 [38] in bubble columns, the power-law dependence of gas holdup on superficial gas velocity (Equation (5) is the basis for many of the correlations available in literature.

$$\epsilon_{gr} = \alpha U_g^{\beta} \tag{5}$$

However, since Equation (5) does not take into account the increase in the riser gas holdup due to the bubbles entrained by the circulating liquid at higher gas velocities in airlift reactors, it cannot be applied directly to these reactors. For this reason, some researchers have also included the liquid velocity in the riser, U_{lr}, in the gas holdup correlations [23]. In this work, U_{lr} was measured using a classic colored dye experiment, by measuring the time taken by the colored dye injected into the system to travel along the axis of the riser. A slight variation of Equation 5 and the correlation by Bello et al., 1985 [23], incorporating the liquid circulation velocity, was developed to correlate the superficial gas velocity with the riser gas holdup, and is as given in Equation (6).

Equation 6 satisfactorily predicts the riser gas holdup for the split airlift reactor used in this study. The mathematical regression of Equation 6 with the experimental data gave alpha= 0.324, and beta = 35.772. Figure 4.4 shows that the experimental gas holdup values for the riser lie within 15 % deviation of the developed model.

$$\epsilon_{gr} = \alpha\left(\frac{U_{gr}}{U_{lr}} + 1\right)^{\beta} \quad (6)$$

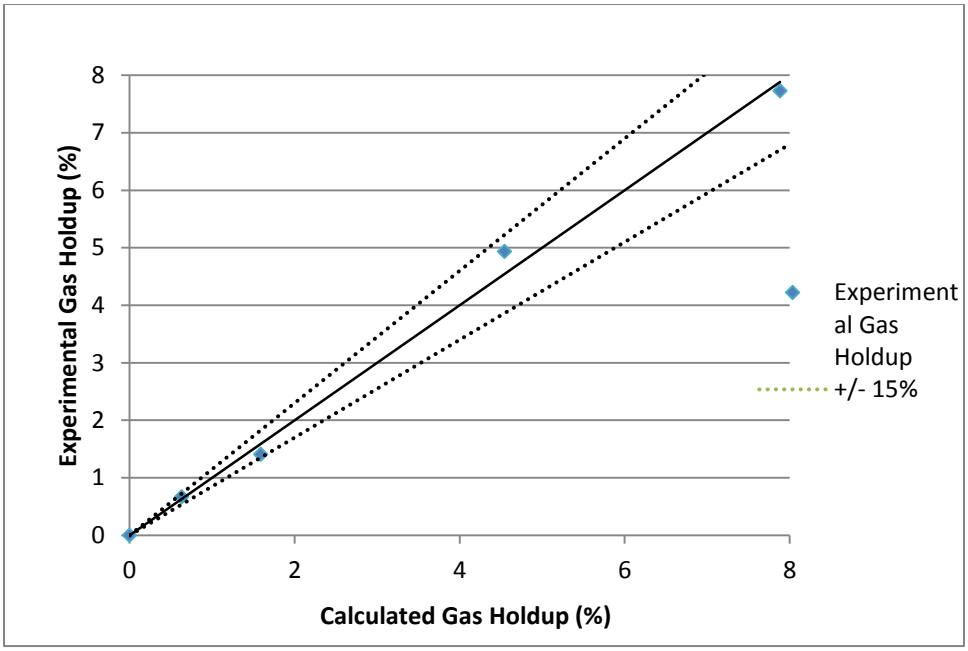

Figure 4.4: Comparison of experimental and calculated gas holdup in the riser

4.1.2 Gas Holdup in the Downcomer. Gas holdup variation in the downcomer was studied at superficial gas velocities ranging from 0.3 cm/s to 2.8 cm/s. The gas holdup in the downcomer was found to vary axially. Figure 4.5 shows the change in the gas holdup at ports 3, 4, and 5, at distances of 52 cm, 76 cm, and 100 cm from the base of the reactor (Figure 2.1) with a change in superficial gas velocity. Similar to the trend

observed in the riser, the gas holdup in the downcomer was seen to increase with an increase in the superficial gas velocity. This can again be attributed to the increase in bubble passage frequency with superficial gas velocity. Figure 4.6 shows the variation of bubble passage frequency at ports 52 cm, 76 cm, and 100 cm above the base in the downcomer.

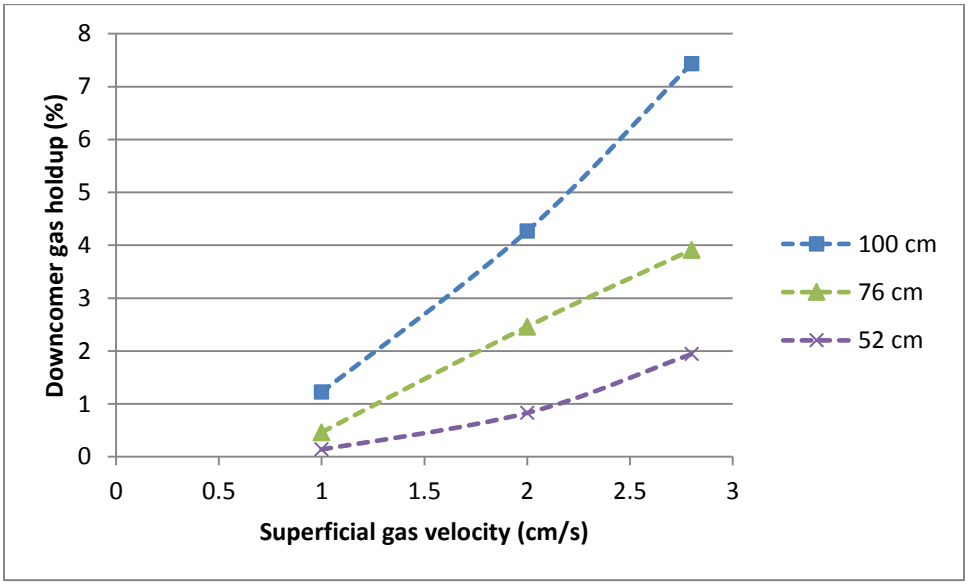

Figure 4.5: Variation of gas holdup in the downcomer with superficial gas velocity (at distance from the base of the reactor)

Since there was no direct gas injection in the downcomer, the gas holdup in the downcomer was as a result of bubble entrainment by the circulating liquid. No bubbles were entrained by the circulating liquid at superficial gas velocity of 0.3 cm/s. An increase in the superficial gas velocity increased the circulation velocity of the liquid and for velocities of 1.0 cm/s and higher, some bubbles were entrained by the liquid circulating into the downcomer. An increase in superficial gas velocity increased the

circulation velocity, resulting in greater bubble entrainment and a consequent increase in the bubble passage frequency and gas holdup values. This can be seen in Figures 9 and 10. For an increase in superficial gas velocity from 1.0 cm/s to 2.8 cm/s, the increase in gas holdup was 500% at port 5 (100 cm), 740% at port 4 (76 cm), and 1300 % at port 3 (52 cm).

The bubble passage frequency in the downcomer was zero at superficial gas velocity of 0.3 cm/s and is therefore, not shown in Figure 4.6. At Ug = 0.3 cm/s, all the bubbles in the riser were disengaged in the separation zone at the top of the reactor, and no bubbles entered the downcomer along with the circulating liquid. A similar result was observed by Renegal et al., 2012 [19] for velocities up to 1.0 cm/s. This can be attributed to the fact that at U_g=0.3 cm/s, the liquid circulation velocity is not enough to entrain the bubbles while flowing down the downcomer. At a slightly higher superficial gas velocity of 1.0 cm/s, some bubbles could be seen entering the downcomer. The entrained bubbles could only be seen until halfway down the axis of the downcomer. At higher superficial gas velocities of 2.0 cm/s and 2.8 cm/s, through visual observation, smaller bubbles were seen traveling all the way to the bottom of the downcomer, and then entering the riser along with the recirculating liquid at the bottom. Also, the concentration of the bubbles could be seen to decrease axially in the downcomer. This is shown in Figure 4.7. In the downcomer, the optical fiber probe was not able to detect any bubbles below port 3 (z=52 cm from the bottom of the reactor). Therefore, the data shown in Figures 4.5, 4.6, and 4.7 is only for ports 3, 4, and 5 in the downcomer. As mentioned earlier, even though a very small number of bubbles could visually be seen entrained by the liquid circulating at the bottom of the downcomer at higher superficial gas velocities of 2.0 and 2.8 cm/s, due to

the number and size being very small, no bubbles were detected by the probe. Hence, no reliable data was gathered for ports 1, and 2 (lower than 52 cms from the base) in the downcomer.

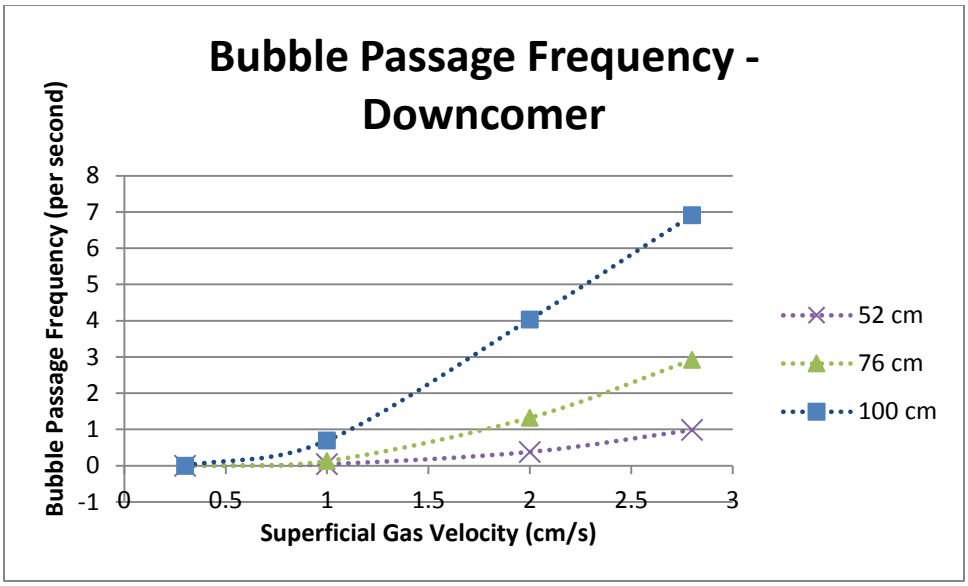

Figure 4.6: Variation of bubble passage frequency in the downcomer with superficial gas velocity

Figure 4.8 shows the axial decrease of gas holdup in the downcomer. The axial decrease in the gas holdup in the downcomer can be attributed to the fact that some bubbles are disengaged in the separation zone, and only a part of them are transported by the liquid circulating through the downcomer. Furthermore, due to buoyancy, the bubbles being transported down the downcomer have a tendency to flow upwards causing an axial decline in the number of bubbles or bubbles concentration (observed visually) in the downcomer. This explains the higher bubble passage frequency towards the top of the downcomer (Figure 4.7). For a given superficial gas velocity, an axial decline in the

bubble passage frequency results in the local gas holdup values decreasing axially in the downcomer. It is also noteworthy to mention that at the studied superficial gas velocities of 2.0 and 2.8 cm/s, a few small bubbles were seen reentering the riser at the bottom, but no bubbles were detected by the probe. Thus, the axial variation shown in Figure 4.8 is limited to ports 3, 4, and 5 in the downcomer.

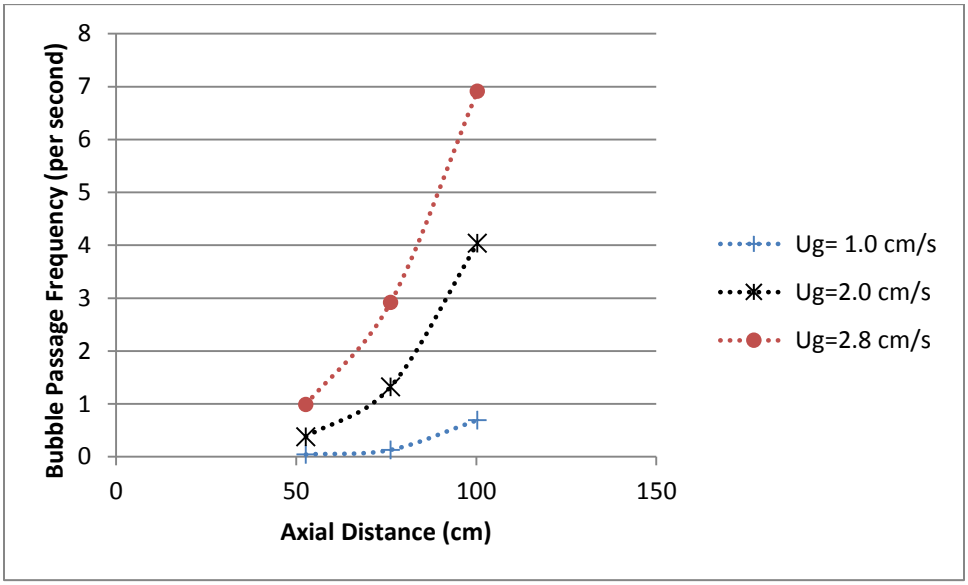

Figure 4.7: Axial variation of bubble passage frequency in the downcomer (shown at different superficial gas velocities)

The axial decrease of gas holdup was 88% at Ug= 1.0 cm/s, 80% at Ug=2.0 cm/s, and 74% at Ug=2.8 cm/s. At higher superficial gas velocities, the liquid circulation velocity increases increasing bubble entrainment by the circulating liquid. At Ug=1.0 cm/s, no bubbles were detected below port 3 in the downcomer. Through visual observation, some small bubbles were seen traveling down to the bottom of the

downcomer at Ug=2.0 cm/s, and Ug=2.8 cm/s, and the bubble density appeared to be higher at the higher superficial gas velocity. This explains higher values of gas holdup near the top of the downcomer. Thus, at a higher liquid circulation velocity, a higher fraction of the bubbles entering the downcomer travels a longer distance axially towards the bottom of the downcomer, and therefore, the percentage axial decrease at superficial gas velocity of 2.8 cm/s is higher than that at 1.0 cm/s.

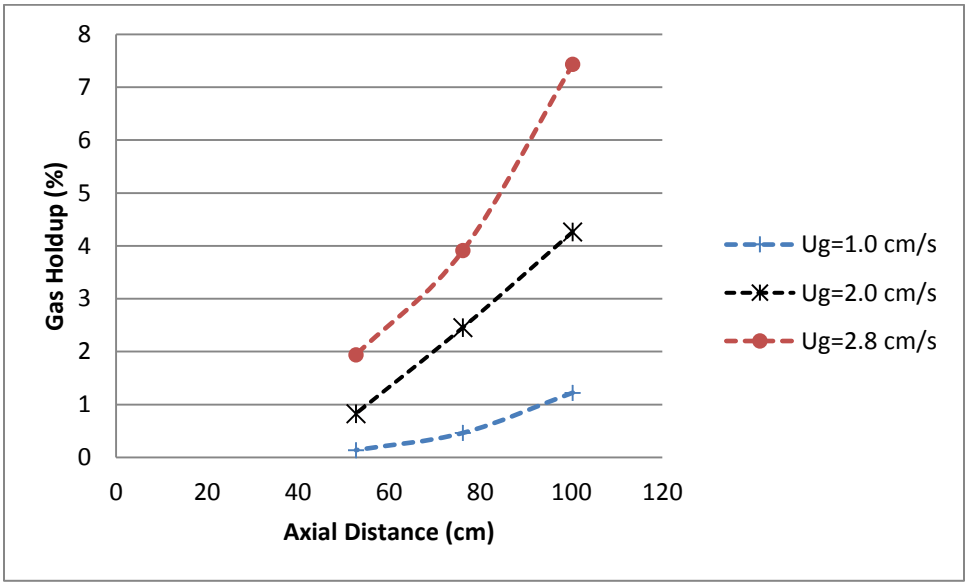

Figure 4.8: Axial variation of gas holdup in the downcomer (shown at different superficial gas velocities)

The correlations available for gas holdup in the downcomer are fewer in number. Some studies suggest a direct relation between the riser and the downcomer gas holdups [12], [39].

$$\epsilon_{gd} = \alpha \ \epsilon_{gr} \tag{7}$$

However, the above Equation 7 fails to account for the fact that the downcomer gas holdup increases with the riser gas holdup only after a certain value of gas holdup has been achieved in the riser and the superficial gas velocity is enough to produce a circulation velocity high enough to entrap and entrain the bubbles into the downcomer. Thus, Equation 7 was modified to Equation 8 ([39], [40] to accommodate this effect.

$$\in_{gd} = \alpha \ \in_{gr} - \beta \tag{8}$$

The value of α has been found to be between 0.8 and 0.9 for most of the cases studied in literature [19], [39]. Equations 7 and 8 for give the gas holdup in the downcomer based on the total volume of the downcomer, and thus, fail to account for the axial variation in the downcomer gas holdup. Figure 4.9 compares the experimental data with that obtained using the correlations given in Table 4.1. It should be noted here that the correlations are for the overall gas holdup in the downcomer while the experimental data presented is at different axial positions in the downcomer. Although the general trend depicted by the correlations is similar to that shown by the experimental data, there is no good agreement between them. Similar to the riser gas holdup correlations, the correlation for downcomer gas holdup given by Blazej et al., 2004 [15] highly over-predicts the gas holdup at the ports 3, 4, and 5 in the downcomer (Figure 4.9). The correlation given by Bello et al., 1985 [23] was only able to predict the gas holdup in the downcomer at gas velocities of 2.0 cm/s and 2.8 cm/s at port 3. Also, the correlations by Chisti et al., 1988 [38], and Bello et al., 1985 [23] gave some non-zero value of downcomer gas holdup even at Ug =0.3 cm/s, which is contrary to the phenomenon observed in this work. As mentioned earlier, no bubbles were entrained into the downcomer at 0.3 cm/s, and hence, the downcomer gas holdup is zero at U_g=0.3 cm/s, which was not depicted by these

correlations. Although, Blazej, 2004 [15] takes into account the zero-downcomer gas holdup condition at 0.3 cm/s, the gas holdup predicted at higher gas velocities is much higher than the experimental values at all the three ports. The different values of gas holdup in the downcomer predicted by the correlations is probably due to the different underlying assumptions, reactor sizes and configurations, gas-liquid systems, and operating conditions used in these studies. This, in addition to their inability to account for the axial variation in gas holdup in the downcomer, is a major drawback of using these correlations.

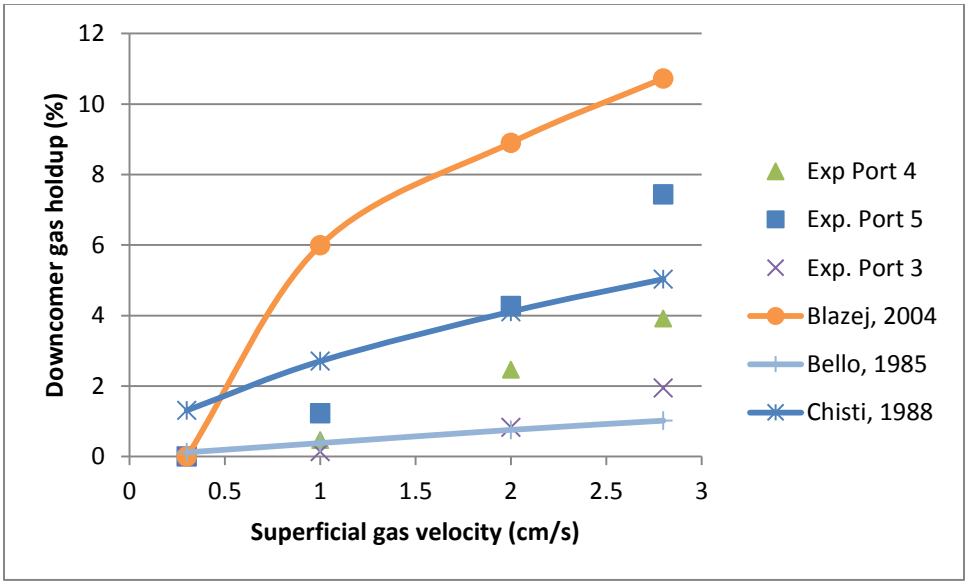

Figure 4.9: Comparison of experimental gas holdup in the downcomer with the correlations

4.1.2.1 Developed correlation. Equation 8 was modified to account for the axial variation in gas holdup, with α and β as functions of z/H_D, i.e. the ratio of the distance of

the downcomer port from the base of the reactor to the total downcomer height. The resulting equation was fitted to the experimental data to obtain the values of α and β.

$$\epsilon_{gd} = \left(1.1603 * \frac{z}{H}^2 + 0.0049 * \frac{z}{H}\right) \epsilon_{gr} - \left(0.87 * \frac{z}{H}^2 - 1.0695 * \frac{z}{H}\right) \quad (9)$$

Equation 9 was able to predict the downcomer gas holdup at ports 3, 4 and five within a deviation of 20%, and the data for port five is shown in Figure 4.10.

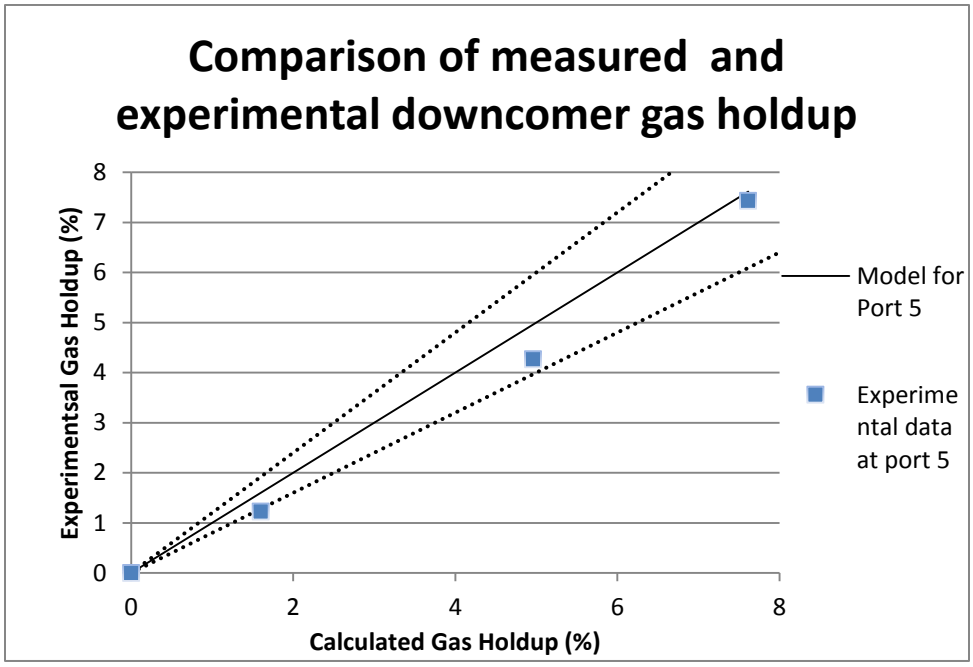

Figure 4.10: Comparison of experimental and calculated gas holdup in the downcomer

4.2 BUBBLE CHORD LENGTH

A bubble moving through liquid experiences a number of forces which collectively define the shape and size of the bubble. This phenomenon gets enhanced in the presence of a swarm of bubbles flowing through liquids, as is the case in airlift reactors. Also, as the dominant force acting on the bubble changes, so does its shape and

size [32]. Not many reliable techniques are available to measure the bubble size, due to which the Sauter mean diameter or the equivalent diameter is used in literature [41]. Thus, bubble size can also be studied through a bubble chord length distribution approach.

Bubble chord length is best represented as a log-normal distribution [32], [42]. A log-normal distribution of the bubble chord length considers a large number of small disintegrated bubbles along with a small number of large coalesced bubbles [32].

Figure 4.11 shows the bubble chord length distribution at the middle of the riser at different superficial gas velocities. As can be seen in the figure, bubble chord length follows log-normal distribution at all superficial gas velocities. With an increase in the superficial gas velocity, the chord length distribution got wider and more spread out. The mean and variance of the bubble chord length data in the riser are given in Table 4.2.

Table 4.2 Mean and Variance of bubble chord length distribution in the riser

Riser	Mean (cm)	Variance (cm^2)
U_g = 0.3 cm/s	0.460	0.015
U_g = 1.0 cm/s	0.569	0.028
U_g = 2.0 cm/s	0.640	0.062
U_g = 2.8 cm/s	0.667	0.076

With an increase in superficial gas velocity, the mean bubble size and the variance increase, lowering the peak and shifting the distribution to the right. This

indicates that the mean size of the bubbles is higher at higher superficial gas velocities, and also the range of bubble sizes is available is wider. This effect can be attributed to the increase in turbulence due to increase in superficial gas velocities, causing an increased bubble interaction.

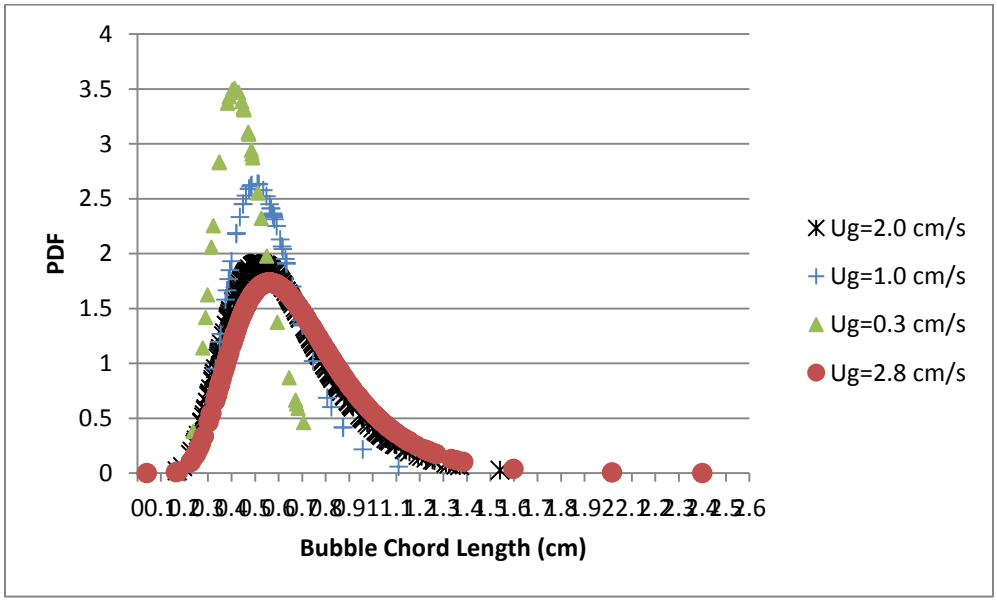

Figure 4.11: Bubble chord length distribution in riser

The bubble chord length distribution for port 5 of the downcomer at superficial gas velocities of 1.0, 2.0, 2.8 cm/s is shown in Figure 4.12. It was visually observed that the bubbles traveling down the axis of the downcomer got successively fewer in number and smaller in size. This was also depicted by the axial variation in bubble passage frequency in Figure 4.7. Due to this reason, sufficient data could not be gathered to depict chord length distribution towards the bottom of the downcomer.

Similar to the observations in the riser, the mean and the variance of the distribution in the downcomer increased with an increase in the superficial gas velocity. This was due to increased number of bubbles being entrained by the circulating liquid and the increased turbulence and bubble interaction.

Thus, in both the riser and the downcomer, an increase in the superficial gas velocity resulted in a higher mean bubble size and wider size distribution. Also, the bubble size was seen (visually) to decrease axially in the downcomer.

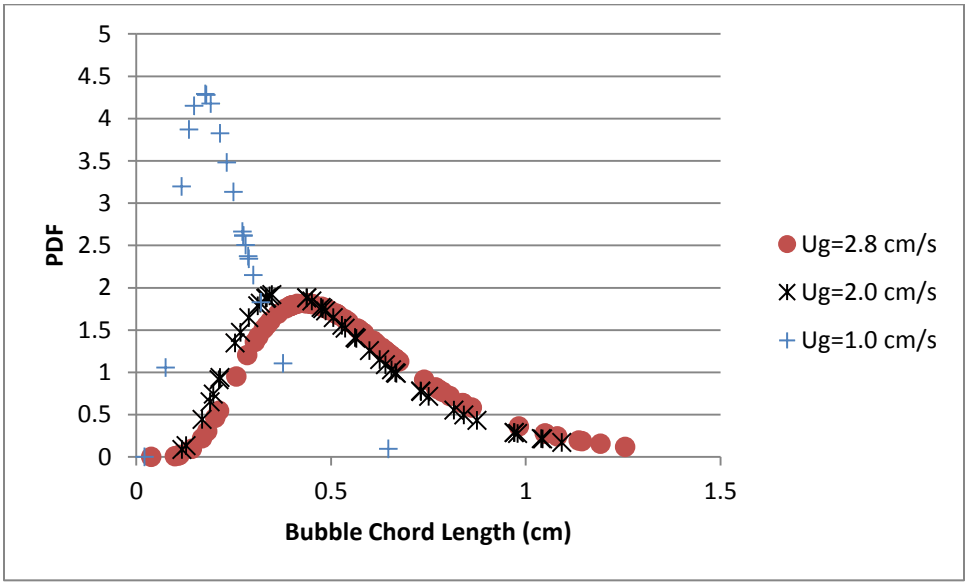

Figure 4.12: Bubble chord length distribution in the downcomer at Port 5 (z=100 cm from the base of the reactor)

4.3 BUBBLE VELOCITY

Bubble rise velocity affects the residence time of the gas bubbles and the gas holdup in the reactor. It is also related to the slip velocity which is used in calculating the lift and drag forces acting on the bubbles, making it critical for computational fluid

dynamics simulations [32]. A few correlations to calculate the bubble velocity are available in the literature [32], [43]. However, since these correlations are based on single bubble studies, they cannot be applied to airlift reactors where swarms of bubbles are present.

The probability distribution for the bubble rise velocity in the middle of the riser is shown in Figure 4.13. As can be seen from Figure 4.13 the mean bubble velocity increases with an increase in superficial gas velocity. For a superficial gas velocity increase from 0.3 to 1.0 cm/s, the mean bubble velocity increased by 51%. The mean and variance of the bubble rise velocity distributions are given in Table 4.3. With an increase in the superficial gas velocity from 0.3 to 2.8 cm/s, he variance of the distribution increased by 520%. This can be attributed to the fact that as the superficial gas velocity increases, the distribution of bubble rise velocity gets wider due to a decrease in the fraction of bubbles at higher bubble rise velocities.

Table 4.3: Mean and Variance of bubble rise velocity distribution in the riser

Superficial Gas Velocity	Mean (cm/s)	Variance $(cm/s)^2$
U_g = 0.3 cm/s	80.451	134.260
U_g = 1.0 cm/s	93.550	544.708
U_g = 2.0 cm/s	111.697	615.227
U_g = 2.8 cm/s	121.776	843.194

The bubble velocity reported in the downcomer is the downward bubble velocity as the optical fiber probe was positioned upwards to face the bubbles flowing downwards. Also, as mentioned earlier, since no bubbles were detected in the downcomer at superficial gas velocity of 0.3 cm/s, and the bubble frequency decreased axially on moving down the downcomer, sufficient data was not obtained to study the downward bubble velocity towards the bottom of the downcomer.

Figure 4.14 shows the downward bubble velocity distribution at port 5 (z=100 cm from the base pf the reactor) in the downcomer. An increase in the superficial gas velocity increases the liquid circulation velocity, along with the number of bubbles being entrained by the circulating liquid. This causes an increase in the interaction among the bubbles which further increases the mean downward bubble velocity. The mean downward bubble velocity increased by 42% as the superficial gas velocity increased from 1.0 to 2.8 cm/s. The variance of the bubble velocity distribution also increased with an increase in superficial gas velocity from 1.0 to 2.8 cm/s by 132%.

4.4 INTERFACIAL AREA

4.4.1 Interfacial Area in the Riser. The variation of interfacial area with superficial gas velocity is shown in figure 4.15. A trend similar to that for the gas holdup in the riser was observed. An increase in the superficial gas velocity in the riser increases the interfacial area. As was the case for gas holdup, the interfacial area in the riser was also measured at each of the five ports in the riser, and the values were not found to be statistically significantly different from each other. Thus, no axial variation of interfacial area was observed in the riser. Interfacial area increased by almost 800% as the

superficial gas velocity increased from 0.3 cm/s to 2.8 cm/s. The increase in interfacial area can be thought to be due to the increase in the bubble passage frequency with the superficial velocity, as shown in Figure 4.2 and explained in section 4.1.1. The rate of increase in interfacial area for a superficial gas velocity increase from 0.3 cm/s to 1.0 cm/s was lower than the rate for an increase in velocity from 1.0 cm/s to 2.8 cm/s. This is depicted by the slope of the curve in Figure 4.15. This phenomenon can also be attributed to the fact that at higher velocities (> 1.0 cm/s) the circulating liquid was able to entrain and carry bubbles into the downcomer, and a few bubbles were seen reentering the riser at the bottom, adding to the bubbles due to gas injection.

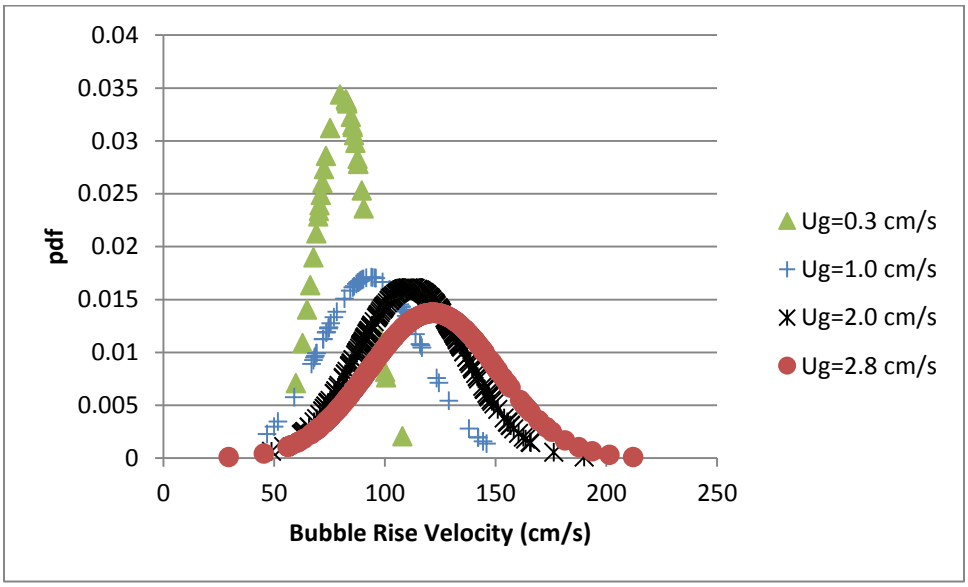

Figure 4.13: Bubble rise velocity distribution in the riser

A limited number of correlations to estimate the interfacial area in airlift reactors are available in the literature. One of the earliest correlations for gas holdup was

developed by Akita et al., in 1974 [44], for bubble columns. Interfacial area (a) has been proposed to depend on the mean bubble diameter (d_s) and gas holdup(ε) [16], [44], [45] as:

$$a = \frac{6\epsilon}{d_s(1-\epsilon)} \tag{10}$$

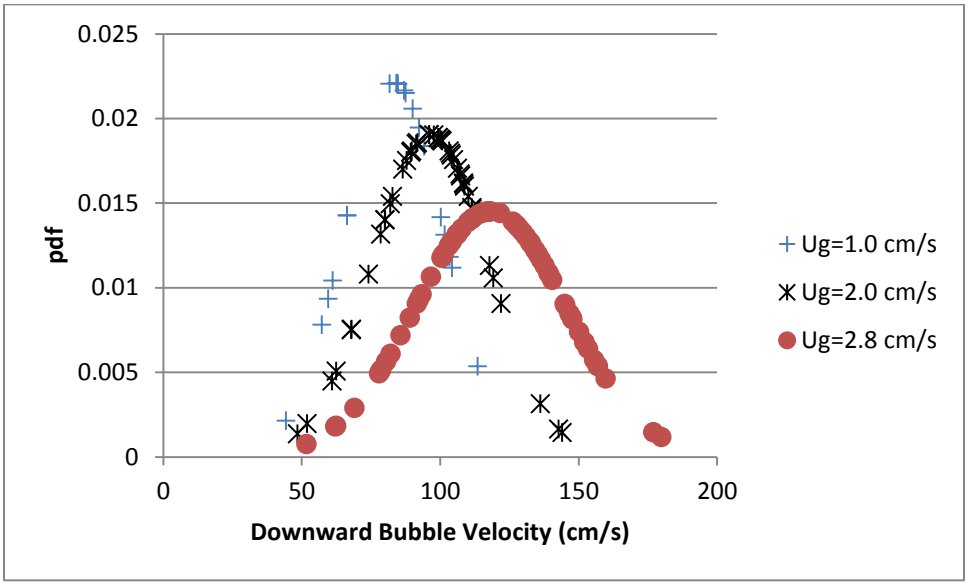

Figure 4.14: Downward bubble velocity distribution in downcomer

Since gas holdup varies between the riser and the downcomer sections, and also axially in the downcomer, Equation 10 can possibly be employed to obtain the interfacial area in the riser and the downcomer using the respective gas holdup values. A number of correlations are available to calculate d_s, however there is a lack of reliability and general consensus with regards to these methods. Also, in bubbly flow regimes, the assumption of bubbles being spherical holds true, and hence, the mean chord length from the chord length distribution (sections 4.2) can substitute the mean bubble diameter. Figure 4.16

shows a comparison of the experimental data with the correlation given by equation 10 for the riser interfacial area. Clearly, the correlation does not agree well with the experimental data.

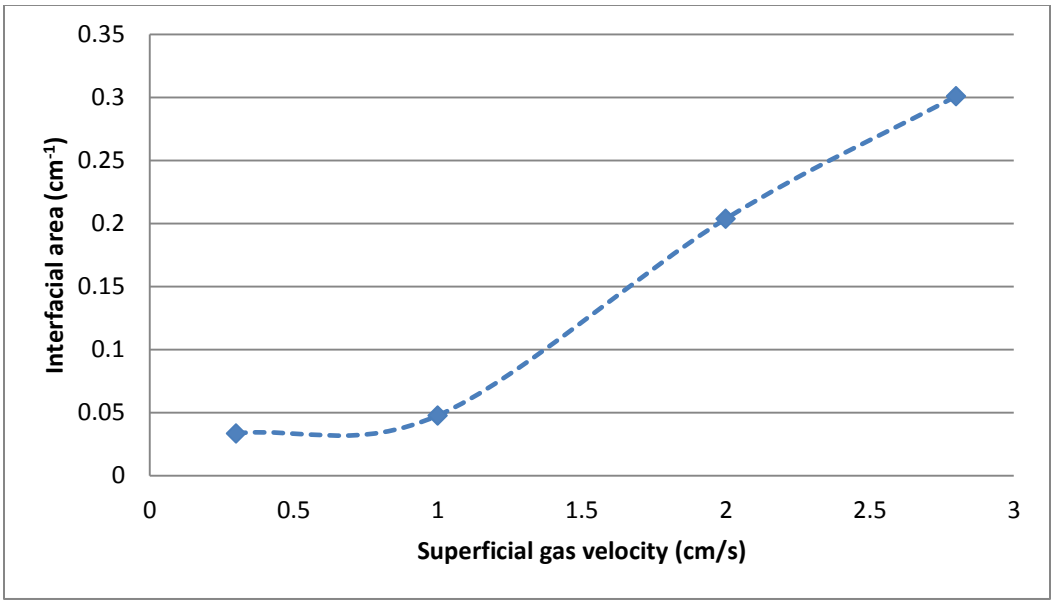

Figure 4.15 Variation of interfacial area in the riser with superficial gas velocity

The interfacial area at any location in the reactor is greatly affected by bubble breakup and coalescence, which further depends on many parameters such as density, viscosity, and surface tension of the fluids in contact, the column diameter, superficial gas velocity, sparger size and configuration, gas holdup and number of bubbles. Thus, a more in-depth and comprehensive study is required to obtain a correlation for interfacial area in airlift reactors in general, and in split airlift reactors in particular.

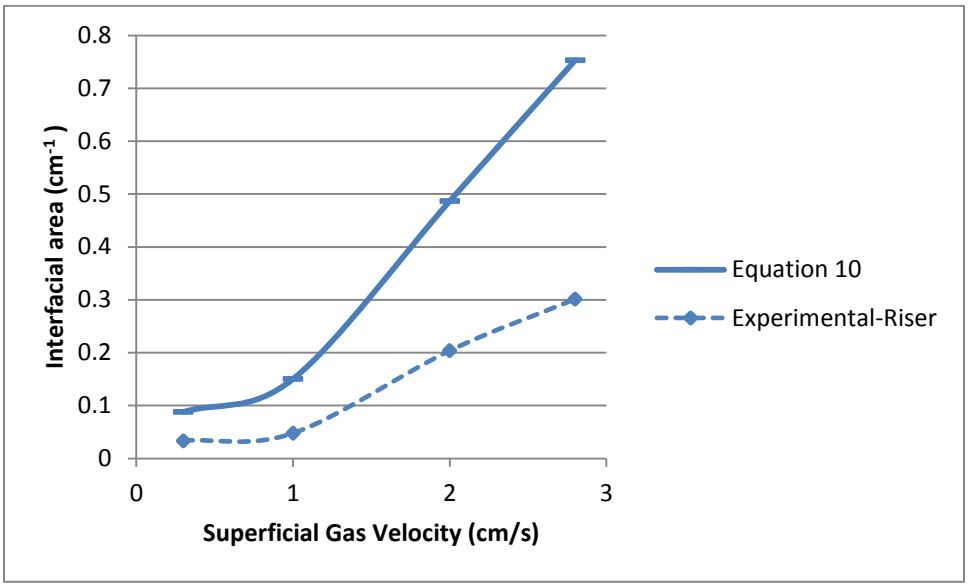

Figure 4.16: Comparison of experimental riser interfacial area with Equation 10

4.4.2 Interfacial Area in the Downcomer. Figure 4.17 depicts the variation of interfacial area in the downcomer with superficial gas velocity. Local values of interfacial area at each of the five ports in the downcomer were found to be statistically significantly different from each other. Similar to the gas holdup trend in the downcomer, the interfacial area increased with an increase in the superficial gas velocity. Increasing superficial gas velocity increased the liquid circulation velocity, which in turn increased the number of bubbles entrained by the circulating liquid.

As mentioned earlier, since the four-point optical probe was not able to detect any bubbles at the bottom two ports in the downcomer, the interfacial area values were available only up to the middle of the downcomer (ports 3, 4, and 5).

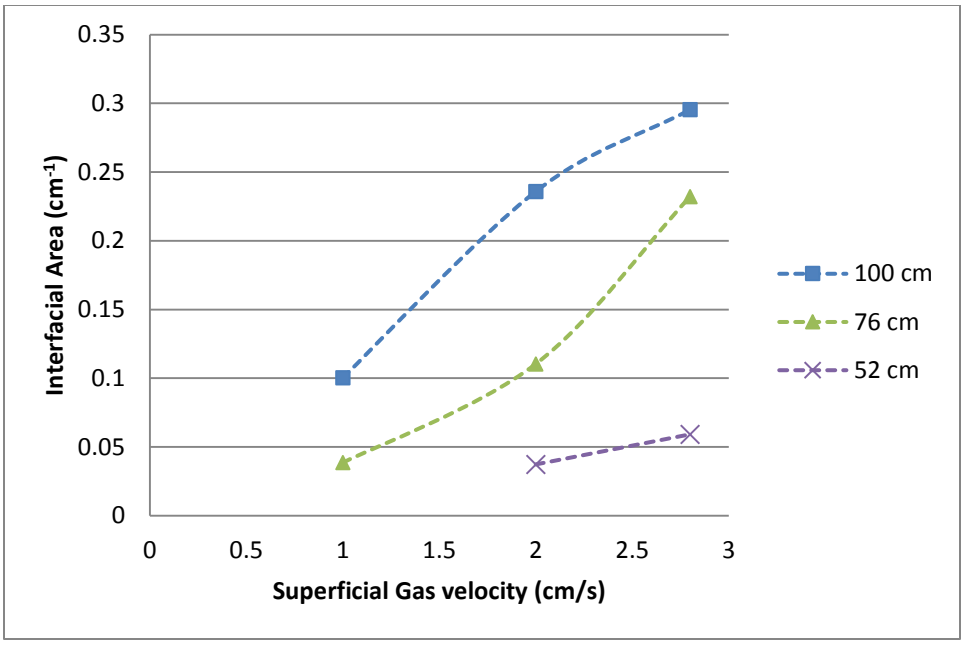

Figure 4.17: Variation of interfacial area in the downcomer with superficial gas velocity

Figure 4.18 shows the axial variation of interfacial area in the downcomer. At a given superficial gas velocity, the interfacial area can be seen to decrease on moving down along the axis of the downcomer. Even though at higher superficial gas velocities, the liquid circulation velocity can entrain bubbles, the buoyant force experienced by the bubbles causes them to move upwards in the riser. Hence, the number of bubbles decreased successively on moving axially downwards in the downcomer, resulting in an axial decline in the interfacial area in the downcomer. Interfacial area increased by 400% at port 5 for a superficial gas velocity increase from 1.0 cm/s to 2.8 cm/s. For port 4, the increase was 532%. At port 3, however, due to a very small number of bubbles being detected by the probe, no reliable interfacial area value was obtained at Ug of 1.0 cm/s. For a Ug increase from 2.0 cm/s to 2.8 cm/s, the interfacial area increased by 160% at port 3.

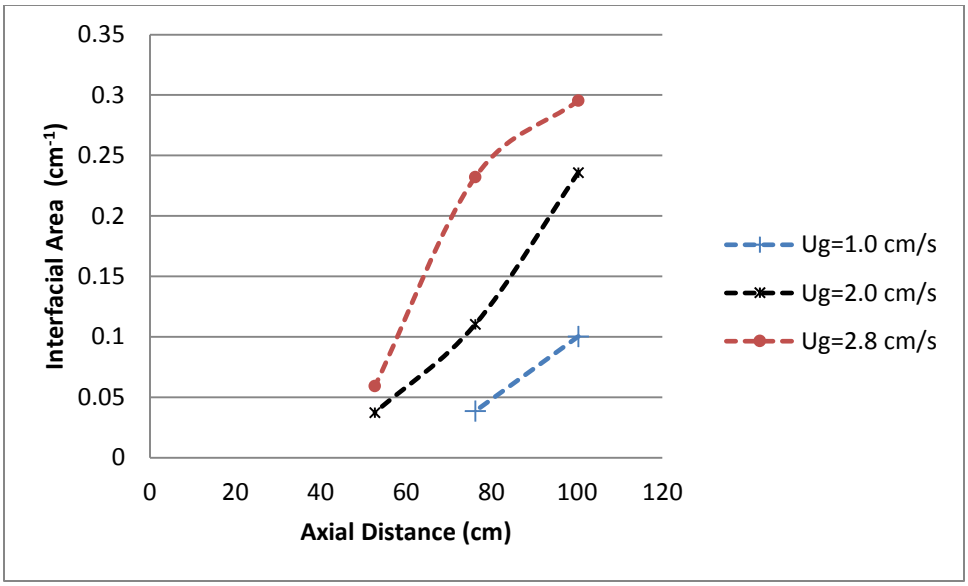

Figure 4.18: Axial variation of interfacial area in the downcomer (shown at different superficial gas velocities)

Equation 10 was also used with the corresponding downcomer gas holdup values to calculate the interfacial area in the downcomer. Figure 4.19 compares the experimental results with those obtained from Equation 10. Again, the correlation does not depict the experimental data well, emphasizing the need for local point measurements, especially in the downcomer of airlift reactors. Also, as stated for the riser, a more comprehensive and in-depth analysis and a wider range of experimental conditions is needed to develop a correlation of interfacial area.

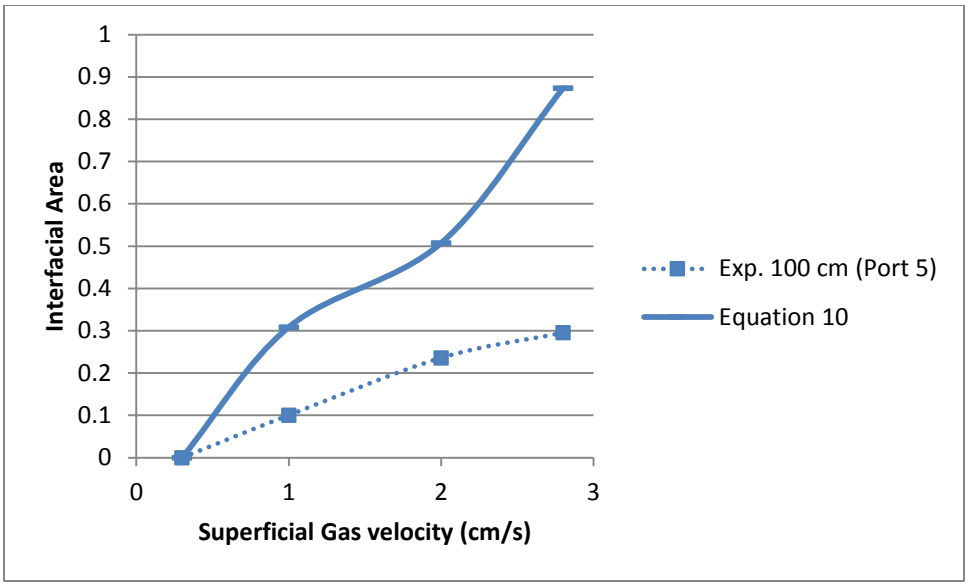

Figure 4.19: Comparison of experimental interfacial area in the downcomer with Equation 10

5. REMARKS

The gas holdup, specific interfacial area, bubble passage frequency, and chord length distribution were studied for the first time in a split airlift reactor for an air-water system at room temperature and pressure conditions. A sophisticated 4-point optical probe technique was successfully employed to study the axial variations in these parameters for change in superficial gas velocity between 0.3 cm/s and 2.8 cm/s. Both the gas holdup and specific interfacial area were found to increase with an increase in the superficial gas velocity in both the riser and the downcomer sections. While the properties remained the same axially throughout the riser section, a significant axial variation was observed in the downcomer for the studied conditions. This was believed to be due to the effect of buoyancy and the presence of a separation zone at the top of the column resulting in very little entrainment of bubbles by the circulating liquid in the downcomer, and hence, a decrease in the number of gas bubbles flowing axially down the downcomer.

New correlations were developed for the gas holdup in the riser and the downcomer sections, taking into account the axial variation in the downcomer. The experimental data was successfully represented by the developed correlations within a deviation of 15 % and 20% in the riser and downcomer sections, respectively. This axial variation in gas holdup and interfacial area in the downcomer shows that using overall parameters to depict the behavior of airlift reactors can be highly misleading, and emphasizes the need to carry out local measurements. Bubble chord length distribution and bubble velocity distribution were also studied in the riser and the downcomer

sections. The distribution of the bubble chord length and bubble velocity was found to be log-normal and normal, respectively. In both the cases the mean and the variance were found to increase with an increase in the superficial gas at the studied conditions.

REFERENCES

[1] C. U. Ugwu, H. Aoyagi, and H. Uchiyama, "Photobioreactors for mass cultivation of algae," *Bioresour. Technol.*, vol. 99, no. 10, pp. 4021–4028, 2008.

[2] A. Sanchez *et al.*, "Bubble-column and airlift photobioreactors for algal culture," *AIChE J.*, vol. 46, no. 9, pp. 1872–1887, 2000.

[3] B. Ketheesan and N. Nirmalakhandan, "Feasibility of microalgal cultivation in a pilot-scale airlift-driven raceway reactor," *Bioresour. Technol.*, vol. 108, pp. 196–202, 2012.

[4] M. Chisti, M.Y.; Moo-Young, "Airlift reactors: Characteristics, applications and design considerations," *Chem. Eng. Commun.*, vol. 60, no. 1–6, pp. 195–242, 1987.

[5] H. P. Luo and M. H. Al-Dahhan, "Airlift column photobioreactors for Porphyridium sp. culturing: Part I. effects of hydrodynamics and reactor geometry," *Biotechnol. Bioeng.*, vol. 109, no. 4, pp. 932–941, 2012.

[6] J. . Merchuk, M. Gluz, and I. Mukmenev, "Comparison of photobioreactors for cultivation of the red microalgaPorphyridium sp," *J. Chem. Technol. Biotechnol.*, vol. 75, no. 12, pp. 1119–1126, 2000.

[7] G. C. Zittelli, L. Rodolfi, and M. R. Tredici, "Mass cultivation of Nannochloropsissp. in annular reactors," *J. Appl. Phycol.*, vol. 15, no. 2, pp. 107–114, 2003.

[8] D. J. Pollard, A. P. Ison, P. A. Shamlou, and M. D. Lilly, "Reactor heterogeneity with Saccharopolyspora erythraea airlift fermentations," *Biotechnol. Bioeng.*, vol. 58, no. 5, pp. 453–463, 1998.

[9] A. S. Mirón, A. C. Gómez, F. G. Camacho, E. M. Grima, and Y. Chisti, "Comparative evaluation of compact photobioreactors for large-scale monoculture of microalgae," *Prog. Ind. Microbiol.*, vol. 35, no. C, pp. 249–270, 1999.

[10] S. J. Heijnen, A. Mulder, R. Weltevrede, P. H. Hols, and H. L. J. M. van Leeuwen, "Large-scale anaerobic/aerobic treatment of complex industrial wastewater using immobilized biomass in fluidized bed and air-lift suspension reactors," *Chem. Eng. Technol. - CET*, vol. 13, no. 1, pp. 202–208, 1990.

[11] M. S. (1973). . Chakravarty, M., Begum, S., Singh, H. D., Baruah, J. N., & Iyengar, "Gas holdup distribution in a gas-lift column," *Biotechnol. Bioeng. Symp.*, vol. 4, pp. 363–378, 1973.

[12] Y. Chisti, *Airlift Bioreactors*. Elsevier, New York, 1989.

[13] Y. Kawase, M. Tsujimura, and T. Yamaguchi, “Gas hold-up in external-loop airlift bioreactors,” vol. 12, pp. 21–27, 1995.

[14] T. Miyahara, M. Hamaguchi, Y. Sukeda, and T. Takahashl, “Size of bubbles and liquid circulation in a bubble column with a draught tube and sieve plate,” *Can. J. Chem. Eng.*, vol. 64, no. 5, pp. 718–725, Oct. 1986.

[15] M. Blažej, M. Kiša, and J. Markoš, “Scale influence on the hydrodynamics of an internal loop airlift reactor,” *Chem. Eng. Process. Process Intensif.*, vol. 43, no. 12, pp. 1519–1527, 2004.

[16] M. Bouaifi, M., Bastoul, D., Roustan, “A comparative study of gas hold-up, bubble size, interfacial area, and mass transfer coefficients in stirred gas-liquid reactors and bubble columns,” *Chem. Eng. Process. Process Intensif.*, vol. 40, no. 2, pp. 97–111, 2001.

[17] X. Lu, J. Ding, Y. Wang, and J. Shi, “Comparison of the hydrodynamics and mass transfer characteristics of a modified square airlift reactor with common airlift reactors,” *Chem. Eng. Sci.*, vol. 55, no. 12, pp. 2257–2263, 2000.

[18] R. Sardeing, P. Painmanakul, and G. Hébrard, “Effect of surfactants on liquid-side mass transfer coefficients in gas-liquid systems: A first step to modeling,” *Chem. Eng. Sci.*, vol. 61, no. 19, pp. 6249–6260, 2006.

[19] A. Rengel, A. Zoughaib, D. Dron, and D. Clodic, “Hydrodynamic study of an internal airlift reactor for microalgae culture,” *Appl. Microbiol. Biotechnol.*, vol. 93, no. 1, pp. 117–129, 2012.

[20] J. C. Merchuk, M. Ronen, S. Giris, and S. Arad, “Light/dark cycles in the growth of the red microalga Porphyridium sp.,” *Biotechnol. Bioeng.*, vol. 59, no. 6, pp. 705–713, 1998.

[21] J. C. Merchuk and Y. Stein, “Local hold-up and liquid velocity in air-lift reactors,” *AIChE J.*, vol. 27, no. 3, pp. 377–388, May 1981.

[22] C. Vial, E. Camarasa, S. Poncin, G. Wild, N. Midoux, and J. Bouillard, “Study of hydrodynamic behaviour in bubble columns and external loop airlift reactors through analysis of pressure fluctuations,” *Chem. Eng. Sci.*, vol. 55, no. 15, pp. 2957–2973, 2000.

[23] R. A. Bello, C. W. Robinson, and M. Moo-Young, “Gas holdup and overall volumetric oxygen transfer coefficient in airlift contactors.,” *Biotechnol. Bioeng.*, vol. 27, no. 3, pp. 369–81, Mar. 1985.

[24] B. J. C. Merchuk, “Airlift Bioreactors : Review of Recent Advances,” *Can. J. Chem. Eng.*, vol. 81, no. August, pp. 324–337, 2003.

[25] S. Zhang, K., Kurano, N., Miyachi, “Optimized aeration by carbon dioxide gas for microalgal production and mass transfer characterization in a vertical flat-plate photobioreactor,” *Bioprocess Biosyst. Eng.*, vol. 25, no. 2, pp. 97–101, 2002.

[26] L. Luo and J. Yuan, “Modeling of mass transfer in an internal loop airlift reactor,” *Chem. Eng. Technol.*, vol. 38, no. 3, pp. 511–520, 2015.

[27] T. Zhang, B. Zhao, and J. Wang, “Mathematical models for macro-scale mass transfer in airlift loop reactors,” *Chem. Eng. J.*, vol. 119, no. 1, pp. 19–26, 2006.

[28] H. P. Luo and M. H. Al-Dahhan, “Local gas holdup in a draft tube airlift bioreactor,” *Chem. Eng. Sci.*, vol. 65, no. 15, pp. 4503–4510, 2010.

[29] B. D. Fernandes, A. Mota, A. Ferreira, G. Dragone, J. A. Teixeira, and A. A. Vicente, “Characterization of split cylinder airlift photobioreactors for efficient microalgae cultivation,” *Chem. Eng. Sci.*, vol. 117, pp. 445–454, 2014.

[30] A. D. Z. Albdiri, A. Ojha, and M. Al-Dahhan, “Study of Local Gas Holdup and Specific Interfacial Area in a Split-Column Airlift Bioreactor Using Sphosticated 4-Point Optical Probe for Culturing Microlgae/Cyanobacteria,” *Chem. Eng. Commun.*, vol. 202, no. 7, pp. 892–898, 2014.

[31] R. F. Xue, J., Al Dahhan, M.H., Dudukovic, M.P., Mudde, “Bubble dynamics measurements using four-point optical probe,” *Can. J. Chem. Eng.*, vol. 81, pp. 375–381, 2003.

[32] A. A. Youssef, “Fluid dynamics and Scle-up of bubble columns with internals,” Washington University, Saint Louis, 2010.

[33] M. Kagumba and M. H. Al-dahhan, “Impact of Internals Size and Con fi guration on Bubble Dynamics in Bubble Columns for Alternative Clean Fuels Production,” 2015.

[34] A. Kataoka, I., Ishii, M., Serizawa, “Local Formulation and measurements of interfacial area concentration in two-phase flow,” *Int. J. Multiph. Flow*, vol. 12, pp. 505–529, 1986.

[35] W. A. Al-Masry, “Effect of liquid volume in the gas-separator on the hydrodynamics of airlift reactors,” *J. Chem. Technol. Biotechnol.*, vol. 74, no. 10, pp. 931–936, 1999.

[36] H. Gourich, B., Azher, N.E., Belhaj, S., Delmas, H., Ziyad, “Contribution to the study of hydrodynamics and gas-liquid mass transfer in a two- and three- phase split-rectangular airlift reactor,” *Chem. Eng. Process*, vol. 44, pp. 1047–1053, 2005.

[37] Y. Gumery, F., Ein-Mozaffari, F., Dahman, “Characteristics of local flow dynamics and macro-mixing in airlift column reactors for reliable design and scale-up,” *Int. J. Chem. React. Eng.*, vol. 7, no. 1, 2009.

[38] M. Chist, M.Y., Halard, B., Moo-Young, “Liquid circulation in airlift reactors,” *Chem. Eng. Sci.*, vol. 43, no. 3, pp. 451–457, 1988.

[39] A. Contreras, Y. Chisti, and E. Molina Grima, "A reassesment of relationship between riser and downcomer gas holdups in airlift reactors," *Chem. Eng. Sci.*, vol. 53, no. 24, pp. 4151–4154, 1998.

[40] F. U. Wenge, Y. Chisti, And M. Moo-Young, "Split-Cylinder Airlift Reactors: Hydraulics And Hydrodynamics Of A New Mode Of Operation," *Chem. Eng. Commun.*, Vol. 155, No. 1, Pp. 19–44, 1996.

[41] W. D. Deckwer, *Bubble column reactors*. Wiley and Sons, New York, 1992.

[42] A. Pohorecki, R.; Moniuk, W.; Bielski, P., Zdrojkowski, "Modeling of coalescence-redispersion in bubble columns," *Chem. Eng. Sci.*, vol. 56, no. 21, pp. 6157–6164, 2001.

[43] C. Wu, "Heat Transfer and Bubble Dynamics in slurry bubble columns for Fischer-Tropsch clean alternative energy," Washington University in Saint Louis, 2007.

[44] K. Akita and F. Yoshida, "Bubble Size, Interfacial Area, and Liquid-Phase Mass Transfer Coefficient in Bubble Columns," *Ind. Eng. Chem., Process Des. Dev.*, vol. 13, pp. 84–90, 1974.

[45] P. Wongsuchoto, P., Pavasant, "Internal liquid circulation in annulus sparged internal loop airlift contractors," *Chem. Eng. J.*, vol. 100, pp. 1–9, 2004.

PAPER

II. A NEW APPROACH FOR EVALUATING THE LOCAL VOLUMETRIC MASS TRANSFER COEFFICIENT IN A SPLIT AIRLIFT REACTOR

ABSTRACT

In this study, a new approach to estimate the local volumetric mass transfer coefficients was developed in a split airlift photobioreactor using the plug flow modeling approach. It was applied to both the gas and liquid phases in the riser and downcomer sections, taking into account local gas holdup and interfacial area variation. An assumption of a constant liquid-side mass transfer coefficient was made, and a numerical solution was developed to fit the model to the oxygen concentration data to estimate the liquid-side mass transfer coefficient. The approach was applied to an air-water system at superficial gas velocities of 1.0 to 2.8 cm/s, and the liquid-side mass transfer coefficient was found to increase from 0.11 m/s to 0.37 m/s. A parametric analysis showed the liquid-side mass transfer coefficient to be insensitive to changes in the downcomer superficial gas velocity, and thus, the mass transfer process was believed to be dominated by the local gas holdup and interfacial area. This observation emphasizes the need for local measurements and correlations of gas holdup and interfacial area, and also validates the need and application of the presented mass transfer model. The availability of the local interfacial area data also allowed the estimation of local volumetric mass transfer coefficient. The local volumetric mass transfer coefficient was found to be constant axially in the riser, and was higher than that in the downcomer. The local volumetric mass transfer coefficient in the downcomer decreased on moving axially downwards. The

fitted volumetric mass transfer coefficient was usually found to be a magnitude higher, and out of range of the overall volumetric mass transfer coefficients estimated from the correlations available in literature.

Keywords: Mass Transfer, Airlift Reactors, Local Mass Transfer Coefficient

1. INTRODUCTION

Airlift photobioreactors are widely used in biochemical processes, besides their application in chemical and other industries. Their advantageous characteristics like simple construction, pneumatic operation, low shear stress, and efficient heat and mass transfer capabilities [1] make them a better choice for multiphase bioprocess operations than conventional reactors [2], [3].

Hydrodynamics and interphase mass transfer studies are critical to the design and scale-up of airlift bioreactors in general. Airlift bioreactors are generally known to have high mass transfer rates and have been studied well in literature. [4]–[6]] have studied the volumetric mass transfer coefficient under different experimental conditions. Some other studies have focused on studying the mass transfer process in various solute concentration solutions [7]. These studies have modeled airlift bioreactors as continuously stirred tank reactors to estimate volumetric mass transfer coefficients ($k_l a$, s^{-1}). However, due to a lack of verification of the modeling representation other models such as axial dispersion models and tanks in series models have been applied to estimate mass transfer coefficient in airlift reactors [8]–[11]. These models consist of a set of partial differential equations or ordinary differential equations coupled with various boundary and initial conditions to be solved to estimate mass transfer coefficients. Zhang et al., 2006 [12], experimentally verified the application of plug flow model to airlift reactors. They first applied the axial dispersion model to an external loop airlift reactor, and then compared the results with the simplified plug flow model, and did not observe any significant difference between the two approaches. In their study, they came up with

a rather complex analytical solution to solve the partial differential equations for the plug flow modeling approach to calculate the overall volumetric mass transfer coefficients. They then used the experimentally measured oxygen concentration data to fit the complex analytical solution to extract the overall mass transfer coefficient. Luo and Yuan, 2015 [13], estimated the mass transfer coefficients in a draft tube airlift reactor by considering both the liquid and gas phases to be axially dispersed using an axial dispersion model. They fitted for the overall volumetric mass transfer coefficient for the entire reactor. Even though they accounted for the riser and downcomer sections separately in their model, they used parameters such as overall gas holdup to estimate the overall mass transfer coefficient, and hence did not account for any variation of these parameters in the reactor while numerically solving the differential equations. Luo et al., 2008 [14], and Cheng-Shing, 2003 [15], suggested that local measurements give a better understanding of the actual process than relying on overall parameters. Pallapothu et. al, 2012 [16] have also suggested that to thoroughly study the mass transfer process it is important to separate k_l (cm/s) and a (cm^{-1}). All the methods to estimate the volumetric mass transfer coefficient ($k_l a$, s^{-1}) through processing the experimental data using analytical or numerical analysis have focused on treating $k_l a$ (s^{-1}) as a global parameter representing the whole reactor with an inherent assumption that its value stays constant throughout the reactor which may not always be the case, especially in airlift reactors. This is mainly due to the lack of availability of proper measurement techniques to measure local properties such as gas holdup, interfacial area, and other bubble dynamic properties which have been overcome in Paper I.

The overall volumetric mass transfer coefficient accounts for both the liquid and the gas side resistances to mass transfer. However, for the measurement technique that relies on the absorption of oxygen (and other sparingly soluble gases) in water, the gas side resistance across the gas-liquid interface can be considered to be negligible when compared to the resistance posed by the liquid side, and hence, mass transfer can be thought to be dominated primarily by the liquid side [3]. Thus the overall volumetric mass transfer coefficient can be represented by $k_l a$ (s^{-1}), which is the product of the liquid-side mass transfer coefficient, k_l (cm/s), and the gas-liquid interfacial area, a (cm^{-1}). Furthermore, according to film theory, the liquid side mass transfer coefficient, k_l (cm/s), is the diffusivity, *D*, of the gas in the liquid divided by the fictitious transport film thickness between the gas-liquid interface and the bulk liquid, δ. Now as the interfacial area, *a*, decreases on moving down the downcomer due to a decrease in the number and size of the bubbles descending axially down the downcomer [Paper I], the assumption of a constant value of $k_l a$ (s^{-1}) then implies that the liquid-side mass transfer coefficient, k_l(cm/s), would increase axially downwards. This further implies that the fictitious film thickness, δ, decreases on moving down the axis of the downcomer. This contradicts the fact that the gas-liquid interaction decreases axially downwards in the downcomer due to reduced number and size of bubbles and gas-liquid interaction which must cause negligible, if any, change in δ. Hence, the assumption of a constant liquid-side mass transfer coefficient, k_l (cm/s), stemming from the more appropriate assumption of a constant film thickness, δ, could be a better approach towards evaluating and understanding the local volumetric mass transfer coefficient and its variation across airlift reactors in general, and bioreactors in particular.

In Paper I, the use of a four-point optical fiber probe technique allowed for the measurement of local gas holdup and interfacial area along the axis of the riser and downcomer sections, besides bubble frequency, velocity, and chord length. This availability of local measurements at various axial locations in the riser and downcomer of airlift reactors further allows for correctly modeling the mass transfer process with a varying volumetric mass transfer coefficient. Also, the split airlift bioreactor used in Paper I, has been shown to outperform bubble column and draft tube airlift reactor for microalgae culturing [17]. Thus, due to the availability of local measurements in the split airlift reactor in Paper I, and its ability to outperform other airlift bioreactors and bubble columns [17] it was chosen as the bioreactor for this study (Figure 3.1). Accordingly, in this study, a constant liquid-side mass transfer coefficient, k_l (cm/s), is assumed and is used together with the local interfacial area, a (cm^{-1}), to estimate the local volumetric mass transfer coefficient, $k_l a$ (s^{-1}). The liquid and gas phases are modeled as plug flow, and the axial variation in the gas holdup and the interfacial area is also accounted for to estimate the local volumetric mass transfer coefficient in the studied split airlift reactor. The results of varying $k_l a$ are then compared to the results obtained if the $k_l a$ is assumed to be constant using the conventional method used in literature of fitting the numerical data to the plug flow model with a constant overall volumetric mass transfer coefficient ($k_l a$) throughout the reactor.

2. MASS TRANSFER MODEL

An internal loop airlift reactor (draft tube or split airlift) can be broadly divided into four parts: the mixing section at the bottom, the riser, the separation zone at the top, and the downcomer. This is schematically shown in Figure 2.1. For the purpose of modeling, the separation zone at the top and the mixing section at the bottom were considered to act as extensions or continuation in length of the riser and the downcomer sections, respectively (Figure 2.1). The liquid and gas phases in the riser and downcomer were modeled as plug flow based on the following assumptions: (i) There was no axial dispersion in the reactor; (ii) The reactor operates isothermally; (iii) Velocity and density of the fluids were the same radially. These assumptions are similar to the ones found in other studies [13], [17]. In addition to these assumptions, in literature even the gas holdup and interfacial area are considered to be constant throughout the reactor [12], [13] mainly due to the difficulty in carrying out local measurements. According to Luo et al., 2014, this assumption may, however, be incorrect and inapplicable to real industrial reactors. In Paper I, gas holdup and interfacial area measured at the radial center in a split airlift reactor were found to be constant axially throughout the length of the riser but varied significantly axially along the downcomer.

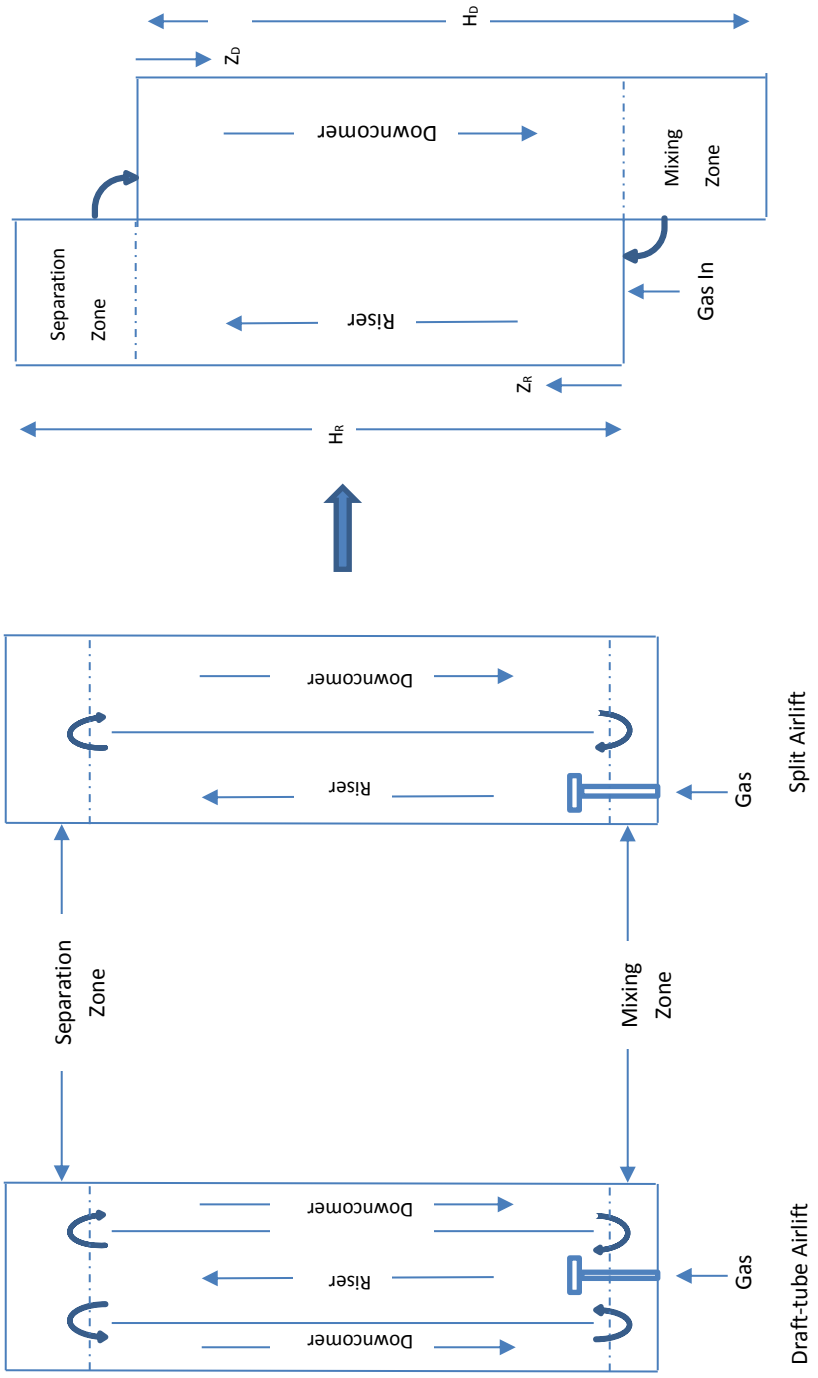

Figure 2.1: Schematic representation of the internal-loop airlift reactors and the modeling scheme used in this study

The general plug flow model for a two-phase system is given in Equations (1) and (2) (for the gas and liquid phases, respectively). Equations (1) and (2) have been derived from the general mass balance equation for a general transported gas without axial dispersion. They consist of the change of concentration balanced by the advection and the source terms combined. As mentioned earlier, the gas side resistance can be considered to be negligible when compared to the resistance posed by the liquid side, and hence, mass transfer can be thought to be controlled by the liquid side [3].

$$\frac{\partial C_{gj}}{\partial t} = -\frac{1}{\epsilon_j}\frac{\partial U_{gj} C_{gj}}{\partial z} - \frac{1}{\epsilon_j} k_l a \left(\frac{C_g^*}{H} - C_{lj}\right) \quad (1)$$

$$\frac{\partial C_{lj}}{\partial t} = -\frac{1}{1-\epsilon_j}\frac{\partial U_{lj} C_{lj}}{\partial z} + \frac{1}{1-\epsilon_j} k_l a \left(\frac{C_g^*}{H} - C_{lj}\right) \quad (2)$$

The subscript j can be set equal to r for the riser section and equal to d for the downcomer section to denote the gas and liquid phases in them. C_g and C_l denote the concentration of the transported gas in the gas and the liquid phases, respectively; C_L^* is the dissolved saturation concentration of the gas; U_{lj} and U_{gj} denote the liquid circulation and the superficial gas velocities based on the cross-sectional area of section j, respectively; ϵ is the gas holdup in section j; H is the Henry's law constant; and $k_l a$ (s^{-1}) is the volumetric mass transfer coefficient.

The advection term in Equations (1) and (2) consists of the overall superficial gas and liquid circulation velocities, $U_{g,overall}$ and U_l and the transported gas concentrations in the gas and liquid phases, C_g and C_l, respectively, and can further be expanded to give Equations (3) and (4).

$$\frac{\partial C_{gj}}{\partial t} = -\frac{U_{gj}}{\epsilon_j}\frac{\partial C_{gj}}{\partial z} - \frac{C_{gj}}{\epsilon_j}\frac{\partial U_{gj}}{\partial z} - \frac{1}{\epsilon_j} k_l a \left(\frac{C_g^*}{H} - C_{lj}\right) \quad (3)$$

$$\frac{\partial C_{lj}}{\partial t} = -\frac{U_{lj}}{1-\epsilon_j}\frac{\partial C_{lj}}{\partial z} - \frac{C_{lj}}{1-\epsilon_j}\frac{\partial U_{lj}}{\partial z} + \frac{1}{1-\epsilon_j} k_l a \left(\frac{C_g^*}{H} - C_{lj}\right) \quad (4)$$

Thus, the plug flow model for the gas and the liquid phases in the extended riser section (riser and the separation zone) and the extended downcomer section (downcomer and the bottom mixing zone) based on Equations (3) and (4) are as described below.

$$\frac{\partial C_{gr}}{\partial t} = -\frac{U_{gr,overall}}{\epsilon_r}\frac{\partial C_{gr}}{\partial z} - \frac{C_{gr}}{\epsilon_r}\frac{\partial U_{gr,overall}}{\partial z} - \frac{1}{\epsilon_r} k_l a \left(\frac{C_g^*}{H} - C_{lr)}\right) \quad (5)$$

$$\frac{\partial C_{lr}}{\partial t} = -\frac{U_{lr}}{1-\epsilon_r}\frac{\partial C_{lr}}{\partial z} - \frac{C_{lr}}{1-\epsilon_r}\frac{\partial U_{lr}}{\partial z} + \frac{1}{1-\epsilon_r} k_l a \left(\frac{C_g^*}{H} - C_{lr)}\right) \quad (6)$$

$$\frac{\partial C_{gd}}{\partial t} = \frac{U_{gd}}{\epsilon_d}\frac{\partial C_{gd}}{\partial z} + \frac{C_{gd}}{\epsilon_d}\frac{\partial U_{gd}}{\partial z} - \frac{1}{\epsilon_d} k_l a \left(\frac{C_g^*}{H} - C_{ld}\right) \quad (7)$$

$$\frac{\partial C_{ld}}{\partial t} = \frac{U_{ld}}{1-\epsilon_d}\frac{\partial C_{ld}}{\partial z} + \frac{C_{ld}}{1-\epsilon_d}\frac{\partial U_{ld}}{\partial z} + k_l a \left(\frac{C_g^*}{H} - C_{ld}\right) \quad (8)$$

Equations (5)-(8) completely define the gas and liquid phases in the riser and the downcomer sections accounting for the variations in the liquid and gas phase concentrations, gas holdup, interfacial area, and superficial gas and liquid circulation velocities. In the riser, the gas velocity available for advection is the overall superficial gas velocity in the riser, $U_{gr,overall}$, which consists of the superficial gas velocity due to gas injection in the riser, U_{gr}, and that due to circulation from the downcomer. More details on the overall superficial gas velocity are given in section 4.3.

Since the liquid circulation velocities in both the riser and the downcomer sections (U_{lr} and U_{ld}) do not change with respect to the axial direction, *z*, the derivative in the second term in Equations (6) and (8) can be set to zero. The method to measure them is given in the next section.

In the literature, the superficial gas velocity in the riser is commonly estimated on the drift flux model given in Equation 31 [13] . The drift flux model is based on the gas holdup in the riser, which was measured at the radial center, and was found to be constant axially in the riser at the studied conditions. Then, based on Equation 31, the overall

superficial gas velocity in the riser, $U_{gr,overall}$, is considered to be constant axially, making its derivative in the second term in Equation (5) zero. It must be noted that the drift flux model was used to calculate $U_{gr,overall}$ because the local bubble velocity, U_b, and gas holdup, $\in$, were measured at the radial center at different axial locations in the riser [Paper I]. However, to understand the actual variation of $U_{gr,overall}$ in the riser, U_b, and $\in$ can be measured radially to obtain a radial average of $U_{gr,overall}$ at the axial locations.

Again, since the local gas holdup and bubble velocity in the downcomer were measured at the radial center in the downcomer [Paper I], the steady state continuity equation based on the balance of gas between the riser and the downcomer was used to estimate U_{gd}. This U_{gd} is based on the total volume of gas in the downcomer and its cross-sectional area, and was thus assumed to be constant. However, in reality, the local number of bubbles, bubble velocity and gas holdup in the downcomer was seen to vary axially [Paper I], giving rise to an axial variation in U_{gd}. Hence, the derivative of the superficial gas velocity in the downcomer U_{gd}, with the axial location z is non-zero. However, due to complexity of solving for the $\frac{C_{gd}}{\in_d}\frac{\partial U_{gd}}{\partial z}$ term, or accounting for it while fitting the numerical concentration data to obtain the mass transfer coefficient, and the lack of radially averaged local bubble velocity, and gas holdup at the different axial locations in the downcomer to account for the axial variation, U_{gd} was assumed to be based on the total gas volume entering the downcomer, and constant axially. Hence, Equation (7) was simplified by setting its derivative with respect to axial distance, z, and equal to zero. However, a parametric analysis of U_{gd} was also performed to study its effect on the fitted k_l (cm/s), and it was found to be negligible. Details of this analysis are given in section 5.4.

Following the above observations and assumptions, the plug flow model without axial dispersion for an internal loop airlift reactor was then reduced to Equations (9)-(12).

$$\frac{\partial C_{gr}}{\partial t} = -\frac{U_{gr}overall}{\epsilon_r}\frac{\partial C_{gr}}{\partial z} - \frac{1}{\epsilon_r} k_l a \left(\frac{C_g^*}{H} - C_{lr}\right) \quad (9)$$

$$\frac{\partial C_{lr}}{\partial t} = -\frac{U_{lr}}{1-\epsilon_r}\frac{\partial C_{lr}}{\partial z} + \frac{1}{1-\epsilon_r} k_l a \left(\frac{C_g^*}{H} - C_{lr}\right) \quad (10)$$

$$\frac{\partial C_{gd}}{\partial t} = \frac{U_{gd}}{\epsilon_d}\frac{\partial C_{gd}}{\partial z} - \frac{1}{\epsilon_d} k_l a \left(\frac{C_g^*}{H} - C_{ld}\right) \quad (11)$$

$$\frac{\partial C_{ld}}{\partial t} = \frac{U_{ld}}{1-\epsilon_d}\frac{\partial C_{ld}}{\partial z} + k_l a\left(\frac{C_g^*}{H} - C_{ld}\right) \quad (12)$$

Also, as shown in Paper I, the downcomer bubble dynamics is strongly influenced by that in the riser. Therefore, the four Equations ((9)-(12)) must be solved simultaneously, constrained by the boundary and initial conditions given by Equations (13), (14), and (14). Equation (13) is the initial condition that states that initially, at time *t=0*, transported gas concentration in the gas phase and the dissolved gas concentration is zero in both the riser and the downcomer. Also, at the bottom of the reactor, for *z=0*, the liquid from the downcomer enters the riser, and hence, the dissolved transported gas concentration in the riser and downcomer is the same at this location (Equation (14)). The sparger is located at the bottom of the riser (z=0), and hence the inlet gas phase concentration is zero (Equation (14)). Equation (15) gives the homogeneous Neumann boundary condition at z=h.

Initial Condition (t=0):

$C_{lr}(z,0)=C_{ld}(z,0)=0, \qquad C_{gr}(z,0)=C_{gd}(z,0)=0$ (13)

Boundary Conditions:

At z=0:

$C_{lr}(0, t) = C_{ld}(0,t), \qquad C_g(0,t)=C_g^*$ (14)

At z=h:

$$\frac{\partial C_{lr}}{\partial z} = \frac{\partial C_{gr}}{\partial z} = \frac{\partial C_{ld}}{\partial z} = \frac{\partial C_{gd}}{\partial z} = 0 \quad (15)$$

The mass transfer model given by the partial differential Equations (9) through (12) cannot be solved analytically due to the variation in the local gas holdup and interfacial area [Paper I], and is hence solved numerically. The equations are solved by discretizing the equations in space and time domains with $z=i\Delta z$ (i=0, 1, 2….M), and $t=n\Delta t$ (n=0, 1, 2,…N). An upwind difference scheme is applied to the time derivative, and a central difference scheme is applied to the space derivative terms. The discretized equations are as follows:

$$\frac{C_{gri}^{n+1}-C_{gri}^{n}}{\Delta t} = -\frac{U_{gr,overall}}{\epsilon_{ri}} \frac{C_{gri+1}^{n}-C_{gri-1}^{n}}{2\Delta z} - \frac{1}{\epsilon_{ri}} k_l a_i \left(\frac{C_{gri}^{n}}{H} - C_{lri}^{n}\right) \quad (16)$$

$$\frac{C_{lri}^{n+1}-C_{lri}^{n}}{\Delta t} = -\frac{U_{lr}}{1-\epsilon_{ri}} \frac{C_{lri+1}^{n}-C_{lri-1}^{n}}{2\Delta z} + \frac{1}{1-\epsilon_{ri}} k_l a_i \left(\frac{C_{gri}^{n}}{H} - C_{lri}^{n}\right) \quad (17)$$

$$\frac{C_{gdi}^{n+1}-C_{gdi}^{n}}{\Delta t} = \frac{U_{gd}}{\epsilon_{di}} \frac{C_{gdi+1}^{n}-C_{gdi-1}^{n}}{2\Delta z} - \frac{1}{\epsilon_{di}} k_l a_i \left(\frac{C_{gdi}^{n}}{H} - C_{ldi}^{n}\right) \quad (18)$$

$$\frac{C_{ldi}^{n+1}-C_{ldi}^{n}}{\Delta t} = \frac{U_{ld}}{1-\epsilon_{di}} \frac{C_{ldi+1}^{n}-C_{ldi-1}^{n}}{2\Delta z} + \frac{1}{1-\epsilon_{di}} k_l a_i \left(\frac{C_{gdi}^{n}}{H} - C_{ldi}^{n}\right) \quad (19)$$

The boundary and initial conditions are also discretized on the *t*-*z* plane as given in Equations (20), (21), and (22).

Initial Condition (t=0) :

$C_{lri}(0)=C_{ldi}(0)=0$, $C_{gri}(0)=C_{gdi}(0)=0$ (20)

Boundary Conditions:

At z=0:

$C_{lr0}(t) = C_{ld\,0}(t)$, $C_{gr0}(t)=C_g^*$ (21)

At z=MΔz:

$$\frac{C_{lrM+1}-C_{lrM-1}}{2\Delta z}=\frac{C_{grM+1}-C_{grM-1}}{2\Delta z}=\frac{C_{ldM+1}-C_{ldM-1}}{2\Delta z}=\frac{C_{gdM+1}-C_{gdM-1}}{2\Delta z}=0 \qquad (22)$$

Equations (16)-(19) can be rewritten for each point in the space domain and solved simultaneously. Experimental data can be gathered for all variables and parameters except k_l(cm/s), which is assumed to be constant and is explained in the next section. With the assumption of a constant k_l (cm/s), and also since it is the only unknown, experimental concentration data can be fitted to the above model equations to estimate k_l(cm/s). The parameters used for solving the above equations are explained in the next section.

For 1<i<M-1 (Riser Section)

$$\begin{aligned} A_{gri}C_{gri-1}^{n+1}+C_{gri}^{n+1}-A_{gri}C_{gri+1}^{n+1}&=-A_{gri}C_{gri-1}^{n}+\left(1+\frac{B_{gri}}{H}\right)C_{gri}^{n}+A_{gri}C_{gri+1}^{n}-B_{gri}C_{lri}^{n}\\ A_{lri}C_{lri-1}^{n+1}+C_{lri}^{n+1}-A_{lri}C_{lri+1}^{n+1}&=-A_{lri}C_{lri-1}^{n}+(1-B_{lri})C_{lri}^{n}+A_{lri}C_{lri+1}^{n}+\frac{B_{lri}}{H}C_{lri}^{n}\end{aligned} \qquad (23)$$

For 1<i<M-1 (Downcomer Section)

$$\begin{aligned} A_{gdi}C_{gdi-1}^{n+1}+C_{gdi}^{n+1}-A_{gdi}C_{gdi+1}^{n+1}&=-A_{gdi}C_{gdi-1}^{n}+\left(1+\frac{B_{gdi}}{H}\right)C_{gdi}^{n}+A_{gdi}C_{gdi+1}^{n}-B_{gdi}C_{ldi}^{n}\\ A_{ldi}C_{lri-1}^{n+1}+C_{ldi}^{n+1}-A_{ldi}C_{ldi+1}^{n+1}&=-A_{ldi}C_{ldi-1}^{n}+(1-B_{ldi})C_{ldi}^{n}+A_{ldi}C_{ldi+1}^{n}+\frac{B_{ldi}}{H}C_{ldi}^{n}\end{aligned} \qquad (24)$$

Where

$$\begin{aligned} &A_{gri}=\frac{-U_{gr,overall}\Delta t}{\epsilon_{ri}*4*\Delta x}, \quad A_{lri}=\frac{-U_{lr}\Delta t}{(1-\epsilon_{ri})*4\Delta x}, \quad A_{gdi}=\frac{-U_{gd}\Delta t}{\epsilon_{di}*4\Delta x}, \quad A_{ldi}=\frac{-U_{ld}\Delta t}{(1-\epsilon_{di})*4\Delta x},\\ &B_{gri}=-\frac{k_l a\,\Delta t}{\epsilon_{ri}}, \quad B_{lri}=\frac{k_l a\,\Delta t}{1-\epsilon_{ri}}, \quad B_{gdi}=-\frac{k_l a\,\Delta t}{\epsilon_{di}}, \quad B_{ldi}=\frac{k_l a\,\Delta t}{1-\epsilon_{di}}\end{aligned} \qquad (25)$$

Clearly, Equations in sets (23) and (24) are coupled with each other and can be solved simultaneously along with the initial and boundary conditions given by Equations (20)-(22). The liquid side mass transfer coefficient, k_l(cm/s) was assumed to be constant. No axial variation in the gas holdup and interfacial area in the riser was observed [Paper I], and hence the experimental values for these parameters in the riser was used at all the nodes in the mesh selected for numerical analysis and data fitting. In the downcomer,

however, gas holdup and interfacial area varied axially [Paper I]. Since in Paper I, the experimental values for the downcomer were available only at the five axial measurement ports, and a large mesh size based on just the five axial ports would cause significant error, the gas holdup and interfacial area correlations developed for the downcomer were used to facilitate a suitable mesh size to obtain proper accuracy. The mesh size chosen was $\Delta z=0.1$ and $\Delta t=0.01$, and since measuring the properties at each node in the mesh would be experimentally impractical, the correlations developed by Paper I, were used for the axial variation of the key parameters of Equations(9)-(12), namely ε(z), and a(z). The model was fitted to the experimental data to extract the liquid-side mass transfer coefficient, k_l (cm/s). Then, the interfacial area data was used to calculate the local volumetric mass transfer coefficient.

$$k_l a = k_l * a_i \tag{26}$$

For the sake of comparison, the conventional assumption of constant overall volumetric mass transfer coefficient, $k_l a_{overall}$ (s^{-1}), commonly used in all the literature, can also be applied to the same model (Equations (23)-(24)) subject to the constraints (Equations (20)-(22)), by replacing $k_l a$ in the equations by $k_l a_{overall}$ (s^{-1}). This method obviously does not account for changes in the interfacial area, a, and a constant $k_l a_{overall}$ (s^{-1}) was then extracted by fitting the model to the experimental concentration data.

3. EXPERIMENTAL SETUP

The numerical solution of the plug flow model explained in section 2 requires for the experimental setup to provide for axial measurement ports to carry out local measurements of the gas holdup, interfacial area, and the transported gas concentration. As mentioned earlier, Luo and Al Dahhan, 2005 [17], found the split airlift photobioreactor to outperform the bubble column and draft tube airlift reactor for culturing microalgae. Thus, experiments were performed in an internal loop split airlift reactor shown in Figure 3.1. The setup was adapted from Luo and Al Dahhan, 2005 [17], and Paper I, and consists of an acrylic column of the height of 150 cm, and an inside diameter of 13 cm. The column is split into half by an acrylic sheet, 105 cm tall, which divides it into the riser and the downcomer sections. The transport gas used for the purpose of mass transfer was oxygen, and for that air was introduced into the riser section using a sparger, 5 cm in diameter, with 1 mm openings. The column was provided with five ports each in the riser and the downcomer sections, at a distance of 24 cm apart. These ports were used for measuring the oxygen concentration in the liquid and the gas phases in this work and are the same as the ones used in Paper I for the local gas holdup and interfacial area measurements. The rate of airflow was controlled by a calibrated rotameter and the measurements were done at three superficial gas velocities of 1.0 cm/s, 2.0cm/s, and 2.8 cm/s, based on the cross-sectional area of the riser. These velocities were selected based on Luo and Al Dahhan, 2015 [17] who cultured microalgae *Porphyridium* in a split airlift reactor with the same dimensions as used in this study. All experiments were carried out at room temperature and atmospheric pressure.

An optical oxygen probe from Ocean Optics Inc. was used to measure the dissolved liquid phase oxygen concentrations (C_l) at superficial gas velocities of 1.0, 2.0, and 2.8 cm/s. First the reactor was sparged with nitrogen to deoxygenate the water, and then gas flow was quickly switched to air and concentration data was recorded until dissolved oxygen saturation was achieved. A classic colored-dye tracer experiment was used to measure the superficial liquid velocity, U_{lr}. A drop of colored dye was introduced and the moving front of the color was tracked with time to estimate the liquid circulation velocity needed in the model. The gas holdup and interfacial area data used in the mass transfer model has been adapted from Paper I, using the data and the developed correlations. Details of the measurement techniques are given in the next section.

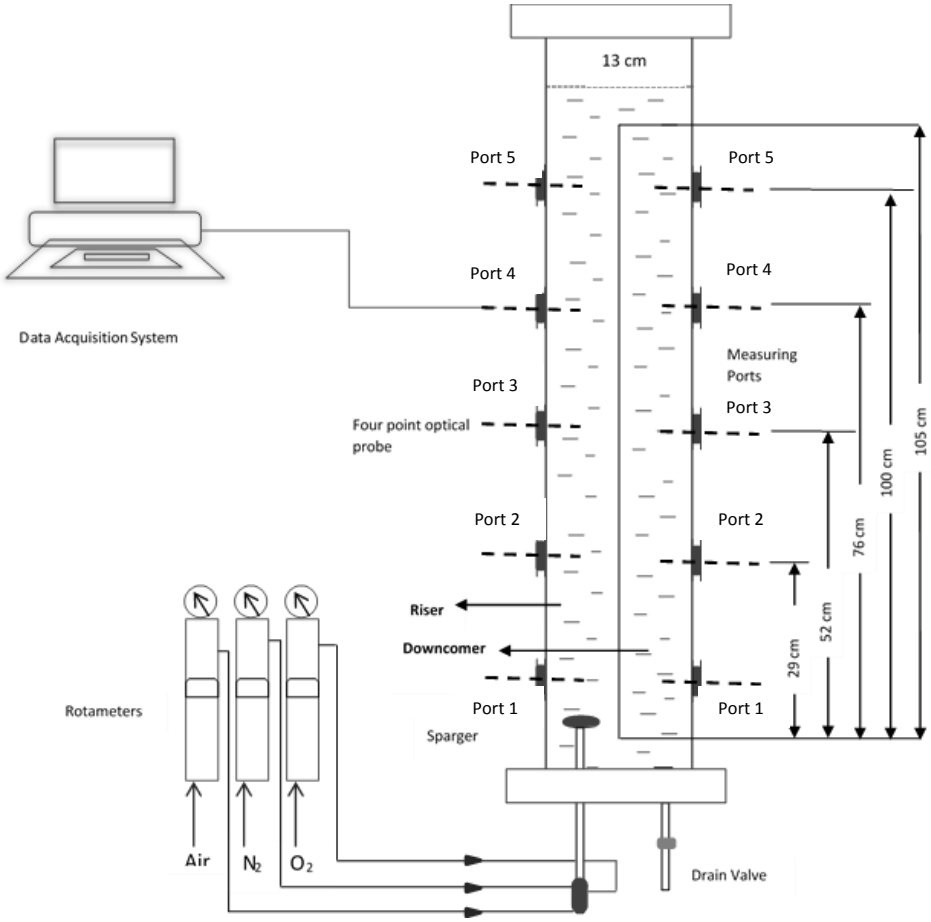

Figure 3.1: Schematic representation of the split airlift reactor used in this study

4. MEASUREMENT TECHNIQUES

The measured and estimated parameters in this section were used to fit the liquid phase concentration data to the numerical model for both the riser and the downcomer sections. k_l (cm/s) was the only unknown parameter, and its value was determined by fitting the oxygen concentration data to the numerical model and minimizing the sum of the squares of the residual between the calculated and measured data at all the axial ports in the riser and downcomer sections.

4.1 OXYGEN CONCENTRATION

The dissolved liquid phase oxygen concentrations, $C_l(t)$, at each port in the riser and the downcomer for superficial gas velocities of 1.0, 2.0, and 2.8 cm/s (based on the riser cross-sectional area) was measured using the optical oxygen probe from Ocean Optics Inc. The optical oxygen probe was connected to a spectrophotometer connected to a data acquisition system. The tip of the probe has a light-sensitive coating, which was quenched based on the oxygen concentration, schematically shown in Figure 4.1. The liquid and gas phase oxygen concentrations were measured at each of the 5 ports in the riser and the downcomer sections. First, the reactor was sparged with nitrogen to deoxygenate the water, and then a step change in oxygen concentration was made by switching the gas phase from nitrogen to air. Dissolved oxygen concentration was recorded at intervals of 1 second at each port in the riser and the downcomer.

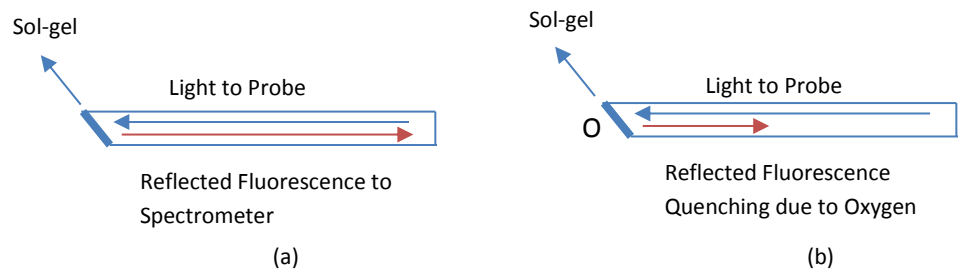

Figure 4.1: Schematic representation of (a) optical oxygen probe (Ocean Optics) and (b) fluorescence quenching in the presence of oxygen

Due to a delay in the sensor response, the actual oxygen concentration, $C_l(t)$, is different from that measured by the probe, $C_{sensor}(t)$, and must, therefore, be de-convoluted. The probe delay constant, k_{sensor} , was estimated using the two-point calibration method [18]. The delay constant for the probe was found to be 1 s^{-1}. The actual dissolved concentration was then used to fit the model.

$$C_l(t) = C_{sensor}(t) + \frac{1}{k_{sensor}} \frac{dC_{sensor}(t)}{dt} \tag{27}$$

The value of the Henry's Law constant for oxygen in water, *H*, was taken to be 0.032 [19].

4.2 LOCAL GAS HOLDUP AND INTERFACIAL AREA

The gas holdup and interfacial area data used in the mass transfer model was adapted from Paper I. In Paper I, a sophisticated four-point optical fiber probe technique was used to measure the local gas holdup and interfacial area at the radial center at the axial ports in the riser and downcomer sections, at velocities of 1.0, 2.0, and 2.8 cm/s (based on the riser cross-sectional area). The experimental data was also used to develop correlations for the axial variation of the gas holdup and interfacial area. The four-point

optical probe technique uses a source to send light signals thought to the probe tip. Due to a difference in the refractive indices of the liquid and the gas phases, the intensity of light reflected back from the tip is different if the probe is in the liquid than in the gas phase. A data processing algorithm [20] was adapted to measure the gas hold-up ($\in$) and specific interfacial area (a) from the voltage signal collected by the data acquisition system. Details of the technique can be found in Paper I.

For a given superficial gas velocity, no axial variation of gas holdup and interfacial area was observed in the riser, and hence the experimental data for the riser from Paper I was used to solve the model.

Due to the axial variation in the properties in the downcomer, correlations were developed for the downcomer in Paper I. As explained before, to enhance accuracy, the grid size used is small as compared to the distance between the axial ports. Thus, the mass transfer model is being solved by numerical discretization, and therefore, knowledge of $\in_{gd}$ and a is needed at more points in the space regime than what is measured in the experiments in Paper I. Hence, correlations for the gas holdup and interfacial area in the downcomer, from Paper I have been used to estimate these properties at the discretized axial locations to solve the mass transfer model. The correlations are as given below.

$$\in_{gdi}= \left(1.608 * \frac{z_i}{H_D} - 0.5153\right) 0.324 \left(\frac{U_{gr}}{U_{lr}} + 1\right)^{35.772} - \left(0.177 * \frac{z_i}{H_D} - 0.425\right) \quad (28)$$

$$a_{di} = \alpha * z_i - \beta \quad (29)$$

Where the values of α and β are 0.0049 and 0.1826, 0.0042 and 0.1911, and 0.0026 and 0.1545 for U_{gr} 2.8 cm/s, 2.0 cm/s, and 1.0 cm/s, respectively. Z_i is the

distance in the downcomer from the base of the reactor, and H_D is the height of the downcomer.

4.3 SUPERFICIAL GAS VELOCITY

The gas volume in the riser consists of both the gas injected through the sparger and that entering the riser from the downcomer due to circulation. The superficial gas velocity due to gas injection from the sparger, U_{gr}, can be calculated based on the riser cross-sectional area (A_r) and the volumetric gas flow rate (Q).

$$U_{gr} = \frac{Q}{A_r} \tag{30}$$

To account for the gas entering from the downcomer and that due to injection, the overall superficial gas velocity, $U_{gr,overall}$, based on the total gas volume, has been adapted from [13]. The drift flux model for two-phase flow is given in Equation (31) [21]. This has been used in literature to calculate the superficial gas velocity in the riser of airlift reactors [13].

$$\in_r = \frac{U_{gr,overall}}{C_o(U_{gr,overall}+U_{lr})+\vartheta_{gjr}} \tag{31}$$

The gas holdup, $\in_r$, was as measured in Paper I. Since the reactor is operated in bubbly flow regime and a uniform bubble distribution was observed, the distribution parameter, C_o, was taken to be 1. U_{lr} is the liquid circulation velocity as calculated in section 4.4. ν_{gjr} was the drift velocity and was estimated as follows [22]:

$$\vartheta_{gjr} = \vartheta_\infty(1-\in_r)^n \tag{32}$$

ν_∞ is the bubble terminal velocity, taken to be 0.25 m/s for bubble sizes up to 10 mm [13], n was taken to be 2 [13], [22].

The difference of the overall riser superficial gas velocity, $U_{gr,overall}$, and that due to gas injection, U_{gr}, is balanced with the downcomer-superficial gas velocity, U_{gd}, through the continuity equation. The downcomer superficial gas velocity is, therefore, calculated using Equation (33).

$$U_{gd} x\, A_d = (U_{gr,overall} - U_{gr}) x\, A_r \quad (33)$$

Similar to the riser superficial gas velocity, the superficial gas velocity in the downcomer, U_{gd}, was estimated based on the total gas volume entering the downcomer, and the cross-sectional area of the downcomer. As explained in section 2, in reality, the number of the bubbles and the local gas holdup in the downcomer decrease on moving axially downwards [Paper I], however, U_{gd}, has been estimated based on the assumption that it is constant axially in the downcomer. A detailed analysis for the validity of this assumption is explained in section 5.4.

4.4 LIQUID CIRCULATION VELOCITY

A colored dye tracer experiment was used to measure the liquid circulation velocity. The time taken by the front of the colored dye to travel the entire height of the downcomer and riser was used to calculate the superficial liquid velocity as:

$$U_{Lr} = \frac{H_r\,(1-\epsilon_r)}{t_r} \qquad U_{Ld} = \frac{H_d\,(1-\epsilon_d)}{t_d} \quad (34)$$

5. RESULTS AND DISCUSSION

5.1 MODEL VALIDATION

Following the plug flow reactor (PFR) model with the assumption of a constant liquid-side mass transfer coefficient, k_l (cm/s), the estimated oxygen concentration data from the model by fitting for k_l (cm/s) was compared with the experimental concentration from the optical oxygen probes. Figures 5.1 and 5.2 compare the experimental results with the calculated dissolved oxygen data for a superficial gas velocity of 2.0 cm/s at Port 3, at the axial distance of z=52 cm from the base of the reactor. Clearly, the PFR model agrees well with the experimental data for both the riser and the downcomer.

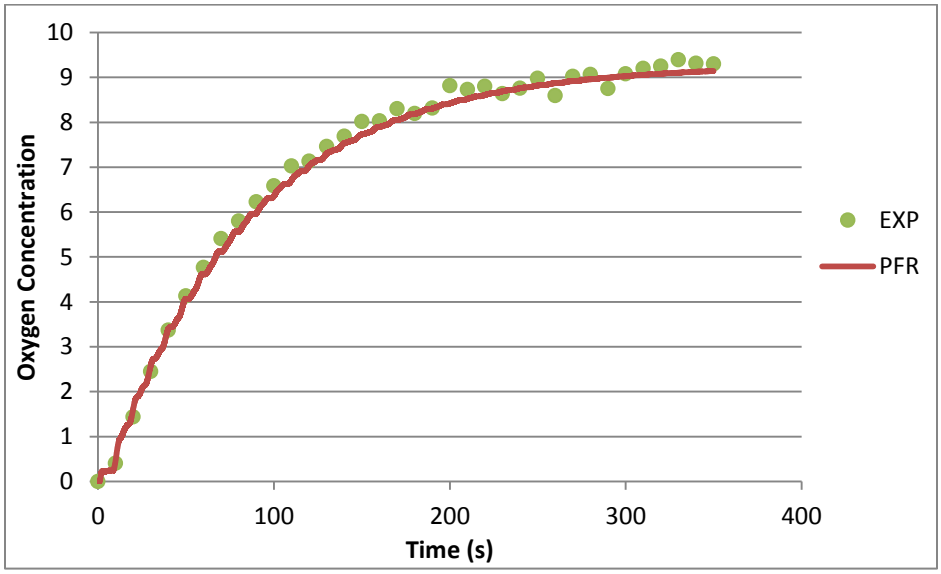

Figure 5.1: Comparison of the experimental and estimated dissolved oxygen concentration at z=52cm (Port 3) in the riser at U_{gr} =2.0 cm/s

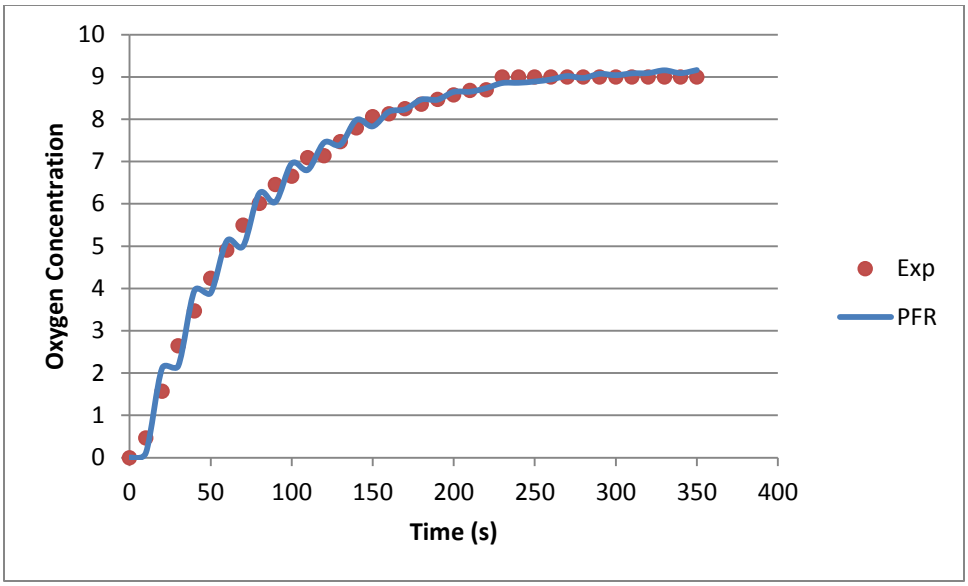

Figure 5.2: Comparison of the experimental and estimated dissolved oxygen concentration at z=52cm (Port 3) in the downcomer at U_{gr} =2.0 cm/s

Thus, Figures 5.1 and 5.2 validate the use of the plug flow model given by Equations (1)-(4) in the split airlift reactor shown in Figure 3.1. Since the plug flow reactor model was developed for a constant liquid side mass transfer coefficient, k_l (cm/s), throughout the reactor, fitting the experimental data of oxygen concentration from any axial location in the riser or the downcomer with the corresponding estimated oxygen concentration data from the model did not significantly vary the fitted value of k_l (cm/s).

5.2 LIQUID-SIDE AND LOCAL VOLUMETRIC MASS TRANSFER COEFFICIENT

Figure 5.3 shows the variation of the liquid side mass transfer coefficient (k_l, cm/s) with superficial gas velocity. The fitted value of k_l (cm/s) varied from 0.11 cm/s at 1.0 cm/s to 0.37 cm/s at 2.8 cm/s superficial gas velocity. The increase in the liquid side mass transfer coefficient (k_l, cm/s) with an increase in the superficial gas velocity is a

direct consequence of increased mixing and interaction between the liquid and the gas phases at higher gas velocities. Although no studies focus on estimating k_l (cm/s) directly from experimental data, the increase in k_l with superficial gas velocity (as shown in Figure 5.3) is similar to the results observed for the overall mass transfer coefficient in literature [3], [13].

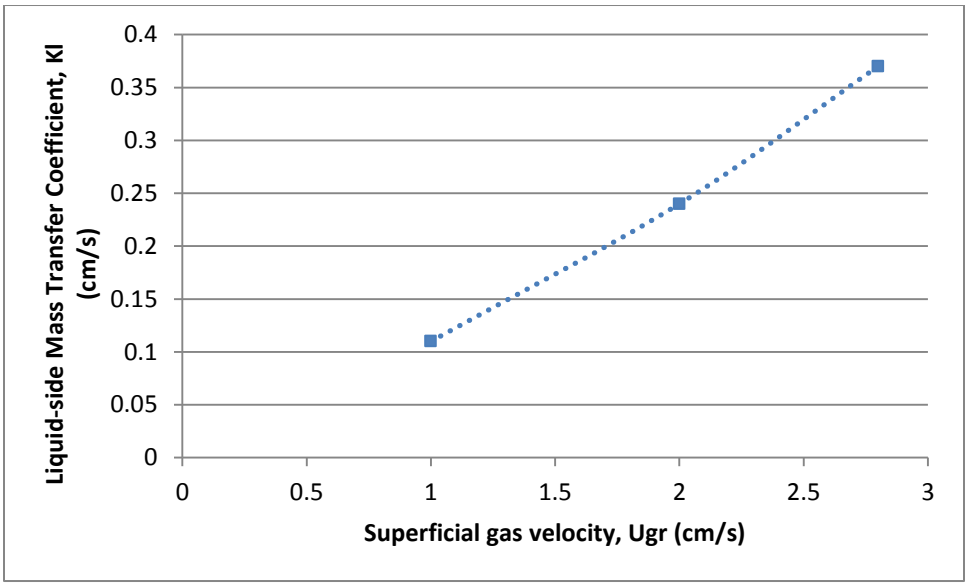

Figure 5.3: Variation of the liquid-side mass transfer coefficient, k_l, with superficial gas velocity, U_{gr}

The local volumetric mass transfer coefficient, $k_l a$ (s^{-1}), was estimated based on the interfacial area data measured in Paper I and the liquid-side mass transfer coefficient values using Equation (26). The interfacial area measured at the radial center in the riser and the downcomer (Paper I), was found to increase with an increase in superficial gas

velocity. It did not vary significantly axially in the riser, but varied axially in the downcomer resulting in an axial variation of $k_l a$ (s^{-1}) in the downcomer.

The local volumetric mass transfer coefficient, $k_l a$ (s^{-1}), for the riser, calculated using Equation (26), is shown in Figure 5.4.

The axial variation of the local volumetric mass transfer coefficient in the downcomer is shown in Figure 5.5. In Figures 5.4 and 5.5, $k_l a$ (s^{-1}) can be seen to increase with an increase in the superficial gas velocity. This trend for the general increase of the mass transfer coefficient with the superficial gas velocity is the same as that reported in the literature [13], [23], and is due to increased gas-liquid interaction and interfacial area at higher flow rates. However, it must be noted at this point that the studies available for mass transfer coefficient in airlift reactors are for the overall mass transfer coefficient and the Figures 5.4 and 5.5 are for the local ones.

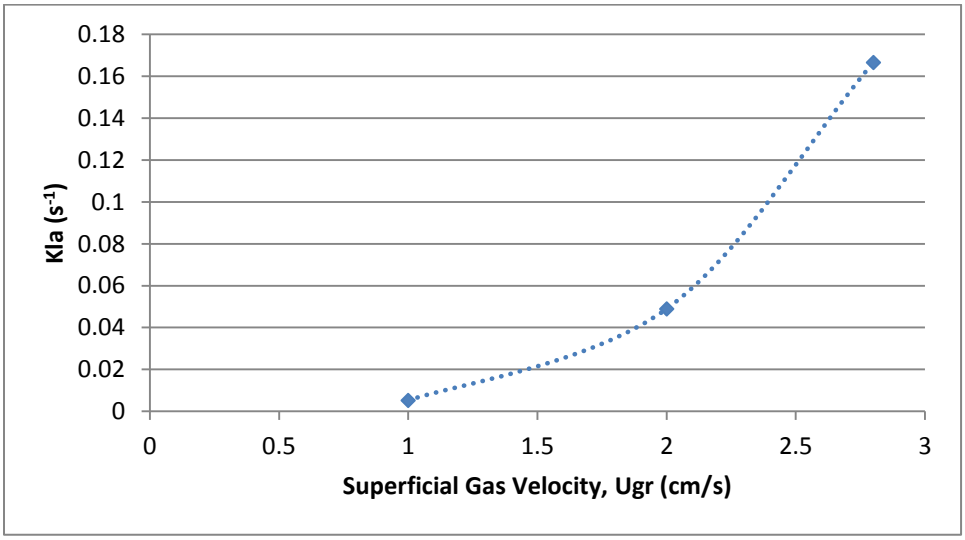

Figure 5.4: Variation of local volumetric mass transfer coefficient, $k_l a$, in the riser with superficial gas velocity, U_{gr}

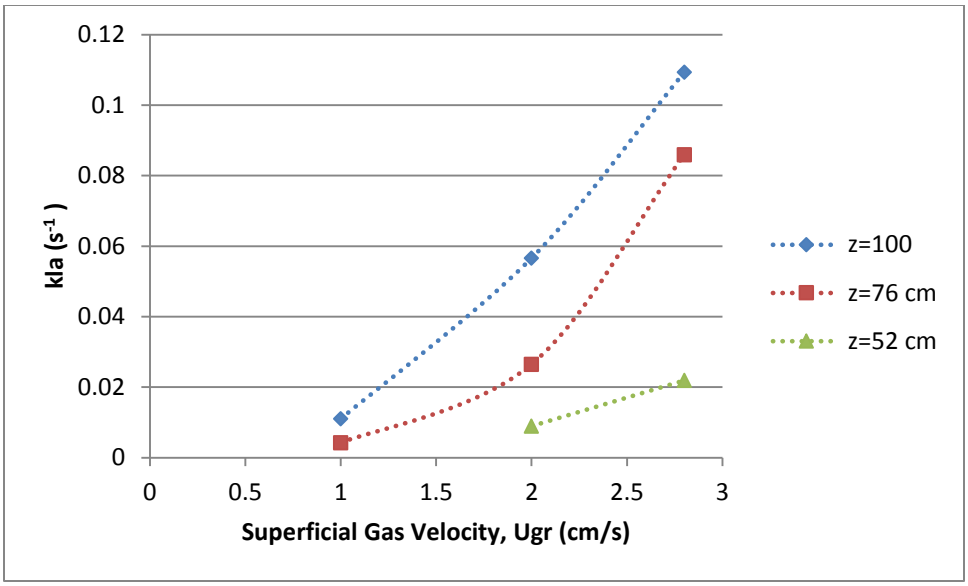

Figure 5.5: Variation of local volumetric mass transfer coefficient, $k_l a$, in the downcomer with superficial gas velocity, U_{gr} (Port 5:z=100cm; Port 4: z=76cm; Port 5: z=52cm)

Figure 5.6 compares the local volumetric mass transfer coefficient, $k_l a$ (s^{-1}), with a few correlations available in literature. These correlations evaluate the overall volumetric mass transfer coefficient based on the overall gas holdup and interfacial area in the reactor, and have been given in Table 5.1. As mentioned earlier, the trend for increase in volumetric mass transfer coefficient with superficial gas velocity is the same for the correlations as well as the local $k_l a$ (s^{-1}) in the riser and at different axial locations in the downcomer in this study. Also, since a direct comparison of the experimental data with the correlations was not possible due to the different of nature (local versus overall) of $k_l a$, the range of the values of the volumetric mass transfer coefficient for a superficial gas velocity increase from 1.0 to 2.8 cm/s is given in Table 5.1. At superficial gas velocity of 1.0 cm/s, the local $k_l a$ in the riser and downcomer was within the range of magnitude of the overall estimated from the correlations. However, the local $k_l a$ value

estimated in this study was still always higher than that estimated by any correlation. The local $k_l a$ in the riser and the downcomer was always a magnitude higher than the overall $k_l a$ obtained from Alibajnic, 2007 [24], Bello, 1985 [25], and Li, 1995 [26] at superficial gas velocities of 2.0 and 2.8 cm/s, and from Blazej, 2004 [27] at 2.8 cm/s. Also, as was expected, no correlation was able to predict the local values of $k_l a$ in the riser and the downcomer of the split airlift reactor.

Table 5.1: Correlations for overall $k_l a$ in literature

	$k_l a$	Estimation Method	Range of $k_l a$ (s^{-1}) (Ugr 1.0-2.8 cm/s)
Albijanic, 2007 [24]	Overall	$k_l a=0.28*(1+d\sigma/dC_A)^{0.71} *U_{gr}^{0.77}$	0.008-0.018
Blazej, 2004 [27]	Overall	$k_l a=0.91*\varepsilon_{gr}^{1.39}$	0.0024-0.026
Bello, 1985 [25]	Overall	$k_l a=5.5x10^{-4}*(1+A_d/A_r) *U_{gr}^{0.8}$	0.005-0.011
Li et al., 1965 [28]	Overall	$k_l a=0.0343*U_{gr}^{0.524}$	0.0031-0.0052
Riser	Local	Fitting, Plug Flow Model	0.0053-0.17
Downcomer, Port 5 (z=100 cm)	Local	Fitting, Plug Flow Model	0.011-0.11
Downcomer, Port 4 (z=76 cm)	Local	Fitting, Plug Flow Model	0.004-0.086
Downcomer, Port 3 (z=52 cm)	Local	Fitting, Plug Flow Model	0.009(at 2.0 cm/s)-0.022

5.3 PITFALLS OF CONVENTIONAL METHOD TO ESTIMATE OVERALL MASS TRANSFER COEFFICIENT

For the sake of comparison, the plug flow model given by Equations 9-12 was solved for overall mass transfer coefficient, $k_l a_{overall}$ (s^{-1}), under the assumption of a

constant $k_l a_{overall}$ (s^{-1}) throughout the reactor. The initial and boundary conditions and the methodology adapted was as explained in section 2, without accounting for the variation of interfacial area, and assuming $k_l a_{overall}$ (s^{-1}) to be the same throughout the reactor. This method is conventionally used in literature to estimate the overall mass transfer coefficient. The variation of $k_l a_{overall}$ (s^{-1}) with superficial gas velocity (Figure 5.7) follows the general trend for an increase in $k_l a_{overall}$ (s^{-1}) with superficial gas velocity [3], [13], [23].

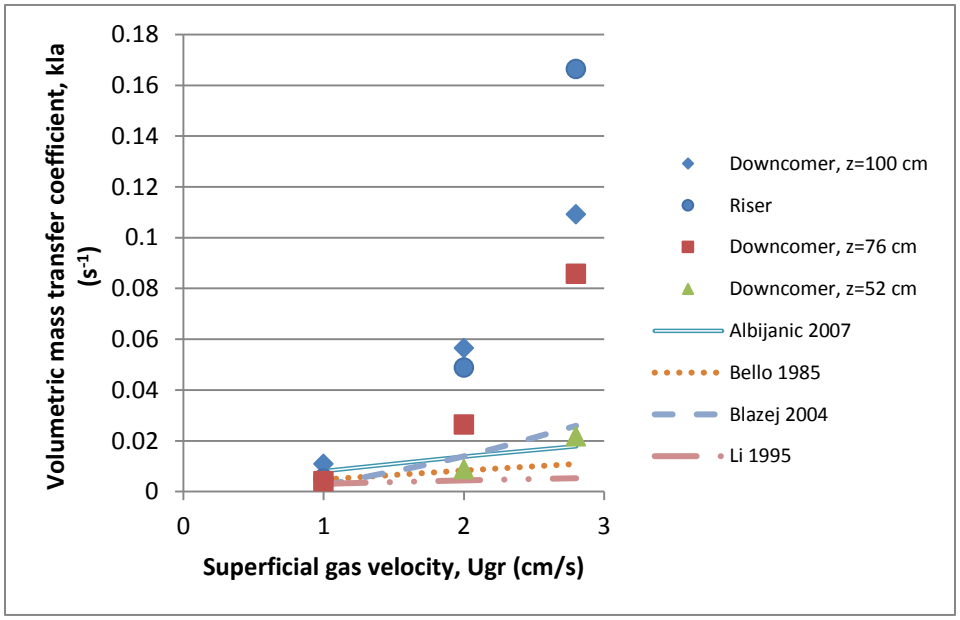

Figure 5.6: Comparison of local $k_l a$ (s^{-1}) with correlations in literature

Figure 5.7 also compares the overall and the local volumetric mass transfer coefficient for the riser. At each of the studied superficial gas velocities, the local volumetric mass transfer coefficient for the riser was higher than its overall counterpart. At a superficial gas velocity of 2.0 cm/s, the global mass transfer coefficient was 75%

lower than the local mass transfer coefficient. Also, from Figure 5.6, it can be seen that the difference between the global and the local volumetric mass transfer coefficients increases as superficial gas velocity increases. This may be because, at higher velocities, both the interfacial area and liquid-side mass transfer coefficient increases compounding the effect of velocity on the local volumetric mass transfer coefficient. Such a large difference between local and overall values emphasizes the need for local measurements to truly analyze and understand the gas-liquid mass transfer behavior, especially for scale-up operations.

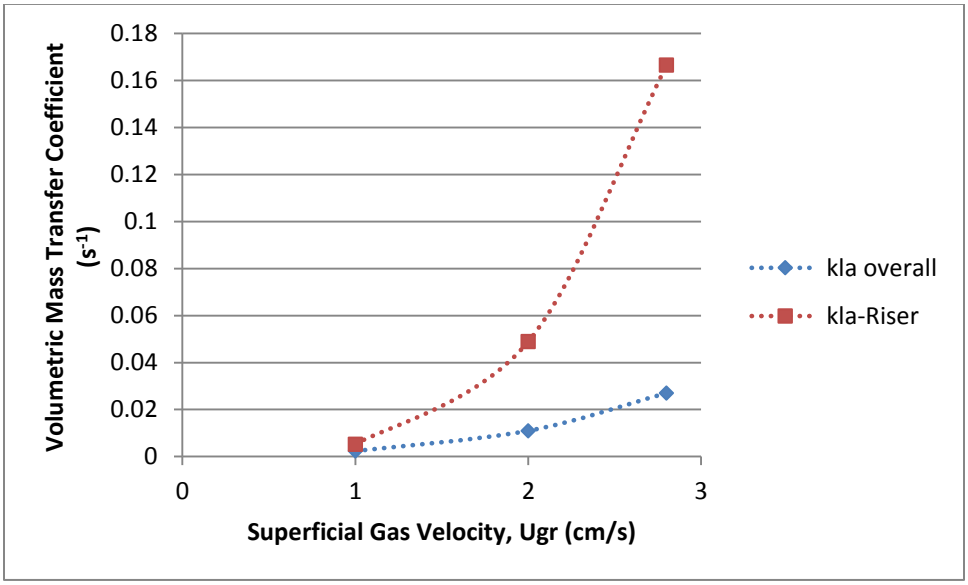

Figure 5.7: Comparison of overall and local volumetric mass transfer coefficient with superficial gas velocity, U_{gr}

The fitted constant value of $k_l a_{overall}$ was then used back in Equation (26) to calculate the liquid-side mass transfer coefficient, designated as k_l^*(to differentiate it from k_l fitted when $k_l a$ varies in the reactor), using the local interfacial area, a, [Paper I].

According to Paper I, since the number and size of bubbles traveling down the downcomer decreases, gas-liquid interaction must also decrease, increasing the fictitious film thickness, δ, on moving down the downcomer. Now, as defined by the film theory, since k_l^* is the gas-liquid diffusivity, D, divided by the fictitious film thickness, δ, therefore, for a constant diffusivity, D, an increase in film thickness, δ, down the downcomer must decrease the value of k_l^* on moving down the downcomer. However, when the fitted constant value of $k_l a_{overall}$was used in Equation (26) to calculate k_l^*, the decrease in the interfacial area on moving axially downwards resulted in an axial increase of k_l^* in the downcomer to (Figure 5.8). This is in contradiction to the above expected phenomenon. Thus, the assumption of a constant global overall volumetric mass transfer coefficient is highly misleading, and the assumption of a constant liquid-side mass transfer coefficient is a more appropriate one.

Also, the range of $k_l a_{overall}$ (s^{-1}) was found to be within that of the correlations as shown in Figure 5.9. This confirms the validity and application of the numerical solution to the model, and the model in general to airlift reactors. However, since $k_l a_{overall}$ (s^{-1}) is within the range of the correlations, and the correlations do not come close to predicting the values of the local $k_l a$ (s^{-1}) (Figure 5.6), the assumption of a constant $k_l a_{overall}$ (s^{-1}) throughout the reactor and not accounting for the local gas holdup and interfacial area is not appropriate.

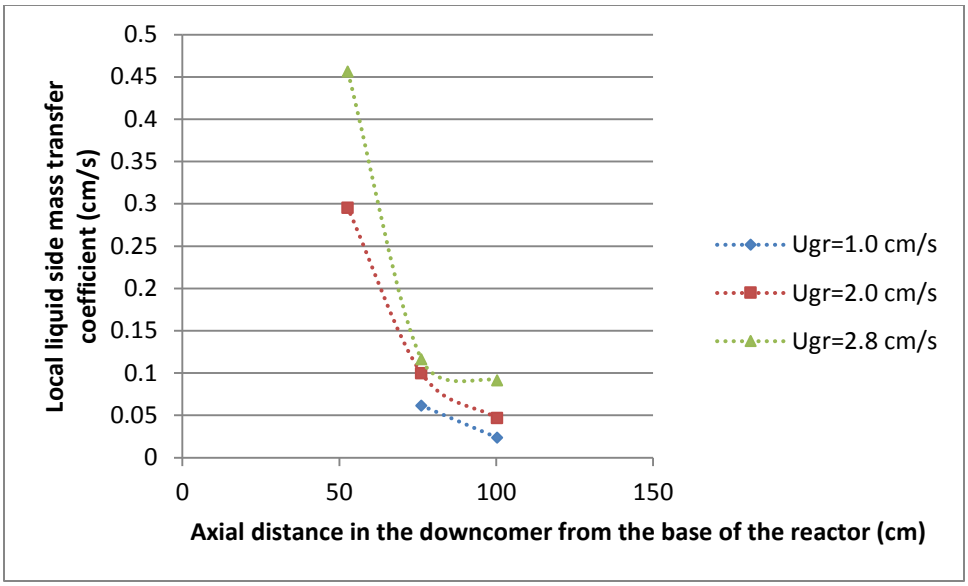

Figure 5.8: Axial variation of the local liquid side mass transfer coefficient (k_l^*) in the downcomer, based on the conventional method used in literature

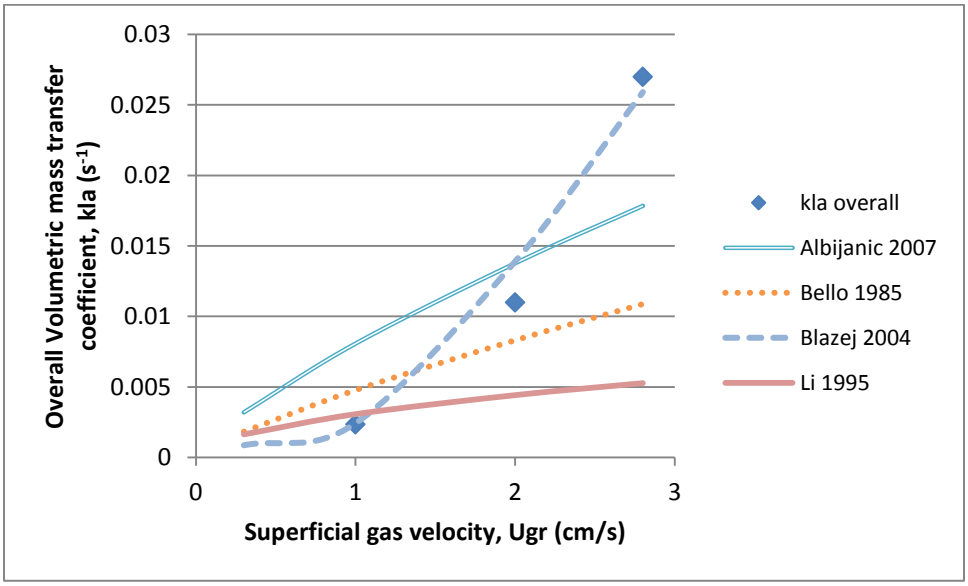

Figure 5.9: Comparison of $k_l a_{overall}$ (s^{-1}) with the correlations

5.4 INSENSITIVITY OF THE FITTED k_l TO U_{gd}

Fundamentally, the superficial gas velocity, U_g is related to the true bubble velocity, U_b, and the gas holdup, ε (Equation (9)) [3], [29].

$$U_{gi} = U_{bi} * \in_i \quad (35)$$

In Paper I, the local bubble velocity and gas holdup measured at the radial center in the downcomer was seen to decrease axially downwards. Since no radial measurements were done to evaluate the radially averaged local bubble velocity and gas holdup, an average superficial gas velocity could not be obtained at the axial locations in the downcomer. However, using the local values of bubble velocity and gas holdup at the radial center, the superficial gas velocity at the radial center at different axial locations was calculated from Equation (35). Then, to gain some insight into the effect of U_{gd} on the mass transfer process, and also provide a means to validate the use of the assumption of a constant U_{gd} in the mass transfer model, U_{gd}, calculated based on Equation (33), was substituted with the highest and lowest observed downcomer superficial gas velocities at the radial center in the plug flow model to fit for k_l (cm/s).

Also, since the number and size of the bubbles decreased axially downwards, no reliable data was available for ports below Port 3 (z=52 cm from the base of the reactor) [Paper I]. Hence, the highest and the lowest observed local bubble velocity and gas holdup values available were at ports 5 and 3, respectively. The mean local bubble velocity and gas holdup of 96.46 cm/s and 4.27% at port 5, and 77.34 cm/s and 0.83% at port 3, at superficial gas velocity, U_{gr}, of 2.0 cm/s were used in Equation 35. The results obtained from fitting for the liquid-side mass transfer coefficient, k_l (cm/s) at the different downcomer superficial gas velocities are as given in Table 5.2.

Table 5.2: Comparison of the fitted value of k_l (cm/s) at the highest and the lowest observed superficial gas velocities in the downcomer

Downcomer Superficial Gas Velocity, U_{gd} (cm/s)	Based on the continuity equation (Equation (33))	Highest Observed (port 5) based on Equation (35)	Observed U_{gd} (port 4) based on Equation (35)	Lowest Observed (port 3) based on Equation (35)
	0.7	4.1	2.8	0.6
Fitted k_l (cm/s)	0.24	0.23	0.23	0.24

The fitted liquid-side mass transfer coefficient, k_l (cm/s) at the lowest observed downcomer superficial gas velocity of 0.6 cm/s. was the same as that obtained by assuming a constant U_{gd} through the downcomer. Also, the fitted k_l (cm/s) at the highest observed downcomer superficial gas velocity of 4.0 cm/s was less than 5% lower than the value of 0.24 obtained at a constant U_{gd} through the downcomer. This analysis implies that the variation in the local gas holdup and interfacial area dominate the process of mass transfer through the downcomer, and since the axial variation of local gas holdup and interfacial area was appropriately accounted for in the mass transfer model, the variation in U_{gd} did not significantly affect the fitted k_l (cm/s). This validates the assumption of a constant U_{gd} based on the total gas volume through the downcomer for fitting for the liquid-side mass transfer coefficient, k_l (cm/s) for the split airlift photobioreactor and the conditions used in this study. Further, a parametric analysis of gas holdup and interfacial area on the fitted value of k_l (cm/s) showed a variation of

about 50%. This observation, once again, stresses the importance of incorporating local measurements to evaluate k_l (cm/s) and $k_l a$ (s^{-1}).

U_{gd} can be assumed to be constant in the downcomer. It can be taken to be in the range of the highest and the lowest observed values at the axial locations in the downcomer, or to be a weighted average of the axial values in the downcomer. However, since measuring the local bubble velocity and gas holdup at the axial locations in the downcomer to evaluate the true superficial gas velocity at the axial locations (Equation (35)) can be a tedious and time consuming process, the drift flux modeling approach coupled with the continuity equation (Equations (31)-(33)) can be safely and easily used to calculate U_{gd}.

6. REMARKS

A plug flow mass transfer model was developed for an internal loop airlift reactor. A finite difference numerical method was used to solve the model for the gas and liquid phases. A new approach of assuming a constant liquid-side mass transfer coefficient, k_l(cm/s), was developed, validated, and successfully implemented in a split airlift reactor. k_l(cm/s) was seen to increase with an increase in the superficial gas velocity. The local liquid-side mass transfer coefficient, k_l (cm/s), increased by 200% as the superficial gas velocity increased from 1.0cm/s to 2.8 cm/s. The local interfacial area data from Paper I, was used to estimate the local volumetric mass transfer coefficient, $k_l a$ (s), at different axial locations in the riser and the downcomer. Due to a decrease in local interfacial area on moving down the downcomer, an axial decrease of $k_l a$ (s) was observed in the downcomer. The assumption of a constant liquid-side mass transfer coefficient, k_l (cm/s), was found to be more appropriate than assuming a constant overall volumetric mass transfer coefficient, $k_l a_{overall}$ (s^{-1}), which lead to highly misleading results such as the increase in liquid-side mass transfer coefficient in regions of decreased gas-liquid interaction. Also, the local mass transfer coefficient was found to be higher than its overall counterpart. At a superficial gas velocity of 2.0 cm/s, the local $k_l a$ was 518% higher than the overall $k_l a_{overall}$ in the riser. Thus, the assumption of $k_l a_{overall}$ used in literature, can result in erroneous findings, especially in special systems such as the culturing of microorganisms in airlift reactors, further emphasizing the need to carry out local measurements to truly understand the mass transfer process.

The use of the assumption of a constant downcomer superficial gas velocity to fit the oxygen concentration data to obtain the liquid-side mass transfer coefficient, k_l (cm/s) was validated by replacing the constant U_{gd} with the highest and the lowest observed superficial gas velocity based on the local bubble velocity and gas holdup at the axial locations in the downcomer. Change in the superficial gas velocity in the downcomer did not seem to significantly affect the fitted k_l (cm/s) for the split airlift photobioreactor used in this work. Therefore, to advance the understanding of the effect of downcomer superficial gas velocity, U_{gd} can be estimated by measuring the local radial bubble velocity and gas to estimate the radially averaged superficial gas velocity at various axial locations in the downcomer, and using a weighted average of the axial values to account for the whole downcomer. However, due to the ease of application and calculation, the drift flux model, coupled with the continuity equation seems to be a less cumbersome choice. Nevertheless, the stark difference between the overall volumetric mass transfer coefficient (conventional approach in literature) and the local volumetric mass transfer coefficient (new approach developed in this work) emphasizes the need to measure the local gas holdup, interfacial area, and bubble velocity and use these local parameters in mass transfer models instead of the overall ones.

REFERENCES

[1] C. W. Siegel, M.H., Robinson, "Applications of Airlift GAs-Liquid-Solid Reactors in Biotechnology," *Chem. Eng. Sci.*, vol. 47, no. 13–14, pp. 3215–3229, 1992.

[2] Y. Xu, L. Luo, and J. Yuan, "CFD simulations to portray the bubble distribution and the hydrodynamics in an annulus sparged air-lift bioreactor," *Can. J. Chem. Eng.*, vol. 89, no. 2, pp. 360–368, 2011.

[3] Y. Chisti, *Airlift Bioreactors*. Elsevier, New York, 1989.

[4] G. Olivieri, A. Marzocchella, and P. Salatino, "Hydrodynamics and mass transfer in a lab-scale three-phase internal loop airlift," *Chem. Eng. J.*, vol. 96, no. 1, pp. 45–54, 2003.

[5] M. K. Moraveji, M. M. Pasand, R. Davarnejad, and Y. Chisti, "Effects of surfactants on hydrodynamics and mass transfer in a split-cylinder airlift reactor," *Can. J. Chem. Eng.*, vol. 90, no. 1, pp. 93–99, 2012.

[6] a. Couvert, M. Roustan, and P. Chatellier, "Two-phase hydrodynamic study of a rectangular air-lift loop reactor with an internal baffle," *Chem. Eng. Sci.*, vol. 54, no. 21, pp. 5245–5252, 1999.

[7] E. Camarasa, E., Meleiro, L.A.C., Carvalho, "A complete model for oxidation airlift reactors," *Comput. Chem. Eng.*, vol. 25, pp. 577–584, 2001.

[8] J. Dhaoudi, H., Poncin, S., Hornut, J.M., Wild, G., Oinas, P., Korpijarvi, "Mass transfer in an external-loop airlift reactor: experiments and modeling," *Chem. Eng. Sci.*, vol. 52, no. 21/22, pp. 3909–3917, 1997.

[9] J. C. Merchuk and Y. Stein, "Local hold-up and liquid velocity in air-lift reactors," *AIChE J.*, vol. 27, no. 3, pp. 377–388, May 1981.

[10] I. Sikula, M. Juraščík, and J. Markoš, "Modeling of fermentation in an internal loop airlift bioreactor," *Chem. Eng. Sci.*, vol. 62, no. 18–20, pp. 5216–5221, 2007.

[11] H. Znad, M. Tokumura, and Y. Kawase, "Axial distribution of oxygen concentration in different airlift bioreactor scales: Mathematical modeling and simulation," *Chem. Eng. Technol.*, vol. 29, no. 9, pp. 1042–1047, 2006.

[12] T. Zhang, B. Zhao, and J. Wang, "Mathematical models for macro-scale mass transfer in airlift loop reactors," *Chem. Eng. J.*, vol. 119, no. 1, pp. 19–26, 2006.

[13] L. Luo and J. Yuan, "Modeling of mass transfer in an internal loop airlift reactor," *Chem. Eng. Technol.*, vol. 38, no. 3, pp. 511–520, 2015.

[14] H. P. Luo and M. H. Al-Dahhan, "Local characteristics of hydrodynamics in draft tube airlift bioreactor," *Chem. Eng. Sci.*, vol. 63, no. 11, pp. 3057–3068, 2008.

[15] C.-S. Lo and S.-J. Hwang, “Local hydrodynamic properties of gas phase in an internal-loop airlift reactor,” *Chem. Eng. J.*, vol. 91, no. 1, pp. 3–22, 2003.

[16] S. K. Pallapothu and A. M. Al Taweel, “Effect of contaminants on the gas holdup and mixing in internal airlift reactors equipped with microbubble generator,” *Int. J. Chem. Eng.*, vol. 2012, 2012.

[17] H. P. Luo and M. H. Al-Dahhan, “Airlift column photobioreactors for Porphyridium sp. culturing: Part I. effects of hydrodynamics and reactor geometry,” *Biotechnol. Bioeng.*, vol. 109, no. 4, pp. 932–941, 2012.

[18] L. Han, “Hydrodynamics, back-mixing, and Mass Transfer in a Slurry Bubble Column Reactor for Fischer-Tropsch Alternative Fuels,” 2007.

[19] D. W. Perry, R.H., Green, *Perry’s chemical engineers’ handbook*. New York: McGraw Hill, 2008.

[20] R. F. Xue, J., Al Dahhan, M.H., Dudukovic, M.P., Mudde, “Bubble dynamics measurements using four-point optical probe,” *Can. J. Chem. Eng.*, vol. 81, pp. 375–381, 2003.

[21] J. A. Zuber, N., Findlay, “No TitleAverage Volumetric Concentration in Two-Phase Flow Systems,” *J. Heat Transf.*, vol. 87, no. 4, p. 453, 1965.

[22] G. B. Wallis, *One-dimensional two-phase flow*. New York, McGraw-Hill, 1969.

[23] Z. Deng, T. Wang, N. Zhang, and Z. Wang, “Gas holdup, bubble behavior and mass transfer in a 5m high internal-loop airlift reactor with non-Newtonian fluid,” *Chem. Eng. J.*, vol. 160, no. 2, pp. 729–737, 2010.

[24] M. N. Albijanic, B., Havran, V., Petrovic, D. Lj., Duric, M., and Tekic, “Modeling and simulation of the polymeric nanocapsule formation process,” *AIChE Jour*, vol. 53, no. 11, pp. 2987–2904, 2007.

[25] R. A. Bello, C. W. Robinson, and M. Moo-Young, “Gas holdup and overall volumetric oxygen transfer coefficient in airlift contactors.,” *Biotechnol. Bioeng.*, vol. 27, no. 3, pp. 369–81, Mar. 1985.

[26] G. Li, S. Yang, Z. Cai, and J. Chen, “Mass transfer and hydrodynamics in an airlift reactor with viscous non-Newtonian fluid,” *Chinese Journal of Chemical Engineering*. 1995.

[27] M. Blažej, M. Juraščík, J. Annus, and J. Markoš, “Measurement of mass transfer coefficient in an airlift reactor with internal loop using coalescent and non-coalescent liquid media,” *J. Chem. Technol. Biotechnol.*, vol. 79, no. 12, pp. 1405–1411, 2004.

[28] G.-Q. Li, S.-Z. Yang, Z.-L. Cai, and J.-Y. Chen, “Mass transfer and gas-liquid circulation in an airlift bioreactor with viscous non-Newtonian fluids,” *Chem. Eng. J. Biochem. Eng. J.*, vol. 56, no. 2, pp. B101–B107, 1995.

[29] M. Hamed, “Hydrodynamics , Mixing , and Mass Transfer in Bubble Columns with Internals,” 2012.

PAPER

III. LOCAL GAS HOLDUP AND BUBBLE DYNAMICS INVESTIGATION DURING MICROALGAE CULTURING IN A SPLIT AIRLIFT PHOTOBIOREACTOR

ABSTRACT

To make the process of microalgae cultivation for bioenergy, and wastewater and flue gas treatment economically viable, it is important to completely understand gas-liquid interaction inside photobioreactors in real microalgae cultures completely. However, due to limitations of the conventional measurement techniques in the literature, only the overall parameters (such as over gas holdup, interfacial area, etc.) are studied, and that too mostly in air-water systems. Thus, the variation of local parameters such as local gas holdup and bubble dynamics properties like bubble passage frequency, bubble chord length and velocity, and interfacial area in real culturing systems remains unclear. In this study, these properties were studied inside a split- airlift photobioreactor at superficial gas velocities of 1.0, 2.0, and 2.8 cm/s while culturing microalgae *Scenedesmus sp.* These measurements were made at the radial center of the riser and the downcomer sections of the split airlift photobioreactor along the axial height. The viscosity of the medium was seen to increase with the optical density of the culture, while the surface tension remained the same throughout the experiment. Bubble passage frequency, gas holdup, and interfacial area were seen to increase with an increase in superficial gas velocity, and decrease with optical density which is related to the growth of microalgae. The bubble chord length and bubble velocity distributions became wider

at higher superficial gas velocities and higher optical densities; while no significant axial variation in the bubble properties was observed in the riser, an axial variation in these properties was observed in the downcomer due to a decrease in the number of bubbles descending through the downcomer. New correlations, accounting for the change in optical density as well as superficial gas velocity, to predict the gas holdup in the riser and at different axial locations in the downcomer were also developed.

Keywords: Airlift Photobioreactors, Microalgae Culture, Local Bubble Dynamics, Local Gas Holdup

1. INTRODUCTION

Microalgae are versatile fast growing unicellular microorganisms that became increasingly popular as the third generation of biofuels. Since microalgae absorb carbon dioxide from the atmosphere to photosynthesize and produce sugars, lipids, and proteins which can further be processed into biofuels and biodiesel, they are considered to be a carbon neutral source of energy. The high rates of biomass productivity and high oil content of microalgae are the main advantages of culturing microalgae for clean bioenergy production. For the process of photosynthesis, microalgae use much more carbon dioxide as compared to terrestrial plants, helping in carbon dioxide sequestration. Also, microalgae also help in abating environmental pollution by absorbing nutrients such as carbon dioxide, nitrates, and phosphates required for microalgae culturing from waste water and flue gasses, in turn treating them. Besides environmental applications like clean bioenergy product, carbon sequestration, and wastewater and flue gas treatment, microalgae also find application in aquaculture feed, pharmaceuticals, and human and animal nutrients. Despite the many advantages and applications of microalgae, limited research and development in the field render large-scale, commercial production of microalgae uneconomical. This is mainly due to a lack of a comprehensive approach to understand and quantify the interaction between the various phenomenon that affects microalgae cultures in photobioreactors. Gas holdup and the bubble dynamic properties such as bubble passage frequency, chord length, bubble velocity, and interfacial area are important parameters that affect the growth of microalgae inside photobioreactors. Investigating these parameters in real microalgae cultures can lay the

foundation to the improved process of operation and design, and scale-up and optimization of the process of microalgae culturing to be economically feasible.

Microalgae are cultivated in open as well as closed reactors equipped with bubbling or sparging systems for the introduction of air, CO_2, and other gasses needed for culturing. Due to the inherent constraints of open reactors, closed reactors are a better choice for culturing microalgae under controlled, and contamination-free environment [1], especially for high-value products and bioenergy production for microalgae species that are highly sensitive, in general. Enclosed photobioreactors (PBRs) are found in horizontal and vertical configurations. In recent studies, it has been shown that the vertical PBR configuration has a higher productivity and light distribution than its horizontal counterpart [2], [3]. Airlift reactors and bubble columns are common types of enclosed PBRs. Since both bubble columns and airlift reactors are pneumatically operated devices, they minimize the shear stress exerted on the microalgae cells, while promoting efficient mixing. Airlift reactors have been found to outperform bubble columns for microalgae culturing due to the additional advantage of ordered mixing and liquid recirculation, as opposed to the random mixing and back mixing found in bubble columns [4], [5]. Also, they are easier to design and scale-up and provide higher transfer coefficients [1], [4], [5]. Airlift reactors, with different configurations, ranging from tubular to draft-tube and split cylinder reactors have been studied in the literature, with the former being the least efficient for the mass production of microalgae cultures. In conventional draft-tube airlift PBRs, the presence of an internal dark zone in the inner tube (draft tube) due to limited to no light penetration, especially for dense cultures, does not allow for optimal light distribution. Hence, the draft tube airlift reactors have shown

to have lower production rates than split airlift PBRs [4], [5]. Draft tube airlift PBRs have an increased fraction of the dark cycle which further makes controlling the medium temperature quite a task. This can be particularly detrimental to species that are very sensitive to temperature fluctuations, and can also lead to a higher loss of medium due to evaporation. The split airlift photobioreactor can overcome the shortcomings of the draft tube airlift reactor. In fact, Luo and Al Dahhan, 2012 [4], performed a study to culture microalgae *Porphyridium* under controlled environment in a bubble column, draft-tube, and split airlift photobioreactors, and found that the highest biomass productivity and rate of growth were achieved in the split airlift photobioreactor.

In general, airlift PBRs have been studied extensively in the literature [6]–[10], [Paper I], with emphasis on bubble dynamics and mass transfer. Properties like gas holdup, interfacial area, and mass transfer coefficient are important for the design and scale-up of these reactors. Also, the gas holdup and interfacial area determine the interaction between the gas and the liquid phases inside the reactor, which is particularly crucial from the point of microalgae cultivation. Studies on the overall gas holdup and interfacial area in airlift reactors available in the literature [6], [11], [12] have developed correlations to relate the holdup and interfacial area to parameters such as superficial gas velocity, density, viscosity, etc. In Paper I the local variation in the gas holdup, bubble frequency, chord length, and velocity, and interfacial area in an air-water system in the riser and the downcomer sections was studied independently, and correlations were also developed to account for the axial variation in these properties. However, this study was carried out in an air-water system, and not in a real microalgae culture. Due to the empirical nature of these correlations, they have limited applicability, and hence,

extrapolation of the findings of such correlations to other systems can result in significant errors. Furthermore, the stark difference in the rheological properties of a microalgae culture and an air-water system renders these studies inapplicable to a real culture, especially as the culture grows in density. To mimic the changes in the culture properties with time, some other researchers have studied these properties in mediums of different solute concentrations [10], [13]. These studies give a better understanding of the changes in bubble dynamics and mass transfer properties with changes in operating conditions and medium properties than the more commonly studied air-water systems. However, they didn't reflect the real systems properly due to the differences with the presence of cells, and possibly other particulates from the dead and ruptured cells. Fernandez, 2014 [14], studied the gas holdup and volumetric mass transfer coefficient in water and in the culturing medium used for growing microalgae, without the presence of algae. Luo and Al Dahhan, 2012 [15], showed that the viscosity of the microalgae culture *Porphyridium* grown in different airlift PBRs changed with time as the culture grew in density, affecting properties such as gas holdup. This further emphasizes the need to carry out local measurements in a real microalgae culture and also track these changes as the medium grows in density, viscosity, and surface tension.

Additionally, all of the above studies have focused on evaluating the overall bubble dynamic parameters like the overall gas holdup and interfacial area and studied the variation in these properties with respect to operating parameters like superficial gas velocity, sparger design, and top and bottom clearance. All of the studies, except Paper I, simply measure these properties based on the riser section of the PBR, and fail to account for the variation in properties between the riser and the downcomer, and any axial

variation that may exist. Thus, they fail to provide a thorough understanding of the process, which becomes particularly problematic during scale-up operations [16]. The dearth of studies focusing on local parameters is due to the difficulty associated with carrying out local measurements and lack of reliable techniques to do so. While Paper I did measure local variations in these parameters, they only used an air-water system, which is also a shortcoming in their study as mentioned earlier. Thus, a thorough understanding of the basic bubble dynamics and mass transfer properties in an actual culture is crucial [17]. The combined effect of the lack of measurements in actual microalgae cultures and local measurements poses serious hindrances to true understanding of the entire culturing system, leaving room for error in the design and scale up process.

In light of the above discussion, this study aims at experimentally investigate the gas holdup and bubble dynamic properties in a microalgae culture in a split airlift PBR by employing a four-point optical fiber probe technique [18], [Paper I]. The split airlift PBR used in Paper I, based on the work of Luo and Al Dahhan, 2012 [4], has been used since such configuration outperforms the 3-dimensional bubble columns and draft tube PBRs [4]. Gas holdup and bubble dynamics properties namely bubble passage frequency, chord length, bubble velocity, and interfacial area, have been measured in this study locally along the axes of the riser and the downcomer sections. The changes in the properties over the growth period of the microalgae culture due to an increase in the culture density have been studied. The effect of the superficial gas velocity on the local properties has also been analyzed.

2. EXPERIMENT

2.1 MICROALGAE CULTURE

Green fresh water algae *Scenedesmus sp.*, was selected as the strain to study. *Scenedesmus sp.* has been shown to be a good candidate for biofuel production [19], and to outperform Chlorella in removing effluents from flue gases [20], [21]. Also, the oil obtained from microalgae *Scenedesmus* meets the standards for biodiesel in terms of linolenic acid concentration, iodine value, and oxygen stability [21]. *Scenedesmus sp*. was grown in a fresh water medium using reverse osmosis (RO) water and Proline F/2 algae food, prepared according to the manufacturer's instructions. Microalgae cultures were first prepared in 1000 ml Erlenmeyer flasks under room temperature and pressure conditions, and then transferred to the studied split airlift reactor.

2.2 EXPERIMENTAL SETUP

The split airlift PBR used in this study is schematically shown in Figure 2.1 [4], [Paper I]. The reactor consisted of an acrylic column with an inside diameter of 13 cm, and a 105 cm split plate in the middle, dividing the column in two equal halves – the riser and the downcomer. A ring-type sparger with a diameter of 5 cm, and 1mm openings along its circumference was installed at the bottom of the riser to introduce compressed air. The reactor had a working liquid volume of 15 liters. The airflow rate in the reactor was maintained by a calibrated rotameter for superficial gas velocities of 1.0, 2.0, 2.8 cm/s, based on the cross-sectional area of the riser. These velocities are based on the study by Luo and Al Dahhan, 2012 [4], as superficial gas velocities higher than 3.0 cm/s

in a reactor of the dimensions mentioned above causes too much turbulence and increases the shear stress on the microalgae cells. The riser and the downcomer sections were equipped with 5 ports each, 24 cm apart, along the axis of the reactor. These ports provided for local measurements of local gas holdup, bubble dynamics, and interfacial area of green, fresh water algae *Scenedesmus* which was the liquid medium in the reactor. A bank of 12 cool white fluorescent grow lights (*Agrobrite* T5, 54W, 6400K) were used to provide the light necessary for growth and photosynthesis of the algae culture inside the PBR. These lights do not cause excessive heating effects, and were thus, used for microalgae culturing as it is greatly affected by temperature fluctuation. The lights were arranged symmetrically around the reactor, at a distance of 0.5 m from the reactor's surface.

2.3 PHOTOBIOREACTOR OPERATION

The split airlift photobioreactor (Figure 2.1) was operated in batch mode at room temperature and pressure conditions. First, the reactor was filled with fresh water algae growth medium (RO water and Proline F/2 algae food). Compressed air was introduced in the sparger by means of a calibrated rotameter. Flow rate of air enriched with 3% CO_2 was adjusted to obtain the studied superficial gas velocities of 1.0, 2.0, and 2.5 cm/s based on the cross-sectional area of the riser. The dynamic height of the liquid for each studied superficial gas velocity was always maintained at 122 cm above the base of the reactor. This was done in order to have a constant top clearance between the dynamic liquid height and the top flange of the PBR, which has been shown to affect the bubble dynamic properties in airlift reactors [4]. Next, the reactor was inoculated with algae

Scenedesmus sp. amounting to 150 ml, or 1% of the reactor volume. After adjusting the dynamic liquid height, the reactor was operated at a low superficial gas velocity of 0.5 cm/s for 14 hours under normal room light to allow the algal species to acclimatize, following which the superficial gas velocity to be studied was adjusted. Then, all the lights were turned on to illuminate the surface of the reactor with an average surface illumination of 350 $\mu E/m^2s$. A four-point optical fiber probe technique explained in Paper I, and originally adapted from Xue, 2003 [18] was used for this purpose. Gas holdup and interfacial area were measured at all the 10 ports in the reactor for the following 10 days. Although the microalgae culture inside the reactor continued to grow past the 10 days, for up to 22 days, after 10 days, microalgae was seen to accumulate on the tips of the optical fiber probe used for local measurements, rendering it unusable. The optical density, viscosity, and surface tension of the liquid media were also measured regularly.

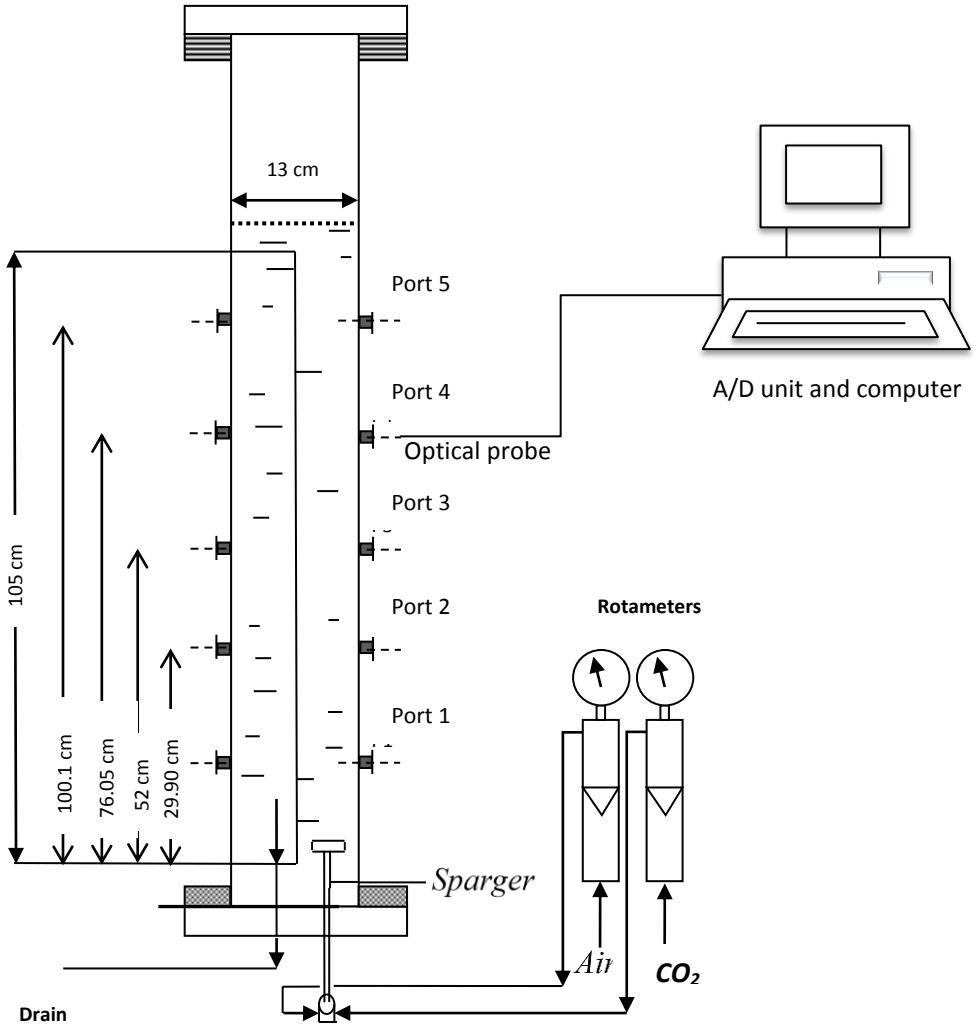

Figure 2.1: Schematic representation of split airlift PBR

3. MEASUREMENT TECHNIQUES

3.1 GAS HOLDUP AND BUBBLE DYNAMICS

To investigate the local gas holdup and bubble dynamic properties inside the split airlift reactor, a four-point optical probe technique originally developed by Xue et al., 2003 [18], and schematically shown in Figure 3.1, was employed. In literature, this technique has been applied successfully applied in bubble columns for local measurements of these properties [22], [23], [Paper I]. It consists of a four-point optical fiber probe, a light source, and a photodiode to detect the light reflected back by the probe tip. Light from the source travels through the optical fibers to the probe tip, and due to the difference in the refractive indices of the liquid and gas phases, only half the light is reflected back by when the tip is in contact with the liquid phase, while all of it is reflected back when the tip is in contact with the gas phase.

The probe tips were always positioned to face the oncoming bubble, that is, downwards in the riser, and upwards in the downcomer. The reflected light detected by the photodiode was converted into voltage signals and an algorithm developed by Xue et al., 2003 [18] was used to process the data to calculate the local gas hold-up and bubble dynamic properties at the different axial locations in the split airlift PBR. At each studied superficial gas velocity, an average of three measurements at the radial center of each of the axial locations in the riser and the downcomer was used.

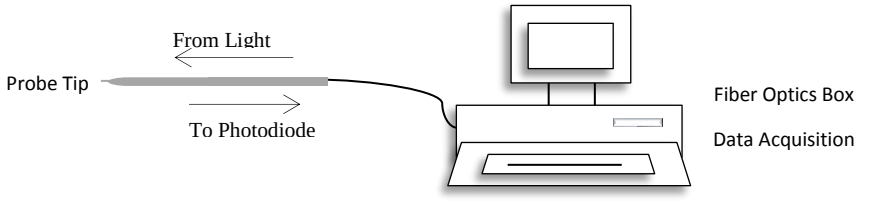

(a)

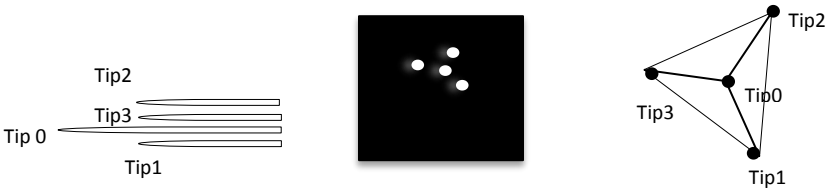

(b)

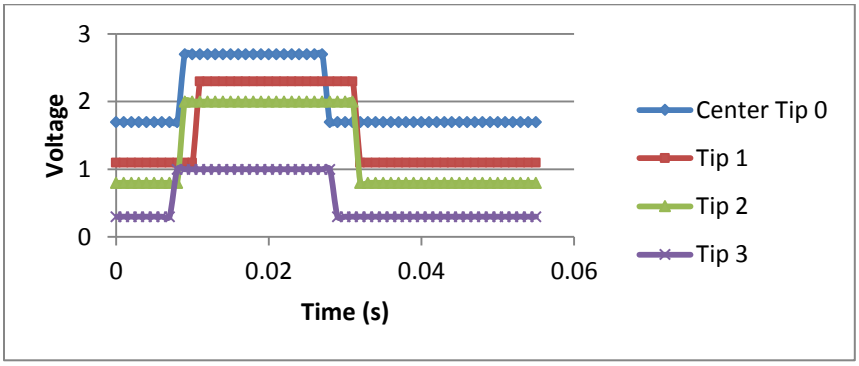

(c)

Figure 3.1: 4-Point optical fiber probe technique (Paper I)
(a) Schematic representation of the 4-point optical fiber probe technique
(b) Schematic representation of the probe tip
(c) Typical response of a bubble striking the probe tip

Xue et al., 2003 [18] calculated the local gas holdup based on the time spent by the tip in the gas phase (T_G) versus the total measurement time (T).

$$\varepsilon_g = \frac{T_G}{T} \tag{1}$$

To account for all the bubbles hitting the tip, local gas holdup can be estimated as given in Equation (2).

$$\varepsilon_g = \frac{\sum (v_i . t_{G,i})}{\sum (v_i . (t_{G,i} + t_{L,i}))} \tag{2}$$

Where, v_i is the velocity of the i^{th} gas-liquid interface (bubble leading phase), $t_{G,i}$ is the time interval that the probe tip spends in the i^{th} gas (bubble), $t_{L,i}$ is the time interval that the probe tip spends in the i^{th} liquid [18].

For interfacial area measurement, Xue et al., 2003 [18] modified the interfacial area equation developed by Kataoka et al., 1986 [24] (Equation (3) to account for the bubbles that hit the center tip, but miss the others. This is given in Equation (4).

$$a = \frac{1}{\Delta T} \sum_N \frac{1}{V \cos\phi} \tag{3}$$

$$a = \frac{1}{\Delta T} \sum_N \frac{1}{V \cos\phi} \cong \frac{1}{\Delta T} \frac{N}{N_{measured}} \sum_{N_{measured}} \frac{1}{V \cos\phi} \tag{4}$$

$$N = N_{measured} + N_{missed}$$

In Equation (4), V is the magnitude of the bubble velocity vector, N is the total number of the gas-liquid interfaces passing the probe in time, ΔT and ϕ is the angle between the velocity vector and the normal vector of the interface (bubble's surface).

Details for the measurement of bubble chord length and bubble velocity have been presented in Xue et al., 2003 [18].

3.2 LIQUID-PHASE PROPERTIES

A 100 ml algae sample was withdrawn from the top of the reactor, about 10 cm below the liquid level once a day for measuring the liquid-phase properties such as optical density, viscosity, and surface tension. To maintain a constant dynamic liquid height, the same amount of the growth medium was added to the reactor every time a sample was withdrawn from it. The sample was divided into three parts for the measurement of optical density, viscosity, and surface tension, explained as follows:

3.2.1 Optical Density. Optical density is a commonly used parameter to assess the growth of a microalgae species. It is based on the amount of light that is retarded by a medium. A Thermo Spectronic 20+ spectrometer with cuvettes of a path length of 1 cm was used to measure the optical density of the sample at 660 nm. Three samples were taken to measure the optical density of the culture. The standard deviation of the samples was observed to be low, and hence an average of the three readings was recorded.

3.2.2 Viscosity and Surface Tension. Owing to the increase in the optical density of a culture due to growth, the viscosity and surface tension of the medium also change. DV1 digital viscometer by Brookfield was used to measure the viscosity of the culture. Surface tension of the culture was measured using a Sensadyne Surface Tensiometer.

4. RESULTS AND DISCUSSION

The changes in the optical density, viscosity, and surface tension of the microalgae culture were recorded as it grew in density for a period of 10 days. As mentioned earlier, to monitor these changes, a 100 ml sample was withdrawn from the top of the reactor for viscosity and optical density measurements. The local gas holdup and interfacial area in the riser and the downcomer were also measured at the 10 axial ports. Also, it should be noted that since, at each superficial gas velocity, the rate of increase in the culture density was different an exact match of the optical density for gas holdup and other bubble dynamics properties was not possible. The results obtained are as discussed below.

4.1 THE CHANGE IN OPTICAL DENSITY WITH MICROALGAE GROWTH

Optical density measurement of the culture denotes the photosynthetic growth of the culture over time. An increase in the superficial gas velocity in the reactor increases mixing and agitation, and also, improves the circulation of microalgae cells between the illuminated surface and the darker interiors of the reactor. Also, higher superficial gas velocities are associated with higher mass transfer. However, very high superficial gas velocities lead to a lot of turbulence inside the reactor, increasing shear stress on the cells which can potentially rupture the cells and stunt growth. Thus, a trade off needs to be achieved such that the superficial gas velocity is sufficient to keep the culture well mixed to prevent settling and achieve proper movement of cells between the well-lit exterior and the dark interior of the PBR, and to avoid the effects of photoinhibition and

photolimitation. The increase in optical density was studied at each superficial gas velocity as a reference for the intensity of microalgae growth, and is shown in Figure 4.1.

As the microalgae cells grow and multiply the optical density of the medium increases. For the first couple of days, the optical density of the culture was not significantly different at all the three studied superficial gas velocities. The rate of increase of the optical density was low up to day 3 and higher after that. Therefore, for the purpose of evaluation and analysis, the growth period of 10 days was divided into three zones based on three optical density ranges. Zone I was for the optical density increase up to 0.08, Zone II is from optical density of 0.08 to 0.19, and Zone III is from optical density of 0.19 to 0.30. In Zone I, there was no significant difference between the optical densities at superficial gas velocities 1.0 and 2.0 cm/s. The optical density at 2.8 cm/s was the same at the beginning of Zone I, and was 55% higher than that at 1.0 and 2.0 cm/s. In Zone II, the optical densities at superficial gas velocities at 2.0 and 2.8 cm/s were not significantly different from each other, and were 21% higher than those at 1.0 cm/s. Similar to Zone I, no significant difference in the optical density values was observed between the two higher superficial gas velocities of 2.0 and 2.8 cm/s in Zone III, while that at superficial gas velocity of 1.0 cm/s was 13% lower by the end of Zone III.

4.2 THE CHANGE IN SURFACE TENSION AND VISCOSITY WITH MICROALGAE GROWTH

The surface tension of the sample was found to be close to that of water at all times, in all the three Zones. Surface tension varied from ~ 0.071-0.0726 N/m. No

significant change in surface tension of the algae culture was observed during the course of the experiment.

The microalgae culture was observed to have a Newtonian behavior over the studied conditions. Figure 4.2 shows the variation of viscosity over the growth of microalgae with optical density. Higher optical densities imply higher cell growth increasing the viscosity of the medium. The rate of change of viscosity was higher at the lower optical densities in Zone I (up to optical density of 0.08), and Zone II (optical density 0.08-0.19), while becoming almost zero in Zone III (optical density 0.19-0.30). The viscosity of the medium increased by 19% in Zone I, by 28.5% in Zone II, and remained the same in Zone III.

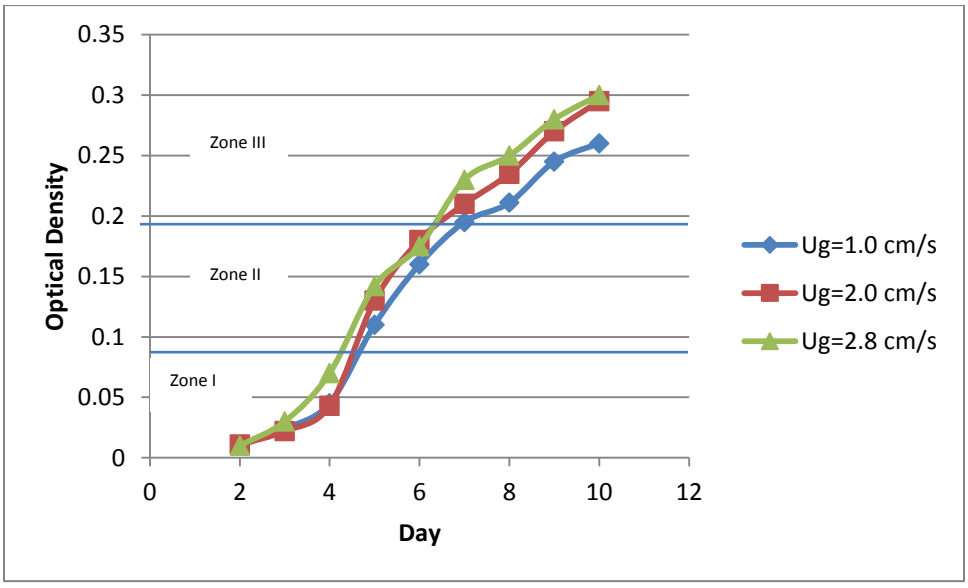

Figure 4.1: Optical density variation at different superficial gas velocities

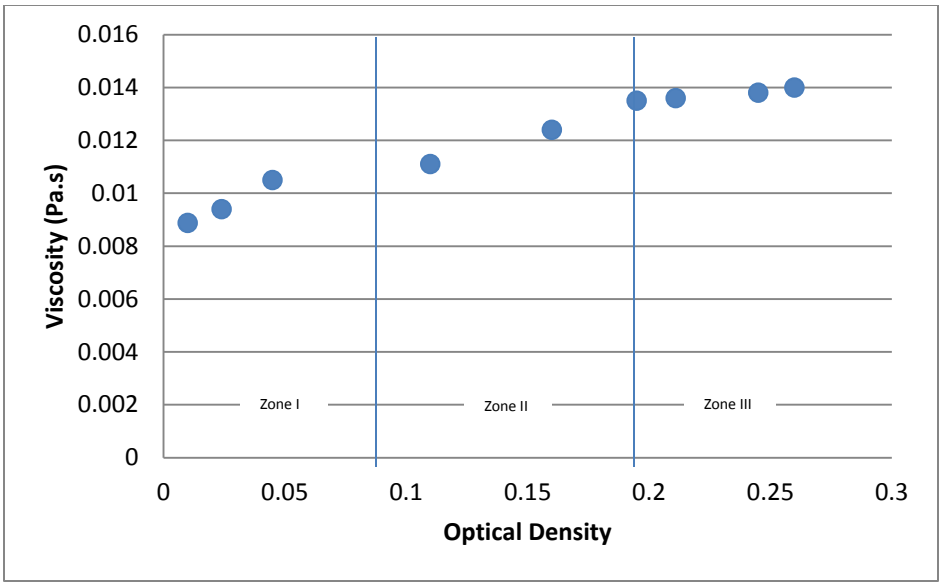

Figure 4.2: Increase in viscosity with optical density of the culture

4.3 BUBBLE PASSAGE FREQUENCY

At each optical density measurement, the bubble frequency in the column was measured at the axial ports in the riser and the downcomer sections at the studied superficial gas velocities of 1.0, 2.0, and 2.8 cm/s (based on the riser cross-sectional area).

4.3.1 Bubble Passage Frequency in the Riser. In the riser, no significant axial variation of bubble passage frequency was observed at the radial center. The variation of the riser bubble passage frequency at different superficial gas velocities in the three zones is shown in Figure 4.3. Also, increasing the superficial gas velocity increases the gas throughput in the reactor leading to an increase in the number of bubbles, and thus, the bubble passage frequency. These findings are similar to those found in literature [Paper I]. Also, as can be seen from Figure 4.3, as the optical density of the microalgae culture increased the bubble frequency decreased over the entire growth period of 10 days, across

all the three zones, at each superficial gas velocity. The decrease in the bubble frequency with an increase in the optical density of the culture can be attributed to decrease in mixing in higher optical density and viscosity solutions. Bubble passage frequency in airlift reactors, especially for microalgae systems, is rarely studied in literature. Some researchers have evaluated the effect of change in the viscosity of the liquid on the bubble passage frequency. Since an increase in optical density leads to a consequent increase in viscosity of the medium (Figure 4.2), thus, the results of this study have been found to be similar to those found in literature. Esmaeili et. al., 2016 [25] studied non-Newtonian liquids with different viscosities in a bubble column, and found the bubble frequency of the lesser viscous liquids to be higher than the ones with a higher viscosity. Similar results were observed by Kuncova and Zahradnik, 1995 [26], in a Newtonian Saccharose solution in a bubble column. The decrease of bubble frequency in higher viscosity solutions was mainly due to increased viscous forces on bubbles promoting bubble coalescence. Also, the effect of increase in optical density on the bubble passage frequency was higher at higher superficial gas velocity. In Zone I, bubble passage frequency did not vary significantly at superficial gas velocity of 1.0 cm/s. It decreased by 9.5%, and 11.6 % at velocities of 2.0 and 2.8 cm/s, respectively. In Zone II, the bubble passage frequency decreased almost linearly by 28.5% at 1.0 cm/s, and 13% at 2.0 cm/s. At superficial gas velocity of 2.8 cm/s, the bubble passage frequency in Zone II remained about constant at a 12% lower value than that at the end of Zone I. In Zone III, bubble passage frequency decreased by 37% at the superficial gas velocity of 1.0 cm/s. At the higher velocities of 2.0, and 2.8 cm/s, the bubble passage frequency did not vary significantly, with averages of 3241 and 4667 bubbles/second, respectively.

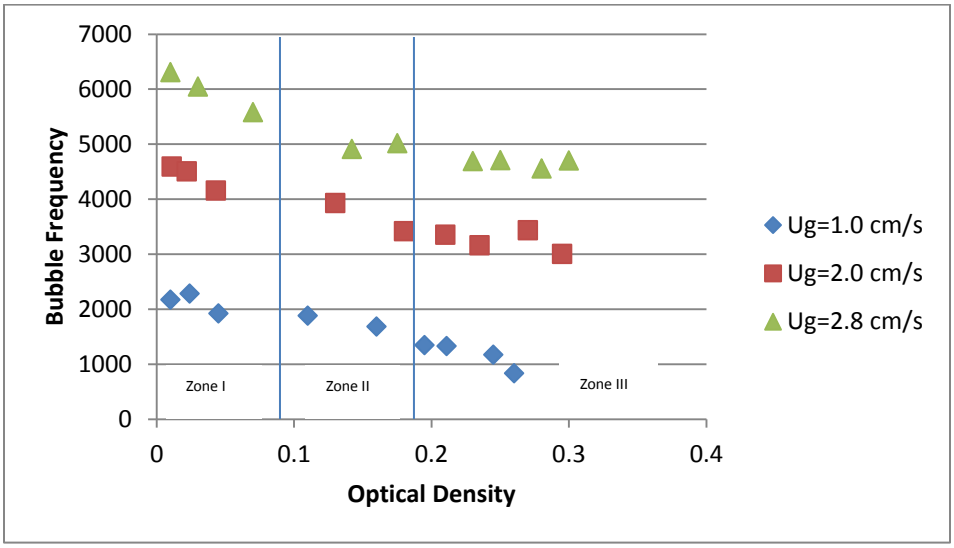

Figure 4.3: Variation of bubble frequency with optical density in the riser

4.3.2 Bubble Passage Frequency in the Downcomer. The variation of downcomer bubble passage frequency with changes in the optical density of the medium at different superficial gas velocities is shown in Figure 4.4. The bubble frequency at higher superficial gas velocities was higher mainly due to two reasons. At higher superficial gas velocities, gas throughput and turbulence in the reactor are higher, contributing to the higher bubble passage frequency [25], [26], [Paper I]. Also, the liquid circulation velocity increases with an increase in superficial gas velocity, increasing the number of bubbles entrained by the circulating liquid, and thus the bubble passage frequency [Paper I]. However, unlike in the riser, no steady decrease in bubble passage frequency with optical density was observed in the downcomer, and it varied from one zone to another. During the initial growth period, in Zone I, the impact of increase in optical density on the bubble passage frequency was more pronounced at the higher superficial gas velocities of 2.0 and 2.8 cm/s. Towards the end of the experiment, in Zone

III, the bubble frequency at each of the studied superficial gas velocities did not change significantly with optical density.

In Zone I, the bubble passage frequency in the riser did not vary significantly at superficial gas velocities of 1.0, and 2.8 cm/s, and the average value at these velocities was 1982 and 5305 bubbles/second, respectively. It decreased linearly by 12% in Zone I at the velocity of 2.0 cm/s. At the beginning of Zone II, the bubble passage frequency was lower by 37%, 57%, and 63% from the corresponding values in Zone I, at velocities of 1.0, 2.0, and 2.8 cm/s, respectively. Through Zone II, the bubble passage frequency at 1.0 cm/s decreased by 60%, but did not vary significantly for the velocities of 2.0, and 2.8 cm/s. In fact, the bubble passage frequency in the downcomer at port 5 (Z=100 cm from the base of the reactor) was the same at the velocities of 2.0 and 2.8 cm/s. No effect of the increase of optical density due to the growth of the culture was observed on the bubble passage frequency in the downcomer in Zone II for 2.0 and 2.8 cm/s, and for all the three velocities, 1.0, 2.0, and 2.8 cm/s, in Zone III. Also, the difference in the bubble passage frequency at different superficial gas velocities diminished in Zones II and III.

In the downcomer, an axial variation in bubble frequency measured at the radial center of the downcomer was observed. The variation of bubble frequency with optical density at different axial locations in the downcomer is shown in Figure 4.5. As the liquid moves from the riser to the downcomer, some of the gas bubbles rising up in the riser are carried with the circulating liquid into the downcomer. Only the smaller bubbles descend axially downwards in the downcomer, and the bigger ones are disengaged in the separation zone at the top of the reactor. The bigger the size of the bubble, more are the buoyant forces experienced by it, and hence, only the smaller bubbles manage to flow

down the downcomer. A steep linear decrease in the bubble frequency in the downcomer was observed at ports 4 and 5, at distances 76 and 100 cm from the base of the reactor, respectively, in Zone I. The difference between the bubble frequencies at the axial locations shown in Figure 4.5 decreased as the optical density of the microalgae culture increased from Zone I to Zone III. In Zone II, while the change in optical density did not affect the bubble passage frequency at port 3 (z= 52 cm), a linear decrease was observed at axial ports 4 and 5 (z=76, and 100 cm, respectively). Also, it must be mentioned at this point that no bubbles were detected by the optical fiber probe in the downcomer below an axial height of 52 cm (Port 3) from the base of the reactor. On visual observation, very few tiny bubbles were seen to be present below z==52 cm (Port 3). They were mainly concentrated at the radial center of the downcomer, but they were too small and few in number to be detected by the probe.

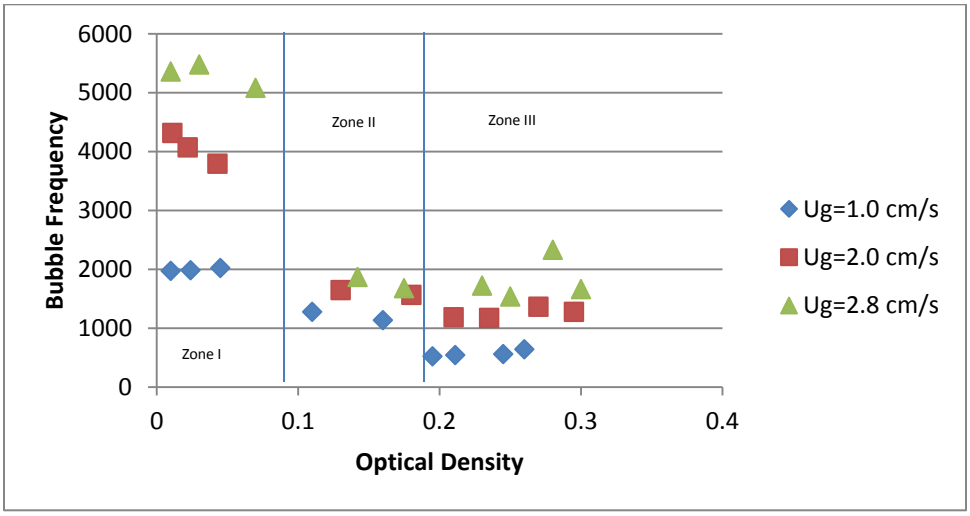

Figure 4.4: Variation of bubble frequency with optical density at Port 5 in the downcomer (z=100 cm from the reactor base)

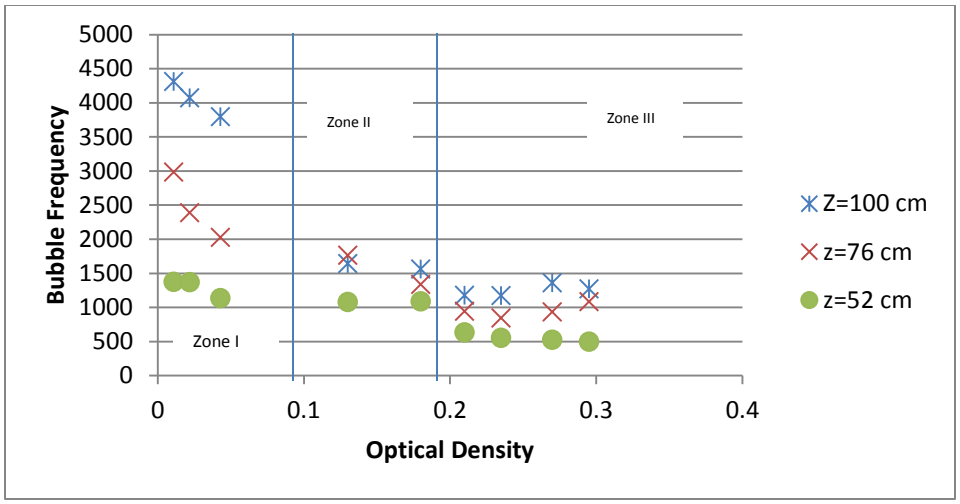

Figure 4.5: Variation of bubble frequency at different axial locations in the downcomer at Ug=2.0 cm/s

4.4 GAS HOLDUP

4.4.1 Gas Holdup in the Riser. The effect of increase in microalgae growth expressed in terms of optical density on the gas holdup in the riser at different superficial gas velocities is shown in Figure 4.6. Since the bubble frequency in the riser did not vary axially, no significant axial variation of gas holdup measured at the radial center was observed in the riser. As can be seen from Figure 4.6, gas holdup was higher at higher superficial gas velocity. The increase of gas holdup with superficial gas velocity has been commonly observed in literature [8], [9], [13], [14], [25], [27]–[29]. The increase in the gas throughput and turbulence at higher superficial gas velocities increases the bubble passage frequency and hence, the gas holdup.

Figure 4.6 also shows the variation of gas holdup with growth in microalgae leading to an increase in the optical density of the culture. The decrease in gas holdup over the entire growth period, across the three zones I, II, and III, with an increase in optical density as seen in Figure 4.6 is due to a decrease in the bubble passage frequency

and gas holdup with optical density. In the literature gas hold has been found to decrease with an increase in viscosity in various Newtonian and non-Newtonian fluids in airlift reactors, mainly due to decreased turbulence and mixing at higher viscosities, decreasing bubble interaction [9], [10], [29]. Since an increase in the optical density of the medium increases the viscosity (Figure 4.2), the results found in this study are similar to those found in literature. In these studies, the decrease in gas holdup with an increase in viscosity was explained to be mainly due to increased bubble size and decreased bubble frequency at higher viscosities. In this study as well, as is explained in sections 4.3 and 4.5, a decrease in bubble passage frequency and an increase in the mean bubble chord length was observed at higher optical densities and viscosities. Rajarajan et al., 1996 [30], found that with an increase in viscosity of the liquid, the gas holdup value in a glycerol-water solution first increased and reached a maximum, and then decreased.

Also, as can be seen from Figure 4.6, In Zone I, at superficial gas velocities of 1.0 cm/s, the gas holdup value decreased linearly by 15%, and did not vary significantly from the average value of 5.17% and 6.66% gas holdup at velocities of 2.0, and 2.8 cm/s, respectively. In Zone II, while the gas holdup values at velocities 1.0 and 2.0 cm/s decreased linearly, that at 2.8 cm/s did not vary significantly. The gas holdup at 1.0 and 2.0 cm/s in Zone II was lower than the values in Zone I, but that at 2.8 cm/s was higher by 8% than the corresponding values in Zone I. In Zone III, the gas holdup did not vary with the increase in the optical density of the medium for the velocity of 1.0 cm/s, and its average value was 2.6%. At the higher velocities of 2.0 and 2.8 cm/s, gas holdup value in the riser decreased linearly by 21.5% and 16.4%, respectively.

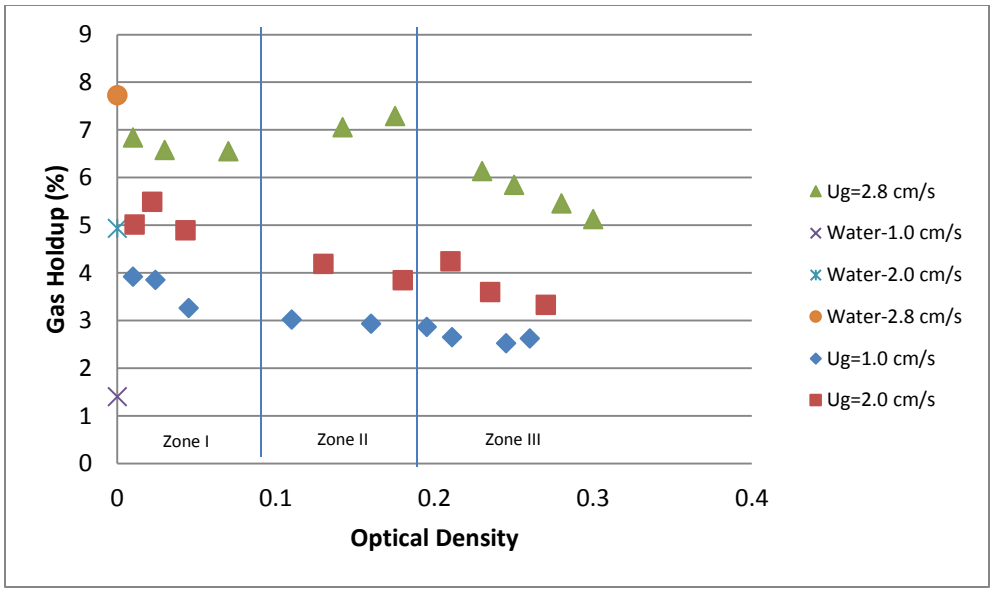

Figure 4.6: Variation of gas holdup in the riser with optical density

Figure 4.6 also gives the gas holdup of water at the three studied superficial gas velocities (optical density of 0) from Paper I. As can be seen from the figure, the gas holdup of microalgae culture at the beginning of the growth period (in Zone I) is 11.6% lower at the superficial gas velocity of 2.8 cm/s; it is almost the same at superficial gas velocity of 2.0 cm/.s; and it is 48.7% higher at 1.0 cm/s. Also, as discussed above, the gas holdup of the culture decreases with an increase in its optical density over the growth of microalgae, therefore, the use of a constant value for the air-water gas holdup for microalgae cultures can lead to erroneous results and conclusions.

Table 4.1 gives a few correlations for internal loop airlift reactors available in literature, and Figure 4.7 compares the gas holdup data observed in this study with that estimated from the given correlations. Figure 4.7 is for superficial gas velocity of 2.0 cm/s. Of all the correlations given in Table 4.1, only the ones by Chakravarty, 1973 [31], and Kawase, 1998[11] account for the change in medium properties, such as viscosity

and surface tension. All the other correlations in Table 4.1 are based only on the superficial gas velocity, and hence they gave a constant value of gas holdup at a given superficial gas velocity and fail to account for any changes due to changes in properties of the medium. The correlation given by Blazej, 2004 [32] was a whole magnitude higher than the highest observed gas holdup value in the riser, while that given by Chakravarty, 1973 [31] was a magnitude lower. The correlation given by Chisti, 1988 [33] is able to predict the gas holdup in the microalgae culture during the initial growth phase (Zone I), however, since it does not account for any changes in the medium properties, it fails to account for the change in gas holdup in the riser as the microalgae culture grows and its optical density increases in Zones II, and III. Figure 4.7 further stresses the limitations of existing correlations and the need to carry out local measurements in real culturing medium.

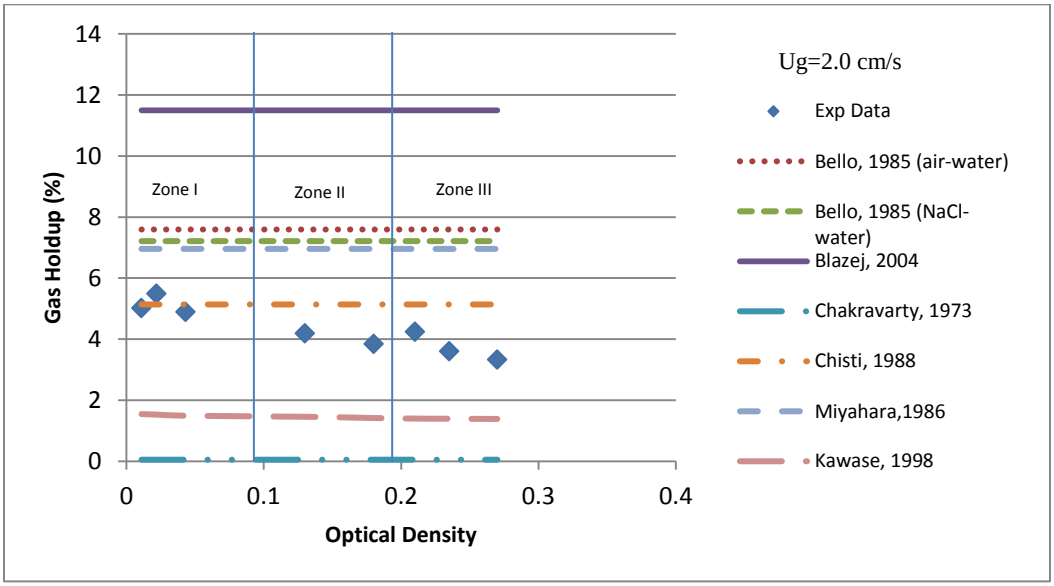

Figure 4.7: Comparison of gas holdup in the riser at U_g=2.0 cm/s with correlations given in Table 4.1

Due to the inability of the correlations available in literature, an attempt was made to quantify the limited data available for the variation in gas holdup with optical density at superficial gas velocities 1.0, 2.0, and 2.8 cm/s. The correlation given in Equation (5) accounts for the effect of change in superficial gas velocity and optical density of microalgae *Scenedesmus*. Figure 4.8 shows that the correlation given in Equation (5) satisfactorily depicts the riser gas holdup observed in this study. The average absolute relative error (AARE) was 5.5% was achieved for the developed correlation. Despite the low AARE for the developed correlation, it was developed based on a limited set of data, and hence, more experimental data is needed to further improve this investigation.

$$\in_{gr} = \left(25982 * U_{gr}^{2} - 971.56 * U_{gr} + 2.0917\right) * O.D. + (170.9 * U_{gr} + 2.0067) \quad (5)$$

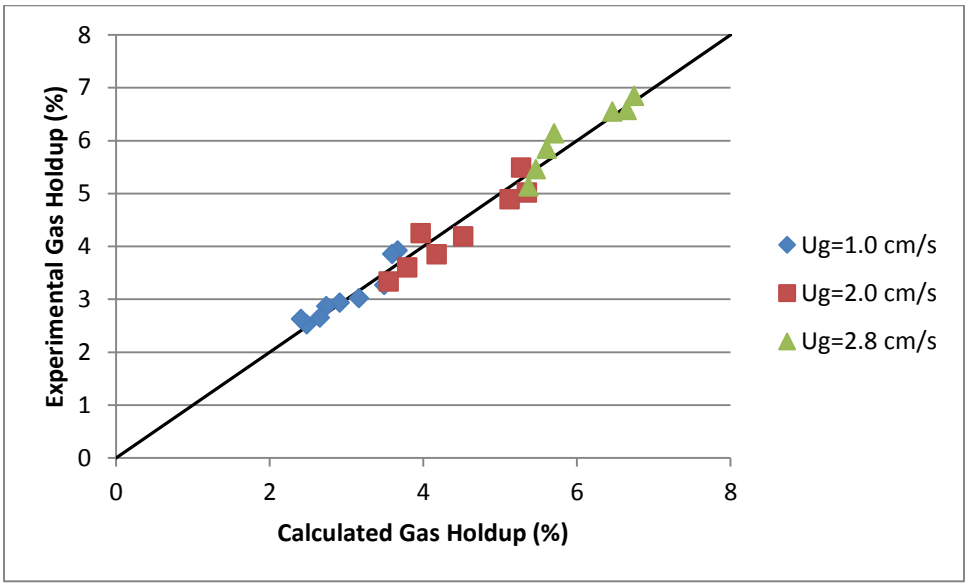

Figure 4.8: Comparison of experimental gas holdup with the developed correlation

Table 4.1: Literature reported correlations for overall gas holdup, ε_g
(Subscript 'r' denotes the riser and 'd' denotes the downcomer)

Reference	Parameters	Correlation
Bello et al., 1985 [34]	Air - Water/NaCl solution A_d/A_r = 0.11-0.69	$\epsilon_{gr} = 0.16 * \left(\frac{U_{gr}}{U_l}\right)^{\alpha} (1 + \frac{A_d}{A_r})$ $\epsilon_{gd} = 0.89 * \epsilon_r$ $\alpha = 0.56\ for\ water$ $\alpha = 0.58\ for\ NaCl\ solution$
Blazej et al., 2004 [32]	Air – Water Reactor Volume : 10.5 L A_d/A_r = 1.23	For 10.5 L $\epsilon_{gr} = 0.829 * {U_{gr}}^{0.505}$ $\epsilon_{gd} = 0.875 * \epsilon_{gr} - 0.0095$
Chakravarty et al., 1973 [31]	$\epsilon_{gr} = \left[(\mu_l - \mu_w)^{2.75} + 161\frac{(73.3-\sigma)}{(74.1-\sigma)}\right] x10^{-4} U_{gr}^{0.88}$ $\epsilon_{gd} = 1.23x\left[\frac{(74.2-\sigma)}{(79.3-\sigma)}\right] x10^{-2} x U_{gr}^{0.88} (\frac{A_r}{A_d})^{1.08} {\mu_l}^{0.45}$	
Chisti et al., 1988 [33]	A_d/A_r = 0.25 -0.44	$\epsilon_{gr} = 0.65 * U_{gr}^{0.603} (1 + \frac{A_d}{A_r})^{-0.258}$ $\epsilon_{gd} = 0.46 * \epsilon_{gr} - 0.0244$
Miyahara et al., 1986 [12]	Air – Non-Newtonian Sols A_d/A_r = 0.128 – 0.808	$\epsilon_{gr} = \frac{0.4\sqrt{Fr}}{1 + 0.4\sqrt{Fr}(1 + \frac{U_l}{U_{gr}})}$ $Fr = \frac{(U_{lr} + U_{gr})^2}{g d_r}$
Kawase et al., 1998 [11]	$\frac{\epsilon_{gr}}{1-\epsilon_{gr}} = \frac{(\frac{U_{gr}}{n})^{(n+2)/(2(n+1))}}{2^{\frac{3n+5}{n+1}} \left(\frac{g^n k}{\rho_l}\right)^{\frac{1}{2(n+1)}} (1 + \frac{A_d}{A_r})^{3(n+2)/4(n+1)}}$ N=1 for Newtonian fluids; K= viscosity of fluid	

4.4.2 Gas Holdup in the Downcomer. Similar to the trend observed in the riser the gas holdup in the downcomer was found to be higher at higher superficial gas velocities. Figure 4.9 depicts this phenomenon. In the downcomer, only the smaller bubbles were transported down the downcomer along with the circulating liquid, and the bigger bubbles were disengaged in the separation zone at the top of the reactor. An increase in superficial gas velocity increases the liquid circulation velocity and the number of bubbles. This further increases the number of bubbles being entrained by the liquid circulating in the downcomer, thus increasing gas holdup in the downcomer at higher superficial gas velocities.

Gas holdup in the downcomer decreased with an increase in microalgae growth and optical density. In Zone I, the gas holdup at velocities 1.0 and 2.8 cm/s decreased by 13% and 7.6 %, respectively, and was almost constant at the velocity of 2.0 cm/s. In Zone II, gas holdup decreased by 43%, 16.5%, and 7.5% at velocities 1.0, 2.0, and 2.8 cm/s, respectively. In Zone III, the gas holdup value remained constant at a value of 1.68% for velocity of 1.0 cm/s, and decreased by 58%, and 28% for velocities of 2.0, and 2.8 cm/s, respectively. The decrease in gas holdup at each superficial gas velocity in Zones II and III was more than the corresponding decrease in Zone I because of higher optical densities in Zones II and III. At higher optical densities the number of bubbles being entrained by the circulating liquid decreased leading to a decrease in gas holdup. Also, the combined effects of buoyancy and the resistance to flow at higher optical density (and thus higher viscosity) of the medium, makes the flow of the bubbles downwards through the downcomer more difficult. As a result, it was also observed that when the optical density of the medium was high, there was increased bubble coalescence in the separation

zone at the top of the reactor, and a lot of bubbles could be visibly seen popping and escaping the surface of the liquid from the top.

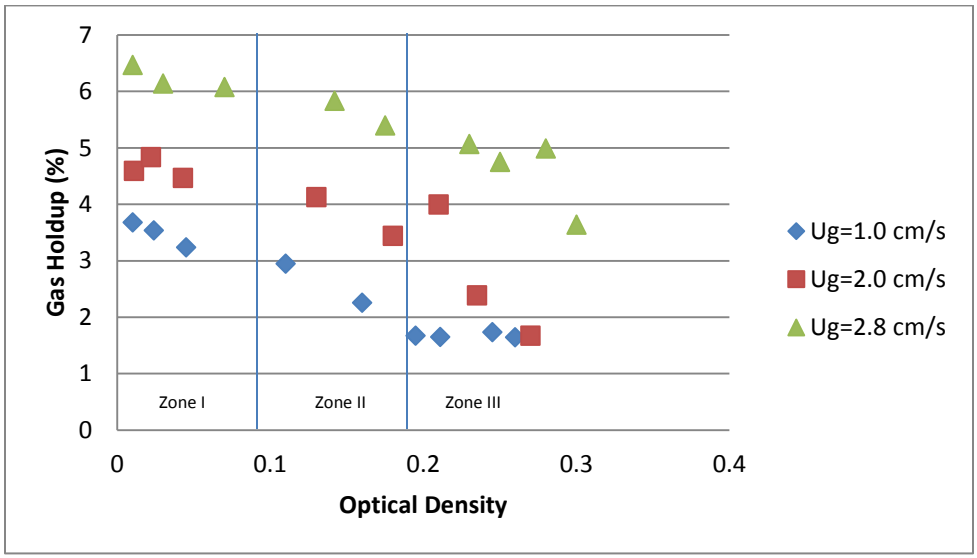

Figure 4.9: Variation of gas holdup in the downcomer with optical density at Port 5 (z=100cm, form the base of the reactor)

In addition to the above findings, an axial decrease in gas holdup was observed in the downcomer. This variation at superficial gas velocity of 2.0 cm/s can be observed in Figure 4.10, which gives the variation of gas holdup with optical density at three different axial locations, ports 5, 4, and 3 in the downcomer (z=100, 72, 52 cm, from the base of the reactor). In Zone I, gas holdup decreased by 14%, 10%, and 13.5% at distances of 52, 76, 100 cm from the base of the reactor, corresponding to ports 3, 4, and 5, respectively. In Zone II this decrease was 21.7%, 23%, and 28% at the three ports, respectively. At the top of the downcomer, at z=100 cm from the base of the reactor (Port 5), the overall decrease in gas holdup over all the three zones is much more than at z=76 and 52 cm

(Ports 4 and 3). This may be due to the proximity of port 5 to the separation zone where larger bubbles were seen to escape the liquid phase. The gas holdup in Zone III did not vary at any of the three ports. It was visually observed that only the smaller bubbles travelled axially downwards with the circulating liquid in the downcomer, which explains this decrease in the gas holdup values. This decrease may thus be attributed to the combined effects of buoyancy and bubble size. This trend of axial variation in the downcomer has been found to be similar to the one found in air-water system in Paper I. A similar trend was seen at the superficial gas velocities of 2.0 and 2.8 cm/s.

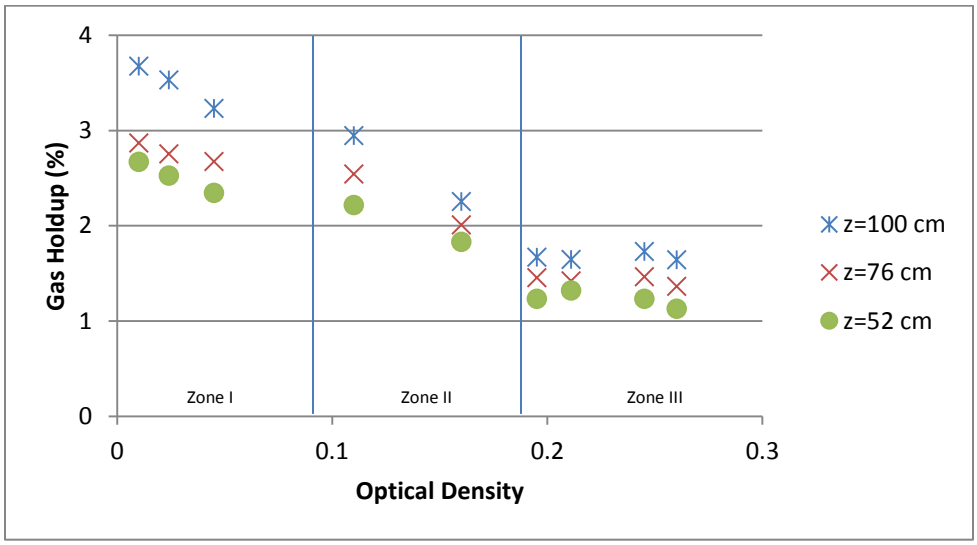

Figure 4.10: Variation of gas holdup at different axial locations in the downcomer at Ug=2.0 cm/s

Again, a comparison of the local gas holdup in the downcomer with the correlations given in Table 4.1 is given in Figure 4.11. Similar to the comparison for the riser gas holdup, the gas holdup predicted by the correlations given by Bello, 1985 [34],

Blazej, 2004 [32], Chakravarty, 1973 [31], and Miyahara, 1986 [12] did not come close to predicting the downcomer gas holdup at any of the axial locations. In Zone I, the gas holdup measured at Port 3 (z=52 cm from the base) in the downcomer was the same as predicted by Chisti, 1988 [33], while the values of gas holdup at Ports 4, and 5 (Z=76, 100 cm from the base respectively) in the downcomer were 21.7% and 49.6% higher. However, as the gas holdup at each axial location decreased with an increase in optical density of the microalgae culture the trend was different in Zones II and III. Towards the end of Zone II, the gas holdup values at the end of Zone II at the ports was within the range predicted by Chisti, 1988 [33] and Kawase, 1998 [11]. In Zone III, the gas holdup at ports 3 and 4 (z=52, 76 cm) was almost the same as that obtained from Kawase, 1998, while the values of gas holdup at port 5 (Z= 100 cm) was slightly higher by 13%. Despite the fact that the gas holdup values observed in the downcomer in this study fell within the range predicted based on Chisti, 1988 [33] and Kawase, 1998 [11], no correlation was able to account for the change in gas holdup due to growth and the change in the properties of the microalgae culture.

In Paper I, it was shown that the gas holdup in the downcomer is directly affected by that in the riser. Hence, a correlation to predict the change in the downcomer gas holdup based on the holdup in the riser, and also account for the axial variation was developed. It is given in Equation (6).

Equation (6) was developed mainly to facilitate the use of local gas holdup values for the calculation of mass transfer coefficient in the mass transfer study in Paper IV. The experimental data was always within 18% deviation of that calculated by the correlation in Equation (6) at velocities of 1.0, 2.0, and 2.8 cm/s. These correlations have been

developed based on a very limited set of experimental data and must not be treated as comprehensive correlations. Figure 4.12 compares the downcomer gas holdup at 1.0 cm/s.

$$\epsilon_{gdi} = \left(a_1 * \frac{z_i^2}{h} + a_2 \frac{z_i}{h} + a_3\right) \epsilon_r - \left(a_4 * \frac{z_i}{h}^2 + a_5 \frac{z_i}{h} + a_6\right) \quad (6)$$

Table 4.2: Values of coefficients for correlation of gas holdup in the downcomer (Equation (6))

U_g (cm/s)	a_1	a_2	a_3	a_4	a_5	a_6	α	β
1.0	4.8	-5.53	2.63	-13.13	16.38	-6.35	0.0049	0.1862
2.0	1.79	-1.8	1.57	-3.67	3.77	-2.65	0.0042	0.1911
2.8	-1.78	2.068	0.5295	18.38	-21.38	3.68	0.0026	0.1545

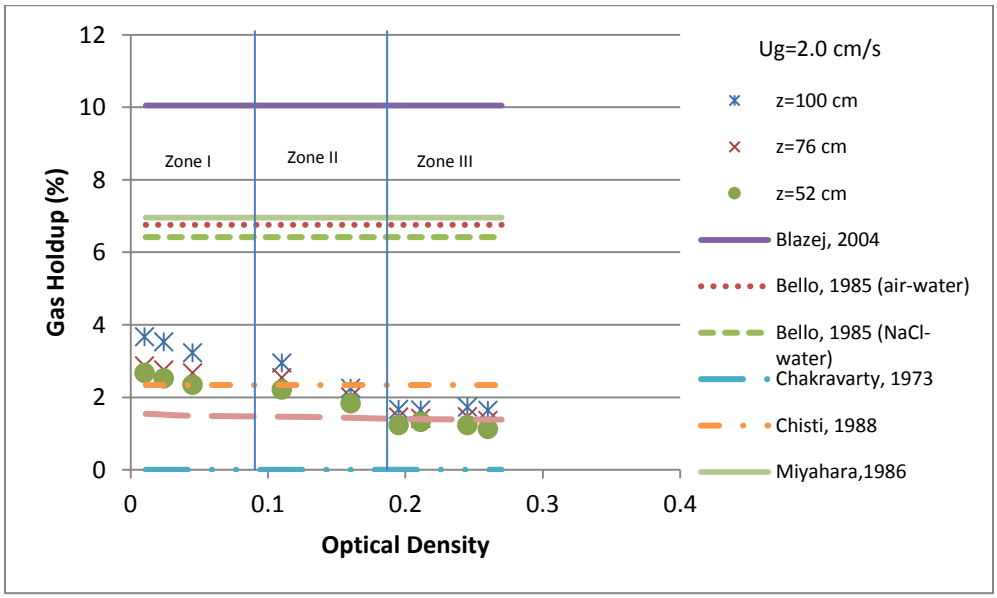

Figure 4.11: Comparison of gas holdup at different axial locations in the downcomer with correlations in Table 4.1 at Ug=2.0 cm/s

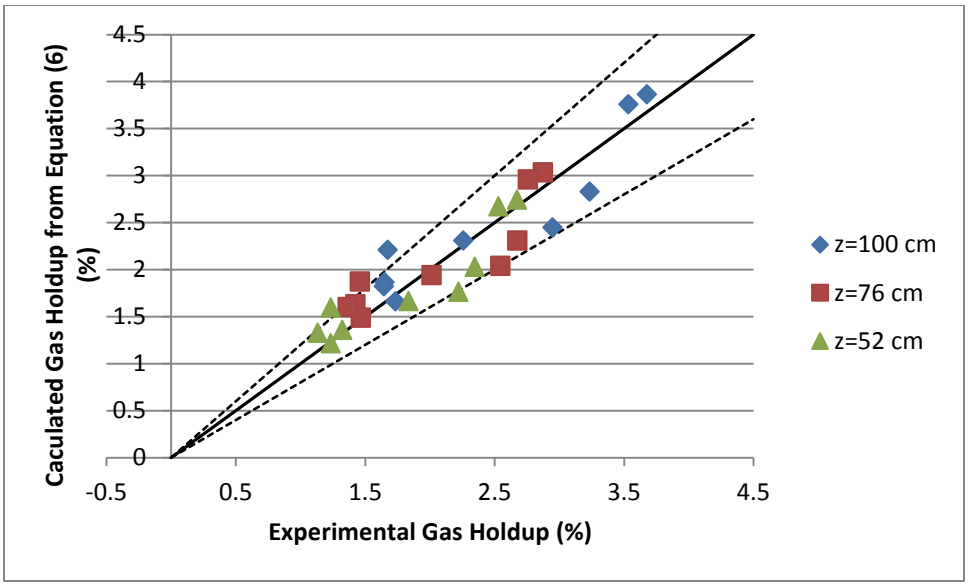

Figure 4.12: Comparison of experimental gas holdup in the downcomer with the developed correlation

4.5 BUBBLE CHORD LENGTH

The size and shape of a bubble in an airlift reactor depends on the physical properties of the liquid, reactor configuration and operating conditions, and the type of gas distributor [35], [36]. Due to the presence of swarm of bubbles in airlift reactors, and the lack of reliable techniques to measure their size, bubble size is usually studied as bubble chord length distribution [22].

Bubble chord length distribution is studied through a lognormal distribution [22], [37]. Such a distribution consists of a probability distribution of chord length of disintegrated small bubbles as well as large coalesced bubbles [22].

The bubble chord length distribution at the middle of the riser at different superficial gas velocities is given in Figure 4.13. Table 4.3 gives the mean and the variance of the bubble chord length distribution at optical density of 0.12 (Zone II). With

an increase in the superficial gas velocity, the mean and variance of the distribution increase. Similar results have been found in literature [Paper I], [38], [39].

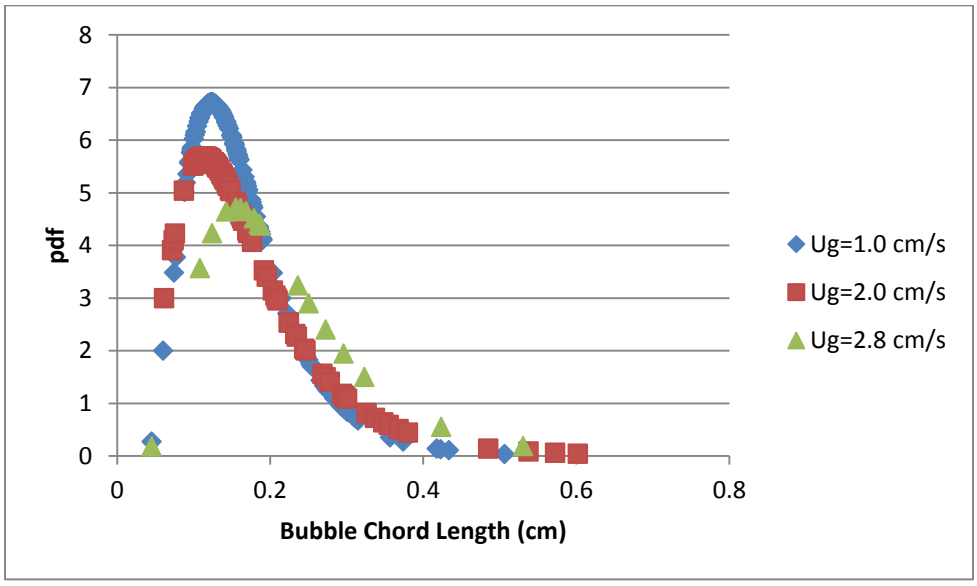

Figure 4.13: Bubble chord length distribution in riser at optical density=0.12 (Zone II)

In homogenous regimes, the effect of bubble breakup and coalescence on bubble chord length distribution is seen to negligible, and it is mainly affected by the liquid viscosity [10]. Figure 4.14 shows the bubble chord length distribution at the superficial gas velocity of 2.0 cm/s in Zones I, II, and III, at the optical densities of 0.01, 0.12, 0.27, corresponding to viscosities of 0.009, 0.0128, 0.014 Pa.s, respectively. On moving from Zone I towards Zone III, with an increase in optical density, the mixing intensity decreases while the drag force on the bubbles increases, increasing the mean bubble size and distribution. Also shown in Figure 4.14, the mean and the standard deviation of the bubble chord length distribution in pure water was greater than that of the microalgae

culture in all the three zones. The higher mean and variance in water may be due to the lower optical density, and hence lower viscosity of water, resulting in a wider distribution.

Table 4.3: Mean and Variance of bubble chord length distribution in the riser at optical density= 0.12 (Zone II)

Riser	Mean (cm)	Variance (cm^2)
U_g = 1.0 cm/s	0.164	0.006
U_g = 2.0 cm/s	0.175	0.011
U_g = 2.8 cm/s	0.221	0.013

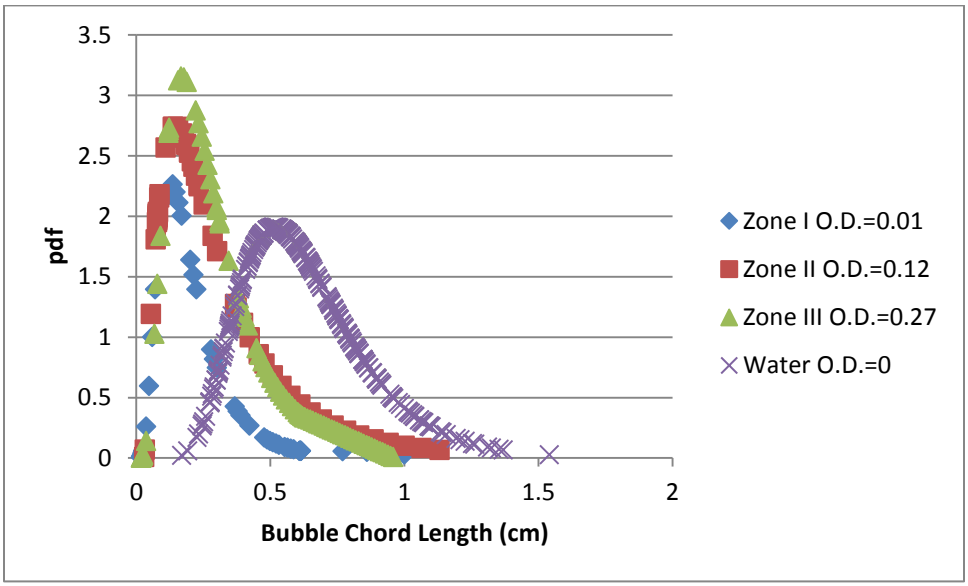

Figure 4.14: Bubble chord length distribution in riser at superficial gas velocity 2.0 cm/s

The bubble chord length distribution in the downcomer at z=100 cm (Port 5) from the base of the reactor is shown in Figure 4.15. As the bubbles descending down the downcomer decreased both in number and in size, the optical probe could not gather enough data, and hence the chord length distribution shown in Figure 4.15 is for z=100 cm (Port 5).

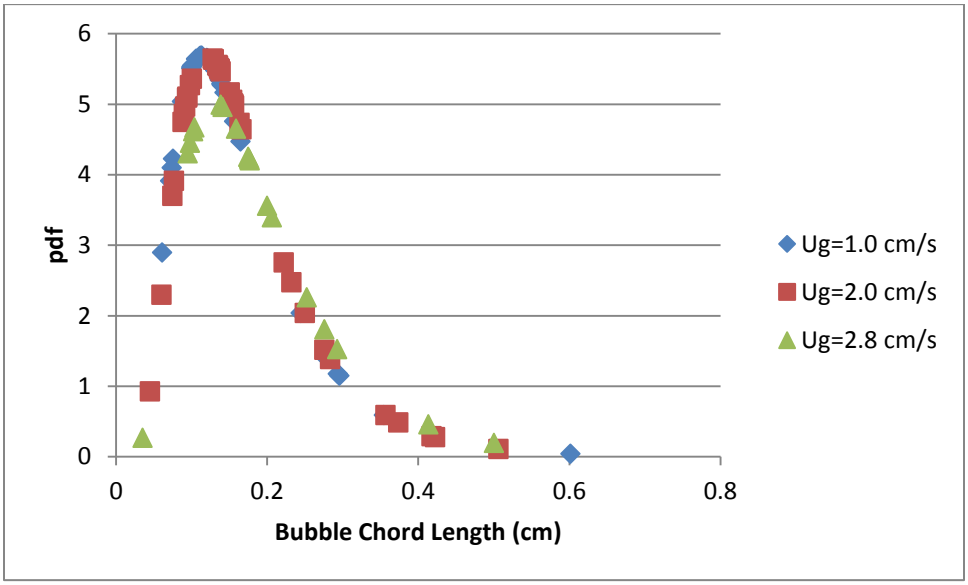

Figure 4.15: Bubble chord length distribution in downcomer at Port 5 (z=100cm, form the base of the reactor) optical density= 0.12(Zone II)

Similar to the riser, the mean and the variance of the distribution in the downcomer increased with the superficial gas velocity, but not to the same extent. The effect of superficial gas velocity on the chord length distribution in the downcomer was much less than that observed in the downcomer. This can be attributed to the fact that at higher velocities more number of bubbles is entrained by the circulating liquid, but even the buoyant forces acting on the bubbles are higher at higher gas velocities. The mean

and variance of the bubble chord length in the downcomer at optical density of 0.12 (Zone II), and at z=100cm (Port 5) from the base of the reactor is given in Table 4.4.

Figure 4.16 gives the bubble chord length distribution in the downcomer at port 5 (z=100 cm from the reactor base) at three optical densities of 0.01, 0.12, and 0.27 in Zones I, II, and III, respectively. The effect of change in optical density of the culture on the chord length distribution in the riser is not significant; however, it differs considerably from the chord length distribution at the same location for air-water system. The mean and the variance of the distribution in air-water are much higher than that in the microalgae culture, again possibly due to lower optical density and viscosity of water. Higher viscosity increases the viscous forces on the bubbles, further reducing bubble frequency and interaction among bubbles, resulting in a narrower distribution.

Table 4.4: Mean and Variance of bubble chord length distribution in the downcomer at optical density= 0.12 (Zone II), at Port 5 (z=100cm, form the base of the reactor)

Riser	Mean (cm)	Variance (cm^2)
U_g = 1.0 cm/s	0.152	0.010
U_g = 2.0 cm/s	0.171	0.011
U_g = 2.8 cm/s	0.196	0.013

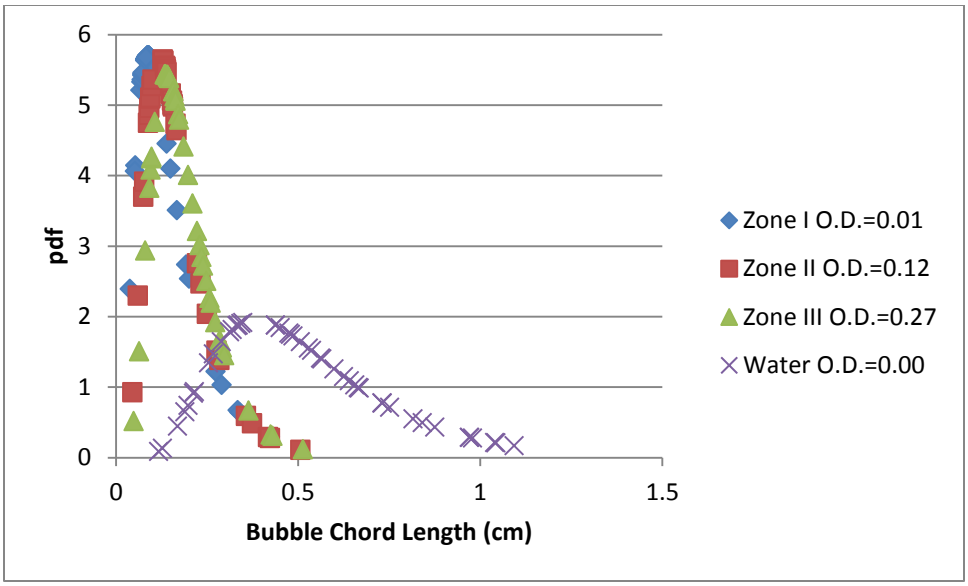

Figure 4.16: Bubble chord length distribution in downcomer Port 5 (Z=100 cm) at superficial gas velocity 2.0 cm/s

4.6 BUBBLE RISE VELOCITY

Bubble rise velocity is an important parameter to be studied for gas-liquid interaction as it affects the residence time and holdup of the gas phase. In microalgae cultures in airlift reactors, the carbon needed for growth and photosynthesis is transferred from the gas phase to the liquid, and hence, the bubble rise velocity can provide an important insight into the interaction between the two phases. The correlations to calculate the bubble rise velocity available in literature are based on single bubbles, and hence cannot be extrapolated to airlift reactors [22].

Bubble rise velocity is usually studied as a probability distribution function [23]. Figure 4.17 shows the bubble rise velocity in the riser middle. As was expected, the mean bubble rise velocity value increased with an increase in superficial gas velocity, and the distribution became wider. This trend is similar to that found in literature [Paper I] [10]. This increase in bubble rise velocity is thought to be due to the increase in the number of

bubbles with an increase in superficial gas velocity, consequently decreasing the drag force on the bubbles, and increasing the bubble rise velocity [10]. The mean and the variance of the bubble rise velocity at an optical density of 0.12 (Zone II) are given in Table 4.5. The higher variance at higher gas velocities denotes a decrease in the fraction of bubbles at higher bubble rise velocities [Paper I].

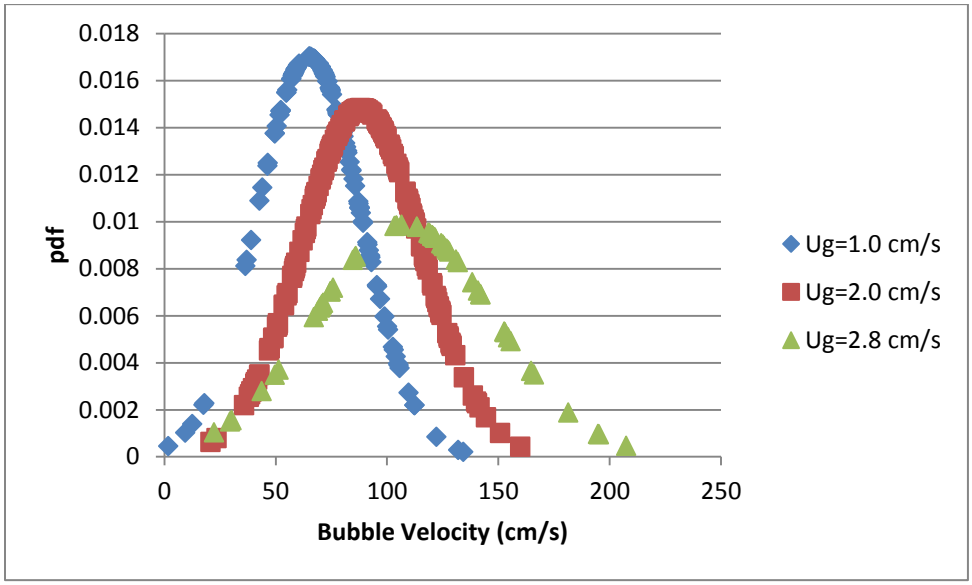

Figure 4.17: Bubble rise velocity distribution in the riser at optical density=0.12 (Zone II)

Table 4.5: Mean and Variance of bubble rise velocity distribution in the riser at optical density=0.12

Superficial Gas Velocity	Mean (cm/s)	Variance $(cm/s)^2$
U_g = 1.0 cm/s	64.947	549.675
U_g = 2.0 cm/s	88.415	723.715
U_g = 2.8 cm/s	107.874	1631.336

Bubble rise velocity is directly proportional to bubble size, and is said to increase with the increase in liquid viscosity, due to an increase in bubble size [10], [25].Thus, the increase in viscosity due to an increase in the optical density of the medium explains the increase in the mean bubble velocity. The effect of increase of optical density of the medium on the bubble rise velocity is shown in Figure 4.16, in Zones I, II, and III, at the optical densities of 0.01, 0.12, 0.27, corresponding to viscosities of 0.009, 0.0128, 0.014 Pa.s, respectively. Increase in the optical density of the microalgae culture increases the mean and the variance of the distribution. As mentioned earlier, since the bubble rise velocity is directly affected by the bubbles size, therefore, the higher mean bubble size for pure water (optical density of 0.00) than that observed in Zone III (optical density =0.27) in the microalgae culture (Figure 4.14) lead to a higher mean bubble velocity in water than that observed in the microalgae culture.

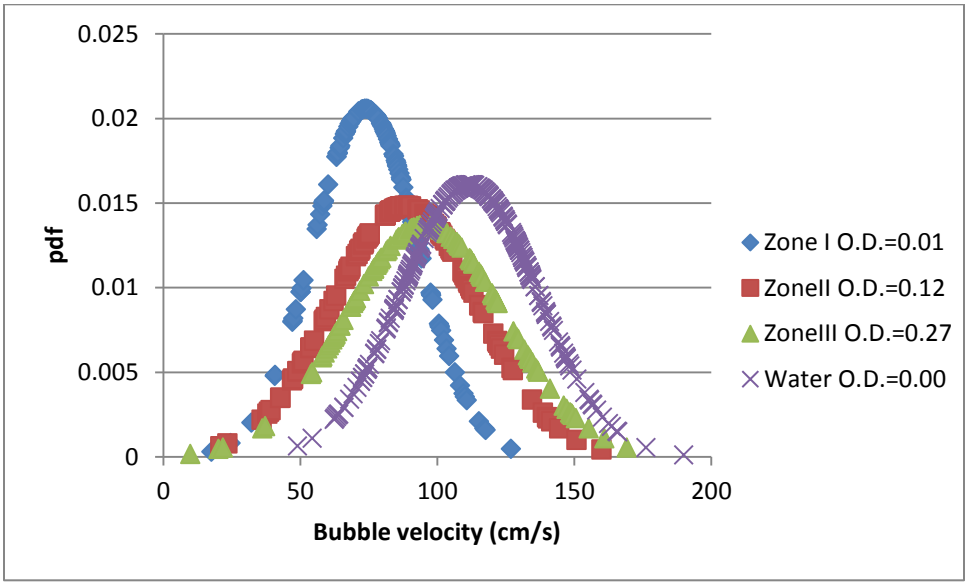

Figure 4.18: Bubble rise velocity distribution in the riser at different optical densities in the three zones

To measure the bubble dynamics properties in the downcomer, the tip of the optical fiber probe was positioned upwards to face the down flowing bubbles. Thus, the bubble velocity reported for the downcomer is the downward bubble velocity.

The downward bubble velocity distribution in the downcomer is given in Figure 4.19. The liquid circulation velocity increases with an increase in the superficial gas velocity, and thus more bubbles are entrained by the circulating liquid, and they flow at a faster rate. This increases the mean downward bubble velocity at higher gas velocities [Paper I]. Table 4.6 gives the mean and variance of the downward bubble velocity at z=100 cm (Port 5) in the downcomer.

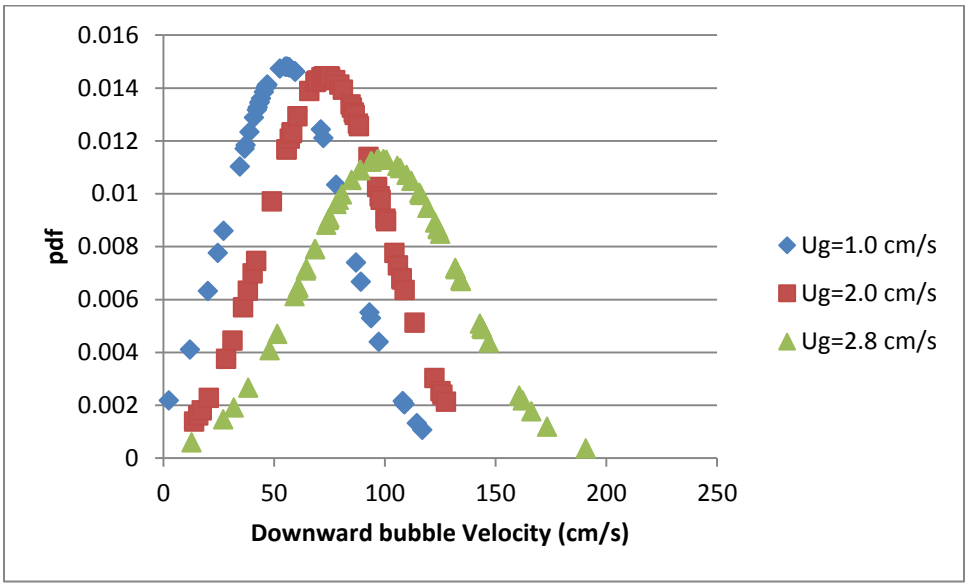

Figure 4.19: Downward bubble velocity distribution in downcomer at Port 5 (z=100cm, form the base of the reactor), and optical density of 0.12 (Zone II)

Table 4.6: Mean and Variance of downward bubble velocity distribution in the riser at optical density=0.12 (Zone II)

Superficial Gas Velocity	Mean (cm/s)	Variance $(cm/s)^2$
U_g = 1.0 cm/s	55.20	726.08
U_g = 2.0 cm/s	73.63	762.85
U_g = 2.8 cm/s	98.30	1246.39

No significant effect of optical density was observed on the downward bubble velocity, and is shown in Figure 4.20, in Zones I, II, and III, at the optical densities of 0.01, 0.12, 0.27, corresponding to viscosities of 0.009, 0.0128, 0.014 Pa.s, respectively. This can be attributed to two opposing effects. On one hand, the increase in the liquid circulation velocity with superficial gas velocities aids the downward flow of the bubbles, while on the other the increase in buoyancy due to increased bubble size at higher optical densities (and thus higher viscosities) opposes it. Also, the mean of the downward bubble velocity was higher in water than that observed in the microalgae culture in the three zones. This, again, can be attributed to the lower optical density, and hence, the viscosity of water as compared to that of the microalgae culture, causing the bubble to flow at relatively higher velocities.

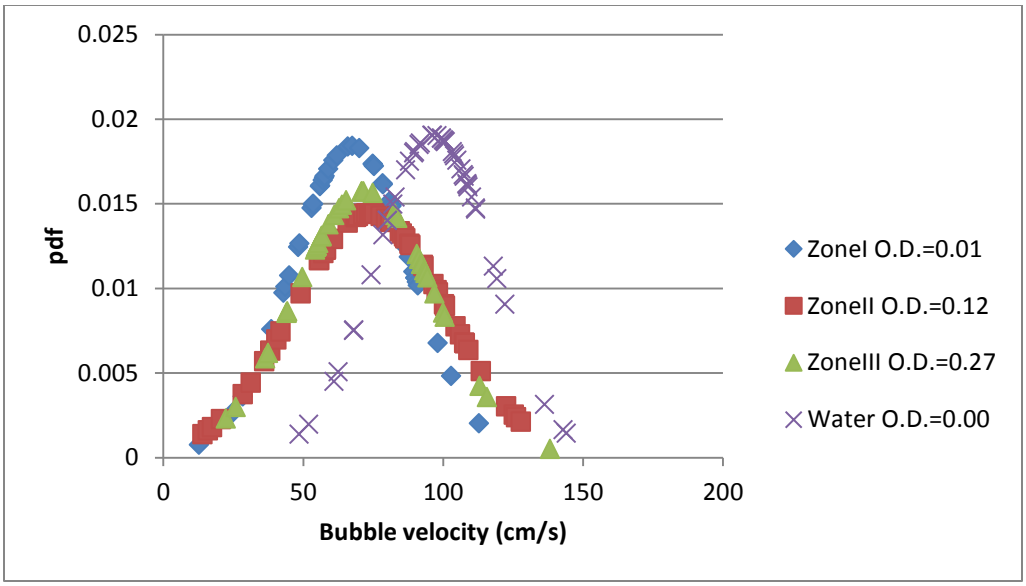

Figure 4.20: Effect of optical density on the downward bubble velocity distribution in downcomer at Port 5 (z=100cm, form the base of the reactor) at Ug=2.0 cm/s

4.7 INTERFACIAL AREA

4.7.1 Interfacial Area in the Riser. Interfacial area is an important parameter directly affecting the mass transfer between the gas and the liquid phases, and is especially important in culturing microalgae and cyanobacteria. Interfacial area was seen to increase with superficial gas velocity, and this trend for the riser is shown in Figure 4.21. Interfacial area is directly affected by gas holdup, and thus, the increase in gas holdup with superficial gas velocity (Figure 4.7) warrants an increase in the interfacial area. The interfacial area at higher gas velocities was always observed to be higher. This can be attributed to the increase in the bubble passage frequency and gas holdup with superficial gas velocity [Paper I] [29]. The effect of increased superficial gas velocity on the interfacial area in the riser was much more pronounced at lower fluid optical density (in Zones I and II). In Zone I, the interfacial area values at velocities 2.0 and 2.8 cm/s were higher than that at 1.0 cm/s by 35.7% and 120.6%, respectively. In Zone III, the

interfacial area values at 2.0 and 2.8 cm/s were the same, however, the value at 1.0 cm/s was 30% lower than them. Similar to the riser gas holdup, no statistically significant difference was observed in the axial the interfacial area in the riser.

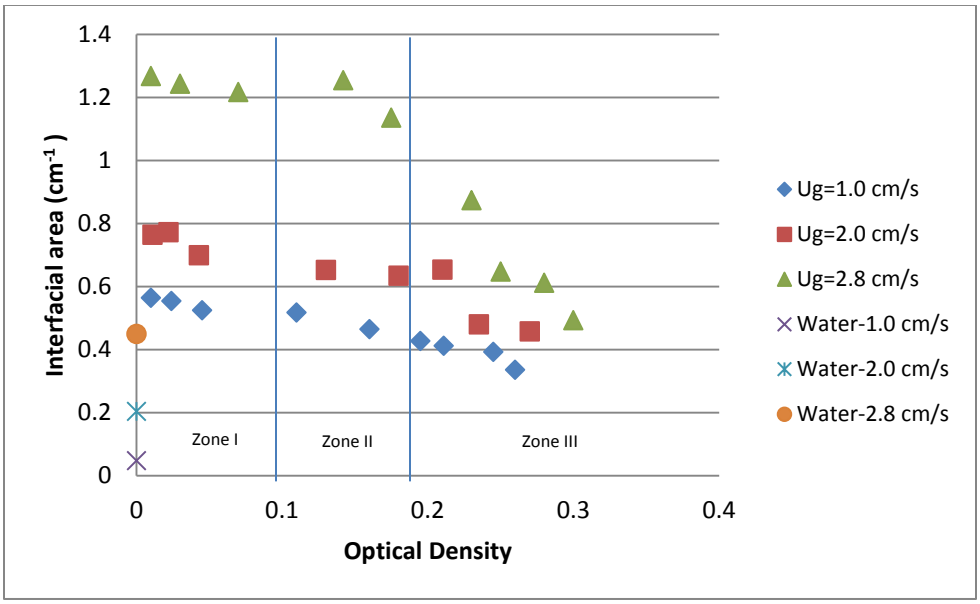

Figure 4.21: Variation of interfacial area in the riser

Figure 4.21 also shows the effect of optical density of the culture on the riser interfacial area across the three zones. Interfacial area decreased with an increase in optical density at by about 10% in Zone I at all the superficial gas velocities. In Zones II, the decrease in interfacial area with optical density was 17%, and 9% at superficial gas velocities of 1.0, and 2.8 cm/s, respectively, while the interfacial area at 2.0 cm/s remained constant at an average value of 0.64/cm. In Zone III, a decrease of 21%, 27%, and 43.7% at superficial gas velocities of 1.0, 2.0, and 2.8 cm/s, respectively was observed. The decrease in interfacial area with increase in the viscosity of the medium is

also found in literature [29]. Interfacial area is directly affected by bubble passage frequency and gas holdup in the medium. Since both these properties were seen to decrease with an increase in optical density and viscosity (Figures 4.3 and 4.6, respectively) of the medium, interfacial area decreased as well.

The interfacial area for water at the three superficial gas velocities [Paper I], is also shown in Figure 4.21. At the beginning of the culture (Zone I), the interfacial area of microalgae system was much higher than that of water. Over the growth period of microalgae in the reactor, the interfacial area dropped, and was almost the same as that of water at the end of Zone III at the superficial gas velocity of 2.8 cm/s. At velocities of 2.0 and 1.0 cm/s, however, even at the end of the growth period, the interfacial area of the culture was 55.3%, and 83.6% higher than the corresponding values for water, respectively.

4.7.2 Interfacial Area in the Downcomer. The interfacial area in the downcomer at different superficial gas velocities is shown in the Figure 4.22. Similar to the trend observed in the riser, the interfacial area values were higher at higher gas velocities. Higher superficial gas velocities result in higher bubble passage frequency and gas holdup and as a result increase the interfacial area.

In Zone I, the interfacial area at superficial gas velocity of 1.0 cm/s was constant at an average value of 0.52/cm, while that at, 2.0 and 2.8 cm/s decreased by 10%. In Zone II, the interfacial area value in the downcomer decreased with an increase in the optical density of the medium. At port 5 (z=100 cm from the base of the reactor), interfacial area decreased by 52%, 17%, and 8% at superficial gas velocities of 1.0, 2.0, and 2.8 cm/s. The decrease in the downcomer interfacial area with an increase in optical density in all

the three zones is similar to that observed in the riser. In Zone III, the interfacial area decreased by 47.6%, 13%, and 34.7%.

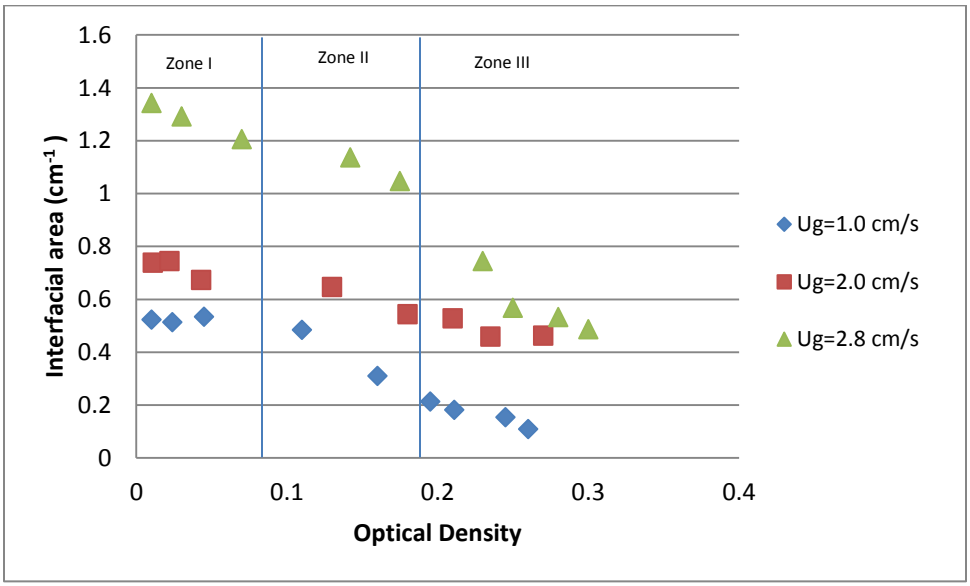

Figure 4.22: Variation of interfacial area with superficial gas velocity in the downcomer Port 5 (z=100cm, form the base of the reactor)

Contrary to the observation in the riser, a significant axial variation of interfacial area values was observed in the downcomer. As can be seen from Figure 4.23, and similar to the trend of gas holdup in the downcomer, the interfacial area in the downcomer decreased axially down the downcomer. Due to the buoyant forces acting on the gas bubbles, the number of the holdup and the number of gas bubbles decreased along the axis of the downcomer. This decrease can be seen in all the three zones as the optical density increases. In Zone I, interfacial area at port 3 (z=52 cm) decreased by 12.7%, was constant at port 4 (z=76 cm), and decreased by 9.5% at port 5 (z=100 cm). A higher decrease in interfacial area values was observed in Zone II, at 18%, 22%, and 21%, at

ports 3, 4, and 5, respectively. In Zone II, the decrease was 22.7%, 26%, and 13%, for the three ports. Again, since very few small bubbles were observed towards the bottom of the downcomer, no valid data for measurements was gathered at locations below z=52 cm.

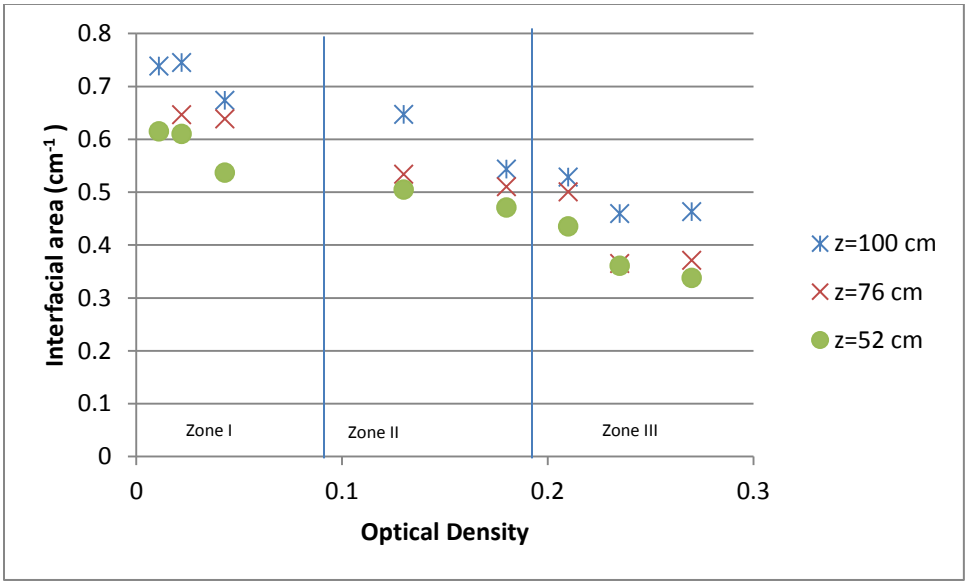

Figure 4.23: Axial variation of interfacial area in the downcomer at Ug=2.0 cm/s

5. REMARKS

Microalgae *Scenedesmus* was successfully grown in a split airlift PBR at three different superficial gas velocities of 1.0, 2.0, 2.8 cm/s. The viscosity of the medium increased with increase in the optical density, but no change in the medium's surface tension, which was always close to that of water, was observed. A four-point optical fiber probe was successfully employed in the *Scenedesmus* culture inside the split airlift PBR to study the local gas holdup, and bubble dynamics for 10 days during the growth period. Measurements beyond the 10 days duration were not possible due to the algae cells sticking to the tips of the probe, rendering the probe unfit. Therefore, for future work it is recommended that the fiber optic probe be coated with a substance that would inhibit the accumulation and sticking of the microalgae cells on the tip. The local bubble passage frequency, gas holdup, and interfacial area were seen to increase with an increase in the superficial gas velocity in both the riser and the downcomer sections. There was no significant variation in the axial properties in the riser, however, an axial variation in these properties was observed in the downcomer. The mean and the variance of the bubble chord length and bubble velocity distribution were found to increase with increase in superficial gas velocity. The increase in the optical density and viscosity of the microalgae culture due to growth was seen to affect the measured properties. At each superficial gas velocity, bubble passage frequency, gas holdup, and interfacial area decreased with an increase in the optical density, and the viscosity of the medium. The effect of superficial gas velocity on the gas holdup and interfacial area was greater during the earlier growth periods, at lower optical densities of the medium. The gas holdup and

interfacial area of the microalgae system was found to be different from that of air-water system. This observation emphasizes the continuing need to study these parameters in real culturing medium.

Also, as a first attempt, new correlations to account for the change in gas holdup with the increase in optical density were developed in the riser and downcomer. The axial variation of gas holdup was also accounted for in the downcomer correlation. Though these correlations satisfactorily depicted the data measured in this study, they need to be improved by carrying more experiments, for longer durations and at more superficial gas velocities.

REFERENCES

[1] A. S. Mirón, A. C. Gómez, F. G. Camacho, E. M. Grima, and Y. Chisti, "Comparative evaluation of compact photobioreactors for large-scale monoculture of microalgae," *Prog. Ind. Microbiol.*, vol. 35, no. C, pp. 249–270, 1999.

[2] M. Cuaresma, M. Janssen, C. V??lchez, and R. H. Wijffels, "Horizontal or vertical photobioreactors? How to improve microalgae photosynthetic efficiency," *Bioresour. Technol.*, vol. 102, no. 8, pp. 5129–5137, 2011.

[3] C. Posten, "Design principles of photo-bioreactors for cultivation of microalgae," *Eng. Life Sci.*, vol. 9, no. 3, pp. 165–177, 2009.

[4] H. P. Luo and M. H. Al-Dahhan, "Airlift column photobioreactors for Porphyridium sp. culturing: Part I. effects of hydrodynamics and reactor geometry," *Biotechnol. Bioeng.*, vol. 109, no. 4, pp. 932–941, 2012.

[5] B. Wang, C. Q. Lan, and M. Horsman, "Closed photobioreactors for production of microalgal biomasses," *Biotechnol. Adv.*, vol. 30, no. 4, pp. 904–912, 2012.

[6] Y. Chisti, *Airlift Bioreactors*. Elsevier, New York, 1989.

[7] C.-S. Lo and S.-J. Hwang, "Local hydrodynamic properties of gas phase in an internal-loop airlift reactor," *Chem. Eng. J.*, vol. 91, no. 1, pp. 3–22, 2003.

[8] M. K. Moraveji, M. M. Pasand, R. Davarnejad, and Y. Chisti, "Effects of surfactants on hydrodynamics and mass transfer in a split-cylinder airlift reactor," *Can. J. Chem. Eng.*, vol. 90, no. 1, pp. 93–99, 2012.

[9] E. Molina Grima, a Contreras, and Y. Chisti, "Gas holdup, liquid circulation and mixing behaviour of viscous newtonian media in a split-cylinder airlift bioreactor," *Food Bioprod. Process.*, vol. 77, no. March, pp. 0–5, 1999.

[10] Z. Deng, T. Wang, N. Zhang, and Z. Wang, "Gas holdup, bubble behavior and mass transfer in a 5m high internal-loop airlift reactor with non-Newtonian fluid," *Chem. Eng. J.*, vol. 160, no. 2, pp. 729–737, 2010.

[11] Y. Kawase, M. Tsujimura, and T. Yamaguchi, "Gas hold-up in external-loop airlift bioreactors," vol. 12, pp. 21–27, 1995.

[12] T. Miyahara, M. Hamaguchi, Y. Sukeda, and T. Takahashl, "Size of bubbles and liquid circulation in a bubble column with a draught tube and sieve plate," *Can. J. Chem. Eng.*, vol. 64, no. 5, pp. 718–725, Oct. 1986.

[13] A. Rengel, A. Zoughaib, D. Dron, and D. Clodic, "Hydrodynamic study of an internal airlift reactor for microalgae culture," *Appl. Microbiol. Biotechnol.*, vol. 93, no. 1, pp. 117–129, 2012.

[14] B. D. Fernandes, A. Mota, A. Ferreira, G. Dragone, J. A. Teixeira, and A. A. Vicente, “Characterization of split cylinder airlift photobioreactors for efficient microalgae cultivation,” *Chem. Eng. Sci.*, vol. 117, pp. 445–454, 2014.

[15] H. P. Luo and M. H. Al-Dahhan, “Airlift column photobioreactors for Porphyridium sp. culturing: Part II. verification of dynamic growth rate model for reactor performance evaluation,” *Biotechnol. Bioeng.*, vol. 109, no. 4, pp. 942–949, 2012.

[16] L. Luo and J. Yuan, “Modeling of mass transfer in an internal loop airlift reactor,” *Chem. Eng. Technol.*, vol. 38, no. 3, pp. 511–520, 2015.

[17] C. U. Ugwu, H. Aoyagi, and H. Uchiyama, “Photobioreactors for mass cultivation of algae,” *Bioresour. Technol.*, vol. 99, no. 10, pp. 4021–4028, 2008.

[18] R. F. Xue, J., Al Dahhan, M.H., Dudukovic, M.P., Mudde, “Bubble dynamics measurements using four-point optical probe,” *Can. J. Chem. Eng.*, vol. 81, pp. 375–381, 2003.

[19] L. Gouveia and A. C. Oliveira, “Microalgae as a raw material for biofuels production,” *J. Ind. Microbiol. Biotechnol.*, vol. 36, no. 2, pp. 269–274, 2009.

[20] J. R. Miranda, P. C. Passarinho, and L. Gouveia, “Bioethanol production from Scenedesmus obliquus sugars: The influence of photobioreactors and culture conditions on biomass production,” *Appl. Microbiol. Biotechnol.*, vol. 96, no. 2, pp. 555–564, 2012.

[21] P. D. V. Makareviciene, V. Andrulevičiūtė, V. Skorupskaitė, and J. Kasperovičienė, “Cultivation of Microalgae Chlorella sp. and Scenedesmus sp. as a Potentional Biofuel Feedstock,” *Environ. Res. Eng. Manag.*, vol. 57, no. 3, pp. 21–27, 2011.

[22] A. A. Youssef, “Fluid dynamics and Scle-up of bubble columns with internals,” Washington University, Saint Louis, 2010.

[23] M. Kagumba and M. H. Al-dahhan, “Impact of Internals Size and Con fi guration on Bubble Dynamics in Bubble Columns for Alternative Clean Fuels Production,” 2015.

[24] A. Kataoka, I., Ishii, M., Serizawa, “Local Formulation and measurements of interfacial area concentration in two-phase flow,” *Int. J. Multiph. Flow*, vol. 12, pp. 505–529, 1986.

[25] J. Esmaeili, A., Guy, C., Chaouki, “Local hydrodynamic parameters of bubble column reactors operating witj non-Newtonian liquids: Experiments and model development,” *AIChE J.*, vol. 62, no. 4, pp. 1382–1396, 2016.

[26] G. Kuncová and J. Zahradník, “Gas holdup and bubble frequency in a bubble column reactor containing viscous saccharose solutions,” *Chem. Eng. Process. Process Intensif.*, vol. 34, no. 1, pp. 25–34, 1995.

[27] Z. Bin Huang and Z. M. Cheng, “Liquid circulation hydrodynamics in an external loop airlift reactor,” *Can. J. Chem. Eng.*, vol. 91, no. 2, pp. 223–230, 2013.

[28] A. Sanchez *et al.*, “Bubble-column and airlift photobioreactors for algal culture,” *AIChE J.*, vol. 46, no. 9, pp. 1872–1887, 2000.

[29] Q. Wu, X. Wang, T. Wang, M. Han, Z. Sha, and J. Wang, “Effect of liquid viscosity on hydrodynamics and bubble behaviour of an external-loop airlift reactor,” *Can. J. Chem. Eng.*, vol. 91, no. 12, pp. 1957–1963, 2013.

[30] J. Rajarajan, D. Pollard, A. P. Ison, and P. A. Shamlou, “Gas holdup and liquid velocity in airlift bioreactors containing viscous newtonian liquids,” *Bioprocess Eng.*, vol. 14, no. 6, pp. 311–315, 1996.

[31] M. S. (1973). . Chakravarty, M., Begum, S., Singh, H. D., Baruah, J. N., & Iyengar, “Gas holdup distribution in a gas-lift column,” *Biotechnol. Bioeng. Symp.*, vol. 4, pp. 363–378, 1973.

[32] M. Blažej, G. M. Cartland Glover, S. C. Generalis, and J. Markoš, “Gas-liquid simulation of an airlift bubble column reactor,” *Chem. Eng. Process. Process Intensif.*, vol. 43, no. 2, pp. 137–144, 2004.

[33] M. Chist, M.Y., Halard, B., Moo-Young, “Liquid circulation in airlift reactors,” *Chem. Eng. Sci.*, vol. 43, no. 3, pp. 451–457, 1988.

[34] R. A. Bello, C. W. Robinson, and M. Moo-Young, “Gas holdup and overall volumetric oxygen transfer coefficient in airlift contactors.,” *Biotechnol. Bioeng.*, vol. 27, no. 3, pp. 369–81, Mar. 1985.

[35] S. V. Kazakis, N.A., Mouza, A.A., Paras, “Experimental study of bubble formation at metal porous spargers: Effect of liquid properties and sparger characteristics on the initial bubble size distribution,” *Chem. Eng. J.*, vol. 137, no. 2, pp. 265–281, 2008.

[36] R. Schäfer, C. Merten, and G. Eigenberger, “Bubble size distributions in a bubble column reactor under industrial conditions,” *Exp. Therm. Fluid Sci.*, vol. 26, no. 6–7, pp. 595–604, 2002.

[37] A. Pohorecki, R.; Moniuk, W.; Bielski, P., Zdrojkowski, “Modeling of coalescence-redispersion in bubble columns,” *Chem. Eng. Sci.*, vol. 56, no. 21, pp. 6157–6164, 2001.

[38] T. Wang and J. Wang, “Numerical simulations of gas-liquid mass transfer in bubble columns with a CFD-PBM coupled model,” *Chem. Eng. Sci.*, vol. 62, no. 24, pp. 7107–7118, 2007.

[39] L. Fadavi, A., Chisti, Y., Chriastel, “Bubble Size in a forced circulation loop reactor,” *J. Chem. Technol. Biotechnol.*, vol. 83, pp. 105–108, 2008.

PAPER

IV. ESTIMATING THE LOCAL VOLUMETRIC MASS TRANSFER COEFFICIENT FOR MICROALGAE SCENEDESMUS IN A SPLIT AIRLIFT PHOTOBIOEACTOR

ABSTRACT

In this study, a plug flow model without axial dispersion was applied to evaluate the liquid-side mass transfer coefficient in a *Scenedesmus* culture grown in a split airlift photobioreactor at superficial gas velocities of 1.0, 2.0, and 2.8 cm/s. At each superficial gas velocity, the liquid-side mass transfer coefficient, assumed to be constant throughout the reactor, was seen to increase with an increase in superficial gas velocity. Using the local interfacial area, local volumetric mass transfer coefficient was also calculated. The local volumetric mass transfer coefficients in the riser and the downcomer were dominated by gas holdup and interfacial area, and were favored by higher superficial gas velocities and lower optical densities of the microalgae culture. The effect of optical density on the liquid side and the local volumetric mass transfer coefficient was analyzed over the growth period divided into three zones; Zone I for optical density up to 0.08, Zone II, optical density between 0.08 and 0.19, and Zone III for optical density between 0.19 and 0.30. While the local volumetric mass transfer coefficient was constant axially in the riser, it decreased axially on moving down the downcomer. The estimated local volumetric mass transfer coefficient was always found to be higher than that estimated from the available correlations.

Keywords: Liquid-side Mass Transfer Coefficient, Local Volumetric Mass Transfer Coefficient, Split Airlift Reactor, Photobioreactor, Microalgae Culture, Plug Flow Model

1. INTRODUCTION

Microalgae are a versatile source used for energy, nutrients, flue gas and wastewater treatment, high value pharmaceutical products, and aquaculture. A number of photobioreactor (PBR) configurations have been researched in literature, and considerable data is available on their advantages and disadvantages. Photobioreactors are broadly classified into two categories- open and closed systems. Open systems require vast land areas. They are prone to contamination and susceptible to changes in the environment and fluctuation in temperature. Thus, open systems are suitable only for the mass production of robust microalgae strains, but due to inefficient mixing and energy utilization, they have poor productivity. Higher biomass productivity and better reactor control can be achieved through closed systems. Closed systems vary from flat-plate PBRs to tubular and vertical PBRs. Flat-plate photobioreactors have high efficiency and biomass productivity [1], large illuminated areas, relatively inexpensive, and easier to clean. Tubular PBRs also provide large illuminated areas, and are commonly used for outdoor cultures. They, however, have poor mixing and mass transfer capabilities causing huge gradients of pH, oxygen, and carbon dioxide inside the reactor [1]. Microalgae are sensitive to changes in pH, which also affects the growth rate. Carbon dioxide is a major requirement for microalgae culturing and also affects pH, and must be well distributed inside the reactor in order to produce healthy cultures. Oxygen is a byproduct of photosynthesis, and it is released as a microalgae culture grows and multiplies. Oxygen buildup in a microalgae system inhibits growth, and thus, it must be transferred effectively from the liquid culture to the gas phase [2]. Vertical PBRs are pneumatically

operated devices that are easier to construct, minimize the effects of photoinhibition and photo-oxidation, exert low shear stress on the algae cells, and provide for efficient mixing and mass transfer.

Despite the potential of microalgae and the different variations of PBRs available, its application on a commercial scale is still not feasible. While open systems remain to be the most cost-effective PBR configuration from the point of view of construction, the low biomass productivity and quality deems the biomass unfit for bulk, and high-value products. The major impediment towards the application and employment of the closed system reactor configurations on a commercial scale are the difficulties associated with scale-up. The flat-plate PBRs are difficult to scale-up for large cultures [1]. Scale-up of tubular reactors requires for longer tubes, which further worsens the problem of inefficient mixing and mass transfer, making them unsuitable for mass cultivation operations. Vertical PBRs such as bubble columns and airlift reactors are perceived as the most promising PBR type for mass cultivation [1], [3]. Vertical PBRs are easier to scale-up than their other counterparts [4]. Another hindrance towards mass cultivation of microalgae is the lack of comprehensive research on the hydrodynamics and mass transfer processes in PBRs. A number of studies on mass transfer in bubble columns, and airlift reactors are available in literature [5]–[7], with an emphasis of estimating and investigating the mass transfer coefficient ($k_l a$) through mechanistic or empirical methods. Due to the presence of ordered mixing and liquid recirculation, exposure and light availability to the culture is better in the case of airlift reactors than in bubble columns. In fact, the split airlift reactor [4] was shown to outperform bubble column and draft-tube airlift reactor for culturing microalgae *Porphyridium* [4]. The gas-phase used

in these studies is usually air, with pure oxygen sometimes used as a tracer for mass transfer analysis, the liquid-phase varies from tap water and sea water [8], [Paper II] to alcohol solutions and different CMC solution concentrations [9], [10]. Limited literature on the study of mass transfer processes in real microalgae cultures is available [11]–[15], however, the different algae strains, PBR geometry and volume, and the methods used for estimating the mass transfer coefficient prevent a direct comparison among them. Also, variation in $k_l a$ has been studied with respect to superficial gas velocity, power input, and gas holdup in various liquids, but no attempt has been made to track the changes in $k_l a$ with an increase in the culture density as it grows inside a PBR.

The methods used to measure the mass transfer coefficient ($k_l a$) vary from empirical to theoretical, first-principles and mechanistic models [6], [8], [14], [16], [17], [18]. Even though the procedures and techniques vary from one study to another, the assumption of a constant overall volumetric mass transfer coefficient is common to all. Recently a new approach to estimate the mass transfer coefficient was introduced by assuming a constant liquid-side mass transfer coefficient (k_l) as opposed to the conventional assumption of constant $k_l a$ found in the literature [Paper II]. In Paper I, the local interfacial area and gas holdup, measured using a four-point optical fiber probe, was found to vary between the riser and the downcomer, and decrease axially down the downcomer due to a decrease in gas-liquid interaction and the number of bubbles in the downcomer. In Paper II it was shown that the decrease in local interfacial area axially down the downcomer, coupled with the assumption of a single constant $k_l a$ for the entire reactor, leads to the erroneous implications of increase in the liquid-side mass transfer coefficient (k_l) on moving axially down the downcomer. According to the film theory of

mass transfer, k_l is defined as the diffusivity of a gas in a liquid divided by the fictitious gas-liquid film thickness [19]. The diffusivity of a gas in liquid is constant for a given gas-liquid system, and the film thickness increases with a decrease in gas liquid interaction. Thus, the increase in k_l in regions of lower gas-liquid interaction in the downcomer arising due to the assumption of a constant $k_l a$ is highly inaccurate and misleading [Paper II]. They further applied and verified the new approach using an air-water system inside a split airlift reactor.

In this study, microalgae *Scenedesmus* was grown inside a split airlift PBR, and local volumetric mass transfer coefficient was measured using the new modified approach suggested in Paper II. The variation in the local mass transfer coefficient, $k_l a$ (s^{-1}) was studied with respect to changes in superficial gas velocity and the optical density of the culture as it photosynthesizes and grows. Also, the variation in the local mass transfer coefficient from one point to another was also analyzed.

2. MASS TRANSFER IN MICROALGAE CULTURES

The gas and the liquid phases in the split airlift PBR, compressed air and microalgae culture respectively, were modeled as plug flow [Paper II]. The plug flow model for dissolved oxygen concentration, derived from the general species mass balance for oxygen, consists of the rate of change of oxygen with time, transport of oxygen via advection, and the source term. The model is based on the following assumptions: (i) axial dispersion in the reactor was assumed to be negligible; (ii) the reactor was assumed to operate isothermally; (iii) velocity and density of the fluids was assumed to be the same radially. The source term for oxygen species in microalgae culture consists of the oxygen transfer rate (OTR) from the gas phase to the liquid, and the oxygen production rate (OPR) due to photosynthesis by the microalgae cells for growth and maintenance.

$$\frac{\partial C_l}{\partial t} = -\frac{U_l}{1-\epsilon}\frac{\partial C_l}{\partial z} + \frac{1}{1-\epsilon}(OTR - OPR) \quad (1)$$

$$\frac{\partial C_g}{\partial t} = -\frac{U_g}{\epsilon}\frac{\partial C_g}{\partial z} - \frac{1}{\epsilon}(OTR - OPR) \quad (2)$$

Equations (1) and (2) have been derived from the general mass balance equation for plug flow of oxygen in the liquid and gas phases in microalgae cultures (that produce oxygen through the process of photosynthesis). The superficial gas velocity (U_g) in the riser is based on the total volume of gas in the riser, and is constant axially. In the downcomer, however, due to the variation of the true bubble velocity and gas holdup on moving downwards, the superficial gas velocity in the downcomer varies axially [Paper II]. However, the superficial gas velocity in the downcomer has been shown to have no significant effect on the mass transfer process, and so it can also be assumed to constant axially [Paper II]. The above equations also consist of the gas holdup (ε), which has been

shown to vary between in riser and downcomer sections of a split airlift reactor, and also axially in the downcomer [Paper I; Paper III]. Therefore, these equations cannot be solved analytically. To obtain a numerical solution to Equations (1) and (2), the change in oxygen concentration with time is needed at different axial locations in the photobioreactor. To gather the oxygen concentration data, a step change in oxygen concentration was implemented by first stripping the liquid phase of all the dissolved oxygen by sparging nitrogen through the reactor, and then switching the gas flow to compressed air to re-oxygenate the liquid phase until dissolved oxygen saturation, at different axial locations. The time for the step change and for the dissolved oxygen concentration to reach saturation upon re-oxygenation was much lesser than the average growth rate observed in Paper III, at the studied superficial gas velocities. Hence, the contribution of OPR to the oxygen mass balance Equations (1) and (2) was ignored, and the transfer of oxygen from the gas to the liquid phase, OTR, was believed to be the rate limiting step.

Based on the above observation, substituting for OTR and rewriting Equations (1) and (2) for the riser and downcomer sections of the split airlift reactor (Figure 3.1), the plug flow model for the gas and liquid phases, given by Equations (3)-(6), is the same as the mass transfer model in Paper II developed in an air water system. The initial and boundary conditions that supplement the mass transfer model are given in Equations (7)-(9).

$$\frac{\partial C_{gr}}{\partial t} = -\frac{U_{groverall}}{\epsilon_r}\frac{\partial C_{gr}}{\partial z} - \frac{1}{\epsilon_r} K_l a \left(\frac{C_g^*}{H} - C_{lr}\right) \quad (3)$$

$$\frac{\partial C_{lr}}{\partial t} = -\frac{U_{lr}}{1-\epsilon_r}\frac{\partial C_{lr}}{\partial z} + \frac{1}{1-\epsilon_r} K_l a \left(\frac{C_g^*}{H} - C_{lr}\right) \quad (4)$$

$$\frac{\partial C_{gd}}{\partial t} = \frac{U_{gd}}{\epsilon_d}\frac{\partial C_{gd}}{\partial z} - \frac{1}{\epsilon_d}K_l a\left(\frac{C_g^*}{H} - C_{ld}\right) \quad (5)$$

$$\frac{\partial C_{ld}}{\partial t} = \frac{U_{ld}}{1-\epsilon_d}\frac{\partial C_{ld}}{\partial z} + K_l a\left(\frac{C_g^*}{H} - C_{ld}\right) \quad (6)$$

Initial Condition (t=0) :

$C_{lr}(z,0)=C_{ld}(z,0)=0,\ C_{gr}(z,0)=C_{gd}(z,0)=0$ (7)

Boundary Conditions:

At z=0: $C_{lr}(0, t) = C_{ld}(0,t)$, $C_g(0,t)=C_g^*$ (8)

At z=h: $\frac{\partial C_{lr}}{\partial z} = \frac{\partial C_{gr}}{\partial z} = \frac{\partial C_{ld}}{\partial z} = \frac{\partial C_{gd}}{\partial z} = 0$ (9)

In Paper II, a new methodology to estimate the local liquid-side mass transfer coefficient k_l (cm/s), which was assumed to be constant throughout the reactor, was developed. They then used the local interfacial area, *a*, data to estimate the local volumetric mass transfer coefficient, $k_l a$ (s^{-1}). They also proved that the assumption of a constant liquid side mass transfer coefficient, k_l (cm/s) was more fundamentally sound than the assumption of a constant overall volumetric mass transfer coefficient. Thus, the solving procedure developed and verified in Paper II, can be applied to solve equations (3)-(6) to estimate the local volumetric mass transfer coefficient, $k_l a$ (s^{-1}), as the microalgae culture grows and changes in optical density and viscosity.

The local gas holdup (ε_g) and interfacial area (a) measurements required to solve the plug flow model (Equations (3)-(6)) have been obtained from Paper III. The other parameters required to estimate the mass transfer coefficient in split airlift PBR are superficial gas velocity (U_g), liquid circulation velocity (U_l), Henry's law constant (H), details of which are given in the section 4.

Based on Paper II, Equations (3)-(6) can be discretized in the space and time domains ($z=i\Delta z$ (i=0,1,2….M), and $t=n\Delta t$ (n=0,1,2,…N)) by applying an upwind difference scheme to the time derivative, and a central difference scheme to the space derivative terms (Equations (10)-(13)). The discretized initial and boundary conditions are given by Equations (14)-(16) [Paper II].

$$\frac{C_{gri}^{n+1}-C_{gri}^{n}}{\Delta t} = -\frac{U_{groverall}}{\epsilon_{ri}}\frac{C_{gri+1}^{n}-C_{gri-1}^{n}}{2\Delta z} - \frac{1}{\epsilon_{ri}}K_l a_i \left(\frac{C_{gri}^{n}}{H} - C_{lri}^{n}\right) \quad (10)$$

$$\frac{C_{lri}^{n+1}-C_{lri}^{n}}{\Delta t} = -\frac{U_{lr}}{1-\epsilon_{ri}}\frac{C_{lri+1}^{n}-C_{lri-1}^{n}}{2\Delta z} + \frac{1}{1-\epsilon_{ri}}K_l a_i \left(\frac{C_{gri}^{n}}{H} - C_{lri}^{n}\right) \quad (11)$$

$$\frac{C_{gdi}^{n+1}-C_{gdi}^{n}}{\Delta t} = \frac{U_{gd}}{\epsilon_{di}}\frac{C_{gdi+1}^{n}-C_{gdi-1}^{n}}{2\Delta z} - \frac{1}{\epsilon_{di}}K_l a_i \left(\frac{C_{gdi}^{n}}{H} - C_{ldi}^{n}\right) \quad (12)$$

$$\frac{C_{ldi}^{n+1}-C_{ldi}^{n}}{\Delta t} = \frac{U_{ld}}{1-\epsilon_{di}}\frac{C_{ldi+1}^{n}-C_{ldi-1}^{n}}{2\Delta z} + \frac{1}{1-\epsilon_{di}}K_l a_i \left(\frac{C_{gdi}^{n}}{H} - C_{ldi}^{n}\right) \quad (13)$$

Initial Condition (t=0) : $C_{lri}(0)=C_{ldi}(0)=0$, $C_{gri}(0)=C_{gdi}(0)=0$ (14)

Boundary Conditions:

At z=0: $C_{lr0}(t) = C_{ld\,0}(t)$, $C_{gr0}(t)=C_g^*$ (15)

At z=MΔz:

$$\frac{C_{lrM+1}-C_{lrM-1}}{2\Delta z} = \frac{C_{grM+1}-C_{grM-1}}{2\Delta z} = \frac{C_{ldM+1}-C_{ldM-1}}{2\Delta z} = \frac{C_{gdM+1}-C_{gdM-1}}{2\Delta z} = 0 \quad (16)$$

Assuming the liquid side mass transfer coefficient, k_l (cm/s), to be constant [Paper II], Equations (10)-(13), subject to conditions (14)-(16), for the entire space domain (Δz=0.1, Δt=0.01) can be solved simultaneously [Paper II]. The procedure for gathering the experimental data for superficial gas velocity (U_g), liquid circulation velocity (U_l), gas holdup (ε_g), interfacial area (a), Henry's law constant (H), and oxygen concentration is explained in the next section. Since the liquid side mass transfer coefficient, k_l (cm/s), is the only unknown, it can be extracted by fitting the oxygen concentration data to Equations (17)-(19).

For 1<i<M-1 (Riser)

$$A_{gri}C_{gri-1}^{n+1} + C_{gri}^{n+1} - A_{gri}C_{gri+1}^{n+1} = -A_{gri}C_{gri-1}^{n} + \left(1 + \frac{B_{gri}}{H}\right)C_{gri}^{n} + A_{gri}C_{gri+1}^{n} - B_{gri}C_{lri}^{n}$$

$$A_{lri}C_{lri-1}^{n+1} + C_{lri}^{n+1} - A_{lri}C_{lri+1}^{n+1} = -A_{lri}C_{lri-1}^{n} + (1 - B_{lri})C_{lri}^{n} + A_{lri}C_{lri+1}^{n} + \frac{B_{lri}}{H}C_{lri}^{n} \quad (17)$$

For 1<i<M-1 (Downcomer)

$$A_{gdi}C_{gdi-1}^{n+1} + C_{gdi}^{n+1} - A_{gdi}C_{gdi+1}^{n+1} = -A_{gdi}C_{gdi-1}^{n} + \left(1 + \frac{B_{gdi}}{H}\right)C_{gdi}^{n} + A_{gdi}C_{gdi+1}^{n} - B_{gdi}C_{ldi}^{n}$$

$$A_{ldi}C_{lri-1}^{n+1} + C_{ldi}^{n+1} - A_{ldi}C_{ldi+1}^{n+1} = -A_{ldi}C_{ldi-1}^{n} + (1 - B_{ldi})C_{ldi}^{n} + A_{ldi}C_{ldi+1}^{n} + \frac{B_{ldi}}{H}C_{ldi}^{n} \quad (18)$$

Where,

$$A_{gri} = \frac{-U_{groverall}\Delta t}{\epsilon_{ri} * 4 * \Delta x},\ \ A_{lri} = \frac{-U_{lr}\Delta t}{(1-\epsilon_{ri}) * 4\Delta x},\ \ A_{gdi} = \frac{-U_{gd}\Delta t}{\epsilon_{di} * 4\Delta x},\ \ A_{ldi} = \frac{-U_{ld}\Delta t}{(1-\epsilon_{di}) * 4\Delta x}$$

$$B_{gri} = -\frac{K_l a_i \Delta t}{\epsilon_{ri}},\ \ B_{lri} = \frac{K_l a_i \Delta t}{1-\epsilon_{ri}},\ \ B_{gdi} = -\frac{K_l a_i \Delta t}{\epsilon_{di}},\ \ B_{ldi} = \frac{K_l a_i \Delta t}{1-\epsilon_{di}} \quad (19)$$

3. EXPERIMENTAL SETUP

Microalgae *Scenedesmus* was grown in a split airlift PBR shown in Figure 3.1. This type of reactor has been shown to achieve higher biomass productivity than bubble column and draft tube airlift PBR for red marine algae *Porphyridium* [4]. The split airlift PBR in Figure 3.1 has been adapted from [4] and has also been studied in Papers I, II, and III, in which the local gas holdup and interfacial area properties in a microalgae culture grown inside the reactor were measured and evaluated. Since knowledge of the local gas holdup and interfacial area is required to solve the model explained in section 2, this split airlift photobioreactor was used in this study. It consists of an acrylic column with an internal diameter of 13 cm, and a 105 cm long rectangular baffle in the middle, dividing the reactor into riser and downcomer sections. Ports for local measurement have been provided along the axis of the riser and the downcomer as shown in Figure 3.1. A ring sparger was used to introduce compressed air (gas phase) into the riser section. A bank of 12 cool white fluorescent lights (Agrobrite T5, 54W, 6400K) was the light source for microalgae cultivation inside the PBR.

The method for culturing microalgae is similar to the one in Paper III. First, the reactor was filled with fresh water algae growth medium (Proline F/2 algae food-parts A and B mixed in equal parts in reverse-osmosis water). Compressed air, enriched with 3% CO_2, was introduced into the reactor through the sparger, following which the reactor was inoculated with 150 ml (1% of the reactor volume) of *Scenedesmus* culture. The air flowrate was adjusted to give a low superficial gas velocity of 0.5 cm/s based on the cross-sectional area of the riser, to allow the microalgae species to acclimatize for 14

hours. During the acclimatization phase, the room light provided the light necessary for photosynthesis, and the light bank was not turned on until after the first 14 hours. Then, the gas flowrate was increased and set at the superficial gas velocity (1.0, 2.0, 2.8 cm/s) to be studied. The superficial gas velocities to be studied were chosen to be the same as those studied in Paper III, as the local gas holdup and interfacial data is available for these superficial gas velocities [Paper III]. The dynamic liquid height was adjusted at 122 cm above the base of the reactor, and the light bank was switched on to provide an average surface illumination was 350 $\mu E/m^2s$. All the experiments were carried out at room temperature and pressure condition. Optical density, viscosity, and surface tension of the medium were measured every 24 hours for a period of 10 days. The microalgae culture continued to grow up to a total of 22 days in the reactor, but the oxygen concentration data was gathered for only the 10 days period for which the local gas holdup and interfacial area data was available from Paper III. An optical oxygen probe from Ocean Optics was used to measure the dissolved oxygen concentration at all of the ten ports.

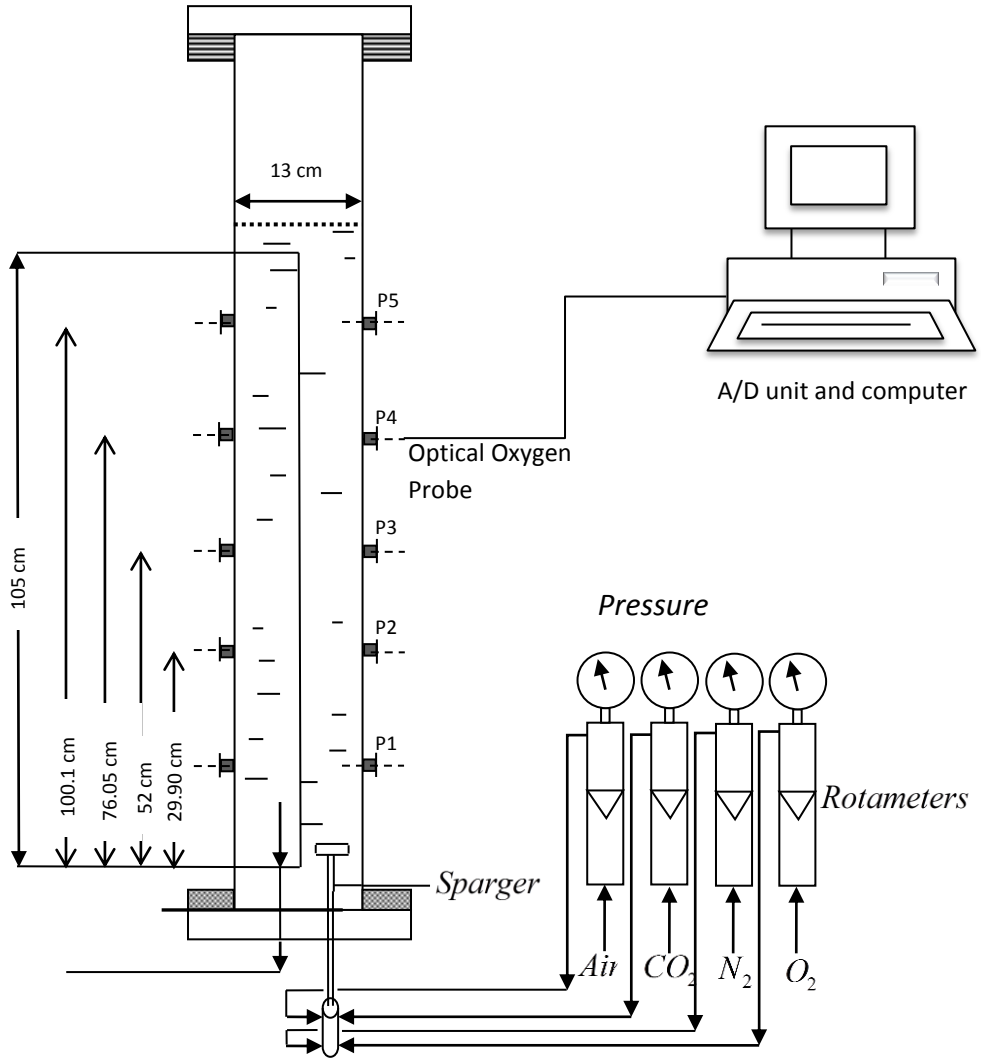

Figure 3.1: Schematic representation of the split airlift photobioreactor

4. MEASUREMENT TECHNIQUES

4.1 OXYGEN CONCENTRATION DATA

Since the gas holdup and interfacial area data (from Paper III) used to solve the model has been obtained at certain specific values of optical density of the microalgae culture, an attempt was made to gather the oxygen concentration data at those specific values of optical density.

An in-situ Neofox oxygen kit from Ocean Optics was used to measure the dissolved oxygen concentrations, $C_l(t)$, at the ports in the riser and the downcomer for superficial gas velocities of 1.0, 2.0, and 2.8 cm/s. The kit consists of an optical oxygen probe, and a fluorimeter assembly. The probe is coated by an active sol-gel coating at the tip. The coating is quenched in the presence of oxygen, and the degree of quenching experienced by the coating varies the fluorescence which is detected by the fluorimeter, and converted into oxygen concentration data. Dissolved oxygen concentration data was measured at each of the 5 ports in the riser and the downcomer sections. A step change in oxygen concentration was made by switching the gas phase between nitrogen and air. First, nitrogen was sparged through the microalgae culture to expel all the dissolved oxygen, and then the gas phase was quickly switched to air. Dissolved oxygen concentration was recorded at intervals of 1 second. The probe delay constant, k_{sensor} , calculated based on the two-point calibration method [18] was used for deconvolution of the actual oxygen concentration, $C_l(t)$, from that measured by the probe, $C_{sensor}(t)$.

$$C_l(t) = C_{sensor}(t) + \frac{1}{k_{sensor}} \frac{dC_{sensor}(t)}{dt} \tag{20}$$

The value of the Henry's Law constant was taken as 0.032 [20].

4.2 LOCAL GAS HOLDUP AND INTERFACIAL AREA

The local gas holdup and interfacial area data for microalgae *Scenedesmus* in the split- airlift PBR shown in Figure 3.1 was taken from Paper III, in which the variation in these parameters was tracked with changes in the optical density as the microalgae culture grew.

The local gas holdup and interfacial area data in the riser did not show any significant axial variation, and hence the experimental values at each optical density were used at all the nodal points in the mesh used for the numerical solution.

The correlation accounting for the axial variation in the local gas holdup and interfacial area in the downcomer have been developed from the data found in Paper III. Although, in their study, measurements of local gas holdup and interfacial area were made at discrete axial ports in the downcomer, but since the mass transfer model requires for a numerical solution, value of gas holdup and interfacial area are needed at more than just the studied locations. Hence, the correlation developed for the axial variation in the downomer gas holdup during the active growth period of microalgae culturing [Paper III] was used. The local interfacial area data in Paper III was used to fit for the correlation and is given in Equation (21). The experimental data was always within 18% deviation of the predicted values by the correlations, and they were used to obtain the local gas holdup and interfacial area values at the all the nodal points in the grid (Δz=0.1) to solve the numerical solution to estimate the liquid side mass transfer coefficient, k_l (cm/s).

$$\in_{gdi} = \left(a_1 * \frac{z_i^2}{h} + a_2 \frac{z_i}{h} + a_3\right) \in_r - \left(a_4 * \frac{{z_i}^2}{h} + a_5 \frac{z_i}{h} + a_6\right), \quad \text{and}$$
$$a_{di} = \alpha * z_i - \beta \tag{21}$$

Values of the parameters used in the above equations are given in Table 4.1. Z_i is the distance in the downcomer from the base of the reactor, and 'h' is the height of the downcomer.

Table 4.1: Coefficients for gas holdup and interfacial area correlations

U_g (cm/s)	a_1	a_2	a_3	a_4	a_5	a_6	α	β
1.0	4.8	-5.53	2.63	-13.13	16.38	-6.35	0.0049	0.186
2.0	1.79	-1.8	1.57	-3.67	3.77	-2.65	0.0042	0.191
2.8	-1.78	2.068	0.5295	18.38	-21.38	3.68	0.0026	0.155

4.3 LIQUID CIRCULATION AND SUPERFICIAL GAS VELOCITY

The technique used to measure the liquid circulation and superficial gas velocities are the same as stated in Paper II.

Colored dye was injected at the top of the downcomer, and the time taken by the front of the dye to travel through the riser and downcomer sections was recorded. Based on that, the liquid circulation velocity was calculated as:

$$U_{Lr} = \frac{H_r\,(1-\epsilon_r)}{t_r} \qquad U_{Ld} = \frac{H_d\,(1-\epsilon_d)}{t_d} \tag{22}$$

The superficial gas velocity in the riser due to gas injection is calculated based on the riser cross-sectional area (A_r) and the volumetric gas flow rate (Q) according to Equation (2l).

$$U_{gr} = \frac{Q}{A_r} \tag{23}$$

But, the overall superficial gas velocity, $U_{gr,overall}$, consists of both, the gas injected into the reactor through the sparger, and the gas entering the riser as result of liquid circulation from the downcomer. The drift flux model for two phase flow (Equation (24)) can be used to calculate the overall superficial gas velocity [17], [21], [Paper II].

$$\epsilon_r = \frac{U_{gr,overall}}{C_o(U_{gr,overall}+U_{lr})+\vartheta_{gjr}} \quad (24)$$

The drift velocity, v_{gjr} was calculated using Equation (25) [17], [Paper II].

$$\vartheta_{gjr} = \vartheta_{\infty}(1-\epsilon_r)^n \quad (25)$$

The bubble terminal velocity, v_{∞}, was assumed to be 0.25 m/s [17], and n was taken to be 2 [17], [22]. A value of unity was taken for the distribution parameter, C_o. The gas holdup data in microalgae *Scenedesmus*, ϵ_r, was taken from Paper III.

The downcomer-superficial gas velocity, U_{gd}, can be assumed to be constant axially through the downcomer [Paper II], and was therefore, calculated based on the difference between the overall riser superficial gas velocity, $U_{gr,overall}$, and that due to gas injection, U_{gr}, using the continuity equation.

$$U_{gd}x\ A_d = (U_{gr,overall} - U_{gr})x\ A_r \quad (26)$$

The superficial gas velocity in the downcomer, U_{gd}, is based on the total gas volume entering the downcomer, and the cross-sectional area of the downcomer. Since the true bubble velocity and local gas holdup in the downcomer decrease on moving axially downwards [Paper I, Paper III], the true local superficial gas velocity also varies axially downwards. However, since the mass transfer coefficient was shown to be insensitive to changes in U_{gd}, it was assumed to be constant for this study as well, and was thus, calculated using Equation (26).

Knowledge of all the above estimated parameters made the Liquid side mass transfer coefficient, k_l (cm/s), to be the only unknown, which was then determined by fitting the oxygen concentration data to the numerical model via least squared error minimization.

5. RESULTS AND DISCUSSION

5.1 PERCENTAGE DISSOLVED OXYGEN

As the microalgae culture grows, the oxygen produced during photosynthesis is released, increasing the dissolved oxygen (DO) levels in the reactor. Since high DO concentrations are known to inhibit growth, they are generally checked on a regular basis. In tubular reactors, DO concentration as high as 400% of air saturation has been observed [3]. Typically, concentrations higher than 120% of air saturation are known to inhibit growth.

The DO levels in the microalgae culture at the three superficial gas velocities of 1.0, 2.0, 2.8 cm/s are shown in Figure 5.1.

The % DO in the microalgae culture increased over time. The %DO varied from about 20% at the beginning of the experiment to all the way up to 30% of air saturation at the highest studied gas velocity. As was expected, the %DO was always within acceptable limits, also suggesting that at the studied gas velocities, the rate of mixing and mass transfer were adequate during the entire growth period. % DO concentrations are generally expected to reach 100% saturation or higher in larger mass cultures.

5.2 LIQUID-SIDE MASS TRANSFER COEFFICIENT, k_l (cm/s)

The liquid-side mass transfer coefficient, k_l (cm/s) was estimated from the mass transfer model as explained earlier. The liquid-side mass transfer coefficient, k_l (cm/s), at the superficial gas velocities of 1.0, 2.0, 2.8 cm/s is shown in Figure 5.2. The k_l (cm/s) value was seen to be higher at the higher superficial gas velocities. An increase in the

superficial gas velocity increases mixing and agitation inside the reactor, improving gas-liquid contact, and hence results in higher values of k_l (cm/s). Based on the film theory of mass transfer, liquid-side mass transfer is defined as the diffusivity of gas in liquid divided by the thickness of the fictitious film between the two phases. With an increase in mixing and agitation due to increase in superficial gas velocity, the thickness of the fictitious film decreases, thus increasing k_l (cm/s). Also, since the mass transfer model was solved under the assumption of a constant k_l (cm/s), as was expected, fitting the oxygen concentration data from any of the 10 measurement ports did not result in any significant variation in k_l (cm/s).

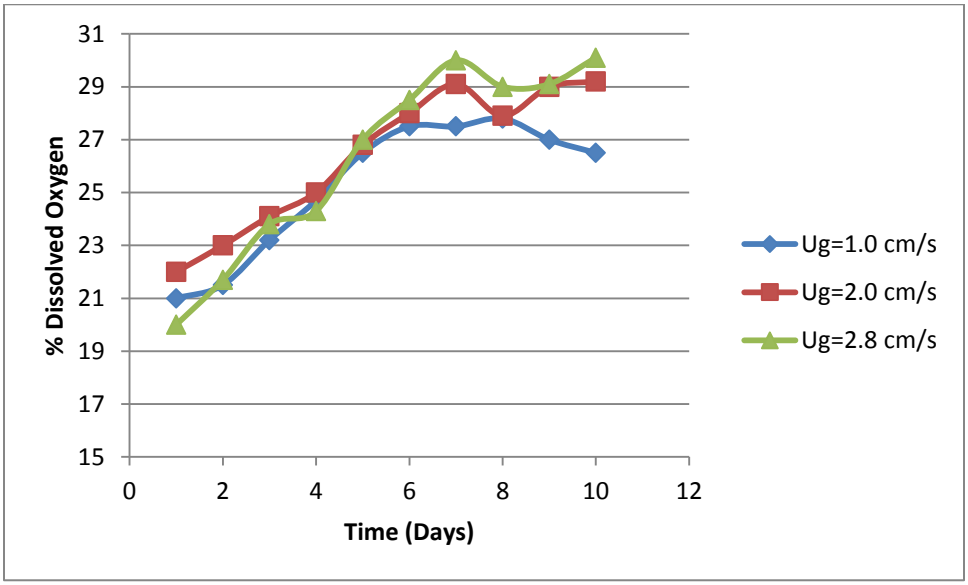

Figure 5.1: Variation of % dissolved oxygen concentration in the reactor

The growth rate data (expressed in terms of optical density) in Paper III, was divided into three distinct zones, namely, Zone I for optical densities up to 0.08, Zone II

for optical densities between 0.08 and 0.19, and Zone III for optical densities between 0.19 and 0.27. For the purpose of analysis, the liquid side mass transfer coefficient, k_l (cm/s), as well as the local volumetric mass transfer coefficient $k_l a$ (s^{-1}) will be analyzed based on these three zones.

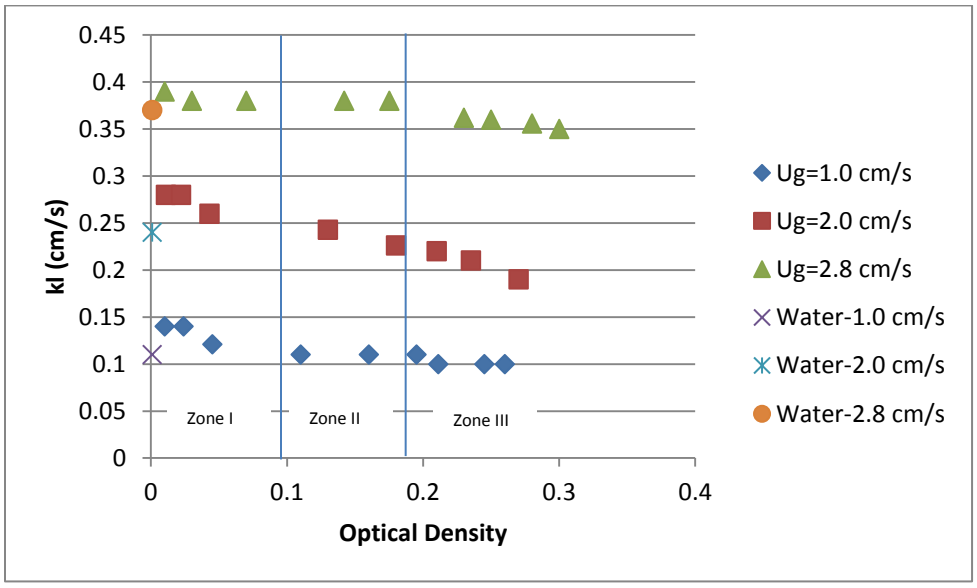

Figure 5.2: Variation of liquid-side mass transfer coefficient, k_l (cm/s)

In Zone I, the liquid side mass transfer coefficient, k_l (cm/s), was constant at the superficial gas velocity of 2.8 cm/s, and decreased by 8%, and 13% at velocities of 2.0, and 1.0 cm/s, respectively. In Zone II, while k_l (cm/s) remained constant at superficial gas velocities of 2.8, and 1.0 cm/s, at 2.0 cm/s, it decreased by the same amount of 8% as in Zone I. In Zone III, k_l (cm/s) at superficial gas velocities of 2.8, and 1.0 cm/s was constant at values 5% and 10% lower than the corresponding values in Zone II,

respectively. Similar to the trend followed by 2.0 cm/s in Zones I and II, the value of k_l (cm/s) decreased in Zone III, but only by a slightly higher percentage (12 %).

Also shown in Figure 5.2 are the k_l (cm/s) values for the air-water system [Paper II]. At superficial gas velocity of 2.8 cm/s, the liquid side mass transfer coefficient, k_l (cm/s) in the microalgae system was almost the same as that of the air water system in Zones I and II, and was slightly lower (5%) in Zone III. At 2.0 cm/s, initially in Zone I, the liquid side mass transfer coefficient, k_l (cm/s) in the microalgae culture was higher than the air water system by 16.7%. Since a steady decline in the value of k_l (cm/s) in the microalgae system was observed at superficial gas velocity of 2.0 cm/s, it was seen to be the same as that of the air water system in the middle of Zone II (day 5). k_l (cm/s) in the microalgae culture was lower than that in the air water system by 21% at the end of Zone III. At superficial gas velocity of 1.0 cm/s, at the beginning of Zone I, the k_l (cm/s) value in the microalgae system was higher than that of the air water system by 27%, but became the same towards the end of Zone I, and remained the same as that of air water system through Zones II and II.

In literature, rarely any attempt has been made to study the liquid-side mass transfer coefficient, k_l (cm/s), and the focus is usually on measuring the overall volumetric mass transfer coefficient. Since, the local volumetric mass transfer coefficient, $k_l a$ (s^{-1}), has been shown to be better at incorporating the fundamental phenomenon of decrease in the liquid side mass transfer coefficient, k_l (cm/s), (due to an increase in the fictitious film thickness) with a decrease in gas-liquid interaction, the local interfacial area during the active growth of the microalgae culture [Paper III] was used to calculate the local volumetric mass transfer coefficient, $k_l a$ (s^{-1}), in the split airlift reactor.

5.3 LOCAL VOLUMETRIC MASS TRANSFER COEFFICIENT, $k_l a$ (s^{-1})

The local volumetric mass transfer coefficient, $k_l a$ (s^{-1}), was calculated according to Equation (27).

$$k_l a = k_l * a_i \tag{27}$$

The local volumetric mass transfer coefficient in the riser is given in Figure 5.3. Since no axial variation of interfacial area was observed in the riser [Paper III] the local volumetric mass transfer coefficient, $k_l a$ (s^{-1}), in the riser did not vary axially. Since the local interfacial area in the riser [Paper III] was measured at the radial center, the value of the local volumetric mass transfer coefficient, $k_l a$ (s^{-1}), reported is also at the radial center. At every stage of the growth, the local volumetric mass transfer coefficient, $k_l a$ (s^{-1}), in the riser was higher at the higher superficial gas velocities. Higher values of the liquid-side mass transfer coefficient, $k_l a$ (cm/s) and the interfacial area, a, at higher superficial gas velocities contributed to the higher values of the local volumetric mass transfer coefficient, $k_l a$ (s^{-1}), in the riser.

As shown by Equation (27), the local volumetric mass transfer ($k_l a$ (s^{-1})) is affected by both the liquid side mass transfer coefficient (k_l, cm/s) and the interfacial area, a. With the growth of the culture, as it grew in optical density, the local volumetric mass transfer coefficient, k_l a(s^{-1}), was seen to decrease at each of the studied superficial gas velocities. This decrease for the riser is shown in Figure 5.3.

In Zone I, even though the value of k_l (cm/s) was constant at velocities of 2.8 and 1.0 cm/s, $k_l a$ (s^{-1}) was seen to decrease with an increase in the optical density of the microalgae culture. $k_l a$ (s^{-1}) decreased by 8% and 12% in Zone I at superficial gas velocities of 2.8 and 1.0 cm/s, respectively. This decrease in $k_l a$ (s^{-1}) can be attributed to

the decrease in the value of interfacial area with increase in the optical density of the microalgae culture [Paper III]. Since at 2.0 cm/s, both the liquid side mass transfer coefficient, k_l (cm/s) (Figure 5.2), and the interfacial area, a [Paper III], decreased in Zone I, the decrease in the value of $k_l a$ (s^{-1}) was higher at 18% than that observed at the velocities of 1.0 and 2.8 cm/s. In Zone II, $k_l a$ (s^{-1}), remained constant at velocities of 1.0, and 2.0 cm/s. In Zone II, $k_l a$ (s^{-1}) decreased by 17%, 10%, and 8% at superficial gas velocities of 1.0, 2.0, and 2.8 cm/s, respectively. In Zone III, the value of $k_l a$ (s^{-1}) decreased by 15 % at superficial gas velocity of 1.0 cm/s, mainly due to the decrease in the interfacial area value in Zone III [Paper III]. The decrease in $k_l a$ (s^{-1}) at 2.0 and 2.8 cm/s was much higher than that at 1.0 cm/s. In Zone III, $k_l a$ (s^{-1}) decreased by 40% and 60% at superficial gas velocities of 2.0, and 2.8 cm/s, respectively. The higher decrease at velocity of 2.0 cm/s is due to the combined effect of decrease in k_l (cm/s) (Figure 5.2) and interfacial area, a [Paper III]. At superficial gas velocity of 2.8 cm/s, the interfacial area, a, decreased by almost 48% in Zone III [Paper III], causing a steep decrease of 60% in the value of $k_l a$ (s^{-1}) in Zone III.

Compared to the local volumetric mass transfer coefficient, $k_l a$ (s^{-1}), for an air-water system [Paper I], the value of $k_l a$ (s^{-1}) for a microalgae system at the corresponding superficial gas velocity was always higher (Figure 4). At the beginning of the growth period, the local volumetric mass transfer coefficient, $k_l a$ (s^{-1}), in the riser for the microalgae system was 330%, 1500%, and 197% higher than that of water at velocities of 1.0, 2.0, and 2.8, cm/s, respectively. This large difference between the $k_l a$ (s^{-1}) values of microalgae and the air-water system are also the combined effect of slightly higher k_l (cm/s), and much higher interfacial area of the microalgae system

[Paper III]. Since the value of $k_l a$ (s^{-1}) decreased with the increase in the optical density of microalgae culture over the growth period, at the end of Zone III, the $k_l a$ (s^{-1}) values for the microalgae culture was the same at the superficial gas velocity of 2.8 cm/s, and 75%, and 700% higher at 2.0, and 1.0 cm/s, respectively. This is due to the fact, that at the end of Zone III, the interfacial area, *a*, in the microalgae culture was the same as that of the air water system at 2.8 cm/s, and still much higher at the velocities of 2.0, and 2.8 cm/s [Paper III].

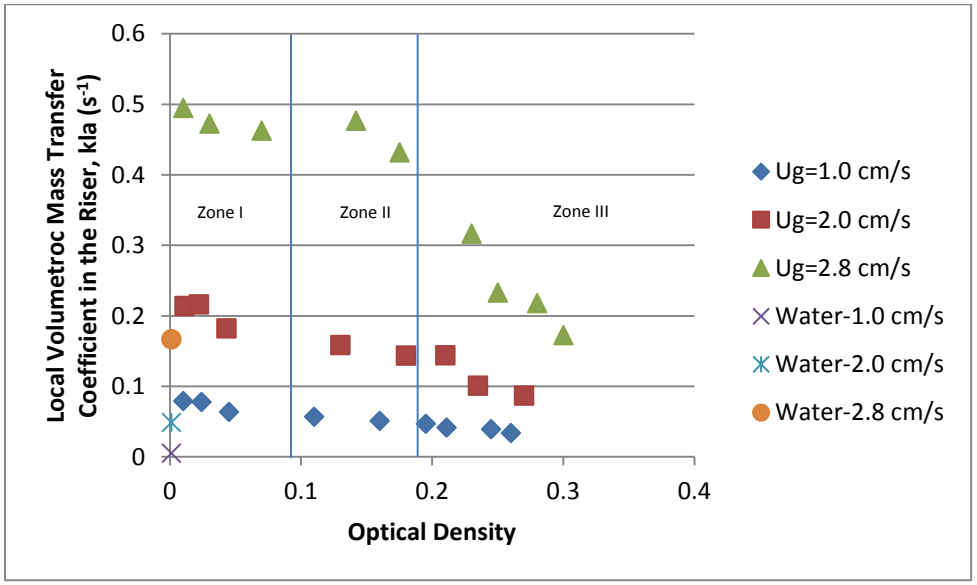

Figure 5.3: Local volumetric mass transfer coefficient, $k_l a$ (s^{-1}) in the riser

The variation of the local volumetric mass transfer coefficient, $k_l a$ (s^{-1}), in the downcomer is shown in Figure 5.4. Figure 5.4 is for the axial position of z=100 cm from the base of the reactor, at port 4 in the downcomer. Similar to the riser and for the same

reasons as stated before, the local volumetric mass transfer coefficient, $k_l a$ (s^{-1}), in the downcomer was always higher at the higher superficial gas velocity.

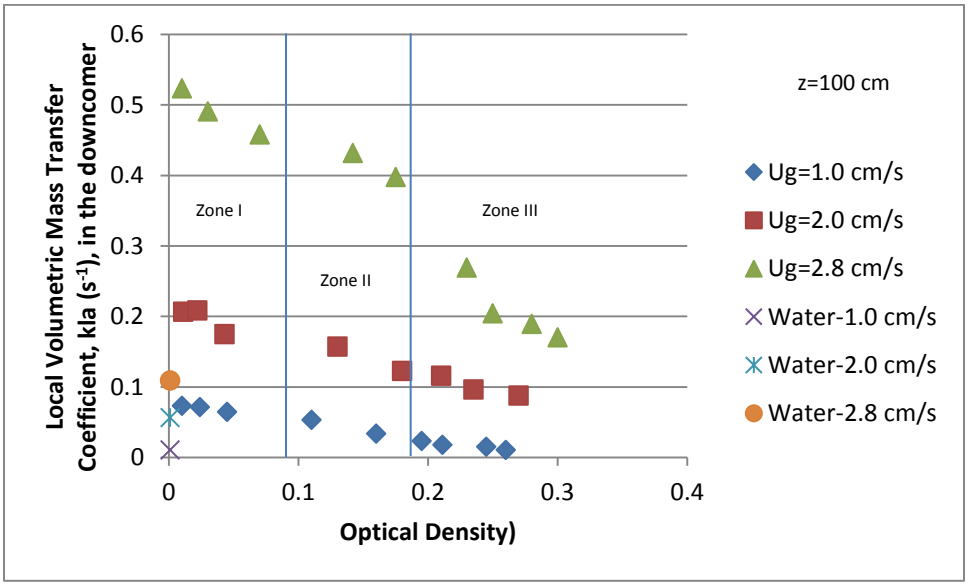

Figure 5.4: Local volumetric mass transfer coefficient, $k_l a$ (s^{-1}), in the downcomer at z=100 cm

Again, as was the case in the riser, the local volumetric mass transfer coefficient, $k_l a$ (s^{-1}), in the downcomer decreased with an increase in the optical density in Zone I. $k_l a$ (s^{-1}) decreased by 11%, 15%, and 12% in Zone I, and by 56%, 22.3%, and 9.7% in Zone II at 1.0, 2.0, and 2.8 cm/s, respectively. This effect is again due to the decrease of interfacial area and liquid side mass transfer coefficient, k_l (cm/s) with increase in optical density of the microalgae culture. In Zone III, the decrease in $k_l a$ (s^{-1}) was 39%, 24%, and 37% at superficial gas velocities of 1.0, 2.0, and 2.8 cm/s, respectively. At each superficial gas velocity, the local interfacial area seemed to dominate Equation (27) in

estimating the local volumetric mass transfer coefficient, $k_l a$ (s^{-1}), and therefore $k_l a$ (s^{-1}), decreased by much larger amounts than the decrease, if any, observed in the values of the liquid-side mass transfer coefficient, k_l (cm/s) with increase in the optical density of the microalgae culture.

In the downcomer, an axial variation in the local interfacial area values was observed [Paper III]. This was mainly due to the decrease in the number and size of the bubbles descending down the downcomer, as well as the decrease in the gas holdup down the downcomer during the growth of microalgae. The axial variation in local interfacial area in the downcomer resulted in the axial variation of local volumetric mass transfer coefficient, $k_l a$ (s^{-1}), in the downcomer. This variation for superficial gas velocity of 2.0 cm/s is shown in Figure 5.5, and a similar variation is observed at the other two studied gas velocities. Since the interfacial area decreased on moving down the downcomer, so did the local $k_l a$ (s^{-1}).

A number of correlations to estimate the overall mass transfer coefficient in airlift PBRs are available in literature [6], [23], [24]. Many researchers have studied the overall volumetric mass transfer coefficient in various microalgae cultures in different PBR configurations and volumes [11], [12], [25], [26]. Although the general phenomenon of improved mass transfer and an increase in the mass transfer coefficient with an increase in the superficial gas velocity found in literature was also observed in this study, a direct comparison with the available literature was not possible due to unavailability of correlations to estimate the local volumetric mass transfer coefficient, $k_l a$ (s^{-1}). However, a comparison with some of the available correlations (Table 5.2, Figure 5.6) shows that even though the local volumetric mass transfer coefficient $k_l a$ (s^{-1}) decreases with

increase in optical density of the medium due to growth, at the end of the 10 days growth period, the k_l a(s^{-1}) was higher than that predicted by the correlations.

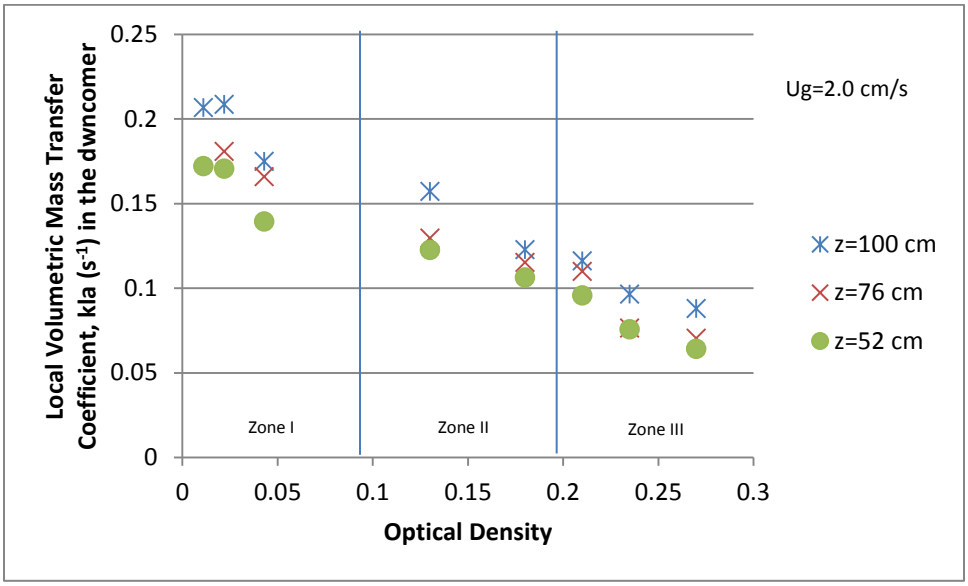

Figure 5.5: Axial variation of local volumetric mass transfer coefficient, $k_l a$ (s^{-1}), in the downcomer at U_g=2.0 cm/s

These correlations (Table 5.2) do not account for the change in $k_l a$ (s^{-1}) due to a change in the interfacial area value as the culture grew in optical density. Thus, no correlation satisfactorily estimated the range of $k_l a$ (s^{-1}) in this study. None of the correlations in Table 5.1 have studied the mass transfer coefficient in a microalgae culture, and hence the applicability of these correlations is highly limited. Very few studies have estimated the mass transfer coefficient in a real microalgae culture. Vega-Estrada et al., 2005 [27], cultured *Haematococcus pluvialis* in a 2L split-cylinder airlift PBR at a superficial gas velocity of 2.4 cm/s and obtained an overall volumetric mass transfer coefficient of 0.009 s^{-1}. Even though the superficial gas velocity in their study

was in the range studied in this work, the local volumetric mass transfer coefficient, $k_l a$ (s^{-1}), was almost two orders of magnitude higher. But this comparison can be highly misleading owing to the different strains, the huge difference in the reactor volumes (2L in their study, and 15 L in this study), and the nature of the mass transfer coefficients (local versus overall) studied in the two works.

Table 5.1: Correlations for overall $k_l a$ in literature

	$k_l a$	Estimation Method	$k_l a$ (s^{-1}) (Ugr 2.0 cm/s)
Blazej, 2004[28]	Overall	$k_l a=0.91*\varepsilon_{gr}^{1.39}$	0.008309552
Bello, 1985 [29]	Overall	$k_l a=5.5x10^{-4}*(1+A_d/A_r)*U_{gr}^{0.8}$	0.01389809
Li et al., 1965 [30]	Overall	$k_l a=0.0343*U_{gr}^{0.524}$	0.004416049

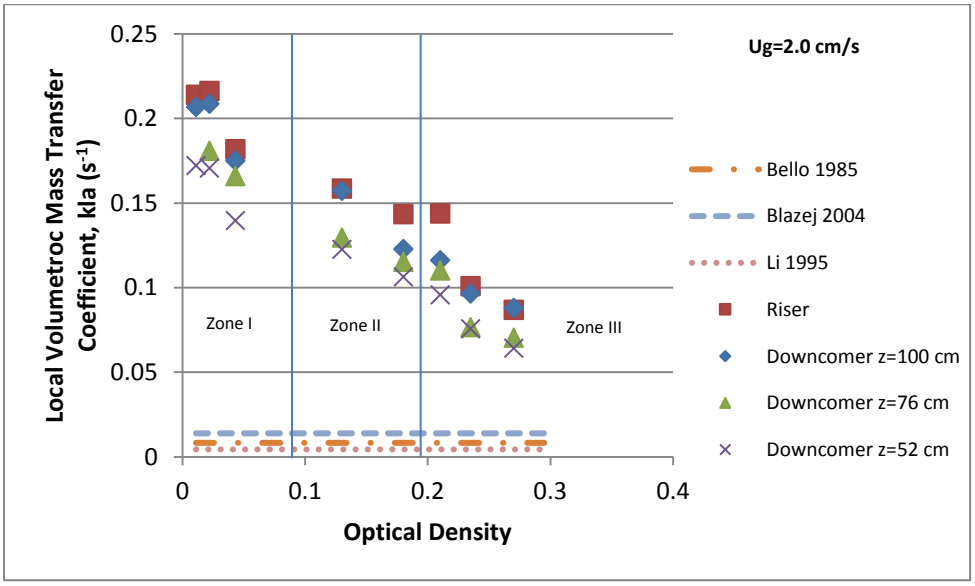

Figure 5.6: Comparison of experimental $k_l a$ (s^{-1}) with correlations in Table 5.1

6. REMARKS

The dissolved oxygen concentration in the microalgae culture of *Scenedesmus sp*., cultivated inside the split airlift PBR was found to increase with the increase in the optical density of the culture, but was always lower than 100% saturation. However, the dissolved oxygen concentration can increase tremendously in large scale commercial culturing operations and inhibit growth, and hence knowledge of the mass transfer coefficient and its variation as the culture grows, provides an important insight into gas-liquid interaction. A new method to estimate the liquid side mass transfer coefficient, k_l (cm/s), developed and verified in Paper II, was successfully applied to a *Scenedesmus* culture in the split airlift PBR. The liquid-side mass transfer coefficient, k_l (cm/s), was assumed to be constant throughout the reactor. As was expected, k_l (cm/s) was affected positively by the superficial gas velocity owing to better mixing and agitation, and a consequent lower thickness of the fictitious gas-liquid film, at higher velocities. Also, the optical density of the medium was seen to affect k_l (cm/s) the most in Zone III for optical densities between 0.19 and 0.30. At all the studied superficial gas velocities the value of the liquid side mass transfer coefficient, k_l (cm/s) of the microalgae culture was higher than that for the air water system at the beginning of the culture. It became the same at the end of the culture at superficial gas velocity of 1.0 cm/s, and was slightly lower than the corresponding air-water values at 2.0 and 2.8 cm/s, respectively. The combined effect of the liquid side mass transfer coefficient, k_l (cm/s) and the local interfacial area was also translated into the trend of the local volumetric mass transfer coefficient, $k_l a$ (s^{-1}), with an increase in the optical density of the culture. The local volumetric mass transfer

coefficient, $k_l a$ (s^{-1}), was seen to be favored by a decrease in the optical density, and an increase in the superficial gas velocity. The interfacial area seemingly dominated the local volumetric mass transfer coefficient, $k_l a$ (s^{-1}), value, and the trend of decrease of the both properties was observed to be the same. While no axial variation was observed in the riser, axial variation of the local volumetric mass transfer coefficient, $k_l a$ (s^{-1}) was observed in the downcomer in this study, due to decrease of axial interfacial area values in the downcomer observed in Paper III. Also, no data on the radial variation of interfacial area was available. Therefore, a radial analysis of the variation of gas holdup and interfacial area, and the consequent variation of $k_l a$ (s^{-1}) in the riser and the downcomer along with changes in the optical density of the medium will provide even more insight into the mass transfer process.

A direct comparison with the correlations available in literature (for overall mass transfer coefficient) was not possible with the local $k_l a$ (s^{-1}) in this study. However, it was seen that the range of the mass transfer coefficient predicted by the correlations was always less than that observed in the microalgae *Scenedesmus* culture. Thus, a detailed study of the change in the mass transfer coefficient for different microalgae species and at more experimental conditions than those studied here is essential to properly characterize $k_l a$ (s^{-1}) for such mediums. Proper knowledge and understanding of $k_l a$ (s^{-1}) in real microalgae cultures will aid the processes of scale-up and optimization, and thus facilitate its commercial development.

REFERENCES

[1] C. U. Ugwu, H. Aoyagi, and H. Uchiyama, "Photobioreactors for mass cultivation of algae," *Bioresour. Technol.*, vol. 99, no. 10, pp. 4021–4028, 2008.

[2] K. Akita and F. Yoshida, "Bubble Size, Interfacial Area, and Liquid-Phase Mass Transfer Coefficient in Bubble Columns," *Ind. Eng. Chem., Process Des. Dev.*, vol. 13, pp. 84–90, 1974.

[3] A. S. Mirón, A. C. Gómez, F. G. Camacho, E. M. Grima, and Y. Chisti, "Comparative evaluation of compact photobioreactors for large-scale monoculture of microalgae," *Prog. Ind. Microbiol.*, vol. 35, no. C, pp. 249–270, 1999.

[4] H. P. Luo and M. H. Al-Dahhan, "Airlift column photobioreactors for Porphyridium sp. culturing: Part I. effects of hydrodynamics and reactor geometry," *Biotechnol. Bioeng.*, vol. 109, no. 4, pp. 932–941, 2012.

[5] M. Chisti, M.Y.; Moo-Young, "Airlift reactors: Characteristics, applications and design considerations," *Chem. Eng. Commun.*, vol. 60, no. 1–6, pp. 195–242, 1987.

[6] Y. Chisti, *Airlift Bioreactors*. Elsevier, New York, 1989.

[7] W. D. Deckwer, *Bubble column reactors*. Wiley and Sons, New York, 1992.

[8] A. Sanchez *et al.*, "Bubble-column and airlift photobioreactors for algal culture," *AIChE J.*, vol. 46, no. 9, pp. 1872–1887, 2000.

[9] V. Sivasubramanian and B. S. N. Prasad, "Effects of superficial gas velocity and fluid property on the hydrodynamic performance of an airlift column with alcohol solution," vol. 1, no. 1, pp. 245–253, 2009.

[10] Z. Deng, T. Wang, N. Zhang, and Z. Wang, "Gas holdup, bubble behavior and mass transfer in a 5m high internal-loop airlift reactor with non-Newtonian fluid," *Chem. Eng. J.*, vol. 160, no. 2, pp. 729–737, 2010.

[11] A. Contreras, Y. Chisti, and E. Molina Grima, "A reassesment of relationship between riser and downcomer gas holdups in airlift reactors," *Chem. Eng. Sci.*, vol. 53, no. 24, pp. 4151–4154, 1998.

[12] F. Camacho Rubio, F. G. Acién Fernández, J. A. Sánchez Pérez, F. García Camacho, and E. Molina Grima, "Prediction of dissolved oxygen and carbon dioxide concentration profiles in tubular photobioreactors for microalgal culture," *Biotechnol. Bioeng.*, vol. 62, no. 1, pp. 71–86, 1999.

[13] B. D. Fernandes, A. Mota, A. Ferreira, G. Dragone, J. A. Teixeira, and A. A. Vicente, "Characterization of split cylinder airlift photobioreactors for efficient microalgae cultivation," *Chem. Eng. Sci.*, vol. 117, pp. 445–454, 2014.

[14] J. C. Merchuk and M. Gluz, “Bioreactors, air-lift reactors,” *Encycl. Bioprocess Technol.*, pp. 320–394, 1999.

[15] C. U. Ugwu, J. C. Ogbonna, and H. Tanaka, “Improvement of mass transfer characteristics and productivities of inclined tubular photobioreactors by installation of internal static mixers,” *Appl. Microbiol. Biotechnol.*, vol. 58, no. 5, pp. 600–607, 2002.

[16] T. Zhang, B. Zhao, and J. Wang, “Mathematical models for macro-scale mass transfer in airlift loop reactors,” *Chem. Eng. J.*, vol. 119, no. 1, pp. 19–26, 2006.

[17] L. Luo and J. Yuan, “Modeling of mass transfer in an internal loop airlift reactor,” *Chem. Eng. Technol.*, vol. 38, no. 3, pp. 511–520, 2015.

[18] L. Han, “Hydrodynamics, back-mixing, and Mass Transfer in a Slurry Bubble Column Reactor for Fischer-Tropsch Alternative Fuels,” 2007.

[19] R. E. Treybal, *Mass-transfer operations*. New York: McGraw-Hill, 1968.

[20] D. W. Perry, R.H., Green, *Perry’s chemical engineers’ handbook*. New York: McGraw Hill, 2008.

[21] J. A. Zuber, N., Findlay, “No TitleAverage Volumetric Concentration in Two-Phase Flow Systems,” *J. Heat Transf.*, vol. 87, no. 4, p. 453, 1965.

[22] G. B. Wallis, *One-dimensional two-phase flow*. New York, McGraw-Hill, 1969.

[23] H. Hikita, S. Asai, K. Tanigawa, K. Segawa, and M. Kitao, “The volumetric liquid-phase mass transfer coefficient in bubble columns,” *Chem. Eng. J.*, vol. 22, no. 1, pp. 61–69, 1981.

[24] J. J. Heijnen and K. Van’t Riet, “Mass transfer, mixing and heat transfer phenomena in low viscosity bubble column reactors,” *Chem. Eng. J.*, vol. 28, no. 2, pp. B21–B42, 1984.

[25] J. . Merchuk, M. Gluz, and I. Mukmenev, “Comparison of photobioreactors for cultivation of the red microalgaPorphyridium sp,” *J. Chem. Technol. Biotechnol.*, vol. 75, no. 12, pp. 1119–1126, 2000.

[26] S. Zhang, K., Kurano, N., Miyachi, “Optimized aeration by carbon dioxide gas for microalgal production and mass transfer characterization in a vertical flat-plate photobioreactor,” *Bioprocess Biosyst. Eng.*, vol. 25, no. 2, pp. 97–101, 2002.

[27] J. Vega-Estrada, M. C. Montes-Horcasitas, A. R. Dom??nguez-Bocanegra, and R. O. Ca??izares-Villanueva, “Haematococcus pluvialis cultivation in split-cylinder internal-loop airlift photobioreactor under aeration conditions avoiding cell damage,” *Appl. Microbiol. Biotechnol.*, vol. 68, no. 1, pp. 31–35, 2005.

[28] M. Blažej, M. Juraščík, J. Annus, and J. Markoš, “Measurement of mass transfer coefficient in an airlift reactor with internal loop using coalescent and non-coalescent liquid media,” *J. Chem. Technol. Biotechnol.*, vol. 79, no. 12, pp. 1405–1411, 2004.

[29] R. A. Bello, C. W. Robinson, and M. Moo-Young, “Gas holdup and overall volumetric oxygen transfer coefficient in airlift contactors.,” *Biotechnol. Bioeng.*, vol. 27, no. 3, pp. 369–81, Mar. 1985.

[30] G.-Q. Li, S.-Z. Yang, Z.-L. Cai, and J.-Y. Chen, “Mass transfer and gas-liquid circulation in an airlift bioreactor with viscous non-Newtonian fluids,” *Chem. Eng. J. Biochem. Eng. J.*, vol. 56, no. 2, pp. B101–B107, 1995.

PAPER

V. DYNAMIC GROWTH INVESTIGATION OF THE MICROALGAE SCENEDESMUS FOR ESTIMATING THE DYNAMIC KINETIC GROWTH MODEL PARAMETERS

ABSTRACT

The three-state dynamic growth model originally developed by Eilers and Peeters, 1988, and modified by Wu and Merchuk, 2001, was applied to microalgae *Scenedesmus,* which has shown to be a good candidate for waste water treatment and biofuel production, to obtain the kinetic growth parameters. The separate effects experiment developed consisted of a tubular airlift photobioreactor with an internal diameter of 0.7 cm, and a total volume of 0.55 L. The intensity of incident light and the ratio of the light/dark phase were the only two variables in the experiment. A bank of white lights was used to vary the incident light intensity, and the light/dark phase was varied by covering parts of the tubular reactor. According to the methodology of Wu and Merchuk, 2001, the cell count and fluorescence data was used to fit the model and determine the parameters.

Keywords: Dynamic Growth Model, Microalgae *Scenedesmus,* Dynamic Growth Kinetics Parameters

1. INTRODUCTION

Microalgae are unicellular organisms that produce complex carbohydrates, and proteins for growth and lipid production through the process of photosynthesis. They require light, carbon dioxide, nitrates, and phosphates for growth and multiplication. The source of the nutrients varies from atmospheric air, waste water and flue gases to specially formulated fresh and salt water growth media. The light required for the process of photosynthesis can be provided either naturally through sunlight, or through artificial sources such as fluorescent lights and LEDs, or a combination of the two for both indoor and outdoor cultures. While controlling the amount of nutrients available is fairly easy, the availability of light can pose a serious problem, especially in large-scale cultures, making it the most important factor controlling the growth rate of microalgae [1]. Whether the culture is irradiated naturally or artificially, there is an exponential decrease in light flux from the surface to the interior of the culture. This effect is more pronounced in mass cultures due to increased mutual shading among the cells [2], [3]. Much like limited light availability, excess light also hampers growth. High light intensities potentially damage D1 protein and reduce the number of active photon traps [4], [5]. The decrease in growth rate due to light limitation is known as photolimitation, while that due to excessive light is known as photoinhibition. Apart from the intensity of light, the frequency and duration of light/dark cycles also affects growth. Studies have shown the enhanced biomass productivity on being exposed to flashing lights [6] Thus, optimization of light flux available to cells is critical to obtain good biomass productivity.

To ensure adequate nutrient and light availability, promote mass transfer, and prevent the cells from agglomerating in large scale cultures, various mixing strategies are employed in photobioreactors (PBRs). Mixing and agitation aids in the movement of the cells between the highly illuminated surface and the darker core of the reactor, thus minimizing the effects of photolimitation and photoinhibition. The movement of the cells in PBRs determines the illumination history of the cells which also affects growth rate [7] (Lee and Pirt, 1981). Hydrodynamic properties such as gas holdup have also been shown to affect the irradiance distribution inside PBRs due to total internal reflection and shading of the culture by the gas bubbles [8].

In literature, the models available to study the process of photosynthesis are broadly categorized as static and dynamic growth models. The static growth rate models [2], [9]–[11] are based on the photosynthesis versus irradiance curves and assume that each cell utilizes light with the same efficiency. As explained above, light availability varies from one point in the reactor to another and from one cell to another. This, in addition to their inability to account for the flashing lights effect, renders static models unfit for large-scale reactors and mass cultures. Thus, integration of fluid dynamics and photosynthesis (Figure 1.2) has been proposed for a complete understanding of the culturing process [1].

A number of dynamic models are available in literature [12]–[15]. While most of the dynamic growth models available include complex calculations, and a very large number of associated growth parameters, the model by Eilers and Peeters, 1988, is a simple three-state mechanistic model that accounts for photoinhibition and recovery, and has been applied in some other works [15]–[17]. Though this model is applicable to large

range of biological systems, and is fairly easier to solve, it fails to account for the decrease in growth rate at very low light intensities. Thus, a modification to the model was introduced by adding a maintenance factor to the three-state model [17]. Due to the complexity of the maintenance process, and as suggested by Lee and Pirt, 1981 [7], the maintenance factor was assumed to be a constant [17]. The dynamic growth parameters for microalgae *Porphyridium* extracted by Wu and Merchuk, 2001 [17], were successfully combined with fluid dynamics and cell trajectories in bench-top and lab-scale bubble columns, and airlift reactors [17]–[19] to explain the growth of the microalgae species. This signifies the importance and application of the dynamics growth parameters in advancing the understanding of the microalgae growth process, and its potential to be applied to large-scale cultures and improve the existing technology.

The modified dynamic growth rate model by Wu and Merchuk, 2001 [17], was applied to red marine algae, *Porphyridium*. However, in this study, the mathematical model developed by Wu and Merchuk, 2001 [17], was applied to a green fresh water algae, *Scenedesmus* sp. *Scenedesmus* is a versatile microalgae species and is a good candidate for biofuel and biodiesel production [20], [21]. The oil obtained from *Scnenedesmus* has been shown to meet the desired standard requirement of linolenic acid, methyl ester, oxidation stability, and iodine value for biodiesel [22]. Also, *Scenedesmus* species is considered to be useful for waste water treatment as well. In the study by Makareviciene et al., 2011, *Scenedesmus* sp. removed more nitrate and phosphate pollutants from waste water the Chlorella sp. Thus, the dynamic growth rate parameters for *Scenedesmus sp.* will add to the knowledge base of the species, and will also be useful in estimating and validating growth rate studies in large scale cultures. This can be

achieved by applying the new approach introduced in Figure 1.2 to integrate dynamic growth model, light intensity model and hydrodynamics in terms of cell trajectory, and the maintenance factor due to shear stress to estimate the microalgae growth and to optimize the culturing process and as well the photobioreactors.

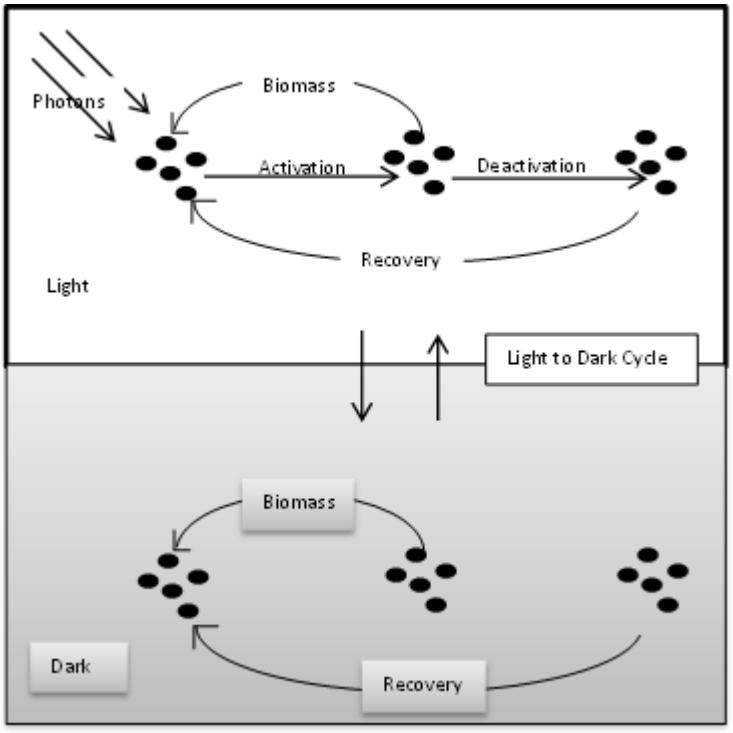

Figure 1.1: Schematic representation of the interaction between fluid dynamics and photosynthesis (adapted from Wu and Merchuk, 2001)

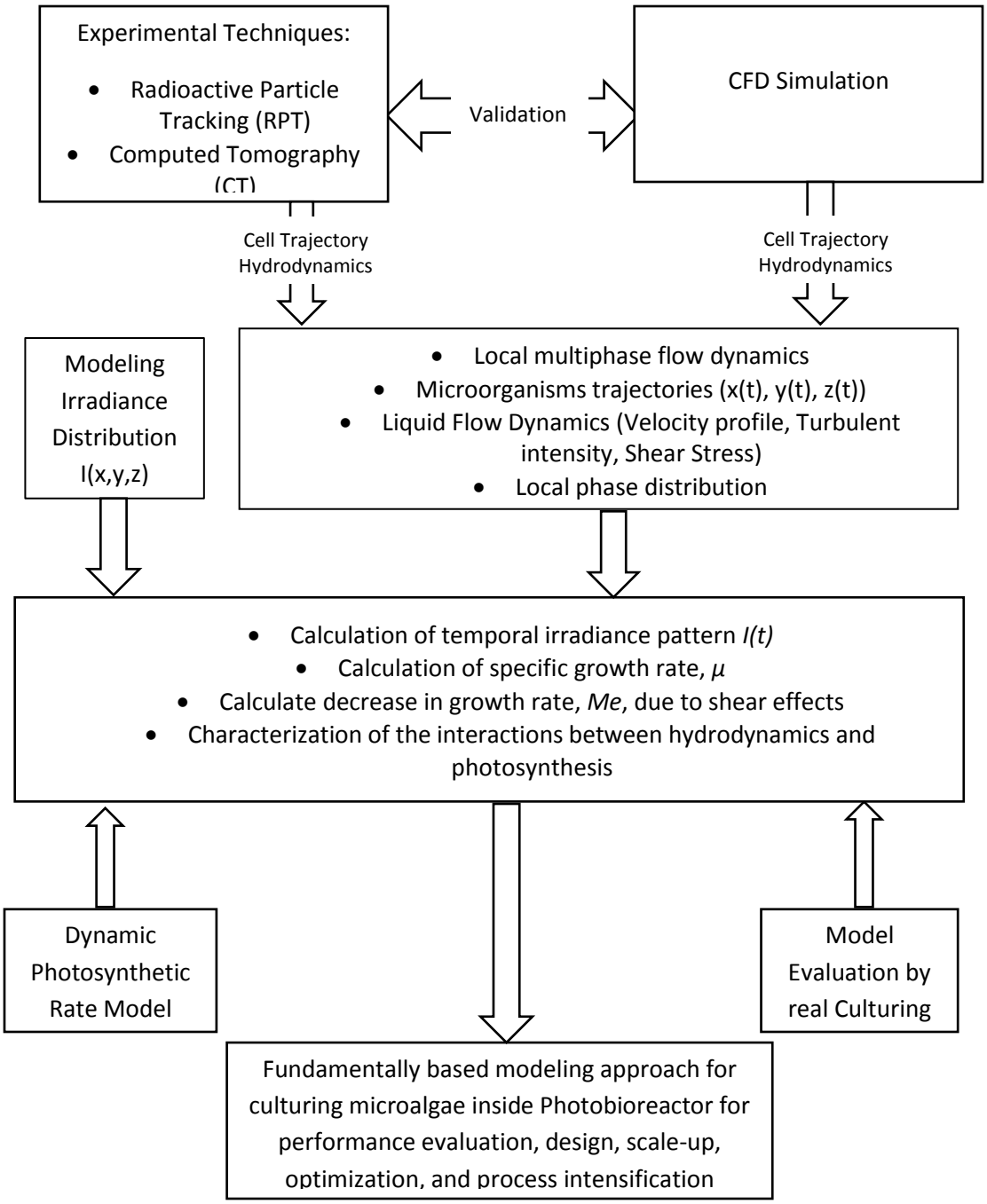

Figure 1.2: Integrated approach for overall analysis of microalgae culturing

2. DYNAMIC THREE-STATE MODEL AND THE CONCEPT OF PHOTOSYNTHETIC FACTORIES (PSFs)

The dynamic three-state model originally developed by Eilers and Peeters, 1988 [15] and modified by Wu and Merchuk, 2001[17] is based on the concept of photosynthetic factories (PSFs), that consist of colored pigments for light trapping, and reaction centers that are activated by incident irradiation. The PSFs are said to exist in three states, namely the resting state (x_1), the activated state (x_2), and the inhibited state (x_3). The model is schematically shown in Figure 2.1.

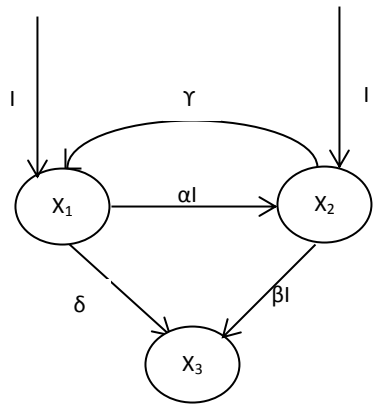

Figure 2.1: Structure of the three states kinetics model (proposed by Eilers and Peeters, 1988 [15])

On incidence of light, the resting PSF x_1 gets activated and transfers to the activated state, x_2. The activated PSFs can either absorb another photon from the incident light and move to the inhibited state, x_3, or transfer energy to acceptors for photosynthesis

and division, and move to x_1. PSFs in the inhibited state x_3 can recover and move back to state x_1. Assuming no limitations due to nutrients availability, the only variable was the availability of light, and hence, the transfer of PSFs involving photon absorption, x_1 to x_2 and x_2 to x_3, were considered to be to be first order reactions, while the other two, x_2 to x_1 and x_3 to x_1, were of zero order [15], [17]. The total process of photosynthetic growth is an integration of all the four transition possibilities shown in Figure 2.1. Accordingly, the process is explained by equation (1), (2), and (3).

$$\frac{dx_1}{dt} = -\alpha I x_1 + \gamma x_2 + \delta x_3 \quad (1)$$

$$\frac{dx_2}{dt} = \alpha I x_1 - \gamma x_2 - \beta I x_2 \quad (2)$$

$$\frac{dx_3}{dt} = \beta I x_2 - \delta x_3 \quad (3)$$

$$x_1 + x_2 + x_3 = 1$$

where α, β, γ, δ, and k are the kinetic parameters, I is the light received by the cells.

The specific growth rate, μ, is then based on the number of cell transitions from the activated state, x_2, to the resting state, x_1. As explained by Wu and Merchuk, 2001 [17], μ, accounts for the negative growth rate due to adverse conditions (Me), and is given in equation (4).

$$\mu = k\gamma x_2 - Me \quad (4)$$

k is the rate constant for the photosynthetic reaction, and Me is the maintenance constant.

As mentioned earlier, the light intensity experienced by a cell in a real culturing environment varies as the cell moves from one point in the reactor to another due to attenuation and mutual shading. Thus, in reality, light intensity, I, is a function of time

which depends on the trajectory of the cell inside the reactor. Also, for simplicity and ease of calculation, as suggested by Eilers and Peeters, 1988 [15], Wu and Merchuk [17] assumed Me to be a constant. However, the decrease in growth rate, accounted for by the maintenance constant, Me, can result from a variety of adverse environmental conditions [17]. Based on the findings in literature that shear stress beyond the critical shear stress damages cells and decreases the growth rate, Wu and Merchuk, 2002 developed an equation for the maintenance factor based on the shear stress experienced by the cells (Equation (5)). This equation for maintenance factor varying with shear stress experienced by the cells is more valid in large scale reactors than assuming a constant value, where the shear stress experienced by the cells is based on the cells trajectory. Wu and Merchuk, 2002 [23], and Luo and Al Dahhan, 2012 [19], applied this maintenance factor equation in bench scale bubble column and lab scale draft tube airlift reactors, respectively, for accounting for the decrease in growth rate due to the shear stress experienced by the cells. However, in the separate effects experiment, developed and implemented based on Wu and Merchuk, 2001 [17], owing to the low gas flow rate (1 vvm), low volume of the reactor (500 ml), and the low density of cells maintained inside the reactor at all times, the effect of shear stress can be ignored and the maintenance constant can be assumed to be a constant.

$$Me = \overline{Me}\, e^{k_m(\tau-\tau_c)} \tag{5}$$

where, Me is the maintenance factor due to shear effects, $\overline{Me}$ is the constant maintenance factor without shear stress (as estimated in Wu and Merchuk, 2001, and in this study), k_m is the extinction coefficient for shear stress, and τ and τ_c are the shear stress and the critical shear stress, respectively.

Therefore, in order to obtain the true kinetic parameters, a separate effects kinetics must be developed for which the intensity of light (taken to be constant for the solution) is known and the maintenance constant can be safely assumed to be constant. The procedure to solve Equations (1)-(4) to obtain the kinetic parameters is explained in section 3.

3. SOLUTION TO THE DYNAMIC THREE-STATE MODEL

The solution to the dynamic three-state model has been adapted from Wu and Merchuk, 2001 [17]. Equations (1)-(3) can be solved simultaneously to obtain the number of cells in the activated state (x_2) to estimate the growth rate, μ. The kinetic growth parameters, α, β, γ, δ, and the photosynthetic rate constant, k can then be determined by fitting the experimental data for specific growth rate to the resulting equation.

To estimate x_2 in terms of the kinetic parameters, an analytical solution to Equations (1)-(3) was obtained by assuming a Quasi steady state [17] under the following assumptions:

(a) The total circulation time (t_c) for completely flowing through the reactor once was divided into a light phase (t_l) and a dark phase (t_d).

(b) The microalgae was considered to experience zero and non-zero light intensity values during the dark and the light phases, respectively.

(c) The non-zero light intensity during the light phase was considered to be a constant [17]. Then, knowing the value of light intensity, Equations (1)-(3) were solved simultaneously.

To facilitate the solution of the modified three-state model (Equations (1)-(3)), a separate effects experiment was needed to satisfy the above mentioned assumptions. This was achieved by the tubular photobioreactor shown in Figure 3.1 (explained in detail in section 4.).

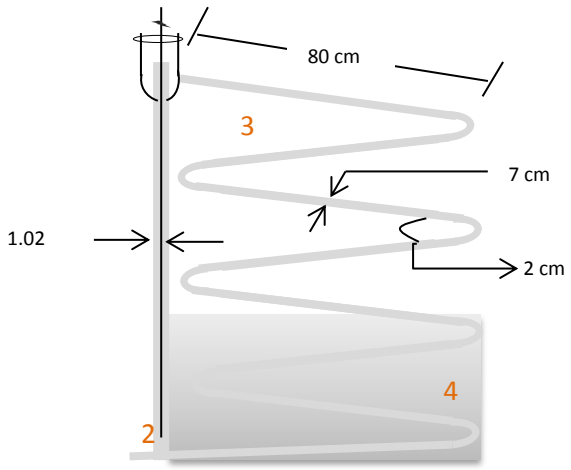

Figure 3.1: Schematic of the tubular loop reactor with air lift pump
((1) Gas inlet, (2) Gas sparger, (3) Illuminated part, (4) Dark part [17])

Solution:

The light illumination, I, was assumed to be constant in the light phase at the beginning of the cycle, $t=0$ ($I>0$, constant). At the end of the light phase, at $t=t_l$, when the PFD is switched off, $I=0$ until the circulation time, $t=t_c$.

The differential equations (1)-(4) can then be solved as follows in two steps ((i) and (ii)).

(i) At $0 < t < t_l$, the PFD is constant, αI and βI are non-zero.

Rearranging Eq. (2),

$$\alpha I x_1 = \frac{dx_2}{dt} + \gamma x_2 + \beta I x_2 \qquad (6)$$

Substitute the derivative of Equations (6) and (3) into Equation (1),

$$\frac{d^2x_2}{dt^2} + (\alpha I + \beta I + \gamma + \delta)\frac{dx_2}{dt} + (\alpha\beta I^2 + \alpha I\delta + \beta I\delta + \delta\gamma)x_2 = \alpha I\delta \qquad (7)$$

The above equations can be solved to obtain the transient values of x_1 and x_2 ($x_{1,l}$ and $x_{2,l}$) during the light period as

$$x_{1,l} = \frac{c(\beta I+\gamma)+bC_1(A+\beta I+\gamma)e^{At}+bC_2(B+\beta I+\gamma)e^{Bt}}{\alpha Ib} \quad (8)$$

$$x_{2,l} = \frac{c}{b} + C_1 e^{At} + C_2 e^{\boldsymbol{B}t} \quad (9)$$

where $a = \alpha I + \beta I + \gamma + \delta,\ \ b = \alpha\beta I^2 + \delta\gamma + \alpha I\delta + \beta I\delta,\ \ c = \alpha I\delta$ (10)

and $A = -\frac{a+\sqrt{a^2-4b}}{2}, \qquad B = -\frac{a-\sqrt{a^2-4b}}{2}.$ (11)

At $t = 0$, $x_1(0) = \frac{c(\beta I+\gamma)+bC_1(A+\beta I+\gamma)+bC_2(B+\beta I+\gamma)}{\alpha Ib}$, $x_2(0) = \frac{c}{b} + C_1 + C_2$ (12)

At $t = t_l$ $x_1(t_l) = \frac{c(\beta I+\gamma)+bC_1(A+\beta I+\gamma)e^{At_l}+bC_2(B+\beta I+\gamma)e^{Bt_l}}{\alpha Ib}$, and

$x_2(t_l) = \frac{c}{b} + C_1 e^{At_l} + C_2 e^{Bt_l}.$ (13)

(ii) At $t_l < t < t_c$, when the PFD is shut off), $I = 0$. Then the solution is

$$x_{1,d} = 1 - e^{-\gamma(t-t_l)}x_2(t_l) + [x_1(t_l) + x_2(t_l) - 1]e^{-\delta(t-t_l)} \quad (14)$$

$$x_{2,d} = e^{-\gamma(t-t_l)}x_2(t_l) \quad (15)$$

At $t = t_c$

$$x_1(t_c) = 1 - e^{-\gamma t_d}x_2(t_l) + [x_1(t_l) + x_2(t_l) - 1]e^{-\delta t_d} \quad (16)$$

$$x_2(t_c) = e^{-\gamma t_d}x_2(t_l) \quad (17)$$

where $t_d = t_c - t_l$.

For quasi-steady state,

$x_1(0) = x_1(t_c)$, and $x_2(0) = x_2(t_c)$ (18)

Equations (12), (16), (17), and (18) give the solution of C_1 and C_2:

$$C_1 = \frac{Bc(u-1)(n-v)+\alpha Ib(n-u)(v-1)+c(\alpha I+\beta I+\gamma)(n-1)(u-v)}{b[B(s-u)(n-v)-A(n-u)(s-v)+(\alpha I+\beta I+\gamma)(s-n)(u-v)]}, \quad (19)$$

$$C_2 = -\frac{Ac(u-1)(s-v)+\alpha Ib(s-u)(v-1)+c(\alpha I+\beta I+\gamma)(s-1)(u-v)}{b[B(s-u)(n-v)-A(n-u)(s-v)+(\alpha I+\beta I+\gamma)(s-n)(u-v)]}, \quad (20)$$

where $s = e^{At_l}, n = e^{Bt_l}, u = e^{\gamma t_d}, v = e^{\delta t_d}$.

Then, for one cycle, the mean specific growth rate is as given by Equation (2).

$$\bar{\mu} = \frac{k\gamma}{t_c}\int_0^{t_c} x_2(t)dt - Me \tag{21}$$

$$\bar{\mu} = \frac{k\gamma}{t_c}\left[\int_0^{t_l} x_{2,l}(t)dt + \int_{t_l}^{t_c} x_{2,d}(t)dt\right] - Me \tag{22}$$

$$\bar{\mu} = \frac{k\gamma}{t_c}\left[\frac{c}{b}t_l + \frac{C_1}{A}(s-1) + \frac{C_2}{B}(n-1) + \left(\frac{c}{b} + C_1 s + C_2 n\right)\frac{u-1}{u\gamma}\right] - Me \tag{23}$$

Since the method to obtain the kinetic parameters is through data fitting, the use of an addition equation based on these parameters will provide for a better fit. Therefore, in addition to equation (23), chlorophyll fluorescence measurements, which have been shown to be a reliable indicator of photoinhibition [23], were used for parameter extraction. The ratio, *q*, of the variable and maximum fluorescence (F_V and F_m), is considered to be a direct indicator of the number of cells that are not inhibited (i.e. are either in resting or active state) [17].

$$\frac{q}{q_{max}} = f\frac{1-x_3}{1}, \tag{24}$$

$$q = f'(1-x_3) = f'(x_1 + x_2), \text{ or} \tag{25}$$

$$x_3 = 1 - \frac{q}{f'}, \tag{26}$$

$$f' = f q_{max} \tag{27}$$

The mean value of q in quasi-steady state was calculated in Wu and Merchuk, 2001 [17] as

$$q = f'(x_1 + x_2) = \frac{f'}{t_c}\int_0^{t_c}[x_1(t) + x_2(t)]dt$$

$$= \frac{f'}{t_c}\left\{\int_0^{t_l}\left[x_{1,l}(t) + x_{2,l}(t)\right]dt + \int_{t_l}^{t_c}\left[x_{1,d}(t) + x_{2,d}(t)\right]dt\right\}$$

$$q = \frac{F_v}{F_m} = \frac{f}{t_c}\left\{\begin{array}{c} t_d + \frac{c}{b}\left(1 + \frac{\beta I\gamma}{\alpha I}\right)t_l + \frac{[x_1(t_l)+x_2(t_l)-1]\left(1-\frac{1}{v}\right)}{\delta} \\ +\frac{C_1}{A}\left(1 + \frac{A+\beta I+\gamma}{\alpha I}\right)(s-1) + \frac{C_2}{B}(1 + \frac{B+\beta I+\gamma}{\alpha I}(n-1) \end{array}\right\} (I>0) \qquad (28)$$

Equations (23) and (28) can then be used to fit the mean specific growth rate, $\bar{\mu}$, and fluorescence measurements, q, and extract the growth parameters.

4. EXPERIMENT

4.1 EXPERIMENTAL SETUP

In order to extract the kinetic parameters α, β, γ, δ, the photosynthetic growth rate, k, and the maintenance constant, Me, the separate effects experiment must satisfy the assumptions of well-defined dark and light phases, zero light intensity during the dark phase, a constant light intensity, I, in the light phase, and a constant maintenance constant, Me. The separate effects tubular airlift PBR used in Wu and Merchuk, 2001 [17], and based on the original idea of Lee and Pirt, 1981 [7], provided for all these conditions, and was designed, developed, and tested in this work. It is schematically shown in Figure 3.1. The PBR is equipped with an airlift pump, and has an internal diameter of 0.7 cm. The reactor had a total volume of 0.55 L and a circulation time of 45.2 s. The tubular design of the reactor allowed for the easy control and variation of light/dark phase, which was achieved by covering a part of the tubes to prevent light penetration. Covering a part of the tubes also satisfied the assumption of zero incident light intensity on the cells during the dark phase. Efficient gas circulation system to help the movement of the cells between the light and the dark phase was achieved through the airlift pump. To satisfy the assumption of constant light intensity during the light phase, the internal diameter of the tubes was 0.7 cm to maintain a thin microalgae culture in order to avoid light variation due to mutual shading. Also, the small diameter tubes helped maintain the change in photon flux density below 10%. Since gas circulation was achieved through an airlift pump, the maintenance constant was assumed to have a fixed value.

4.2 MICROALGAE CULTURE AND PBR OPERATION

A strain of green, fresh water algae *Scenedesmus* was initially grown in Alga-grow growth medium in conical flasks according to the supplier's instructions. The strain and growth medium were obtained from Carolina labs. For obtaining the experimental data, air enriched with 3% carbon dioxide was introduced in the tubular airlift PBR at a constant flow rate of 1 vvm. The PBR was filled with 500 ml of fresh water growth medium and inoculated with 50 ml of microalgae culture. Such a setup allowed for only two variables- the incident PFD on the reactor, and the time spent by the culture in the light phase. A bank of cool white lights was used to provide PFD between 110-550 $\mu E/m^2s$, and part of the tubes was covered to provide the necessary ark phase. The values of the PFD and the time spent in the light phase used for data fitting to equation (23) and (28) are given in Table 5.1. Growth rate and Fluorescent measurements at each experimental condition were taken for an average of 2-3 days ensuring a maximum final cell concentration of $120x10^6$ cells/ml.

5. MEASUREMENT TECHNIQUES

5.1 IRRADIANCE

Light sensor QSL-2101 from Biospherical Instruments Inc. was used to measure the irradiance on the surface of the reactor. The average irradiance studied were 110, 220, 550 $\mu E/m^2s$.

5.2 ILLUMINATED TIME, T_C

The total circulation time through the reactor was 45s. A colored dye technique was used to measure the time taken by the liquid to circulate through each leg of the tubular reactor. Based on that, Illuminated time, t_c, of 45.2, 43, 41.7, 38.2, 36.6, 35 and 28s were studied at each incident PFD.

5.3 FLUORESCENCE, F_V AND F_M

A handy PEA by Hansatech, UK was used to measure the fluorescence of the culture twice a day for the experimentation period. The variable and maximal fluorescence, F_v and F_m, were measured for each sample.

5.4 GROWTH RATE, μ

A cell count measurement was done twice a day for 2-3 days under a microscope. A 100 μL of culture was drawn from the top well of the tubular photobioreactor. Three cell count measurements were made under a microscope to obtain an average cell

number. The slope of the log of the cell count versus time plot was recorded as the growth rate, μ.

The experimental data of μ and F_v/F_m for the different light intensities and illuminated time, t_l is given in Table 5.1.

Table 5.1: Specific growth rate and fluorescence measurement data

Illuminated Time	Illuminated/ Circulation time	I= 107 μEm^{-2}s^{-}		I= 220 μEm^{-2}s^{-}		I= 560 μEm^{-2}s^{-}	
t_l (s)	t_l /t_c	μ (h^{-1})	F_V/F_M	μ (h^{-1})	F_V/F_M	μ (h^{-1})	F_V/F_M
45.2	1.0	0.0415	0.387	0.0462	0.411	0.0471	0.392
45.2	1.0	0.0407	0.421	0.0482	0.413	0.0466	0.383
43.0	0.95	0.0389	0.404	0.0501	0.416	0.0351	0.372
43.0	0.95	0.0394	0.424	0.0517	0.405	0.0410	0.324
41.7	0.92	0.0373	0.435	0.0524	0.422	0.0482	0.336
41.7	0.92	0.0352	0.441	0.0518	0.471	0.0461	0.341
38.2	0.85	0.0361	0.472	0.0463	0.500	0.0412	0.376
38.2	0.85	0.0382	0.480	0.0447	0.520	0.0433	0.357
36.6	0.80	0.0321	0.414	0.0429	0.463	0.0317	0.332
36.6	0.80	0.0342	0.452	0.0437	0.437	0.0368	0.360
35.0	0.77	0.0284	0.406	0.0402	0.381	0.0343	0.311
35.0	0.77	0.0310	0.416	0.0396	0.376	0.0313	0.323
28.0	0.51	0.0262	0.382	0.0353	0.445	0.0301	0.314
28.0	0.51	0.0257	0.395	0.0327	0.431	0.0294	0.309

6. RESULTS AND DISCUSSION

'Scientist' software by Micromath was used to fit the experimental data given in Table 5.1 to equations (23) and (28) through the least square error minimization technique. The goodness of fir (R^2) for the fitting of growth rate and fluorescent values were 0.91 and 0.97, respectively. The 95% confidence interval values of the parameters are given in Table 6.1.

Table 6.1: Dynamic growth parameters for microalgae *Scenedesmus*

Parameter	Value
α	0.018071 ($\mu E/m^2$)
β	8.487×10^{-7}($\mu E/m^2$)
γ	0.000361(s^{-1})
δ	0.000004153(s^{-1})
K	0.08369(-)
Me	0.02126(h^{-1})
f'	0.4505(-)

Thus, the three state dynamic growth model with the fitted kinetic parameters is as given below:

$$\frac{dx_1}{dt} = -0.018071\, I x_1 + 0.000361\, x_2 + 0.000004153\, x_3 \quad (29)$$

$$\frac{dx_2}{dt} = 0.018071 I x_1 - 0.000361 x_2 - 8.487 * 10^{-7}\, I x_2 \quad (30)$$

$$\frac{dx_3}{dt} = 8.487 * 10^{-7} I x_2 - 0.000004153 x_3 \quad (31)$$

$$\mu = 0.08369 * 0.000361\, x_2 - 0.02126 \quad (32)$$

$$\frac{F_V}{F_M} = 0.4505(\, 1 - x_3) \quad (33)$$

Equations (32) and (33) were used to obtain the fitted values which were then compared with the experimental data. The results of the fitted versus experimental data are shown in Figure 6.1.

While the parameters given in Table 6.1 have been derived assuming a constant irradiance at all points inside the reactor, and the experimenters in this study were carried out over a limited range of light/dark ratio (1-0.5) and light intensities, Equations (29)-(33) can be used for any known light intensity, constant or varying.

Equations (29)-(32) can be used to analyze the growth rate over the complete range of light/dark ratio, for different light intensities. The results for this simulation are given in Figure 6.1. Also shown in Figure 6.2 are the simulation results for certain higher light intensities (I=750, 100, and 2000 μE/m^{2}s). As can be seen in Figure 6.2, as the ratio of light/dark phase increases, increasing the exposure of the cells to light, the growth rate at the higher light intensities (I≥750 μE/m^{2}s) tends to be lower than that at the lower light intensities. This may be due to the damage of cell proteins due to excessive light, causing the cells to deactivate and move to the resting state (X3 in Figure 2.1) due to the process of photoinhibition [17]. Although the results of the simulation are based on the assumption of a constant light intensity received by the cells, which is not the case in real culturing systems, nonetheless, the trend from Figure 6.2 suggests that the incident light intensity as well as the ratio of the light/dark cycle must be optimized for efficient microalgae culturing, especially in large-scale reactors. The irradiance in a large scale real culturing system varies from one point to another due to effects of mutual shading by

the cells, movement of microalgae particles within the reactor, gas holdup, and the presence of dark zones in the core of the reactor. This leads to a time series of irradiance experienced by the cells inside the reactor. This also signifies the importance of studying the dynamic growth kinetics model.

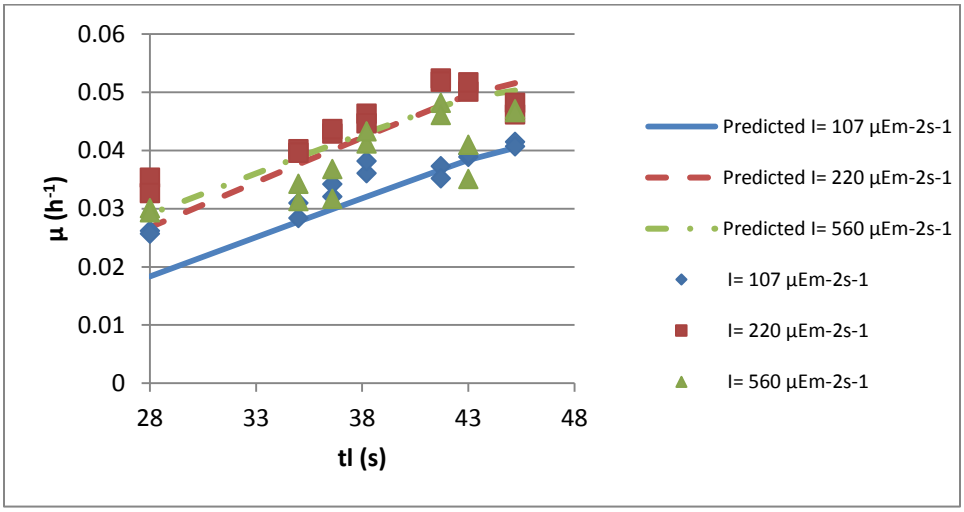

(a)

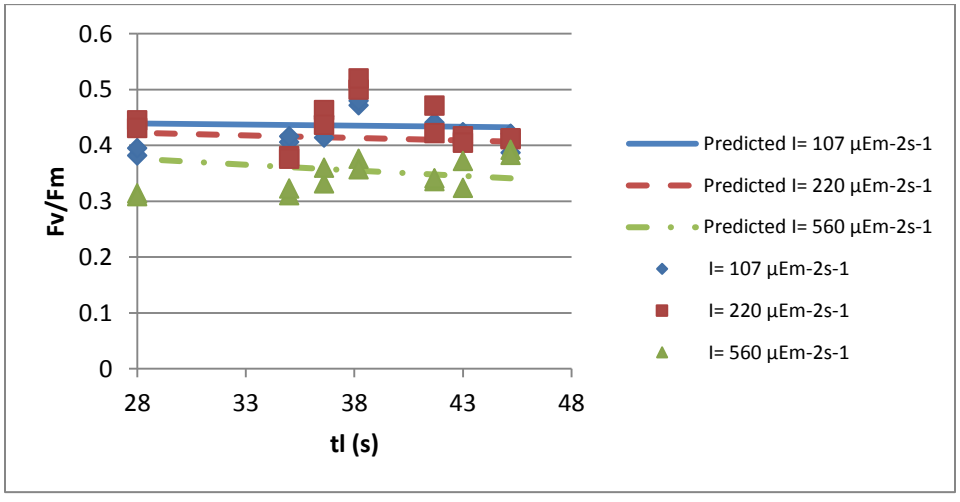

(b)

Figure 6.1: The experimental data and the predicted data from the model for the specific growth rate, μ (a), and the fluorescence measurements (b) (Equations (29)-(32))

The dynamic growth kinetics model for *Scenedesmus sp*. (Equations (29)-(32)) can be applied to both open and closed photobioreactors, provided the trajectory of the particles inside the reactor, and the holdup of the constituent materials is known. Since in large scale real culturing systems, the assumption of constant light intensity experienced by the cells and a constant maintenance constant are not valid, and validated computational fluid dynamics (CFD) simulations can be used to obtain the particle trajectories, liquid velocities, and other turbulent parameters like shear stress. Newton's second law can be used to generate the trajectory of the cells inside the photobioreactor. The particle trajectories can then be used to estimate the light intensity distribution inside the reactor to estimate the light intensity as a function of time (I(t)). In laboratory or pilot plant setups, advanced non-invasive measurement techniques such as Radioactive Particle Tracking (RPT) can be used to obtain the particle trajectories and the needed turbulent parameters to validate the CFD models to further obtain the radial distribution of gas holdup. Validated Computational Fluid Dynamics can also be used to estimate the detailed hydrodynamics of the photobioreactor which can then be used along with Newton's second law to generate the trajectory of the cells inside the photobioreactor to estimate I(t). This I(t) can then be used in equations (29)-(32) to estimate x_2, and the shear stress data can be used in estimating the maintenance constant. Substituting the value of x_2 and the maintenance constant in Equation (32) can then provide the true dynamic growth rate of the culture inside the reactor. . Knowledge of the trajectory of the cells inside the photobioreactor can then be used in conjunction with the above model to track the growth of the microalgae cells, and optimize the environmental and growth conditions for the microalgae to attain faster and more efficient growth. The detailed data

and information obtained from CFD and the above mentioned measurement techniques combined with the dynamic growth model can be used to carry out performance evaluation, and optimize the design and scale-up of large scale microalgae culturing and photobioreactor configurations.

Also, the dynamic growth methodology can be applied to other microalgae strains that have a potential to be used for bioenergy production, carbon sequestration, flue gas and wastewater treatment, as well as other high-value consumer products such as pharmaceuticals, and human nutrition etc. This process of combining the dynamic growth kinetics with the cell trajectories inside photobioreactors is based on integrating fundamental principles of photobioreactor design and growth kinetics, and can thus, bridge the gap between small scale investigational experiments and commercial production, making the whole process of microalgae cultivation for various applications economically feasible.

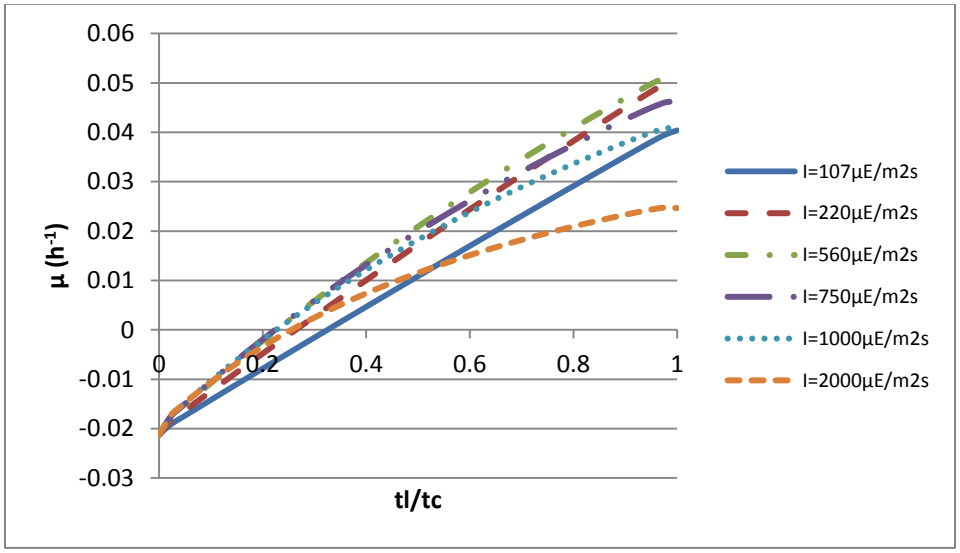

Figure 6.2: Simulation of the effect of different light intensities over the entire range of light/ dark cycle from the dynamic growth model ((29)-(32))

7. REMARKS

A dynamic growth model for microalgae *Scenedesmus* was successfully developed in a separate effects experiment inside a tubular photobioreactor at light intensities of 107, 220, 560 $\mu Em^{-2}s^{-1}$. The ratio of the light to dark phase was varied and the growth rate and fluorescence were evaluated experimentally. The data was fitted to the modified three-state dynamic growth model based on the original idea of Eilers and Peeters, 1988 [15], and modified by Wu and Merchuk, 2001 [17], to estimate the dynamic growth parameters of microalgae *Scenedesmus*. The fitted parameters when substituted back in the model were able to predict the expected growth rate and fluorescence values. The dynamic growth model successfully accounts for the simultaneous processes of photoinhibition and photolimitation that are experienced by the cells in real cultures and can be used with any reactor configuration with a known intensity and variation of light. The ability of the model to incorporate the light history of the cells gives useful insight into the effect of hydrodynamics on the process of photosynthesis. The dynamic growth model of *Scenedesmus* was also used to simulate the growth rate of algae over the entire range of the light/dark cycle, as well as at higher light intensities than those studied in the experiments. The results of the simulation using the fitted parameters indicated that the specific growth rate at light intensities greater than 750 $\mu E/m^2s$ was lesser than that at the lower intensities of 107, 220, and 560 $\mu E/m^2s$, with the difference increasing with an increase in the ratio of the light/dark cycle. This was thought to be due enhanced effect of photoinhibition at the higher intensities. This finding emphasizes the need of integrating the dynamic growth kinetics model with the

photobioreactor hydrodynamics and cell trajectories to optimize the microalgae culturing process to make it economically viable. The studied methodology can be extended to other strains of microalgae with potential for various applications.

REFERENCES

[1] J. C. Merchuk, M. Ronen, S. Giris, and S. Arad, "Light/dark cycles in the growth of the red microalga Porphyridium sp.," *Biotechnol. Bioeng.*, vol. 59, no. 6, pp. 705–713, 1998.

[2] E. Molina Grima, J. A. Sánchez Pérez, F. Garcia Camacho, J. L. Garcia Sánchez, and D. López Alonso, "n-3 PUFA productivity in chemostat cultures of microalgae," *Appl. Microbiol. Biotechnol.*, vol. 38, no. 5, pp. 599–605, 1993.

[3] T. T. Bannister, "Quantitative description of steady state, nutrient-saturated algal growth, including adaptation," *Limnol. Oceanogr.*, vol. 24, no. l, pp. 76–96, 1979.

[4] S. B. Powles, "Photoinhibition of Photosynthesis Induced by Visible Light," *Annu. Rev. Plant Physiol.*, vol. 35, no. 1, pp. 15–44, 1984.

[5] I. Vonshak, A., Guy, R., Poplawsky, R., Ohad, "Photoinhibition and its recovery in two strains of the cyanobacterium Spirulina platensis," *Plant Cell Physiol.*, vol. 29, no. 4, pp. 721–726, 1988.

[6] J. Meyers, "Growth characteristics of algae in realtion to the problems of mass culture," *Algal Cult. from Lab. to Pilot Plant (Burlew, J.S., Ed. Carnegie Inst. Washingt.*, pp. 37–54, 1953.

[7] Y. Lee and J. Pirt, "Energetics of Photosynthetic Algal Growth : Influence of Intermittent," *J. Gen. Microbiol.*, vol. 124, no. 198 I, pp. 43–52, 1981.

[8] A. S. Mirón, A. C. Gómez, F. G. Camacho, E. M. Grima, and Y. Chisti, "Comparative evaluation of compact photobioreactors for large-scale monoculture of microalgae," *Prog. Ind. Microbiol.*, vol. 35, no. C, pp. 249–270, 1999.

[9] J. H. Steele, *Microbial kinetics and dynamics in chemical reactor theory. In Chemical reactor theory: a review*. Lapidus,L., Amundson, N.R., Prentice-Hall Englewood Cliffs, 1977.

[10] S. Aiba, "Growth kinetics of photosynthetic microorganisms," *Adv. Biochem. Eng.*, vol. 23, pp. 85–156, 1982.

[11] N. Banerjee, "Study of algal growth and its engineering aspects for the production of chemicals," University of Mumbai, India, 2010.

[12] P. G. Falkowski and C. D. Wirick, "A simulation model of the effects of vertical mixing on primary productivity," *Mar. Biol.*, vol. 65, no. 1, pp. 69–75, 1981.

[13] K. L. Demnan and A. E. Gargett, "Time and space scales of vertical mixing and advection of phytoplankton in the upper ocean," *Limnol. Oceanogr.*, vol. 28, no. 5, pp. 801–815, 1983.

[14] C. L. Gallegosl and T. Platt, “Vertical advection of phytoplankton and productivity estimates : a dimensional analysis,” *Mar. Ecol. Prog. Ser.*, vol. 26, no. 1982, pp. 125–134, 1985.

[15] J. C. H. Eilers, P.H.C., Peeters, “A model for the relationship between light intensity and the rate of photosynthesis in phytoplankton,” *Ecol. Modell.*, vol. 42, no. 3–4, pp. 199–215, 1988.

[16] S. Rehak, B., Celikovsky, S., Papacek, “Models for photosynthesis and photoinhibition: Parameter identification based on the harmonic irradiation O2 response measurement,” *IEEE Trans. Autom. Control SI*, pp. 101–108, 2008.

[17] X. Wu and J. C. Merchuk, “A model integrating fluid dynamics in photosynthesis and photoinhibition processes,” *Chem. Eng. Sci.*, vol. 56, no. 11, pp. 3527–3538, 2001.

[18] J. C. Wu, X., Merchuk, “Simulation of algae growth in a bench scale internal loop airlift reactor,” *Chem. Eng. Sci.*, vol. 59, pp. 2899–2912, 2004.

[19] H. P. Luo and M. H. Al-Dahhan, “Airlift column photobioreactors for Porphyridium sp. culturing: Part II. verification of dynamic growth rate model for reactor performance evaluation,” *Biotechnol. Bioeng.*, vol. 109, no. 4, pp. 942–949, 2012.

[20] J. R. Miranda, P. C. Passarinho, and L. Gouveia, “Bioethanol production from Scenedesmus obliquus sugars: The influence of photobioreactors and culture conditions on biomass production,” *Appl. Microbiol. Biotechnol.*, vol. 96, no. 2, pp. 555–564, 2012.

[21] L. Gouveia and A. C. Oliveira, “Microalgae as a raw material for biofuels production,” *J. Ind. Microbiol. Biotechnol.*, vol. 36, no. 2, pp. 269–274, 2009.

[22] P. D. V. Makareviciene, V. Andrulevičiūtė, V. Skorupskaitė, and J. Kasperovičienė, “Cultivation of Microalgae Chlorella sp. and Scenedesmus sp. as a Potentional Biofuel Feedstock,” *Environ. Res. Eng. Manag.*, vol. 57, no. 3, pp. 21–27, 2011.

[23] X. Wu and J. C. Merchuk, “Simulation of algae growth in a bench-scale bubble column reactor,” *Biotechnol. Bioeng.*, vol. 80, no. 2, pp. 156–168, 2002.

[24] A. Vonshak, G. Torzillo, and L. Tomaseli, “Use of chlorophyll fluorescence to estimate the effect of photoinhibition in outdoor cultures ofSpirulina platensis,” *J. Appl. Phycol.*, vol. 6, no. 1, pp. 31–34, 1994.

SECTION

4. RECOMMENDATIONS

This study provides useful information on the local gas holdup and bubble dynamics properties such as bubble passage frequency, chord length, velocity, and interfacial area, and local mass transfer coefficient in air-water as well as in a real culture of microalgae *Scenedesmus*. While this information provides more insight into the working of airlift reactors, especially for microalgae cultures, the full potential of this research initiative can only be achieved by carrying out the following recommended studies.

1. Though the four-point optical probe technique was successfully applied in the air-water and microalgae culture, the problems posed due to the physical placement of the probe prevented a complete analysis of the radial profiles of the studied properties. A more precise technique such as Gamma Ray Computed Tomography (CT) can help solve this problem. The findings of this work, when combined with the radial profiles possible through CT experiments will provide the complete picture of the gas-liquid behavior inside the reactor.

2. Radioactive Particle Tracking (RPT) technique can be applied to attain the particle trajectories, liquid profiles, and turbulent parameters inside the split airlift reactor. Combining the particle trajectories with the dynamic growth kinetic parameters can be used to study the flashing lights effect inside the airlift reactor, and the interaction of hydrodynamics and photosynthesis.

3. Findings of this study, combined with information from the above two recommendations can be implemented for CFD model simulations to develop a complete model that integrates local hydrodynamics, mass transfer, and dynamic growth kinetics model. Such a model can then be used to predict the growth rate, biomass productivity, and gas liquid-interaction inside photobioreactors to improve the current understanding of microalgae cultures and photobioreactor designs.

4. The four point optical fiber probe used for gas holdup and bubble dynamics measurement can be coated with a material that inhibits the sticking of microalgae cells to the probe tip without interfering with the mechanism of the technique. This will enable the use of the probe for extended periods of time, over the entire active growth period. Such an optical fiber probe can then also be used as an in-line monitoring and diagnostic tool in commercial and large scale cultures.

5. The study can also be extended to other microalgae strains to evaluate the effect of the microalgae strains on the studied gas holdup and bubble dynamic parameters.

6. Investigations can also be carried out on different photobioreactor configurations, including open raceway ponds.

REFERENCES

[1] M. M. Kulik, "The potential for using cyanobacteria (blue-green algae) and algae in the biological control of plant pathogenic bacteria and fungi," *Eur. J. Plant Pathol.*, vol. 101, no. 6, pp. 585–599, 1995.

[2] R. Vonshak, A., Guy, "Photoadaptation, photoinhibition and productivity in the blue-green alga Spirulina platensis grown outdoors," *Plant Cell Environ.*, vol. 15, no. 5, pp. 613–616, 1992.

[3] M. J. Wijiffels, R.H., Barbosa, "An outlook on microalgal biofuels," *Science (80-.).*, vol. 329, pp. 796–799, 2010.

[4] G. Stephanopoulos, "Challenges in engineering microbes for biofuels production.," *Science*, vol. 315, no. 5813, pp. 801–4, 2007.

[5] A. K. So, M. John-McKay, and G. S. Espie, "Characterization of a mutant lacking carboxysomal carbonic anhydrase from the cyanobacterium Synechocystis PCC6803," *Planta*, vol. 214, no. 3, pp. 456–467, 2002.

[6] P. Lindberg, S. Park, and A. Melis, "Engineering a platform for photosynthetic isoprene production in cyanobacteria, using Synechocystis as the model organism," *Metab. Eng.*, vol. 12, no. 1, pp. 70–79, 2010.

[7] K. Kumar, C. N. Dasgupta, B. Nayak, P. Lindblad, and D. Das, "Development of suitable photobioreactors for CO2 sequestration addressing global warming using green algae and cyanobacteria," *Bioresour. Technol.*, vol. 102, no. 8, pp. 4945–4953, 2011.

[8] A. Hu, Q., Guterman, H., Richmond, "A flat inclined modular photobioreactor for outdoor mass cultivation of photoautotrophs," *Biotechnol. Bioenegineering*, vol. 51, pp. 51–60, 1996.

[9] M. Olaizola, "Commercial production of astaxanthin from Haematococcus pluvialis using 25,000-liter outdoor photobioreactors," *J. Appl. Phycol.*, vol. 12, no. 3, pp. 499–506, 2000.

[10] H. P. Luo and M. H. Al-Dahhan, "Local gas holdup in a draft tube airlift bioreactor," *Chem. Eng. Sci.*, vol. 65, no. 15, pp. 4503–4510, 2010.

[11] H. P. Luo and M. H. Al-Dahhan, "Local characteristics of hydrodynamics in draft tube airlift bioreactor," *Chem. Eng. Sci.*, vol. 63, no. 11, pp. 3057–3068, 2008.

[12] H. P. Luo and M. H. Al-Dahhan, "Verification and validation of CFD simulations for local flow dynamics in a draft tube airlift bioreactor," *Chem. Eng. Sci.*, vol. 66, no. 5, pp. 907–923, 2011.

[13] N. Banerjee, “Study of algal growth and its engineering aspects for the production of chemicals,” University of Mumbai, India, 2010.

[14] J. U. Grobbelaar, “Turbulence in mass algal cultures and the role of light/dark fluctuations,” *J. Appl. Phycol.*, vol. 6, no. 3, pp. 331–335, 1994.

[15] K. L. Terry, “Photosynthesis in modulated light: quantitative dependence of photosynthetic enhancement on flashing rate.,” *Biotechnol. Bioeng.*, vol. 28, no. 7, pp. 988–95, Jul. 1986.

[16] Chisti, Fujimoto, and Moo-Young, “Hydrodynamic and Oxigen Mass Transfer studies in Bubble columns and Airlift Bioreactors,” *Biotechnol. Process. Scale-up Mix.*, pp. 72–81, 1987.

[17] H. P. Luo and M. H. Al-Dahhan, “Airlift column photobioreactors for Porphyridium sp. culturing: Part I. effects of hydrodynamics and reactor geometry,” *Biotechnol. Bioeng.*, vol. 109, no. 4, pp. 932–941, 2012.

[18] C. U. Ugwu, H. Aoyagi, and H. Uchiyama, “Photobioreactors for mass cultivation of algae,” *Bioresour. Technol.*, vol. 99, no. 10, pp. 4021–4028, 2008.

[19] J. . Merchuk, M. Gluz, and I. Mukmenev, “Comparison of photobioreactors for cultivation of the red microalgaPorphyridium sp,” *J. Chem. Technol. Biotechnol.*, vol. 75, no. 12, pp. 1119–1126, 2000.

[20] A. S. Mirón, A. C. Gómez, F. G. Camacho, E. M. Grima, and Y. Chisti, “Comparative evaluation of compact photobioreactors for large-scale monoculture of microalgae,” *Prog. Ind. Microbiol.*, vol. 35, no. C, pp. 249–270, 1999.

[21] G. C. Zittelli, L. Rodolfi, and M. R. Tredici, “Mass cultivation of Nannochloropsissp. in annular reactors,” *J. Appl. Phycol.*, vol. 15, no. 2, pp. 107–114, 2003.

[22] C. U. Ugwu, J. C. Ogbonna, and H. Tanaka, “Light/dark cyclic movement of algal culture (Synechocystis aquatilis) in outdoor inclined tubular photobioreactor equipped with static mixers for efficient production of biomass,” *Biotechnol. Lett.*, vol. 27, no. 2, pp. 75–78, 2005.

[23] Q. Huang, C. Yang, G. Yu, and Z. S. Mao, “CFD simulation of hydrodynamics and mass transfer in an internal airlift loop reactor using a steady two-fluid model,” *Chem. Eng. Sci.*, vol. 65, no. 20, pp. 5527–5536, 2010.

[24] A. Contreras, Y. Chisti, and E. Molina Grima, “A reassesment of relationship between riser and downcomer gas holdups in airlift reactors,” *Chem. Eng. Sci.*, vol. 53, no. 24, pp. 4151–4154, 1998.

[25] J. Vega-Estrada, M. C. Montes-Horcasitas, A. R. Dom??nguez-Bocanegra, and R. O. Ca??izares-Villanueva, “Haematococcus pluvialis cultivation in split-cylinder internal-loop airlift photobioreactor under aeration conditions avoiding cell damage,” *Appl. Microbiol. Biotechnol.*, vol. 68, no. 1, pp. 31–35, 2005.

[26] H. C. Greenwell *et al.*, "Placing microalgae on the biofuels priority list: a review of the technological challenges.," *J. R. Soc. Interface*, vol. 7, no. 46, pp. 703–26, 2010.

[27] J. C. H. Eilers, P.H.C., Peeters, "A model for the relationship between light intensity and the rate of photosynthesis in phytoplankton," *Ecol. Modell.*, vol. 42, no. 3–4, pp. 199–215, 1988.

[28] X. Wu and J. C. Merchuk, "A model integrating fluid dynamics in photosynthesis and photoinhibition processes," *Chem. Eng. Sci.*, vol. 56, no. 11, pp. 3527–3538, 2001.

VITA

Aastha Ojha was born in 1988, in Chandigarh, India. She received her Bachelor of Engineering degree in Chemical Engineering from the Department of Chemical Engineering and Technology, Panjab University, Chandigarh in 2010. She was among the top 3% of the students in the class and received Honors with Distinction. After graduation, Aastha moved to Rolla, Missouri in 2011, to purse her Masters and Doctorate degrees, both in Chemical Engineering, from the Missouri University of Science and Technology. She received her Master of Science degree in Chemical Engineering from Missouri University of Science and Technology in May 2014, and her PhD. in Chemical Engineering in December 2016.